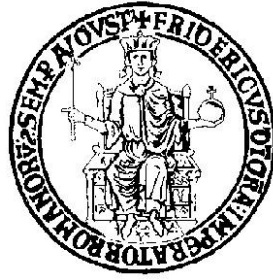# UNIVERSITÀ DEGLI STUDI DI NAPOLI FEDERICO II

Dipartimento di Ingegneria Civile, Edile e Ambientale

Dottorato di Ricerca in Ingegneria dei Sistemi Civili

XXX ciclo

Ph.D. Thesis

Anaerobic processes for waste biomass treatment: applications and mathematical modeling

Vincenzo Luongo

Ph.D. Coordinator

Prof. Ing. Andrea Papola

Promoters

Prof. Ing. Francesco Pirozzi

Dr. Ing. Luigi Frunzo

Table of contents

List of Figures

List of Tables

Chapter 9

__Acknoledgments__

Abstract

The increasing global energy demand and depletion of fossil fuels are driving international policies to promote the use of alternative energy sources, leading to the mitigation of global warming and greenhouse gas (GHG) emissions. In this context, the sustainable valorisation via biological anaerobic processes of organic waste biomasses represents a promising technology for producing renewable energy and value added chemicals in a biorefinery concept.

Anaerobic Digestion (AD) and Dark Fermentation (DF) are the most explored biological routes to produce renewable energy in the form of methane and hydrogen gas, respectively. Due to its high flexibility and applicability to a wide range of organic substrates, AD has been largely adopted in full scale applications, with increasing interest from both academia and industries. Conversely, low biohydrogen yields and incomplete biomass conversion limit DF scaled-up applications as a self-standing biotechnology for energy production. Moreover, the combination of different anaerobic processes, such as DF-AD or DF-Photo-Fermentation (PF), might be adopted to overcome the main drawbacks deriving from the application of DF processes. A significant example is represented by the use of DF by-products, such as organic acids and alcohols, for H_2 production via PF. The combined DF-PF process results in the increase of the total hydrogen yield (usually evaluated in terms of mol H_2 mol $C_6H_{12}O_6^{-1}$) and the production of poly-β-hydroxybutyrate (PHB), which are stored by Purple Non-Sulphur Bacteria, performing the PF step, as a carbon reserve available under nutrient starvation.

In this thesis, different anaerobic technologies have been applied to achieve higher biogas yields and/or by-products valorisation in a biorefinery concept. In particular, the enhancement of AD performances, in terms of biogas productivity, has been addressed by optimizing the crucial start-up phase of an anaerobic fluidized bed reactor. The stability of DF and enhancement of biohydrogen yields have been obtained by optimizing the operative conditions of a DF reactor continuously fed with cheese whey in thermophilic regimen, and by adopting a combined DF-PF configuration for the energetic valorisation of the organic fraction of municipal solid wastes, respectively.

Contextually, the valorisation of Dark Fermentation effluents (DFE) was achieved by i) producing PHB via PF, ii) extracting value added acids with anionic resins or iii) using DFE as a complex media for the dissolution of recalcitrant materials. Furthermore, a 1-D mathematical model has been presented to analyse and predict the microbial colonization of anaerobic multispecies biofilms.

Chapter 1

Anaerobic processes for waste biomass treatment: applications and mathematical modeling

Anaerobic processes for waste biomass treatment: applications and mathematical modeling

1.1 Introduction

The mitigation of environmental impacts and the limitation in use of petroleum based energy sources, have been largely promoted by international policies, in order to reduce the global warming and the greenhouse gas (GHG) emissions phenomena [1]. An economy based on innovative and cost efficient use of bioresources for the green production of both bio-based products and bioenergy could be driven by integrated biorefining systems [2], naturally influenced by the availability and biochemical composition of the utilized biomass. This alternative "*bioeconomy*" refers to a multitude of bio-based production and manufacturing processes, which are based on the use and conversion of bioresources (or generally biomasses) to produce a wide range of value added end-products [3].

Traditionally, biomass is a generic term to define all plants or all materials derived from growing plants. Over the last decades, it has been extended to include such diverse organic sources as algae, municipal solid waste, food wastes, and agro-industrial by-products. Substantially, the definition of biomass moved from a simple ecological concept from an energy-oriented concept as it is possible to read from the Directive 2009/28/EC of the European Parliament: "*The biomass is the biodegradable fraction of products, waste and residues from biological origin from agriculture (including vegetal and animal substances), forestry and related industries including fisheries and aquaculture, as well as the biodegradable fraction of industrial and municipal waste.*" [4].

In this context, the valorisation via biological anaerobic processes of organic compounds contained in wastewaters and/or in waste biomasses, contextually represents a well-known and largely adopted application in developed countries and a promising technology for producing renewable substances, value added chemicals and energy from wastes. The increasing interest on anaerobic processes from both academia and industries relies on their versatility in terms of substrate application range and integration in developed biorefining systems. The most exhaustive definition of biorefinery was introduced by the International Energy Agency (IEA) Bioenergy Task 42 "*Biorefineries*", established in 2007 to acknowledge the increasing relevance of biorefinery in a sustainable bioenergy research policy: "*Biorefining is the*

2

sustainable processing of biomass into a spectrum of marketable products and energy". The Task group describes biorefinery as a sustainable facility combining diverse integrated conversion technologies aimed to produce biofuels, power and chemicals from biomasses. It is evident that anaerobic processes can play a very central role in the biorefinery facilities due to both the possibilities to produce biogas and large amounts of diverse value added by-products [5].

Anaerobic Digestion (AD) is one the most studied and suited technologies for stabilizing organic wastes, due to its limited environmental impacts and high potential for energy recovery [6]. In this process, complex or simple organic compounds, from solid organic wastes to simple sugars or alcohols, can be effectively degraded into digestate through a series of biological reactions operated by specific anaerobic bacterial species, allowing to the final production of a methane rich biological gas as a result of their synergic metabolisms. These microbial groups catalyse the following main reactions: the extracellular hydrolysis of complex particulates to associated monomers (sugars and amino acids); the fermentation of sugars and amino acids to simpler compounds, such as organic acids, alcohols and hydrogen; the syntrophic acetogenesis, converting the latter into acetate and hydrogen; the acetoclastic methanogenesis to convert acetate into methane [7,8]. As widely demonstrated by experimental evidence, the microbial community interactions are strongly affected by various operating and designing conditions, such as the pH value, the operating temperature, the composition of the feedstock, the organic loading rate and the hydraulic retention time.

The enhancement of AD performances in terms of biogas productivity and energy recovery represents a major research interest. For instance, considerable efforts have been recently devoted to the development of high rate reactors with decreasing reactor volume or retention time to maximize community functions and the related methane production [9]. Even though the intensified practice of AD has led to many different modifications to the conventional reactor configurations, anaerobic biofilm reactors represent one of the most promising technologies in the field of high rate digesters [10]. In these systems, microorganisms grow attached to an inert solid surface and/or each other forming micro colonies or biofilms. The adhesion of microorganisms over solid carriers with large specific surface areas, leads to high biomass concentration and high reaction rates, thus reducing the reactor volume needed [11]. Of course, complex mathematical models have been proposed to understand, design and manage

conventional AD reactors [7, 12]. However, the investigation and development of models aimed to understand the ecological interactions and succession occurring in anaerobic biofilms reactors is an open field for academic research.

Over the last decades, increasing attention has been directed towards the study of an alternative anaerobic process, named Dark Fermentation (DF), devoted to the conversion of organic compounds to a hydrogen-rich biogas. This process is strictly connected to the establishment of favourable environmental conditions for the growth of hydrogen producing microorganisms. For instance, under overloading stress conditions, fermentative bacteria, inhabiting the AD reactors and operating the acidogenesis step, might lead to an incomplete biomass conversion with the accumulation of acids and alcohols and predominate over methanogenic trophic groups [13]. Several strategies have been investigated to enhance the development of a fermentative consortium that provides environmental credentials from recovery of renewable energy in the form of bio-H_2, while providing the treatment of the organic waste [14, 15]. In the energy and environmental sector, H_2 has gained considerable interests due to its high specific energy content (122 MJ kg^{-1}), clean combustion and environmental friendliness in production and use [16]. The feedstock composition influence the DF performance: rich in carbohydrates waste biomass is considered to be the most suited for the DF process [13]. However, other factors such as culture temperature, pH, H_2 partial pressure, bioreactor configuration, inoculum source etc. strongly affect the biohydrogen productivity [17]. A key challenge for the DF large scale applications relies on the enhancement of the H_2 yields or the valorisation of the dark fermentation effluent (DFE), typically rich in organic acids and alcohols, remaining as major fermentation by-products within the bulk liquid. Bastidas-Oyanedel et al. 2015 [18] underlined that the DF process could be perfectly integrated in many biorefining systems due to the contextual production of H_2 and high selling price organic acids. Indeed, the DF products could be purified and/or used as platform chemicals in subsequent biological processes for the production of fuels, fine chemicals, and biosyngas [18]. A striking example of a biorefining system is represented by the combination of the DF process with a consequent photo fermentation (PF) stage, usually performed by Purple Non-Sulphur Bacteria (PNSB), which can successfully convert the organic acids, constituting the DFE, and increase the net H_2 production [19]. Under anaerobic conditions, PNSB carry out an anaerobic photosynthesis using light and reduced carbon sources, such as the organic acids and

alcohols contained in DFE, to produce H_2 [20, 21]. The use of light as energy source is regulated by the simple photosystem of PNSB, which allows the accumulation of photons within the cell membrane and a consequent formation of an energy gradient towards the liquid phase. On the other hand, the assimilation of organic acids leads to the formation of a proton gradient which stimulates the production of bio-energy in the form of ATP, leading to the final enzymatic production of H_2 [22, 23]. In some cases, the combined DF–PF process not only results in a higher H_2 production, but also in the possibility of synthetizing poly-β-hydroxybutyrate (PHB), which is a biopolymer precursor of economic interest [24].

Another significant example of biorefining system is provided by the combined production of methane and hydrogen (bio-hythane), deriving from the integration of the AD and DF processes. Hythane, or enriched methane, requires the addition of H_2 to CH_4 gas (5-25% H_2) to increase the H/C ratio and, on turns, to reduce the GHG emissions by widening the narrow flammability range of the biogas, increasing the fuel efficiency and flame speed, and thus reducing combustion duration and improving heat efficiency [25, 26]. The integrated two stages devoted to H_2 and CH_4 production respectively, might involve the use of microalgal and waste biomass as feedstock for profitable clean energy solution [27].

The valorisation of the DFEs could be also obtained by using the organic acids as feedstock for chemical treatments demanding large amounts of acids and energy, such as the denaturation treatment of cement asbestos composites [28], or by recovering the organic acids with *in situ* or down-stream purification technologies [29].

1.2 Scope and structure of the thesis

The main objective of the thesis was to investigate the feasibility and sustainability of diverse anaerobic processes, namely AD, DF and PF, for waste biomasses conversion to biogas. In particular, the work proposed a range of different strategies to increase the efficiency of the above mentioned anaerobic processes in a biorefinery concept. The latter involved the valorisation of the effluents, which have been used for the final production of high-value biochemicals and for the mitigation of environmental risks. To this aim, the work addressed the use of a biofilm reactor for AD maximization, and mainly focused on the application of the DF technology for hydrogen production, with the contextual integration of such process in diverse biorefining systems. The overall structure of the thesis takes the following form:

Chapter 2 introduces AD process by studying the start-up of an anaerobic fluidized bed reactor using Anox Kaldness-K1 as biofilm carrier material;

Chapter 3 focuses on the invasion problem in anaerobic biofilm reactors; specifically, the removal of both carbon and nitrogen compounds are reported as applications of a new introduced 1-D biofilm model;

Chapter 4 elucidates the applicability of DF process to the conversion of cheese whey producing bio-H_2 in a continuous reactor;

Chapter 5 gives a comprehensive explanation of the PF process for H_2 production focussing on the use of DFE as feeding substrate for photo bio reactors;

Chapter 6 compares the photofermentative hydrogen yields and PHB production of pure (*Rhodobacter sphaeroides*) and mixed PNSB cultures during the PF of DFEs;

Chapter 7 reports the recent applications of combined DF-AD systems for the production of biohytane from microalgae biomasses;

Chapter 8 presents a preliminary study related to the use of DFE as a dissolving agent for the hydrothermal denaturation treatment of cement asbestos composites;

Chapter 9 shows the applicability of anionic resins for lactic acid recovery from a synthetic broth mimicking the DFE;

Chapter 10 highlights the major findings and the implications of the research and provides future recommendations.

References

[1] Ghimire, A., 2015. Dark fermentative biohydrogen production from organic waste and application of by-products in a biorefinery concept. PhD thesis, Paris Est, France.

[2] de Jong, E., Jungmeier, G., 2015. Biorefinery concepts in comparison to petrochemical refineries. Industrial Biorefineries & White Biotechnology, pp.3-33.

[3] Sillanpää, M., Ncibi, C., 2017. Biomass: The sustainable core of bioeconomy. a sustainable bioeconomy, Springer International Publishing, pp. 55-78.

[4] Directive 2009/28/EC of the European Parliament and of the Council of 23 April 2009 on the promotion of the use of energy from renewable sources and amending and subsequently repealing Directives 2001/77/EC and 2003/30/EC. Official Journal of the European Union, 5, p.2009.

[5] Cherubini, F., 2010. The biorefinery concept: using biomass instead of oil for producing energy and chemicals. Energy Conversion and Management, 51(7), pp.1412-1421.

[6] Ariunbaatar, J., Panico, A., Esposito, G., Pirozzi, F., Lens, P.N.L., 2014. Pretreatment methods to enhance anaerobic digestion of organic solid waste. Applied Energy, 123, pp.143-156.

[7] Batstone, D.J., Keller, J., Angelidaki, I., Kalyuzhnyi, S.V., Pavlostathis, S.G., Rozzi, A., Sanders, W.T.M., Siegrist, H., Vavilin, V.A., 2002. The IWA Anaerobic Digestion Model no 1 (ADM1). Water Science and Technology, 45(10), pp.65-73.

[8] McKeown, R.M., Hughes, D., Collins, G., Mahony, T. and O'Flaherty, V., 2012. Low-temperature anaerobic digestion for wastewater treatment. Current Opinion in Biotechnology, 23(3), pp.444-451.

[9] Rajeshwari, K.V., Balakrishnan, M., Kansal, A., Lata, K. and Kishore, V.V.N., 2000. State-of-the-art of anaerobic digestion technology for industrial wastewater treatment. Renewable and Sustainable Energy Reviews, 4(2), pp.135-156.

[10] Yeshanew, M.M., Frunzo, L., Luongo, V., Pirozzi, F., Lens, P.N.L., Esposito, G., 2016. Start-up of an anaerobic fluidized bed reactor treating synthetic carbohydrate rich wastewater. Journal of Environmental Management, 184, pp.456-464.

[11] Wang, W., Hou, H., Hu, S., Gao, X., 2010. Performance and stability improvements in anaerobic digestion of thermally hydrolyzed municipal biowaste by a biofilm system. Bioresource Technology, 101(6), pp.1715-1721.

[12] Picioreanu, C., Batstone, D.J., Van Loosdrecht, M.C.M., 2005. Multidimensional modelling of anaerobic granules. Water Science and Technology, 52(1-2), pp.501-507.

[13] Ghimire, A., Frunzo, L., Pirozzi, F., Trably, E., Escudie, R., Lens, P.N.L., Esposito, G., 2015. A review on dark fermentative biohydrogen production from organic biomass: process parameters and use of by-products. Applied Energy, 144, pp.73-95.

[14] Das, D., Veziroğlu, T.N., 2001. Hydrogen production by biological processes: a survey of literature. International Journal of Hydrogen Energy, 26(1), pp.13-28.

[15] Das, D., Veziroğlu, T.N., 2008. Advances in Biological Hydrogen Production Processes. International Journal of Hydrogen Energy 33 (21), pp.6046-6057.

[16] Balat, H., Kırtay, E., 2010. Hydrogen from biomass–present scenario and future prospects. International Journal of Hydrogen Energy, 35(14), pp.7416-7426.

[17] Li, R.Y., Fang, H.H., 2009. Heterotrophic photo fermentative hydrogen production. Critical Reviews in Environmental Science and Technology, 39(12), pp.1081-1108.

[18] Bastidas-Oyanedel, J.R., Bonk, F., Thomsen, M.H. and Schmidt, J.E., 2015. Dark fermentation biorefinery in the present and future (bio) chemical industry. Reviews in Environmental Science and Bio/Technology, 14(3), pp.473-498.

[19] Ghimire, A., Valentino, S., Frunzo, L., Pirozzi, F., Lens, P.N.L., Esposito, G., 2016. Concomitant biohydrogen and poly-β-hydroxybutyrate production from dark fermentation effluents by adapted *Rhodobacter sphaeroides* and mixed photofermentative cultures. Bioresource Technology, 217, pp.157-164.

[20] Cheng, J., Ding, L., Xia, A., Lin, R., Li, Y., Zhou, J., Cen, K., 2015. Hydrogen production using amino acids obtained by protein degradation in waste biomass by combined dark-and photo-fermentation. Bioresource Technology, 179, pp.13-19.

[21] Rai, P.K., Singh, S.P., Asthana, R.K., Singh, S., 2014. Biohydrogen production from sugarcane bagasse by integrating dark-and photo-fermentation. Bioresource Technology, 152, pp.140-146.

[22] Akkerman, I., Janssen, M., Rocha, J., Wijffels, R.H., 2002. Photobiological hydrogen production: photochemical efficiency and bioreactor design. International Journal of Hydrogen Energy, 27(11), pp.1195-1208.

[23] Hu, X., Ritz, T., Damjanović, A., Autenrieth, F., Schulten, K., 2002. Photosynthetic apparatus of purple bacteria. Quarterly Reviews of Biophysics, 35(1), pp.1-62.

[24] Luongo, V., Ghimire, A., Frunzo, L., Fabbricino, M., d'Antonio, G., Pirozzi, F., Esposito, G., 2017. Photofermentative production of hydrogen and poly-β-hydroxybutyrate from dark fermentation products. Bioresource Technology, 228, pp.171-175.

[25] Liu, Z., Zhang, C., Lu, Y., Wu, X., Wang, L., Wang, L., Han, B., Xing, X.H., 2013. States and challenges for high-value biohythane production from waste biomass by dark fermentation technology. Bioresource Technology, 135, pp.292-303.

[26] Roy, S., Das, D., 2016. Biohythane production from organic wastes: present state of art. Environmental Science and Pollution Research, 23(10), pp.9391-9410.

[27] Ghimire, A., Kumar, G., Sivagurunathan, P., Shobana, S., Saratale, G.D., Kim, H.W., Luongo, V., Esposito, G. and Munoz, R., 2017. Bio-hythane production from microalgae biomass: key challenges and potential opportunities for algal bio-refineries. Bioresource Technology, 241, pp.525-536.

[28] Spasiano, D., Luongo, V., Petrella, A., Alfè, M., Pirozzi, F., Fratino, U., Piccinni, A.F., 2017. Preliminary study on the adoption of dark fermentation as pretreatment for a sustainable hydrothermal denaturation of cement-asbestos composites. Journal of Cleaner Production, 166, pp.172-180.

[29] Luongo, V., Palma, A., Rene, E.R., Fontana, A., Pirozzi, F., Esposito, G., Lens, P.N.L., 2017. Lactic acid recovery from a simplified mimic of *Thermotoga neapolitana* fermentation broth using ion exchange resins in batch and fixed-bed reactors. Submitted

Chapter 2

Start-up of an anaerobic fluidized bed reactor treating synthetic carbohydrate rich wastewater

Start-up of an anaerobic fluidized bed reactor treating synthetic carbohydrate rich wastewater

The present chapter studied the start-up process of a mesophilic (37 ± 2 °C) anaerobic fluidized bed reactor (AFBR) operated at a hydraulic retention time (HRT) of 20 days using synthetic carbohydrate rich wastewater. Anox Kaldness-K1 carriers were used as biofilm carrier material. The reactor performance and biofilm formation were evaluated during the process. The start-up process at lower liquid recirculation flow rate enhanced the biofilm formation and reactor performance. The organic substrate composition had a major impact on early colonization of methanogenic archaea onto the surface of the Kaldness carriers during the start-up process. Specific organic substrates favouring the growth of methanogenic archaea, such as acetate, are preferred in order to facilitate the subsequent biofilm formation and AFBR start-up. The supply of 'bio-available' nutrients and trace elements, in particular iron, had an important role on optimal methanogenic activity and speeding-up of the biofilm development on the Kaldness carriers. This work provides possible strategies to optimize the various operational parameters that influence the initial biofilm formation and development in an AFBR and similar high rate anaerobic reactors, hence can be used to reduce the long time required for process start-up.

2.1. Introduction

At present, the global energy demand and environmental concerns on fossil fuel utilization are demanding alternative energy generation options, aimed at combining economic well-being with a green future [1]. Bioenergy production made an impressive progress in addressing the energy demands with sustainable perspectives [2]. In particular, anaerobic digestion (AD) has been recognized as a promising technology for future biofuel production whilst protecting the environment in a cost effective way [3, 4]. Accordingly, intensified practice of the process led to technological modifications and development of high rate AD reactors over conventional typologies [5, 6]. The latter are slow rate AD reactors operated at a longer hydraulic retention time (HRT), and hence impose larger reactor volumes. Instead, the high rate AD reactors are designed to reduce the HRT and increase the biogas production rate [1, 7]. These prominent advantages were achieved via immobilization of microbial biomass in the reactor, i.e. decoupling of a short HRT

and long solid retention time (SRT) [5]. Depending on the biomass retention techniques, various types of high rate AD reactors have been developed, such as up-flow anaerobic sludge blanket (UASB) reactors, anaerobic packed bed reactors (APBR), anaerobic fluidized bed reactors (AFBR) and anaerobic membrane bioreactors (AnMBR) [1].

An AFBR configuration has attracted an increasing attention due to the retention of biomass onto a solid inert biofilm carrier material with a large specific surface area [8]. The reactors have been widely used for the treatment of many industrial and municipal wastewaters since the last two decades [1]. The carrier materials are fluidized by the influent flow and/or through recirculation of the supernatant liquid [9]. The bed fluidization provides adequate mixing and mass transfer compared to the other reactor types [8], thus facilitates the proliferation of microbial biomass and improves treatment efficiency [9]. In spite of these benefits, some common shortcomings such as the longer start-up period, remain the major deterrent for the extensive application of this technology [10]. The start-up period of an AFBR is an important economic aspect of the system, as the desired stable operation and satisfying reactor performance rely on an effective start-up process [7, 11]. Its main task is to retain a proper amount of active and well adapted microbial biomass on the surface of the carrier materials in a possible shorter period of time [5, 10, 11, 12]. The presence of this matured and well-balanced biofilm (e.g. in terms of the ratio of methanogenic archaea to fermentative bacteria) is vital, particularly considering the syntrophic bioconversion of organic matter in the AD process [2]. Due to the very low growth rate of AD microbial biomass, especially methanogenic archaea, the typical long start-up period with the spontaneous development and maturation of the biofilm is a drawback of the AFBR system [13, 14]. It might take several months (2-9 months) to obtain a matured biofilm and stable process [11]. To address these concerns, several studies have focused on the fundamentals of biofilm formation and enhanced development [2, 11, 5, 10].

The biofilm formation process involves three basic successive stages: initial attachment of microbial cells on the surface of the carrier material, irreversible attachment by producing extracellular polymeric substances (EPS) and maturation of the biofilm [2, 11]. In these dynamic processes, various physico-chemical and biological parameters as well as operational conditions are of great relevance, such as hydrodynamic conditions [10], types and nature of carrier material [5], substrate

composition [15], source of inoculum [5] and availability of trace metals [16, 17]. A further understanding of the various factors affecting the start-up process is essential for the development and success of the AFBR configuration [15].

The present work studied the start-up process of an AFBR, investigating various operational parameters that influence the initial biofilm formation and reactor performance during treatment of synthetic carbohydrate rich wastewater at mesophilic (37 ± 2 °C) temperature. Throughout the experiment, the daily methane yield was used as a main indicator of the dynamic steps of biofilm formation and reactor start-up, as indicated by Michaud et al. [12]. The methane yield could be correlated to the AD biomass activity and development of biofilms since it is the result of the balance between the organic carbon flows to anabolism (biofilm growth) and catabolism (methane and other product formation) in the AD process [12, 16]. Theoretically, the methane yield of an AD biomass is 350 mL CH_4 g $COD_{removed}^{-1}$. Reaching this value would indicate that the majority of the carbon is used by the biofilm for anaerobic respiration and maintenance [16]. Moreover, the reactor performance and stability were evaluated by monitoring several parameters such as total organic acids, total alkalinity, pH, chemical oxygen demand (COD), total ammonium and individual volatile fatty acids (VFAs) concentration.

2.2. Materials and methods

2.2.1. Substrate

Synthetically prepared carbohydrate-rich wastewater containing glucose as the sole carbon source was used as the substrate for 57 days. Afterwards, the substrate was changed to a mixture of acetate and propionate at a ratio of 3:1 (v:v). The necessary nutrients and trace elements (TEs) for the AD biomass were supplied according to Table 1. The concentration of nutrients and TEs added was based on literature reports [18, 19]. In order to avoid precipitation in the storage vessels prior to reactor feeding, each solution was prepared separately and mixed based on the proportion given in Table 1. Ammonium bicarbonate (NH_4HCO_3) was used as a source of nitrogen and alkalinity. All reagents were of analytical grade (Sigma-Aldrich®).

Table 1. Composition of nutrients and trace metals solution used in this study.

Solution type		Compound	Metal	Amount (g L^{-1})
A		K_2HPO_4	-	73.12
		KH_2PO_4	-	10.88
B		$CaCl_2\ 2H_2O$	Ca^{2+}	5.96
		$MgCl_2$	Mg^{2+}	10.0
C	I	EDTA	-	64.0
		KOH	K^+	56.0
	II	$FeSO_4\ 7H_2O$	Fe^{2+}	54.8
D		$ZnCl_2$	Zn^{2+}	0.5
		$MnCl_2\ 4H_2O$	Mn^{2+}	5.0
		$CuSO_4\ 2H_2O$	Cu^{2+}	0.38
		$(NH_4)_6Mo_7O_{24}\ 4H_2O$	Mo^{6+}	0.08
		$NiCl_2\ 6H_2O$	Ni^{2+}	0.5
		H_3BO_3	B^{3+}	0.5
		$CoCl_2\ 6H_2O$	Co^{2+}	5.0
		$Na_2SeO_3\ 5H_2O$	Se^{6+}	0.5
		$Na_2WO_4\ 2H_2O$	W^{6+}	0.5
		$AlCl_3\ 6H_2O$	Al^{3+}	0.5

*Total for 1L of substrate = 40 mL **A** + 10 mL **B** +1 mL **C** + 0.1 mL **D**

*each solution was prepared separately and the volume of each solution was taken according to the given proportion

2.2.2. Inoculum

The inoculum was obtained from a full scale AD plant located in Capaccio-Salerno (Italy), treating buffalo manure and dairy wastes at mesophilic conditions. An inoculum from a running full scale AD plant under suspended biomass system has been previously used by several authors [7, 14]. Larger particles and small sticks of the inoculum were removed by centrifugation at 4500 rpm for 10 min (IEC Centra GP8R, USA) and filtered through a sieve with pore size of 1.0 mm. Approximately 800 mL, 62% of the active volume of the reactor, of the centrifuged inoculum was added to the reactor at the start of the experiment. The main physico-chemical characteristics of the inoculum are given in Table 2.

Table 2. Characteristics of the inoculum used in the study

Parameter	pH	TS	VS	Total COD	Total alkalinity	TKN
unit	-	%, wet basis	%, dry basis	mg L^{-1}	mg L^{-1} $CaCO_3$	g/kg
Amount	8.1 ± 0.01	2.18 ± 0.03	1.8 ± 0.05	197.4 ± 1.9	1466.1 ± 1.4	1.4 ± 0.04

2.2.3. Biofilm carrier material

Kaldness-K1, developed by Anox-Kaldness (Veolia, Sweden), was used as biofilm carrier material. Its use has been widely reported for different types of wastewater and is one of the most commonly employed in moving bed biofilm reactors [20, 21]. The Kaldness-K1 carrier is a small cylinder of low density polyethylene, lower than the density of water, with a cross inside and "fins" in the external surface. It has a specific weight of 145 kg m^{-3} and specific surface area of 500 m^2 m^{-3}. To achieve a good substrate removal without crowding the reactor, 20% of the reactor was filled with the Kaldness carriers (volume basis) according to Wang et al. [6].

2.2.4. AFBR configuration and operation

The AFBR reactor consisted of a cylindrical glass column having a dimension of 34 cm height and internal diameter of 24 mm, with an active volume of 1.3 L (Figure 1). The temperature of the reactor was maintained at mesophilic conditions (37 ± 2 °C) by immersing it in a water bath connected to a thermostatic controller. Prior to starting of the operation, the AFBR was purged with argon gas to ensure an initial anaerobic environment. Dark conditions were maintained by wrapping the reactor and tubes with black plastic covers. Liquid recirculation (LR) was performed in up-flow mode using a peristaltic pump (type 505 L, Watson and Marlow, Falmouth, England). Initially, the reactor was operated in batch feeding mode. This was done to initiate the initial contact between the inoculum and the carrier materials as described by Escudie et al. [11], as well as to make sure that the reactor and pipes were leak proof. Afterwards, the batch feeding was switched to semi-continuous mode, i.e. adding the substrate once a day. The semi-continuous operational conditions were set at an OLR of 1 g COD L^{-1} day^{-1} and HRT of 20 days, corresponding to an influent COD concentration of 20 g L^{-1}. Before substrate addition, manual withdrawing of the effluent was conducted at the feeding inlet.

The biogas produced was led to pass through a concentrated NaOH (12%) solution in order to remove CO_2 gas. The methane gas was subsequently measured volumetrically using a water displacement system [22]. The percentage of methane gas was analysed once a week.
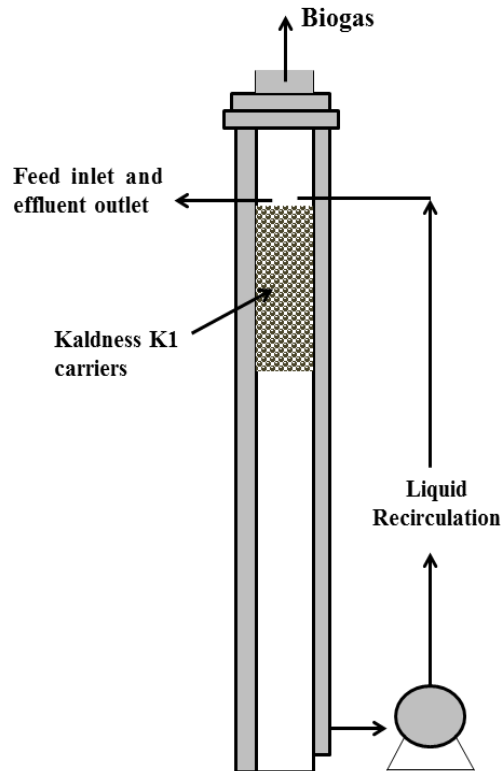
Figure 1. Schematic diagram of the AFBR configuration.

2.2.5. Experimental design

The start-up and operation of the AFBR were followed for 150 days and divided into four main periods. The detailed operational conditions of each period is given in Table 3. The duration of each operational period was 24, 57, 37 and 32 days for period I, II, III and IV, respectively. In period I, two liquid recirculation (LR) flow rates were evaluated in order to select the suitable hydrodynamic conditions: i) continuous LR at a flow rate of 140 mL min^{-1} continuously for 24 h and ii) intermittent LR at a flowrate of 125 mL min^{-1} for fixed time duration (i.e. 10 min day^{-1}, 30 min day^{-1}, 2 h day^{-1} and 4 h day^{-1}). The first LR conditions was applied on days 5, 8 and 12, thereafter intermittent LR was chosen based on the reactor performance. The substrate carbon composition was changed in period II. The concentration of nutrients and TE solution was adjusted based on the reactor performance in period III and IV.

Table 3. Experimental design.

Period	I	II	III	IV
Total duration (day)	24	57	37	32
Feeding mode	Batch	Continuous	Continuous	Continuous
Sole carbon source*	Glucose	Glucose/HAc + HPr	HAc + HPr	HAc + HPr
Major attempts	Hydrodynamic tests	HRT and carbon source changed	Nutrients and TEs solution doubled	Fe²⁺ added five fold

* HAc + HPr : Acetate and propionate with proportion of 3:1 (v/v)

2.2.6. Analytical methods

Total solids (TS), volatile solids (VS), total Kjeldahl nitrogen (TKN) and COD concentrations were measured according to standard methods [23]. The pH was measured using a pH meter (pH/ION, 340i, Germany). The total organic acids and total alkalinity concentration were quantified by titration with H_2SO_4 as described by Pontoni et al. [24]. Also the total ammonium concentration was determined using steam distillation followed by titration with a semi-automatic distillation unit as described by Pontoni et al. [24]. The analysis of lactic acid and the individual VFAs concentration (acetic and propionic acid) were performed using High Pressure Liquid Chromatography (HPLC) as described elsewhere [25]. The methane percentage was quantified using a gas chromatograph (GC, Varian Star 3400) equipped with a Shin-Carbon ST 80/100 column and a thermal conductivity detector with an inject temperature of 120 °C. The carrier gas was argon, operated with a flow rate of 20 mL min⁻¹ at 50 °C.

2.3. Results

The start-up process and reactor performance were evaluated with respect to: i) daily methane yield, HRT, COD removal efficiency and individual VFA patterns throughout the experiment (Figure 2); and ii) pH and total ammonium, total organic acids and alkalinity concentration during the entire reactor operation (Figure 3).
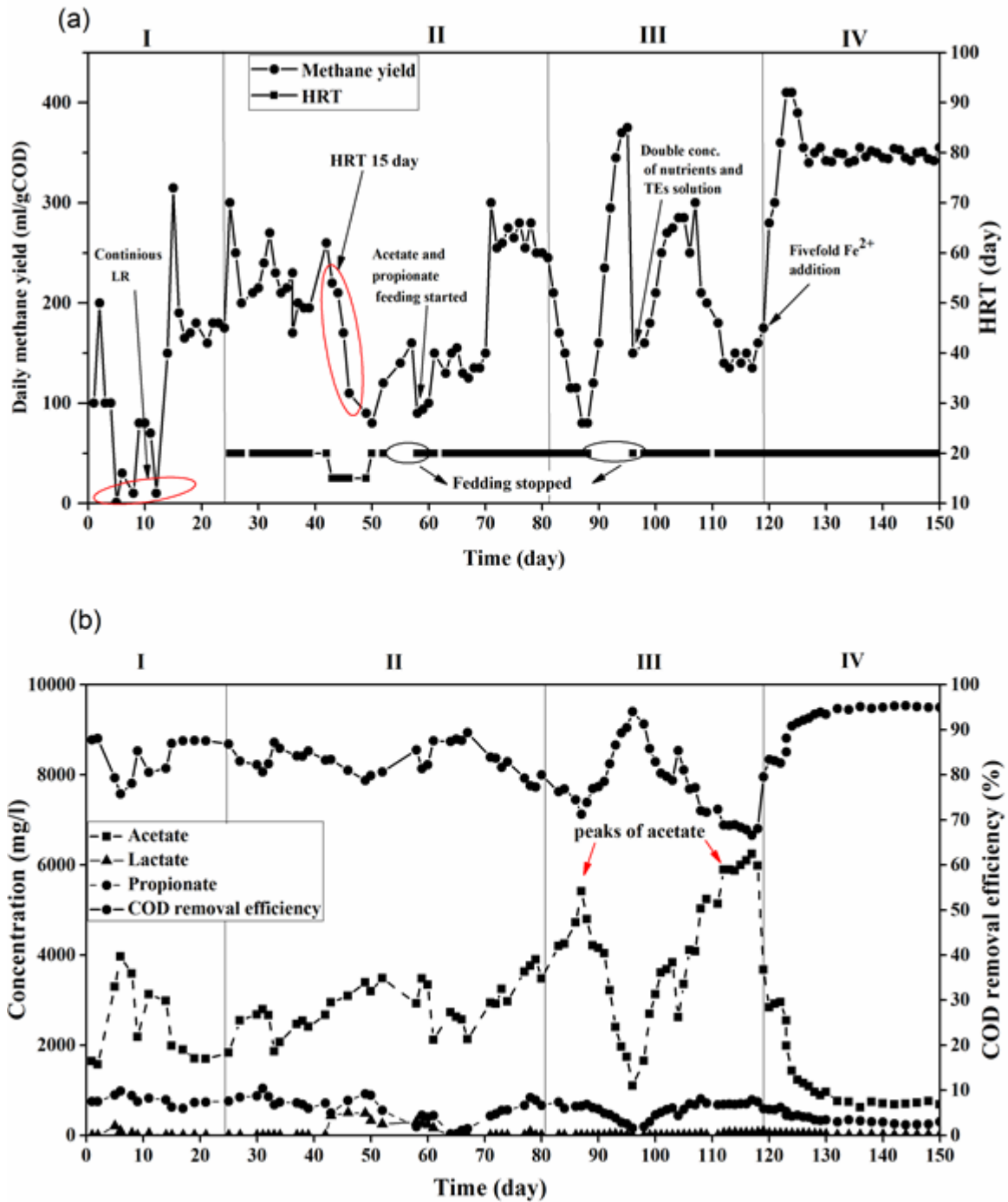
Figure 2. Trends of daily methane yield and HRT (a) and concentration of individual
VFAs and COD removal efficiency (b) as a function of time during the
AFBR start-up process.
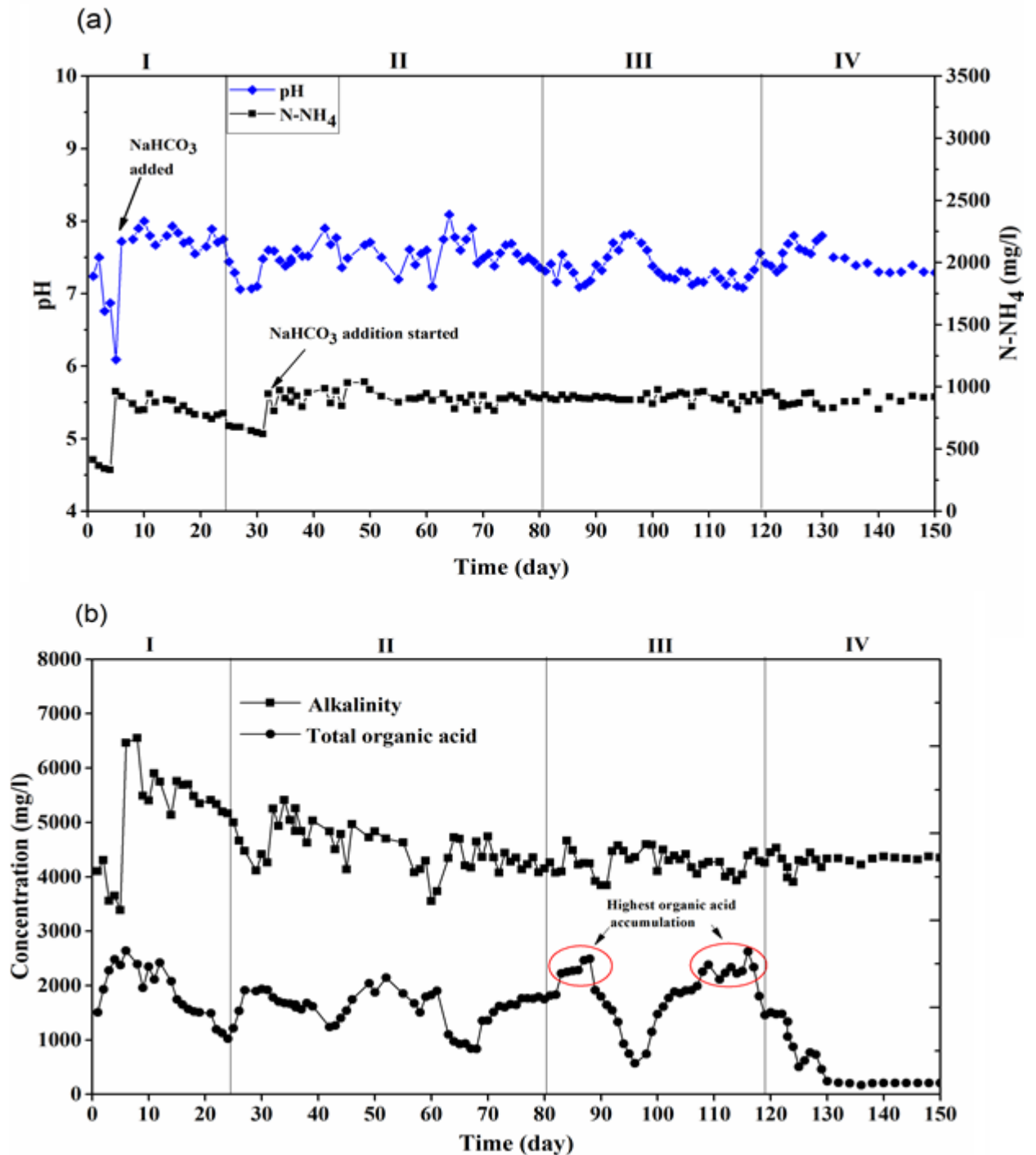
Figure 3. Profiles of pH and total ammonium concentration (a) and total alkalinity
and total organic acid concentration (b) as a function of time during the
AFBR start-up process.

2.3.1. Period I: batch operation and hydrodynamic conditions

During this period, the reactor was operated in batch feeding mode in order to initiate
the adhesion of biomass onto the Kaldness carrier materials [11]. Meanwhile, the
system was also tested for its suitable hydrodynamic conditions, which would favour
biofilm formation and methane yield. When the reactor was subjected to a continuous

LR at 140 mL min^{-1} on days 5, 8 and 12, no methane gas production occurred (Figure 2a). A lower COD removal efficiency and accumulation of total organic acids, particularly acetate, were observed (Figures 2b and 3b). On these operational days (day 1e5), as the total organic acids accumulated (Figure 3b), the pH dropped down to 6.1 (Figure 3a). Hence, external bicarbonate alkalinity was provided by adding sodium bicarbonate (NaHCO$_3$) on day 6 in order to prevent the pH drops. The reactor showed recovery in terms of methane yield when the continuous LR stopped and performed for fixed time intervals (5e10 min day^{-1}). The results suggest that higher hydrodynamic shear stress occurred due to the continuous LR, leading to inhibition of the AD process [26]. Accordingly from day 14, the LR was changed to a lower strength, where the liquid recycled intermittently at 125 mL min^{-1} for 10 min day^{-1} in period I and later increased to 30 min day^{-1}, 2 h day^{-1} and 4 h day^{-1} for periods II, III and IV, respectively. The intermittent LR resulted in a relatively better and more stable daily methane yield between 160 and 190 mL g COD$_{added}^{-1}$ day^{-1} from day 16-24 (Figure 2a) and reduction of total organic acids in the system (Figure 3b). The pH value was stable between the range of 7.0-7.5 (Figure 3a) and the COD removal efficiency exceeded 80% (Figure 2b).

2.3.2. Period II: effect of HRT decrease

As the daily methane yield became stable (from day 16-24), the reactor batch feeding was switched to semi-continuous mode on day 25 at an OLR of 1 g COD L^{-1}. day and HRT of 20 days. Afterwards, the daily methane yield was between 200 and 270 mL g COD$_{added}^{-1}$ day^{-1} (Figure 2a) and the COD removal efficiency exceeded 80% (Figure 2b). A higher total organic acids concentration than the previous operational days was observed (Figure 3b). However, it did not affect the AD process, as reflected by the stable methane yield and pH in the reactor (Figure 3a). During these operational days, microbial attachment and layer formation on the carrier surface were visually noticed (Figure 4a). Therefore, the HRT was decreased from 20 to 15 day on day 43, with the aim of favouring the growth of attached microbial biomass and facilitate the wash out of the suspended biomass from the reactor [10]. However, the daily methane yield gradually decreased from 220 to 90 mL g COD^{-1} day^{-1}, together with a reduction in COD removal efficiency and accumulation of the total organic acids in the system (Figure 2). Besides, lactic acid was also detected, between 500 and 260 mg L^{-1} (Figure 2b), hence the decrease of HRT was kept for only 7 days.

In order to allow the reactor to consume the accumulated organic acids, the feeding was stopped from day 53 for five days. In this situation, the acidogenic microbial groups could rapidly grow and become dominant, outcompeting the methanogens. Most of the methanogenic archaea might remain in suspension and become more susceptible to wash out during the period with a decreased HRT. From day 58 onwards, the substrate was shifted from glucose to an acetate and propionate mixture in 3:1 ratios (v:v), respectively. A nutrients and trace elements (TEs) solution was supplemented to meet the AD microbial requirement based on Table 1. The purpose of shifting the substrates to an organic acid solution was to favour the growth of methanogenic archaea and accelerate their attachment onto the Kaldness carrier materials. In addition, ammonium bicarbonate (NH_4HCO_3) was added as a source of nitrogen and its concentration was maintained around 1000 mg L^{-1} (Figure 3a) for a proper nutrient balanced AD operation [8]. The reactor operation between days 58-70 was considered as an acclimatization phase of the methanogenic archaea to the new influent, in particular the acetoclastic groups. From day 71, a daily methane yield closer to the theoretical value was obtained, i.e. between 250 and 300 mL g COD_{added}^{-1} day^{-1} (Figure 2a). The total organic acids concentration in the system was between 1351 and 1809 mg L^{-1} and reached a plateau (Figure 3b). The COD removal efficiency exceeded 80%. Despite the acetate concentration increased to 3904 mg L^{-1}, apparently no negative effect on the reactor performance was observed. This might be due to the high bicarbonate alkalinity in the system from the ammonium bicarbonate, which provided enough buffering capacity and kept the pH at the desirable range of 7.2-7.8 throughout the experiment, reflecting stable AD operation (Figure 3a).

2.3.3. Period III: trace metal deprivation

While expecting the full conversion of organic substrate into methane, i.e. the exact theoretical daily methane yield (350 $mLCH_4$ g COD^{-1} day^{-1}), the reactor rather suffered a sudden destabilization from day 82 onwards. The daily methane yield decreased gradually and reached as low as 80 mL g COD_{added}^{-1} day^{-1}, corresponding to a 68% decrease (Figure 2a). Herein the acetate concentration, taken as an important indicator for the AD process imbalances [27], accumulated and reached around 4800 mg L^{-1}. The COD removal efficiency dropped from 80 to 73% (Figure 2b). The feeding was stopped from day 89 in order to avoid further acetate accumulation, which might lead to complete process failure. Despite of the continuous supply of

nutrients and TEs solution from period II onwards, the unexpected poor performance, i.e. lower methane yield and acetate accumulation, was caused by deficiency of a nutrient and/or trace metals in the pathways of methane production from acetate, as acetate is the key intermediate for methane production [28].

In order to assess the hypothesis of trace metal deprivation and to overcome the observed process instability, a new solution of nutrients and TEs with the double concentration compared to Table 1 was supplemented from day 96 onwards, without changing any other operational conditions. Subsequently, an improved overall reactor performance was observed: the daily methane yield increased progressively and reached 300 mL g COD_{added}^{-1} day^{-1} and the COD removal efficiency was between 75 and 85% (Figures 2a and b). Oppositely, the concentration of acetate continually builds up and accumulated in the system. On day 108 (after 8 days of supplementation), the reactor experienced again the same situation as before: the concentration of acetate became very high and reached up to 6097 mg L^{-1} (Figure 2b), while the daily methane yield reduced by 55% (Figure 2a) and the COD removal efficiency dropped down from 80 to 67%. The reason for this was supposed to be the deprivation of a single trace metal element, which led to unfavourable acetate degradation.

2.3.4. Period IV: fast recovery upon iron dosing

A stock solution of $FeSO_4$ $7H_2O$ (Table 1) was newly prepared and its supplementation concentration was increased 5 times from day 119 onwards, i.e. the concentration increased from 54.8 to 274 mg L^{-1}. This was done after noticing a color change of the solution in the storage vessel at -4 °C, turning from light yellow to dark red. This is due to the chemical behaviour of Fe^{2+} that has a tendency to be easily oxidized into Fe^{3+} in the presence of oxygen. Interestingly, an immediate response in the reactor performance was observed, as the daily methane yield rapidly increased from 175 to 410 mL g COD_{added}^{-1} day^{-1}, i.e. it was enhanced by 134% (Figure 2a). The accumulated organic acids were rapidly depleted (Figure 3b). In particular, the concentration of acetate decreased from 5997 to 1157 mg L^{-1} and the COD removal efficiency exceeded 90% (Figure 2b). Thereafter, the storage conditions of solution C II (Table 1) was changed to deep freezer (-20 °C). Once all the accumulated organic acids were consumed, the reactor remained very stable and produced the highest observed daily methane yield (between 340 and 345 mL g COD_{added}^{-1} day^{-1}). The

higher methane yield and faster acetate consumption after dosing the Fe^{2+} solution confirms that metal deficiency in the acetoclastic methanogenic pathway, despite of its continuous supplementation.

From day 126 onwards, the reactor produced around 340-345 mL g COD^{-1} day^{-1} of methane, i.e. close to the theoretical daily methane yield (Figure 2a). No further acetate or total organic acids accumulation was observed (Figures 2b and 3b). The COD removal efficiency was between 94 and 95%. The stable daily methane yield and COD removal efficiency as well as the observed biomass on the carriers (Figure 4b) and very low acetate concentration confirmed the formation of a well-matured methanogenic biofilm in the reactor.

2.4. Discussion

2.4.1. Impact of hydrodynamic conditions

This study identified the various operational factors that govern the biofilm formation and effective operation of an AFBR treating synthetic carbohydrate rich wastewater at mesophilic conditions. Period I highlights the major impact of the hydrodynamic conditions on the reactor performance (Figures 2 and 3). The continuous LR inhibited the activity of methanogenic microbial groups. The role of LR in the AFBR system was to provide an efficient contact between the substrate and attached biomass and to promote an effective solid-liquid mass transfer, thus increasing the treatment efficiency [11, 29]. Besides, the LR intensity controlled the biofilm growth and thickness by regulating the microbial cell attachment and detachment on the carrier surface [10, 30]. The stronger hydrodynamic conditions during the reactor start-up creates a high shear stress and physically interrupts the syntrophic association between the various AD microbial groups [29]. Apart from this, strong hydrodynamic conditions can mechanically damage the methanogenic archaea, particularly those having long filamentous cell morphology, such as *methanosaeta concilii* [26]. In addition, from an economic view point, intensive LR would imply high energy demand, posing extra operational costs to the system. Therefore, it is important to ensure a suitable LR intensity that would be compatible with good reactor performance and lower operational costs.

In this study, the intermittent LR at a flow rate of 125 mL min^{-1} was shown to be the optimal hydrodynamic condition for better reactor performance (Figures 2 and 3).

Afterwards, the reactor took less than 10 days to get stabilized and then biomass attachment on to the carrier surface was observed (Figure 4a). These results are in accordance with the work of Cresson et al. [10], who observed better performances and higher attached biomass concentrations during the start-up of an anaerobic inversed turbulent bed reactor having the lowest hydrodynamic strength, based on recirculating the generated biogas at a gas velocity 1 mm s^{-1}, compared to the stronger hydrodynamic conditions (gas velocity 10 mm s^{-1}). Moreover, Lindmark et al. [31] obtained higher cumulative biogas production at a lower mixing intensity of 25 rpm (317 N mL g VS_{added}^{-1}) than the higher mixing intensity of 150 rpm (295 N mL g VS_{added}^{-1}) during AD of the organic fraction of municipal solid waste.

2.4.2. Strategies for early carrier colonization by methanogenic archaea

Previous studies have shown that biofilm formation and development can be enhanced by stepwise shortening of the HRT during the start-up period [11]. This approach creates a competition between the suspended and attached microbial biomass, thus allowing quicker wash out of the suspended biomass from the reactor [11, 13]. In contrast, in this study, lowering of the HRT from 20 to 15 days resulted in a reduction of the daily methane yield from 220 to 90 mL g COD^{-1} day^{-1} (Figure 2a) and total organic acids accumulation (Figure 3b). This was an indication that the majority of the methanogenic archaea might be present in suspension, and become vulnerable for easy wash out from the reactor. Having a relatively higher growth rate, the acidogenic bacteria could become the dominant microbial group and be retained on the surface of the carrier prior to the methanogenic archaea. Therefore, it is crucial to ensure the earlier colonization of methanogenic archaea on the carrier material, since they are the rate-limiting microbial group responsible for the final step of the AD process [3, 7]. The substrate type and composition have been indicated as key factors in determining the dominant AD biomass groups during initial biofilm formation [32]. In this aspect, acidified organic substrates favoured the growth of only acetogens and methanogenic microbial groups and hence their earlier adhesion to the carrier material [14]. In particular, acetate could selectively facilitate the retention of methanogenic archaea, since it is the major metabolic intermediate produced during the AD process [28]. Besides, 70% of the methane produced as an output of the AD process is derived from acetate [3, 14, 25]. Hence, the use of acetate as major carbon

source could be a strategy to induce the initial colonization of methanogenic archaea onto the Kaldness carrier materials during the AFBR start-up process.

For large scale start-up of such a reactor configuration, the acidified substrate can be obtained through biological processes, such as dark fermentation (DF) [33]. In the DF process, complex organic matter is broken down by fermentative bacteria into mainly hydrogen, carbon dioxide and liquid effluent [7]. Several studies have shown that the effluent from the DF process is rich in short chain volatile acids (mainly acetic and butyric acid) [7, 34]. Besides, the DF process allows the use of a wider range of organic wastes, both liquid and solid streams, and hence makes the process more cost-effective [34]. In this perspective, the DF effluent can be used to feed the AFBR system [7].

2.4.3. Bioavailability of trace elements

In the latter periods of the reactor operation (Period III and IV), a deprivation of iron occurred, probably due to the non-bioavailable form of the metal. This was indicated by the decreased daily methane yield and accumulation of acetate, though the nutrients and TEs solution (Table 1) were continuously supplied (Figure 2a and b). This low iron bioavailability was likely caused by the oxidation of iron during storage in the fridge at -4 °C, as indicated by the colour change of the metal solution from light yellow (Fe^{2+}) into dark red (Fe^{3+}). Ma et al. [35] indicated in their review paper that Fe^{2+} was more effective in stimulating the AD microbial groups than Fe^{3+} and Fe^0. Besides, it is noteworthy to mention that the presence of metals inside the AD reactor does not necessary imply that the microorganisms are able to take them up and incorporate them into their catalytic centers and enzymatic reactions [36, 37]. The metal precipitation-solubility and diffusion-adsorption kinetics have a great impact on their bioavailability and bio-uptake during the AD process [17, 37]. These factors depend on the operational conditions of the reactor such as temperature, pH, redox potential, alkalinity, and reactor configuration [36]. Accordingly, trace metals inside the reactor might undergo several physico-chemical processes, and their existing forms are either free ions, complex compounds or precipitates, depending on the reactor operational conditions [36]. From these forms, only free metal ions pass the cell membrane and EPS matrix of the biofilm and are taken up by the biomass constituting the biofilm [37]. Moreover, in anaerobic biofilms and similar aggregates (like granules), a strong bio-sorption of metal ions could occur due to precipitation,

co-precipitation, ion exchange, adsorption and binding by the EPS and bacterial cells
[17, 37]. As a result, the metal bioavailability would be lowered for the microbial
activity.

Methane production from acetate was carried out by acetoclastic methanogens,
predominantly *methanosaeta* and *methanosarcina*, as well as syntrophic acetate
oxidation [3]. The latter is a two-step reaction involving acetate oxidizing bacteria
producing H_2/CO_2 which are subsequently utilized by hydrogenotrophic archaea [28].
These methanogenic groups involve the participation of various metal rich enzymes
and require adequate supply of trace metals such as Ni, Co, Fe, Mo and W, otherwise
deficiency will cause limitation of their activity [19, 36, 38]. In particular, iron is the
most essential trace metal for the AD biomass, as it is used for both electron transport
and catalysts [36, 38]. It is remarkably observed that the supplementation of a suitable
iron form (Fe^{2+}) abated the accumulation of acetate and enhanced the activity of
acetoclastic AD microbial groups (Figures. 2 and 3). After one day supplementation
during Period IV, the reactor restored fully and a high peak of methane yield were
observed. Similarly, Yu et al. [39] observed enhancement of granular biofilm
formation and treatment efficiency of a UASB reactor up on addition of Fe^{2+} at a
concentration of 300 and 450 mg L^{-1} during start-up process using synthetic
wastewater. Table 4 compares the results obtained in this work with previous studies
regarding the effect of iron supplementation on methane yields. The effect of
supplementation is different depending on the operational conditions of the system
such as type of substrate, reactor configuration, temperature, form and amount of
metal supplied (Table 4).

The start-up process was considered completed once the reactor produced a methane
yield closer to the theoretical value (between 340 and 345 mL g COD^{-1} day^{-1}) and was
stable at the given operational conditions. The achievement of stable conditions was
confirmed by the observed well-attached microbial biomass on the surface of the
carrier (Figure 4b).

Table 4. Effect of iron supplementation on methane yield under various conditions.

Substrate[a]	Anaerobic reactor type	Temperature (^{0}C)	Iron supplementation amount	Iron forms	Effect on methane yield[b]	Reference
FW	CSTR	37 ± 1	22.5 mg/L of $FeCl_2.4H_2O$	Fe^{2+}	+	38
Distillery effluent	UASB	35	10 mg/L of $FeSO_4.7H_2O$	Fe^{2+}	+	40
Raw sewage	AnMBR	23 ± 2	26 mg/L of $FeCl_3$	Fe^{3+}	0	41
Glucose	Batch AD	37 ± 2	0, 1, 10, 30 mM Nano zero valent iron (NZVI)	Fe^0	-	42
JPC	CSTR	38 ± 2	Iron added as 0.059 gTS/gVS JPC	ns	+	43
FW	CSTR	37 ± 2	100-1 mg/L of Fe	ns	+	44
RWS	Batch AD	37 ± 2	5 mM of Fe^{2+}	Fe^{2+}	+	45
RWS	Batch AD	10-20	5 mM of Fe^{2+}	Fe^{2+}	-	45
HAc and HPr	Batch AD	55 ± 2	5 and 10 mM of in Fe_3O_4	Fe^{3+}	+	46
HAc and HPr	Batch AD	55 ± 2	5 and 10 mM of $5Fe_2O_3.9H_2O$ (Nano Ferrihydrite)	Nano Fe^{3+}	-	46
HAc and HPr	AFBR	37 ± 2	274 mg/L $FeSO_4.7H_2O$	Fe^{2+}	+	This study

[a]FW: Food waste, JPC: Jatropha press cake, RWS: Rabbit waste slurry, HAc and HPr: acetate and propionate
[b](+) significantly enhanced methane production, (-) suppressed methanogenic activity, (0): did not showed any effect
ns: not specified

(a)   **(b)**

Figure 4. Biofilm development in the AFBR during (a) initial operation, (b) stable operation
in the last period.

2.5. Conclusions

In this study, different operational factors that affect the start-up process of an AFBR
were identified. Hydrodynamic conditions obtained with a lower liquid recirculation,
i.e. at flow rate of 125 mL min^{-1}, were well suited to improve the biofilm formation
and reactor performances. The use of acetate and propionate as substrates enhanced
the growth of methanogenic archaea, favouring their early carrier colonization.
Moreover, the supplementation and bioavailability of trace metals, in particular iron,
was a crucial parameter in sustaining the activity of methanogenic archaea and
accelerating the start-up process. At the end of the start-up process, the reactor
produced a daily methane yield near to the theoretical value, i.e. between 340 and 345
mL g COD^{-1} day^{-1}, with a COD removal efficiency between 94 and 95%.

References

[1]   Van Lier, J.B., van der Zee, F.P., Frijters, C.T.M.J., Ersahin, M.E., 2015. Celebrating 40 years anaerobic sludge bed reactors for industrial wastewater treatment-Review paper. Reviews in Environ Science and Bio/Technology, 14(4), pp.681-702.

[2]   Bialek, K., Kumar, A., Mahony, T., Lens, P.N.L., O' Flaherty. V., 2012. Microbial community structure and dynamics in anaerobic fluidized-bed and granular sludge-bed reactors: influence of operational temperature and reactor configuration. Microbial Biotechnology, 5(6), pp.738-752.

[3]   Aydin, S., Ince, B., Ince, O., 2015. Application of real-time PCR to determination of combined effect of antibiotics on bacteria, methanogenic archaea, archaea in anaerobic sequencing batch reactors. Water Research, 76, pp.88-98.

[4]   Minale M., Worku T., 2014. Anaerobic co-digestion of sanitary wastewater and kitchen solid waste for biogas and fertilizer production under ambient temperature: waste generated from condominium house. International Journal of Environmental Science and Technology, 11(2), pp.509-516.

[5]   Habouzit, F., Hamelin, J., Santa-Catalina, G., Steyer, J.P., Bernet, N., 2014. Biofilm development during the start-up period of anaerobic biofilm reactors: The biofilm archaea community is highly dependent on the support material. Microbial Biotechnology, 7, pp.257-264.

[6]   Wang, W., Hou, H., Hu, S., Gao, X., 2010. Performance and stability improvements in anaerobic digestion of thermally hydrolyzed municipal biowaste by a biofilm system. Bioresource Technology, 101(6), pp.1715-1721.

[7]   Yeshanew, M.M., Frunzo, L., Pirozzi, F., Lens, P.N.L., Esposito, G., 2016. Production of biohythane from food waste via an integrated system of continuously stirred tank and anaerobic fixed bed reactors. Bioresource Technology, 220, pp.312-322.

[8]   Karadag, D., Koroglu, O. E., Ozkaya, B., Cakmakci, M., 2015. A review on anaerobic biofilm reactors for the treatment of dairy industry wastewater. Process Biochemistry, 50(2), pp.262-271.

[9]   Barca, C., Soric, A., Ranava, D., Giudici-Orticoni, M.T., Ferrasse, J.H., 2015. Anaerobic biofilm reactors for dark fermentative hydrogen production from wastewater: A review. Bioresource Technology, 185, pp.386-398.

[10]   Cresson, R., Escudie, R., Carrere, H., Delgenes, J.P., Bernet, N., 2007. Influence of hydrodynamic conditions on the start-up of methanogenic inverse turbulent bed reactors. Water Research, 41(3), pp.603-612.

[11]   Escudie, R., Cresson, R., Delgenes, J.P., Bernet, N., 2011. Control of start-up and operation of anaerobic biofilm reactors: an overview of 15 years of research. Water Resource, 45(1), pp.1-10.

[12]   Michaud, S., Bernet, N., Buffiere, P., Roustan, M., Moletta, R., 2002. Methane yield as a monitoring parameter for the start-up of anaerobic fixed film reactors. Water Research, 36(5), pp.1385-1391.

[13]   Cresson, R., Escudie, R., Steyer, J.P., Delgenes, J.P., Bernet, N., 2008. Competition between planktonic and fixed microorganisms during the start-up of methanogenic biofilm reactors. Water Research, 42(3), pp.792-800.

[14]   Encina, P.A.G., and Hidalgo, M.D., 2005. Influence of substrate feed patterns on biofilm development in anaerobic fluidized bed reactors (AFBR). Process Biochemistry, 40(7), pp.2509-2516.

[15]   D'Acunto, B., Frunzo, L., Klapper, I., Mattei, M.R., 2015. Modeling multispecies biofilms including new bacterial species invasion. Mathematical Biosciences, 259, pp.20-26.

[16]   Cresson, R., Carrere, H., Delgenes, J.P., Bernet, N., 2006. Biofilm formation during the start-up period of an anaerobic biofilm reactor - impact of nutrient complementation. Biochemical Engineering Journal, 30(1), pp.55-62.

[17]   D'Acunto, B., Esposito, G., Frunzo, L., Mattei, M., Pirozzi, F., 2015. Mathematical modeling of heavy metal biosorption in multispecies biofilms. Journal of Environmental Engineering, 142(9).

[18]   Arnaiz, C., Gutierrez, J.C., Lebrato, J., 2006. Support material selection for anaerobic fluidized bed reactors by phospholipid analysis. Biochemical Engineering Journal, 27(3), pp.240-245.

[19] Fermoso, F.G., Collins, G., Bartacek, J., O'Flaherty, V., Lens, P., 2008. Role of nickel in high rate methanol degradation in anaerobic granular sludge bioreactors. Biodegradation, 19(5), pp.725-737.

[20] Rusten, B., Eikebrokk, B., Ulgenes, Y., Lygren, E., 2006. Design and operations of the Kaldnes moving bed biofilm reactors. Aquacultural Engineering, 34(3), pp.322-331.

[21] Aygun, A., Nas, B., Berktay, A., 2008. Influence of high organic loading rates on COD removal and sludge production in moving bed biofilm reactor. Environmental Engineering Science, 25(9), pp.1311-1316.

[22] Esposito, G., Frunzo, L., Panico, A., Pirozzi, F., 2012. Enhanced bio-methane production from co-digestion of different organic wastes. Environmental Technology, 33(24), pp.2733-2740.

[23] APHA. 1998. Standard Methods for the Examination of Water and Wastewater, 20th ed. American Public Health Association/American Water Works Association/Water Environment Federation, Washington DC, USA.

[24] Pontoni, L., Panico, A., Salzano, E., Frunzo, L., Iodice, P., Pirozzi, F., 2015. Innovative parameters to control the efficiency of anaerobic digestion process. Chemical Engineering Transactions, 43, pp.2089-2094.

[25] Yeshanew, M.M., Frunzo, L., Lens, P.N.L., Pirozzi, F., Esposito, G., 2016. Mass loss controlled thermal pretreatment system to assess the effects of pretreatment temperature on organic matter solubilization and methane yield from food waste. Frontiers in Environmental Science, 4, p.62.

[26] Lindmark, J., Thorin, E., Fdhila, R.B., Dahlquist, E., 2014. Effects of mixing on the result of anaerobic digestion: review. Renewable and Sustainable Energy Reviews, 40, pp.1030-1047.

[27] Boe, K., Batstone, D.J., Steyer, J.P., Angelidaki, I., 2010. State indicators for monitoring the anaerobic digestion process. Water Research, 44(20), pp.5973-5980.

[28] Wagner, A.O., Reitschuler, C., Illmer, P., 2014. Effect of different acetate:propionate ratios on the methanogenic community during thermophilic anaerobic digestion in batch experiments. Biochemical Engineering Journal, 90, pp.154-161.

[29] Kundu, K., Bergmann, I., Klocke, M., Sharma, S., Sreekrishnan, T.R., 2014. Influence of hydrodynamic shear on performance and microbial community structure of a hybrid anaerobic reactor. Journal of Chemical Technology and Biotechnology, 89(3), pp.462-470.

[30] D'Acunto, B., Esposito, G., Frunzo, L., Mattei, M.R., Pirozzi, F., 2013. Analysis and simulations of the initial phase in multispecies biofilm formation. Communications in Applied and Industrial Mathematics, 4, pp.1-23.

[31] Lindmark, J., Eriksson, P., Thorin, E., 2014. The effects of different mixing intensities during anaerobic digestion of the organic fraction of municipal solid waste. Waste Management, 34 (8), pp.1391-1397.

[32] Janke, L., Leite, F.A., Nikolausz, M., Radetski, M.C., Nelles, M., Stinner, W., 2016. Comparison of start-up strategies and process performance during semi continuous anaerobic digestion of sugarcane filter cake co-digested with bagasse. Waste Management, 48, pp.199-208.

[33] Ghimire, A., Valentino, S., Frunzo, L., Trably, E., Escudié, R., Pirozzi, F., Lens, P.N.L., Esposito G., 2015. Biohydrogen production from food waste by coupling semi-continuous dark-photofermentation and residue post-treatment to anaerobic digestion: A synergy for energy recovery. International Journal of Hydrogen Energy, 40(46), pp.16045-16055.

[34] Lee, W.S., Chua, A. S.M., Yeoh, H.K., Ngoh, G.C. 2014. A review of the production and applications of waste-derived volatile fatty acids. Chemical Engineering Journal, 235, pp.83-99.

[35] Ma, W., Xin, H., Zhong, D., Qian, F., Han, H., Yuan, Y., 2015. Effects of different states of Fe on anaerobic digestion: a review. Journal of Harbin of Technology, 22(6), pp.69-75.

[36] Ortner, M., Rameder, M., Rachbauer, L., Bochmann, G., Fuchs, W., 2015. Bioavailability of essential trace elements and their impact on anaerobic digestion of slaughterhouse waste. Biochemical Engineering Journal, 99, pp.107-113.

[37] Fermoso, F.G., Bartacek, J., Jansen, S., Lens, P.N.L., 2009. Metal supplementation to UASB bioreactors: from cell-metal interactions to full-scale application. Science of the Total Environment, 407(12), pp.3652-3667.

[38] Wei, Q., Zhang, W., Guo, J., Wu, S., Tan, T., Wang, F., Dong, R., 2014. Performance and kinetic evaluation of a semi-continuously fed anaerobic digester treating food waste: Effect of trace elements on the digester recovery and stability. Chemosphere, 117, pp.477-485.

[39] Yu, H.Q., Fang, H.H.P., Tay, J.H. 2000. Effect of Fe^{2+} on sludge granulation in upflow anaerobic sludge blanket reactor. Water Science and Technology, 41(12), pp.199-205.

[40] Sharma, J., Singh, R., 2001. Effect of nutrients supplementation on anaerobic sludge development and activity for treating distillery effluent. Short communication. Bioresource Technology, 79(2), pp.203-206.

[41] Dong, Q., Parker, W., Dagnew, M., 2015. Impact of $FeCl_3$ dosing on AnMBR treatment of municipal wastewater. Water Research, 80, pp.281-293.

[42] Yang, Y., Guo, J., Hu, Z., 2013. Impact of nano zero valent iron (NZVI) on methanogenic activity and population dynamics in anaerobic digestion. Water Research, 47(17), pp.6790-6800.

[43] Schmidt, T., 2011. Anaerobic digestion of Jatropha curcas L. Press cake and effects of an iron-additive. Waste Management and Research, 29, pp.1171-1176.

[44] Zhang, L., Jahng, D., 2012. Long-term anaerobic digestion of food waste stabilized by trace elements. Waste Management , 32(8), pp.1509-1515.

[45] Sai Ram, M., Singh, L., Suryanarayana, M.V.S., Alam, S. I., 2000. Effect of Iron, Nickel and Cobalt on bacterial activity and dynamics during anaerobic oxidation of organic matter. Water, Air, and Soil Pollution, 117(1), pp.305-312.

[46] Yamada, C., Kato, S., Ueno, Y., Ishii, M., Igarashi, Y., 2015. Conductive iron oxides accelerate thermophilic methanogenesis from acetate and propionate. Journal of Bioscience and Bioengineering, 119(6), pp.678-682.

Chapter 3

Microbial colonization of anaerobic biofilms:
a mathematical model

Microbial colonization of anaerobic biofilms: a mathematical model

A 1-D mathematical model for analysis and prediction of microbial colonization of multispecies biofilms is presented. The model takes into account phenomena of substrate reaction and diffusion, biomass growth, detachment and, in particular, the colonization of new species from bulk liquid to biofilm. The colonization phenomenon is initiated by planktonic cells, present in the bulk liquid but not initially in the biofilm, which thanks to the characteristic porous structure of biofilm matrix, may enter the channels and establish where they find favorable growth conditions. The chapter presents the analysis of the free boundary value problem related to the invasion model of new species in biofilm reactors. In the framework of continuum approach to mathematical modelling of biofilm growth, the problem consists of a system of nonlinear hyperbolic partial differential equations governing the microbial species growth and a system of semi-linear elliptic partial differential equations describing the substrate trends. The model is completed with a system of elliptic partial differential equations governing the diffusion and reaction of planktonic cells, which are able to switch their mode of growth from planktonic to sessile when specific environmental conditions are found. Two systems of nonlinear differential equations for the substrate and planktonic cells mass balance within the bulk liquid are also considered. The free boundary evolution is governed by a differential equation that accounts for detachment. The qualitative analysis is performed and a uniqueness and existence result is discussed. Furthermore, two special models of biological and engineering interest are discussed numerically. The first model application addresses the analysis and prediction of microbial colonization of anaerobic multispecies biofilms for methane production and it is based on the biological framework of ADM1. In the second application, the invasion of Anammox bacteria in a constituted biofilm inhabiting the deammonification units of the wastewater treatment plants is simulated. For both cases, numerical simulations are run to evaluate the influence of the colonization process on biofilm structure and activity.

3.1. Introduction

The term biofilm is used nowadays to indicate the prevailing form of microbial lifestyle, which consists of dynamic complex microbial structures composed of various prokaryotic cells and other microorganisms, forming on solid or liquid surfaces and

encased in a self-produced protective matrix of extracellular polymeric substances (EPS). The roles biofilms exert on both natural and human environments are disparate: they have proven detrimental to human health or undesirable in the open water environment but, on the other hand they can be used beneficially in resource recovery systems as well as water treatment [1]. With specific reference to the last point, biofilm reactors represent the primary means to harness the usefulness of biofilms for pollutant removal from wastewater by means of the synergistic interactions and biochemical transformations characterizing these microbial communities [2]. The biofilm structure results from the interplay of different interactions, such as mass transfer, conversion rates and detachment forces. The main biofilm expansion is due to bacterial growth and to extracellular polymer production. The soluble substrates necessary for bacterial growth are dissolved in the liquid flow and to reach the cells, first they pass through a boundary layer, characterized by a negligible flow over the biofilm/liquid interface, and then through the biofilm matrix. The external fluid flow regulates biofilm growth by establishing the concentration of substrates and products at the solid-liquid interface and shearing the biofilm surface. Other biological phenomena are found to play significant roles in the establishment of mixed species biofilms, i.e. dispersal, bacteriophage, quorum sensing [3].

Among these phenomena, there is a growing interest in the study of microbial invasion and colonization of pre-existing biofilms as it can determine biofilm landscape and contribute to rapid alterations in biofilm populations. Recent advances in microbial ecology have identified motility as one of the main mediator of such process. Indeed, once a motile bacteria, supplied by the liquid phase or the biofilm itself (as a consequence of dispersal phenomenon), has successfully infiltrated the biofilm matrix, it can invade a resident community and establish where the environmental conditions are optimal for its growth. An accurate modeling of such a system has to take all of these factors into account. In a recent contribution [4], the authors have introduced a multispecies biofilm model which explicitly takes into account the invasion phenomenon pursued by planktonic cells. The core of the model lies on the introduction of new state variables which represent the concentrations of planktonic colonizing cells within the biofilm. These cells are supposed to be characterized by a diffusive movement within the biofilm and to be able to give up the ability to move in order to settle down in specific environmental niches.

In this work, we introduce the free boundary value problem for the invasion phenomenon in biofilm reactors which takes into account the dynamics of the bulk liquid phase in terms of both substrates and planktonic cells. The mathematical problem consists of a system of hyperbolic partial differential equations governing the biofilm growth, a system of elliptic partial differential equations for substrate dynamics within the biofilm and a system of elliptic partial differential equations, regulating the diffusion and reaction of planktonic cells. Mass balance equations for the dissolved substrates and planktonic cells within the bulk liquid phase of the biofilm reactor have been taken into account as well. The free boundary evolution is governed by a nonlinear ordinary differential equation.

The qualitative analysis of such a complex system is not an easy task as outlined in [5]. Due to the high non-linearity of the problem, the fixed point theorem seems the natural tool to be used for the existence and uniqueness of the solutions. However, we are considering a moving boundary problem where the domain is not fixed. To overcome this issue, we follow the methodology used in [6] for the analysis of the biofilm reactor model and in [4, 7] for the modeling of the planktonic cells dynamics both within the biofilm and the bulk phase. In particular, we use the method of characteristics to convert the differential problem to an integral one where the unknown functions are defined on a fixed domain and the existence and uniqueness of the solutions are proved in the class of continuous functions.

In addition, the work is completed with some numerical applications related to a real engineering/biological cases which examines the invasion of specific microbial species in a constituted biofilm. More precisely, the first case study investigates the formation and development of an anaerobic multispecies biofilm based on the biological framework of ADM1. The complexity of the microbial ecosystem in anaerobic biofilms has been found to increase over time due to different abiotic and biotic conditions: hydrodynamic conditions [8], types and nature of carrier material [9], substrate composition [4], source of inoculum [9] and availability of trace metals [10, 11, 15]. Indeed, the appearance of new community members in the structure of the multispecies biofilm is probably due to the accumulation of metabolic waste products, such as the acetate for acetogenic bacteria, which can be used as growth substrates by the new colonizer microorganisms, i.e. methanogenic bacteria. The latter show a reduced capability of colonizing the surface but their establishment within the biofilm is strongly affected by the formation of favorable environmental conditions for their

growth. The second case study reproduces the invasion of Anammox bacteria within a multispecies biofilm devoted to the concurrent oxidization of ammonium nitrogen and organic carbon occurring in the biological units of the wastewater treatment plants. Traditionally, ammonium oxidation leads to the formation of residual nitrogen compounds that need to be further removed by means of other treatment phases. The establishment of a biofilm community constituted by Anammox bacteria and Aerobic ammonium oxidizers may lead instead to the complete conversion of ammonium nitrogen to nitrogen gas within a single treatment unit. The establishment of this syntrophy is catalyzed by the formation of an anoxic zone, where the Anammox bacteria can effectively proliferate. The invasion model has been adopted to illustrate the trends related to the establishment of such a multispecies community and to assess the effect of specific operational conditions on the biofilm colonization by Anammox bacteria. For all the cases analyzed real data from existing literature are used to feed numerical simulations, which produce results in nice agreement with experimental findings.

The chapter is organized as follows. In Section 3.2 the invasion moving boundary problem for a biofilm reactor model is introduced: assumptions, boundary and initial conditions are discussed. Section 3.3 introduces the Volterra integral equations. Section 3.4 describes the experimental cases to which the model is applied and presents the numerical results. Finally, in Section 3.5 we present the conclusions and the future recommendations of the work.

3.2. Invasion boundary problem for biofilm reactors

We analyze the free boundary value problem related to the invasion problem in biofilm reactors. In this model we consider the biofilm as constituted by various particulate components (i.e. bacteria, EPS, etc.) growing in a liquid environment, and planktonic cells belonging to various microbial species and able to move within the biofilm and the bulk liquid as well. The biofilm expansion depends on growth limiting nutrients which are dissolved in the liquid region or produced within the biofilm itself. The planktonic cells can diffuse from the bulk liquid to the biofilm, invade, and switch their mode of growth from suspended to sessile when appropriate environmental conditions are found.

The model is formulated for the variables concentration of microbial species in sessile form X_i, the concentration of planktonic invading cells Ψ_i, the concentration of

dissolved substrates S_j, all expressed as functions of time t and z which denotes the spatial coordinate. The substratum is assumed to be placed at $z = 0$. The one-dimensional form of the model writes:

$$\frac{\partial X_i}{\partial t} + \frac{\partial (uX_i)}{\partial x} = \rho_i r_{M,i}(z,t,\boldsymbol{X},\boldsymbol{S}) + \rho_i r_i(z,t,\boldsymbol{\Psi},\boldsymbol{S}), \ \ i = 1,\dots,n \tag{2.1}$$

where ρ_i denotes the constant density of species i, $u(z,t)$ the biomass velocity at which the microbial mass is displaced with respect to the film-support, and $\boldsymbol{X} = (X_1,\dots,X_n)$, $\boldsymbol{S} = (S_1,\dots,S_m)$, $\boldsymbol{\Psi} = (\Psi_1,\dots,\Psi_n)$. The reaction terms $r_{M,i}$ describe the growth of sessile cells, which is controlled by the local availability of nutrients and usually modelled as standard Monod kinetics, and natural cell death. In most biological processes the function $r_{M,i}$ depends on z, t only through the functions $\boldsymbol{X}$ and $\boldsymbol{S}$. The explicit dependence has been considered mainly for mathematical generality. The variable t is positive and $0 \le z \le L(t)$, where $L(t)$ denotes the biofilm thickness at time t. Equation (2.1) without the term r_i was first derived in [12] by mass balance principle. The initial conditions for (2.1) are provided by the initial concentrations $\varphi_i(z)$ of biofilm particulate components

$$X_i(z,0) = \varphi_i(z), \ \ i = 1,\dots,n, \ \ 0 \le z \le L(0). \tag{2.2}$$

The initial concentrations of the invading microbial species are set to zero. The equation in the form (2.1) was presented in [4]. The terms r_i represent the growth rates of the microbial species X_i due to the invasion process which induces the switch of planktonic cells to a sessile mode of growth. This phenotypic alteration is catalyzed by the formation within the biofilm matrix of specific environmental niches. The explicit dependence on z, t has been introduced only for mathematical generality.

Similarly to traditional continuum models of biofilm growth, equations (2.1) can be rewritten in terms of volume fractions $f_i = X_i/\rho_i$, which indicate the fraction of space at a particular location that is occupied by species i,

$$\frac{\partial f_i}{\partial t} + \frac{\partial (uf_i)}{\partial x} = r_{M,i}(z,t,\boldsymbol{X},\boldsymbol{S}) + r_i(z,t,\boldsymbol{\Psi},\boldsymbol{S}).$$

Of course, the sum of all volume fractions at each location and time must always sum to one $\Sigma_i f_i = 1$.

From the equations above it follows immediately that the function $u(z,t)$ satisfies the following problem

$$\frac{\partial u}{\partial x} = \sum_{i=1}^{n} r_{M,i}(z,t,\boldsymbol{X},\boldsymbol{S}) + r_i(z,t,\boldsymbol{\Psi},\boldsymbol{S}), \ \ 0 \le z \le L(t), \ \ u(0,t) = 0, \tag{2.3}$$

where the initial condition $u(0,t)=0$ comes from no flux condition on substratum.

The function $L(t)$ is solution of the following problem

$$\dot{L}(t) = u(L(t),t) - \sigma_d\big(L(t)\big), \ L(0) = L_0. \tag{2.4}$$

Therefore, it is apparent that the evolution of the free boundary depends on the displacement velocity of microbial biomass u and detachment flux σ_d as well. Equation in (2.4) comes from global mass conservation principle.

The diffusion of planktonic cells within the biofilm matrix is governed by the following diffusion-reaction equations

$$\frac{\partial \Psi_i}{\partial t} - \frac{\partial}{\partial z}\left(D_{M,i}\frac{\partial \Psi_i}{\partial z}\right) = r_{\Psi,i}(z,t,\boldsymbol{\Psi},\boldsymbol{S}), \ i = 1,\dots,n, \ 0 < z < L(t), \tag{2.5}$$

where the reaction terms $r_{\Psi,i}$ represent loss terms for the invading species. Homogeneous Neumann conditions are adopted on the substratum at $z = 0$ due to a no-flux conditions and Dirichlet boundary conditions are prescribed on the free boundary $z = L(t)$

$$\frac{\partial \Psi_i}{\partial z}(0,t) = 0, \ \Psi_i(L(t),t) = \psi_i^*(t), \ i = 1,\dots,n \tag{2.6}$$

The initial conditions are set to zero if it is assumed that the invasion process starts at $t = 0$, but specific functions can also be considered.

The functions $\psi_i^*(t)$ denote the concentrations of planktonic cells within the bulk liquid and are governed by the following initial value problem for ordinary differential equations

$$V\dot{\psi}_i^* = -AD_{M,i}\frac{\partial \Psi_i}{\partial z}(L(t),t) + Q\left(\psi_i^{in} - \psi_i^*(t)\right), \ \psi_i^*(0) = \psi_i^{in}, \ i = 1,\dots,n \tag{2.7}$$

Equations (2.7) come from a mass balance within the bulk liquid and account for the inlet and outlet flux to the biofilm reactor and the exchange fluxes to or from the biofilm as well. The bulk liquid is modelled as a completely mixed compartment of volume V and continuously fed and withdrawn at the same flow rate Q. The initial concentrations of planktonic cells within the bulk liquid are provided by the inlet concentrations ψ_i^{in}.

The substrate diffusion within the biofilm is governed by the following reaction-diffusion equations

$$\frac{\partial s_j}{\partial t} - \frac{\partial}{\partial z}\left(D_j\frac{\partial s_j}{\partial z}\right) = r_{S,j}(z,t,\boldsymbol{X},\boldsymbol{S}), \ j = 1,\dots,m, \ 0 < z < L(t), \tag{2.8}$$

where the terms $r_{S,j}$ represent the substrate production or consumption rates due to microbial metabolism and D_j denotes the diffusion coefficient of substrate j within the biofilm. As to the boundary conditions it is assumed that

$$\frac{\partial S_j}{\partial z}(0,t) = 0, \ h \frac{\partial D_j}{\partial D_j^*} \frac{\partial S_j}{\partial z}(L(t),t) + S_j(L(t),t) = S_j^*(t), \ j = 1,\dots,m. \tag{2.9}$$

The first conditions is a no-flux boundary condition on the substratum placed at $z = 0$. The second condition derives from the following reasonings. According to [16] we assume that at a certain distance from the substratum $H(t) = L(t) + h$, with h being a given positive constant, the substrate concentration $S_j(H(t),t)$ is the same as the bulk liquid concentration denoted by $S_j^*(t)$. This dissolved substrate diffuses from the bulk liquid to the biofilm $0 \leq z \leq L(t)$ where it is consumed according to equations (2.8). No biochemical reactions are supposed to occur for $L(t) \leq z \leq H(t)$ which leads to consider homogeneous parabolic equations for $S_j(z,t)$. Solving at steady-state leads to (2.9), where D_j^* represents the diffusion coefficient of substrate j within the bulk liquid. Note that, condition (2.9) reduces to $S_j(L(t),t) = S_j^*$ for $h = 0$.

The functions S_j^* are governed by the following initial value problem for ordinary differential equations

$$V\dot{S}_j^* = -AD_j \frac{\partial S_j}{\partial z}(L(t),t) + Q\left(S_j^{in} - S_j^*(t)\right), \ S_j^*(0) = S_j^{in}, \ j = 1,\dots,m \tag{2.10}$$

Equations above are derived from mass balance on the bulk liquid taking into account the inlet and outlet flux from the reactor and the exchange flux between the biofilm and the bulk liquid. The initial conditions for S_j^* are the same as the inlet concentrations. Finally, due to the slow evolution of the system [6], Ψ_i profiles can be considered to evolve quasi-statically and thus equations (2.8) are rewritten as

$$-D_j \frac{\partial^2 S_j}{\partial z^2} = r_{S,j}(z,t,\mathbf{X},\mathbf{S}), \ j = 1,\dots,m, \ 0 < z < L(t), \tag{2.11}$$

with boundary conditions (2.9). In addition, same arguments as before lead to replace equations (2.5) with the following

$$-D_{M,i} \frac{\partial^2 \Psi_i}{\partial z^2} = r_{\Psi,i}(z,t,\boldsymbol{\Psi},\mathbf{S}), \ i = 1,\dots,n, \ 0 < z < L(t), \tag{2.12}$$

with boundary conditions (2.6).

In conclusion the invasion free boundary problem for biofilm reactor is expressed by equations (2.1)-(2.12). In the next section, following [6-7], an equivalent integral formulation of the problem will be provided. As it will be apparent at the end of the

following section, the integral form of the free boundary problem presents the great advantage that the space variable is defined on a fixed domain whereas in the differential formulation (2.1)-(2.12) the space variable belongs to the moving domain $0 \leq z \leq L(t)$.

3.3. Volterra integral equations

The differential problem introduced in the previous section is herein converted to Volterra integral equations by using the method of characteristics. The characteristic-like lines of system (2.1) are defined by

$$\frac{\partial c}{\partial z_0}(z_0, t) = u(c(z_0, t), t), \; c(z_0, 0) = z_0, \; 0 \leq z_0 \leq L_0, \; t > 0. \tag{3.1}$$

Considering (3.1), equations (2.1) are converted to

$$\frac{dX_i}{dt}(c(z_0, t), t) =$$
$$F_i\big(c(z_0, t), t, \boldsymbol{X}(c(z_0, t), t), \boldsymbol{S}(c(z_0, t), t), \boldsymbol{\Psi}(c(z_0, t), t)\big), 0 \leq z_0 \leq L_0, t > 0, \tag{3.2}$$

with

$$F_i = \rho_i r_{M,i}\big(c(z_0, t), t, \boldsymbol{X}(c(z_0, t), t), \boldsymbol{S}(c(z_0, t), t)\big) +$$
$$+\rho_i r_i\big(c(z_0, t), t, \boldsymbol{S}(c(z_0, t), t), \boldsymbol{\Psi}(c(z_0, t), t)\big) - X_i(c(z_0, t), t) \sum_{i=1}^{n}(r_{M,i} + r_i) \tag{3.3}$$

and initial conditions

$$X_i(c(z_0, 0), 0) = \varphi_i(z_0), \; 0 \leq z_0 \leq L_0. \tag{3.4}$$

Integrating (3.2) and considering (3.4) yields

$$X_i(c(z_0, t), t) = \int_0^t F_i\big(c(z_0, \tau), \tau, \boldsymbol{X}(c(z_0, \tau), \tau), \boldsymbol{S}(c(z_0, \tau), \tau), \boldsymbol{\Psi}(c(z_0, \tau), \tau)\big) d\tau +$$
$$+ \varphi_i(z_0), \; 0 \leq z_0 \leq L_0, \; t > 0. \tag{3.5}$$

The following integral equation for $c(z_0, t)$ is derived from (3.1) and (2.3)

$$c(z_0, t) = z_0 + \int_0^t d\tau \int_0^{z_0} \sum_{i=1}^{n}(r_{M,i}(c(\zeta_0, \tau), \tau, \boldsymbol{X}(c(\zeta_0, \tau), \tau), \boldsymbol{S}(c(\zeta_0, \tau), \tau)) +$$
$$+r_i\big(c(\zeta_0, \tau), \tau, \boldsymbol{S}(c(\zeta_0, \tau), \tau), \boldsymbol{\Psi}(c(\zeta_0, \tau), \tau)\big)\frac{\partial c}{\partial \zeta_0}(\zeta_0, \tau)d\zeta_0, 0 \leq z_0 \leq L_0, \; t > 0. \tag{3.6}$$

From (3.6) it follows easily

$$\frac{\partial c}{\partial z_0}(z_0, t) = 1 + \int_0^t \sum_{i=1}^{n}(r_{M,i}(c(z_0, \tau), \tau, \boldsymbol{X}(c(z_0, \tau), \tau), \boldsymbol{S}(c(z_0, \tau), \tau)) +$$
$$+r_i\big(c(z_0, \tau), \tau, \boldsymbol{S}(c(z_0, \tau), \tau), \boldsymbol{\Psi}(c(z_0, \tau), \tau)\big)\frac{\partial c}{\partial \zeta_0}(z_0, \tau)d\tau, 0 \leq z_0 \leq L_0, \; t > 0. \tag{3.7}$$

The integral equations for $S_j(z,t)$ are obtained by integrating (2.11) and considering the boundary conditions (2.9).

$S_j(z,t) = S_j^*(t) + D_j^{-1}\int_0^z (L-z)r_{s,j}\,(\zeta, \boldsymbol{X}(\zeta,t), \boldsymbol{S}(\zeta,t))d\zeta +$

$+ D_j^{-1}\int_z^L (L-\zeta)r_{s,j}\,(\zeta, \boldsymbol{X}(\zeta,t), \boldsymbol{S}(\zeta,t))d\zeta\, \frac{h}{D_j^*}\int_0^L r_{s,j}\,(\zeta, \boldsymbol{X}(\zeta,t), \boldsymbol{S}(\zeta,t))d\zeta,$

$\quad j = 1, \dots, m,\ 0 \le z \le L(t),\ t > 0.$ (3.8)

Similarly, the following integral equations for Ψ_i are obtained

$\Psi_i(z,t) = \psi_i^*(t) + D_{M,i}^{-1}\int_0^z (L-z)r_{\Psi,i}\,(\zeta, \boldsymbol{\Psi}(\zeta,t), \boldsymbol{S}(\zeta,t))d\zeta +$

$+ D_{M,i}^{-1}\int_z^L (L-\zeta)r_{\Psi,i}\,(\zeta, \boldsymbol{\Psi}(\zeta,t), \boldsymbol{S}(\zeta,t))d\zeta,\ i = 1, \dots, n,\ 0 \le z \le L(t),\ t > 0.$ (3.9)

From (3.8) it follows

$\frac{\partial s_j}{\partial z}\,(L,t) = -D_j^{-1}\int_0^L r_{s,j}\,(\zeta, \boldsymbol{X}(\zeta,t), \boldsymbol{S}(\zeta,t))d\zeta$ (3.10)

Considering (3.10) in (2.10), equation for $S_j^*(t)$ writes

$\dot{S}_j^*(t) = A/V \int_0^L r_{s,j}\,(\zeta, \boldsymbol{X}(\zeta,t), \boldsymbol{S}(\zeta,t))d\zeta + Q\left(S_j^{in} - S_j^*(t)\right) +\ S_j^{in},$
$j = 1, \dots, m,\ t > 0.$

Integrating the last equation over time leads to the following integral equation for $S_j^*(t)$

$S_j^*(t) = \int_0^t \exp\left(-\frac{Q(t-\tau)}{V}\right)d\tau\, A/V \int_0^L r_{s,j}\,(\zeta, \boldsymbol{X}(\zeta,t), \boldsymbol{S}(\zeta,t))d\zeta +\ S_j^{in}$
$j = 1, \dots, m,\ t > 0.$ (3.11)

Following the same reasoning, a similar equation is obtained for $\psi_i^*(t)$

$\psi_i^*(t) = \int_0^t \exp\left(-\frac{Q(t-\tau)}{V}\right)d\tau\, A/V \int_0^L r_{\psi,i}\,(\zeta, \boldsymbol{\Psi}(\zeta,t), \boldsymbol{S}(\zeta,t))d\zeta\ +\ \psi_i^{in},$
$j = 1, \dots, m,\ t > 0$ (3.12)

The integral equation for $L(t)$ is obtained from (2.4)

$L(t) = L_0 + \int_0^t u(L(\tau), \tau)d\tau - \int_0^t \sigma_d\big(L(\tau)\big)d\tau,\ \ t > 0.$ (3.13)

Let us note that, as outlined at the end of Section 2, the integral equations above depend on time and the space variable z_0 defined in the fixed domain $0 \le z_0 \le L_0$. This result is essential to prove the existence and uniqueness of solutions. Indeed, following [6-7], a suitable contractive map can be introduced in the space of continuous functions and the fixed point theorem can be applied. We neglect the calculations since they are a generalization of [6-7] with small modifications.

3.4. Applications of the Invasion Model

In the previous sections, we performed the qualitative analysis for the invasion free boundary value problem of a biofilm reactor model. In particular, a result on the existence and uniqueness of solutions were provided. However, it is apparent that when

complex biological cases are discussed, only numerical simulations can provide satisfactory predictions. The previous qualitative analysis gives a solid base to calculations. For the numerical solution of the model we use an extension of the numerical method proposed in [13]. The code is implemented in MatLab platform and simulations are run for a set target simulation time T that will be specified later on.

3.4.1. Anaerobic biofilm reactor

The model has been applied to simulate the invasion of methanogenic archaea in an anaerobic biofilm operating in a continuous reactor. The analysed scenario describes the dynamics of two microbial species, the fermentative bacteria X_1 and the methanogenic archaea X_2, whose initial concentration within the biofilm has been set to zero.

Table 1. Kinetic-stoichiometric parameters and initial-boundary conditions for AD.

Symbol	Definition	Value	Unit
Y_1	Yield on X_1	0.1	-
Y_2	Yield on X_2	0.05	-
$\mu_{max,1}$	Maximum growth rate of X_1	30	d^{-1}
$\mu_{max,2}$	Maximum growth rate of X_2	5	d^{-1}
Ks_1	S_1 affinity constant for X_1	0.5	$g\ COD\ L^{-1}$
Ks_2	S_2 affinity constant for X_2	0.15	$g\ COD\ L^{-1}$
kd_1	Decay rate of X_1	0.005	d^{-1}
kd_2	Decay rate of X_1	0.005	d^{-1}
Y_ψ	Yield of X_2 on Ψ_2	0.01	-
k_{col}	Maximum colonization rate of Ψ_2	0.001	d^{-1}
k_ψ	Kinetic constant for Ψ_2	0.01	$mg\ COD\ L^{-1}$
φ_1	Initial volume fraction of X_1	1	-
φ_2	Initial volume fraction of X_2	0	-
S_1^{in}	Inlet concentration of S_1	6	$g\ COD\ L^{-1}$
S_2^{in}	Inlet concentration of S_2	0	$g\ COD\ L^{-1}$
L_0	Initial biofilm thickness	0.01	mm

The model takes into consideration three reactive components, dissolved organic matter S_1, acetate S_2 produced by X_1 and consumed by X_2 and methane S_3, which represents the final product of the whole metabolic pathway. According to experimental evidence, the establishment and proliferation of X_2 in sessile form depends on the formation of a favourable environmental niche, which corresponds to the accumulation of acetate. The corresponding substrate concentrations within the bulk liquid $S^*_j(t)$ have been taken

into account as well. Planktonic cells have been considered for X_2. The reaction rates have been defined according to ADM1. The initial biofilm thickness of 0.01 mm has been assumed and the concentration of colonizing archaea in the bulk liquid has been set to $\psi_2(L(t), t) = 0.1\ mg\ COD\ L^{-1}$. Table 1 resumes all the kinetic and stoichiometric parameters and the initial and boundary conditions adopted, such as the concentrations of soluble substrates in the inlet flow rate and the initial biofilm composition used for the specific simulation.

3.4.1.1. Numerical simulations

The simulation reproduces the archaea colonization phenomenon and tracks the dynamics of the bacterial species and the evolution of substrate profiles within the biofilm. The simulation is reported in Figure 1 to Figure 3. In particular, the results are expressed in terms of bacterial volume fractions (A), substrate concentration profiles (B) and methane production (C) at different simulation time (note that biofilm is growing from left to right in all the Figures). The methane production is expressed as the percentage of the maximum theoretical production.
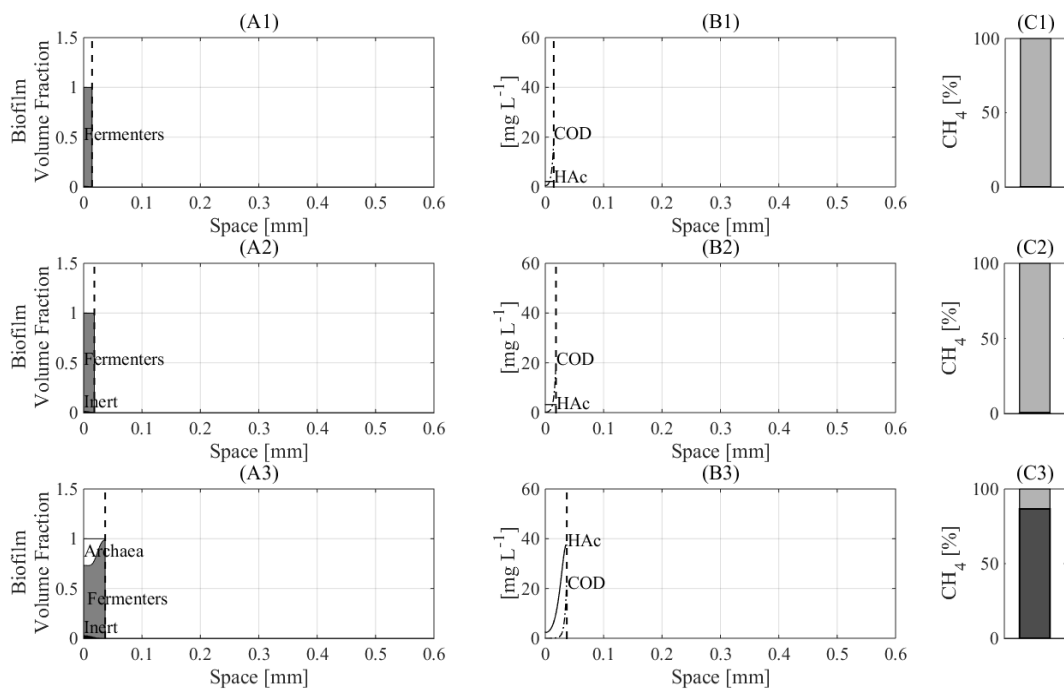
Figure 1. Bacteria volume fractions, substrate concentration trends and substrate to methane conversion efficiency, after 1 (A1, B1, C1), 2 (A2, B2, C2) and 5 (A3, B3, C3) days.
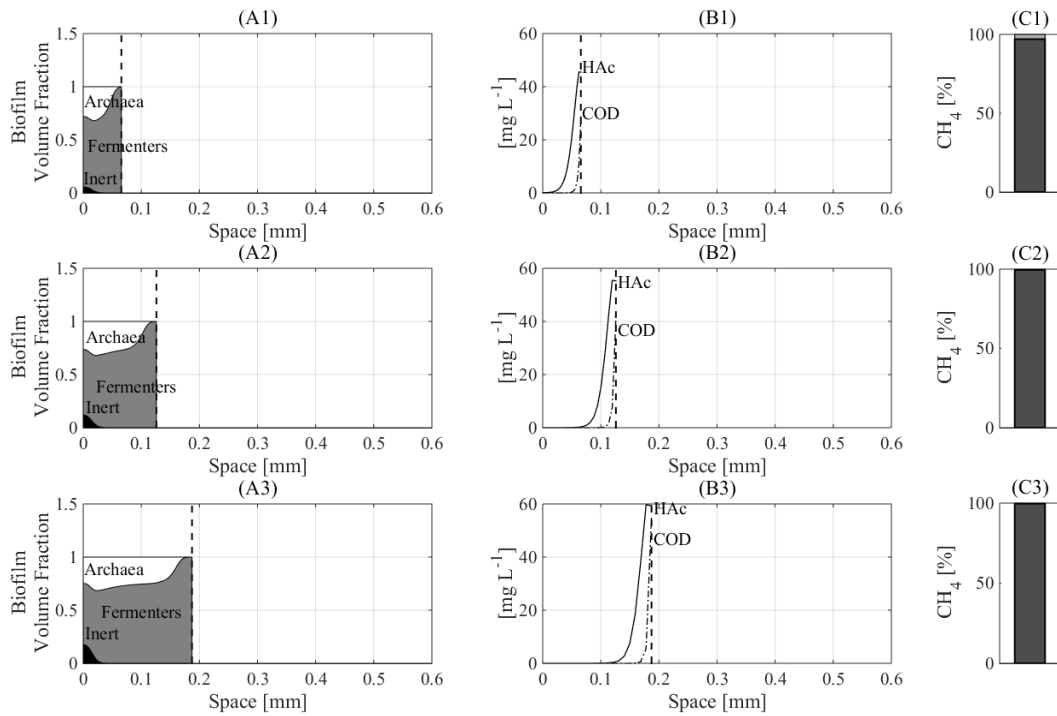
Figure 2. Bacteria volume fractions, substrate concentration trends and
substrate to methane conversion efficiency, after 10 (A1, B1, C1),
20 (A2, B2, C2) and 30 (A3, B3, C3) days.
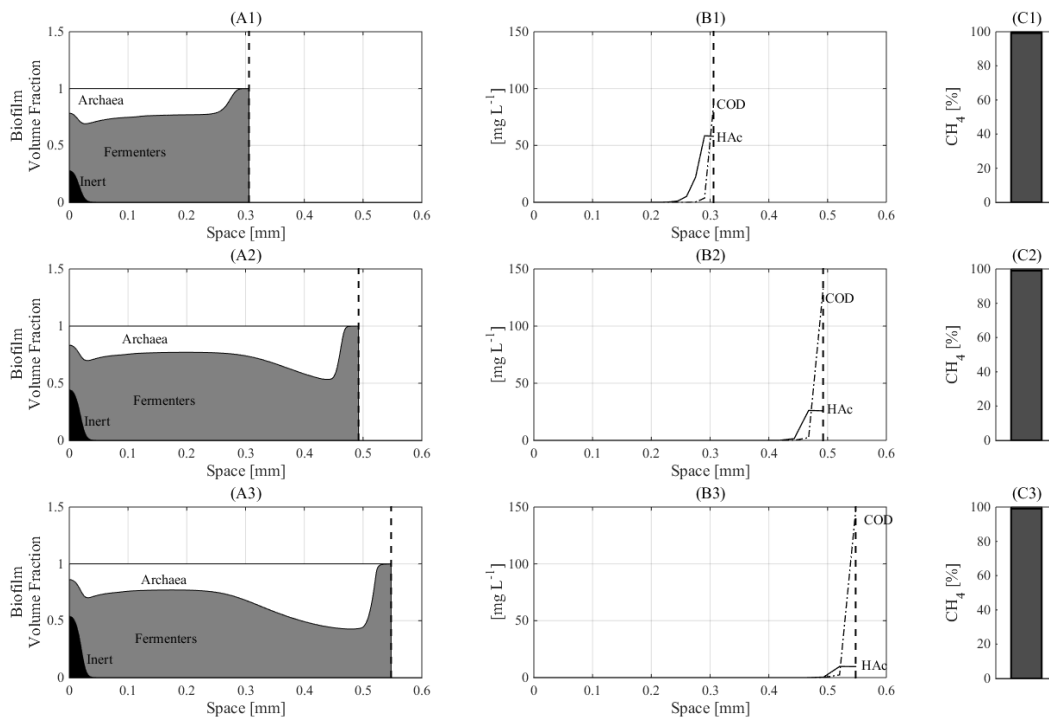
Figure 3. Bacteria volume fractions (A), substrate concentration trends (B) and
substrate to methane conversion efficiency, after 50 (A1, B1, C1),
90 (A2, B2, C2) and 120 (A3, B3, C3) days.

The numerical results show that colonizing bacteria diffuse into the biofilm and grow only where there are favorable environmental conditions for their development (Figure 2 (A1, A2, A3)), as determined by substrates trends (Figure 1 (B3) and Figure 2 (B1, B2, B3)). According to experimental evidence, the archaea cells colonize the inner part of the biofilm, where they found favourable environmental conditions, that is high acetate and low dissolved organic matter concentrations. Under these conditions, archaea can effectually prevail on the fermentative bacteria. During the first days of simulation time, the production of methane is equal to zero due to the absence of methanogenic biomass within the biofilm. As expected, acetic acid shows a constant profile when archaea are not present within the biofilm (Figure 1 (B1, B2)). As soon as archaea start to grow (Figure 1 (A3)), the acetate concentration sharply decreases, (Figure 1 (B3)). The colonization phenomenon completely evolves in Figures 2 and 3. Specifically, the acetate concentration reduces significantly all over the biofilm and a residual dissolved organic matter is found in the bulk liquid (Figure 3 (B1, B2, B3)). Contextually, the maximum methane yield is definitely achieved (Figure 3 (C1, C2, C3)).

Finally, it is important to notice that the diffusion of mobile colonizing archaea into the biofilm allows the colonization of a new species as determined by substrate (i.e. acetic acid) profiles. More precisely, as shown in Figure 4, the biofilm results fully penetrated by ψ_1, which never reaches zero, indicating that merely the contemporary presence of substrates and colonizing motile species can lead to the growth of sessile bacteria. Despite, the concentration of the invading species is higher in the external part of the biofilm, the archaea growth occurs in the inner part of the biofilm where the environmental conditions are more favorable. This fact is consistent with observations that substrate concentrations have a regulatory effect on the dynamics of biofilm structure since the colony size can be directly correlated with the substrate concentration profiles into the biofilm [21].
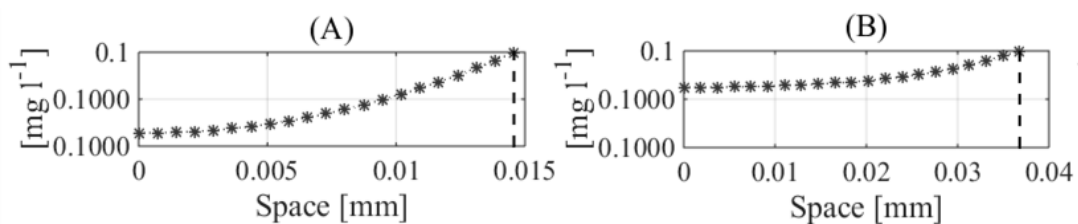
Figure 4. ψ profile within biofilm after 1 (A), and 120 (B) days.

3.4.2. Anammox biofilm reactor

The simulated biofilm system consists of bacterial cells accumulating on a surface surrounded by an aquatic region and reproduces a typical multi-culture and multi-substrate process which establishes in the deammonification units of the wastewater treatment plants. The deammonification process consists in the autotrophic nitrogen removal carried out by two microbial groups, the ammonium oxidizing bacteria AOB X_1 which oxidize ammonium S_1 partially to nitrite S_2 aerobically and the anaerobic ammonium oxidizing bacteria AMX (X_2), which subsequently convert the remaining ammonium and the newly formed nitrite into nitrogen gas and nitrate S_3 in trace concentrations. This process is also known as partial nitritation/anammox [14]. In multispecies biofilms, the AOB and AMX compete with other two major microbial groups: the nitrite oxidizing bacteria NOB (X_3), which oxidize S_2 to S_3 in aerobic conditions and compete with X_1 for oxygen and X_2 for nitrite, and heterotrophic bacteria HB X_4. The latter can be further classified in ordinary heterotrophic organisms oxidizing the organic material and denitrifiers reducing nitrate to nitrite and nitrite to dinitrogen gas by consuming organic substrate S_4. X_4 compete with X_1 and X_3 for oxygen S_5 and with X_3 for nitrite, the limiting substrate of X_2 in most instances. The establishment and proliferation of X_2 in such constituted biofilms strictly depends on the formation of an anoxic zone in the inner parts of the matrix where X_3 cannot grow, due to oxygen limitation.

The mathematical model takes into consideration the dynamics of the five microbial species $X_i(z, t)$, including inert material X_5 which derives from microbial decay, and the five reactive components $S_j(z, t)$ within the biofilm. The corresponding concentrations in the bulk liquid $S^*_j(t)$ are taken into account as well. Planktonic cells have been considered for both X_2 and X_4 species as the model is aimed at simulating the invasion of a constituted biofilm by heterotrophic and Anammox bacteria after the establishment of a favorable environmental niche. Two modelling scenarios have been considered: the case of X_2 as single invading species and the case of X_2 and X_4 invasion and establishment in an autotrophic biofilm. Hereafter, they will be referred as Model 1, considered in Section 3.4.2.1, and Model 2 that will be discussed in Section 3.4.2.2.

3.4.2.1.   Model 1 - One invading species

Model 1 considers a single invading species: the anaerobic ammonium oxidizing bacteria AMX (X_2). The mathematical formalization of the problem is provided below.

The microbial species dynamics is governed by equations (2.1) rewritten in terms of f_i for convenience

$$\frac{\partial X_i}{\partial t} + \frac{\partial (uX_i)}{\partial x} = \rho_i r_{M,i}(z, t, \boldsymbol{X}, \boldsymbol{S}) + \rho_i r_i(z, t, \boldsymbol{\Psi}, \boldsymbol{S}), \quad i = 1, \dots, 5 \tag{4.1}$$

The following initial volume fractions are associated to equations (4.1)

$$f_1(z, 0) = 0.65, \ f_2(z, 0) = 0.0, \ f_3(z, 0) = 0.25, \ f_4(z, 0) = 0.1, \ f_5(z, 0) = 0.0 \tag{4.2}$$

The biofilm is assumed to be initially constituted only by the species X_1, X_3, X_4. The invasion of the species X_2 is simulated. The initial biofilm thickness L_0 is given by

$$L_0 = 0.1 \ mm \tag{4.3}$$

A representation of the initial microbial distribution is reported in Figure 5.
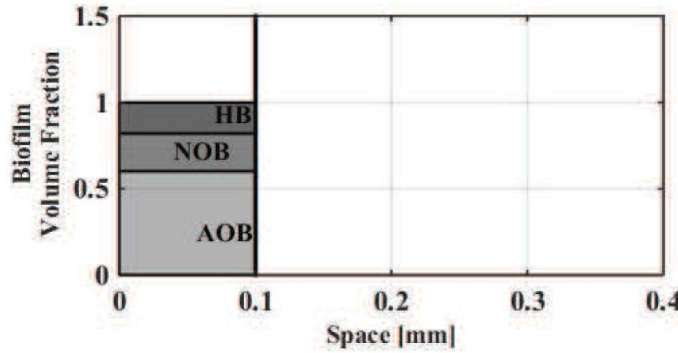
Figure 5. Initial biofilm configuration for Model 1.

The net specific biomass growth rates $r_{M,I}$, $i = 1, \dots, 4$ are expressed as

$$r_{M,i} = \left(\mu_i(\boldsymbol{S}) - k_{d,i}\right)f_i$$

where the function $\mu_i(\boldsymbol{S})$ denotes the *ith* biomass specific growth rate and depends on the anabolic reactions performed by the *ith* microbial species. It is usually formulated as Monod kinetics as detailed below. The term $k_{d,i}$ accounts instead for the forms of biomass loss and energy requirements not associated with growth, including decay, maintenance, endogenous respiration, lysis, predation, death. The net specific growth rates associated to X_i, $i = 1, \dots, 4$ are the the following

$$r_{M,1} = \left(\mu_1(\boldsymbol{S}) - k_{d,1}\right)f_1 = \left(\mu_{max,1} \frac{S_1}{K_{1,1}+S_1} \frac{S_5}{K_{1,5}+S_5} - k_{d,1}\right)f_1 \tag{4.4}$$

$$r_{M,2} = \left(\mu_2(\boldsymbol{S}) - k_{d,2}\right)f_2 = \left(\mu_{max,2} \frac{K_{2,5}}{K_{2,5}+S_5} \frac{S_1}{K_{2,1}+S_1} \frac{S_2}{K_{2,2}+S_2} - k_{d,2}\right)f_2 \tag{4.5}$$

$$r_{M,3} = \left(\mu_3(\boldsymbol{S}) - k_{d,3}\right)f_3 = \left(\mu_{max,3} \frac{S_2}{K_{3,2}+S_2} \frac{S_5}{K_{3,5}+S_5} - k_{d,3}\right)f_3 \tag{4.6}$$

49

$$r_{M,4} = \left(\mu_{4,1}(\boldsymbol{S}) + \mu_{4,2}(\boldsymbol{S}) + \mu_{4,3}(\boldsymbol{S}) - k_{d,4}\right)f_4 = \left(\mu_{max,4}\frac{S_4}{K_{4,4}+S_4}\frac{S_5}{K_{4,5}+S_5} + \right.$$
$$\left. + \beta_1\mu_{max,4}\frac{K_{4,5}}{K_{4,5}+S_5}\frac{S_4}{K_{4,4}+S_4}\frac{S_3}{K_{4,3}+S_3} + \beta_2\mu_{max,4}\frac{K_{4,5}}{K_{4,5}+S_5}\frac{S_4}{K_{4,4}+S_4}\frac{S_2}{K_{4,2}+S_2} - k_{d,2}\right)f_4 \tag{4.7}$$

where $\mu_{max,\,i}$ denotes the maximum net growth rate for biomass i, $K_{i,\,j}$ the affinity constant of substrate j for biomass i, β_1 and β_2 the reduction factor for denitrification nitrate to nitrite and nitrite to nitrogen gas respectively.

The autotrophic performance in the deammonification process relies on the activity of X_1 and X_2 and results in the S_1 conversion to dinitrogen gas via S_2. In aerobic environments, S_1 represents the preferential substrate for X_1 growth (4.4). X_2 proliferate, in turn, on S_1 and S_2 and their metabolic activity is strongly affected by the oxygen concentration, the latter being inhibitory even at low concentrations (4.5). Moreover, they rely on the production of S_2 by X_1, when that substrate is not provided from the bulk liquid. X_3 oxidize S_2 to S_3 under aerobic conditions and thus they compete with X_2 for S_2 (4.6). X_4 are considered facultative bacteria: they can aerobically oxidize the organic matter ($\mu_{4,\,1}$) or perform denitrification reactions over S_3 and S_2 ($\mu_{4,\,2}$ and $\mu_{4,\,3}$ respectively). Indeed, in presence of S_4, S_2 and S_3 can be contextually consumed by X_4 according to equation (4.7). In particular, S_3 and S_2 are reduced to dinitrogen gas in a sequential process which first converts S_3 into S_2, the latter being then reduced to N_2 In addition, the ratios $S_3/(S_2+S_3)$ and $S_2/(S_2+S_3)$ varying between 0-1, indicate the percentage of biomass growing on nitrate and/or nitrite respectively. Inert has been treated as an additional microbial species whose growth rate depends on the decay of all the active species

$$r_{M,5} = k_{d,1}f_1 + k_{d,2}f_2 + k_{d,3}f_3 + k_{d,4}f_4 \tag{4.8}$$

The specific growth rates r_i induced by the switch of the planktonic cells to the sessile mode of growth are defined as

$$r_1 = r_3 = r_4 = r_5 = 0 \tag{4.9}$$

$$r_2 = k_{col,2}\frac{\Psi_2}{k_{\Psi,2}+\Psi_2}\frac{K_{2,5}}{K_{2,5}+S_5}\frac{S_1}{K_{2,1}+S_1}\frac{S_2}{K_{2,2}+S_2}. \tag{4.10}$$

Note that the growth rate terms r_2 for X_2 is newly introduced as Monod kinetics and indicate that the transition of bacteria from planktonic state Ψ_2 into the sessile state X_2 is controlled by the formation of a specific environmental niche which is strictly connected to the local concentration of dissolved substrates. The presence of planktonic

species is fundamental for the occurrence of the invasion process, as better specified in the following.

Remark 1. Consider the second equation in (2.8) with $r_{M,2}$ given by (4.5) and initial condition $f_2(z, 0) = 0$. If it is supposed that $r_2 = 0$, then the mentioned equation admits the unique solution $f_2(z, t) = 0$ and the species X_2 cannot develop.

The diffusion of substrates is governed by

$$\frac{\partial S_j}{\partial t} - D_j \frac{\partial^2 S_j}{\partial z^2} = r_{S,j}(z, t, \mathbf{X}, \mathbf{S}), \quad j = 1, \dots, 5, \tag{4.11}$$

with the following initial-boundary conditions

$$S_j(z, 0) = 0, \quad \frac{\partial S_j}{\partial z}(0, t) = 0, \quad j = 1, \dots, 5, \tag{4.12}$$

$$S_j(L(t), t) = S_j^*(t), \quad j = 1, \dots, 4, S_5(L(t), t) = \overline{S_5} = 1.5 \, mg \, L^{-1} \tag{4.13}$$

The last condition simulates a continuous aeration of the biofilm reactor, [5].

The net substrate conversion rates account for both the microbial production and consumption (positive and negative terms respectively) and can be formulated from the corresponding microbial growth rates through the specific microbial yield Y_i. They are usually expressed as double-Monod kinetics as presented below.

The ammonium conversion rate $r_{S,1}$ is expressed as

$$r_{S,1} = \left(-\frac{1}{Y_1} - i_{N,B}\right)\mu_2 X_2 + \left(-\frac{1}{Y_2} - i_{N,B}\right)\mu_2 X_2 +$$

$$-i_{N,B}\left(\mu_3 X_3 + \mu_{4,1}X_4 + \mu_{4,2}X_4 + \mu_{4,2}X_4\right), \tag{4.14}$$

where Y_i denotes the yield for biomass i and $i_{N,B}$ is the nitrogen content in biomass. Ammonium can be directly consumed by AOB and AMX (first and second term in 4.14), and it is usually uptaken by other microbial species for anabolic reactions (third term in 4.14).

The nitrite and nitrate conversion rates $r_{S,2}$ and $r_{S,3}$ can be written as

$$r_{S,2} = \frac{1}{Y_1}\mu_1 X_1 - \left(\frac{1}{Y_2} + \frac{1}{1.14}\right)\mu_2 X_2 - \frac{1}{Y_3}\mu_3 X_3 +$$

$$-\left(1 - \frac{1}{Y_4}\right)\frac{1}{1.14}\mu_{4,2}X_4 + \left(1 - \frac{1}{Y_4}\right)\frac{1}{1.72}\mu_{4,3}X_4, \tag{4.15}$$

$$r_{S,3} = \left(\frac{1}{1.14}\right)\mu_2 X_2 + \frac{1}{Y_3}\mu_3 X_3 + \left(1 - \frac{1}{Y_4}\right)\frac{1}{1.14}\mu_{4,2}X_4 \tag{4.16}$$

In aerobic environments, nitrite S_2 are produced through the ammonium conversion catalyzed by AOB and they are further oxidized to nitrate S_3 by NOB (first and third term in 4.15). Obviously, the latter represents a production rate for nitrate (second term in 4.16) Conversely, in anoxic conditions AMX bacteria convert nitrite and ammonium

in dinitrogen gas (second term in 4.15), while HB consume both the oxidized nitrogen compounds by reducing nitrate to nitrite (fourth and third term in 4.15 and 4.16 respectively) and by using nitrite as oxygen source (fifth term in 4.15).

The organic carbon conversion rate $r_{S,4}$ is expressed by

$$r_{S,4} = -\frac{1}{Y_4} \left(\mu_{4,1} X_4 + \mu_{4,2} X_4 + \mu_{4,3} X_4 \right) \tag{4.17}$$

and indicates the S_4 consumption due to X_4 metabolism in both aerobic and anoxic conditions.

Finally, $r_{S,5}$ describes the oxygen conversion rate within the multispecies biofilm

$$r_{S,5} = \left(1 - \frac{3.43}{Y_1} \right) \mu_1 X_1 + \left(1 - \frac{1.14}{Y_3} \right) \mu_3 X_3 + \left(1 - \frac{1}{Y_4} \right) \mu_{4,1} X_4, \tag{4.18}$$

where the three terms in (4.18) are net consumption rates due to AOB, NOB and HB species using oxygen for their metabolisms.

The functions $S^*_j(t)$ are governed by the following initial value problem for ordinary differential equations

$$V S^*_j = -A D_j \frac{\partial S_j}{\partial z} (L(t), t) + Q \left(S^{in}_j - S^*_j(t) \right), \ j = 1, \dots, 4, \tag{4.19}$$

The initial conditions for S^*_j are the following

$$S^{in}_j = 1200 \ mgN \ L^{-1}, \ S^{in}_2 = S^{in}_3 = 0, \ S^{in}_4 = 120 \ mgCOD \ L^{-1}. \tag{4.20}$$

The inlet concentrations are non-zero only for S_1 and S_4, reproducing the case of a biofilm reactor fed with a wastewater containing both ammonium nitrogen and organic carbon.

The diffusion and reaction of planktonic cells within the biofilm matrix is governed by the following equations

$$\frac{\partial \Psi_i}{\partial t} - D_{M,i} \frac{\partial^2 \Psi_i}{\partial z^2} = r_{\Psi,i}(z, t, \mathbf{S}, \mathbf{\Psi}), \ i = 1, \dots, 5, \tag{4.21}$$

where $D_{M,i}$ denotes the diffusivity coefficient. The conversion rates of planktonic cells due to invasion process are expressed by

$$r_{\Psi,i} = -\frac{1}{Y_{\Psi,i}} r_i, \ i = 1, \dots, 5, \tag{4.22}$$

with $Y_{\Psi,i}$ being the yield of sessile species on planktonic ones. They are assumed proportional to r_i, i.e. described by the same Monod kinetics [4]. The following initial-boundary conditions are associated to equations (4.21)

$$\Psi_i(z,0) = 0, \ \frac{\partial \Psi_i}{\partial z}(0,t) = 0, \ \Psi_i(L(t),t) = \psi_i^*(t), \ i = 1, \dots, 5. \tag{4.23}$$

The functions $\psi_i^*(t)$ satisfy the following initial value problem for ordinary differential equations

$$V\psi_i^* = -AD_{M,i}\frac{\partial \Psi_i}{\partial z}(L(t),t) + Q\left(\psi_i^{in} - \psi_i^*(t)\right), \ i = 1, \dots, 5, \tag{4.24}$$

$$\psi_1^{in} = 0, \ \psi_2^{in} = 1.0 \ mgCOD \ L^{-1}, \ \psi_3^{in} = \psi_4^{in} = \psi_5^{in} = 0. \tag{4.25}$$

Note that for $i = 1$ equation for Ψ_1 is homogeneous because of hypothesis (4.9) and equation for ψ_1^* do not contain the term ψ_1^{in} because of hypothesis (4.25). Therefore, the system of the two equations admits the unique solution $\Psi_1(z, t) = 0$, $\psi_1^*(t) = 0$. Same result holds for $\Psi_3(z, t) = 0$, $\psi_3^*(t) = 0$, $\Psi_4(z, t) = 0$, $\psi_4^*(t) = 0$, $\Psi_5(z, t) = 0$, $\psi_5^*(t) = 0$.

The biofilm reactor is characterized by the following operational parameters: the flow rate Q is set to 3.15 L d^{-1}, the surface area available for biofilm attachment and proliferation A is equal to 1 m^2 and the reactor volume is of 3.15 L, leading to a hydraulic retention time of 1 day.

The values of the stoichiometric and kinetic parameters used for numerical simulations are adopted from [2] and are reported for convenience in Tables 2-3.

Table 2. Kinetic and stoichiometric parameters used for numerical simulations AMX.

Symbol	Definition	Value	Units
Y_1	X_1 yield on S_1	0.150	$g\ COD\ g\ N^{-1}$
Y_2	X_2 yield on S_1	0.159	$g\ COD\ gN^{-1}$
Y_3	X_3 yield on S_1	0.041	$g\ COD\ gN^{-1}$
Y_4	X_4 yield on S_4	0.63	$g\ COD\ g\ COD^{-1}$
$\mu_{max,1}$	Maximum growth rate of X_1	2.05	d^{-1}
$\mu_{max,2}$	Maximum growth rate of X_2	0.08	d^{-1}
$\mu_{max,3}$	Maximum growth rate of X_3	1.45	d^{-1}
$\mu_{max,4}$	Maximum growth rate of X_4	6.0	d^{-1}
$K_{1,1}$	S_1 affinity constant for X_1	2.4	$mg\ N\ L^{-1}$
$K_{1,5}$	S_5 affinity constant for X_1	0.6	$mg\ O_2\ L^{-1}$
$K_{2,1}$	S_1 affinity constant for X_2	0.07	$mg\ N\ L^{-1}$
$K_{2,2}$	S_2 affinity constant for X_2	0.05	$mg\ N\ L^{-1}$
$K_{2,5}$	S_5 inhibiting constant for X_2	0.01	$mg\ O_2\ L^{-1}$
$K_{3,2}$	S_2 affinity constant for X_3	5.5	$mg\ N\ L^{-1}$
$K_{3,5}$	S_5 affinity constant for X_3	2.2	$mg\ O_2\ L^{-1}$
$K_{4,4}$	S_4 affinity constant for X_4	4.0	$mg\ COD\ L^{-1}$
$K_{4,5}$	S_5 affinity/inhibiting constant for X_4	0.2	$mg\ O_2\ L^{-1}$
$K_{4,2}$	S_2 affinity constant for X_4	0.5	$mgN\ L^{-1}$
$K_{4,3}$	S_3 affinity constant for X_4	0.5	$mgN\ L^{-1}$
$k_{d,1}$	Decay constant for X_1	0.0068	d^{-1}
$k_{d,2}$	Decay constant for X_2	0.0026	d^{-1}
$k_{d,3}$	Decay constant for X_3	0.04	d^{-1}
$k_{d,4}$	Decay constant for X_4	0.06	d^{-1}

Table 3. Additional parameters used for numerical simulations.

Symbol	Definition	Value	Units
$i_{N,B}$	N content of biomass	0.07	$g\ N\ g\ COD^{-1}$
β_1	Reduction factor for denitrification NO₃-NO₂	0.8	-
β_2	Reduction factor for denitrification NO₂-N₂	0.8	-
$k_{col,2}$	Maximum colonization rate of ψ_2	0.0001	d^{-1}
$k_{col,4}$	Maximum colonization rate of ψ_4	0.0001	d^{-1}
$Y_{\psi,2}$	Yield of X_2 on ψ_2	0.001	-
$Y_{\psi,4}$	Yield of X_4 on ψ_4	0.001	-
$k_{\psi,2}$	Kinetic constant for ψ_2	0.000001	$mg\ COD\ L^{-1}$
$k_{\psi,4}$	Kinetic constant for ψ_4	0.000001	$mg\ COD\ L^{-1}$

The simulation results for the multispecies biofilm performance when the AMX invasion is considered are reported in Figs. 6-8. After one day of simulation time (Figure 6-A), it is possible to notice that the microbial distribution into the biofilm is still affected by the initial conditions and the colonization phenomenon has not occurred yet. After 5 days of simulation time (Figure 6-B), the biofilm experiences oxygen limitation, due to the low concentration maintained within the bulk liquid. As a consequence, the NOB concentration significantly decreases with respect to the initial fraction, with the AOB and HB being the two species proliferating the most. The AOB activity is confirmed by the decrease in S_1 concentration within the bulk liquid with respect to the inlet concentration and a concurrent increase in S_2 concentration (Figure

8-A, B). Note that the latter keeps higher than S_3 concentration as the metabolic activity of NOB is limited by the low oxygen concentration. The organic carbon is completely depleted within the biofilm and its concentration keeps lower than 1 mg L^{-1}.
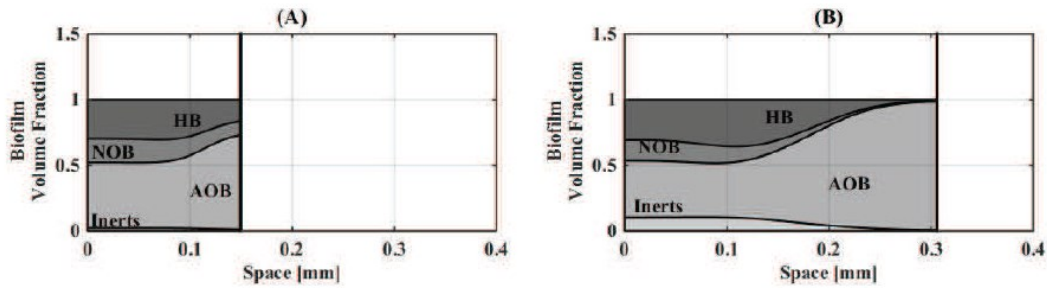
Figure 6. Microbial species distribution of a multispecies biofilm undergoing ψ_2 colonization after 1(A) and 5(B) days simulation time.
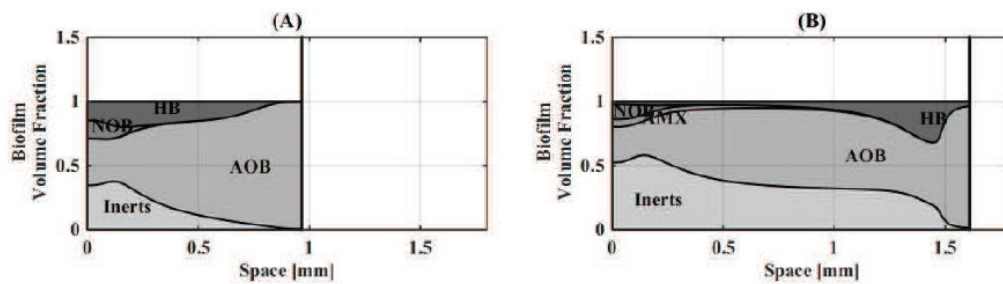
Figure 7. Microbial species distribution of a multispecies biofilm undergoing ψ_2 colonization after 20(A) and 50(B) days simulation time.

Figure 7-A displays biofilm configuration after 20 days of system operation: nevertheless the concomitant formation of an anoxic zone in the inner part of the biofilm (Figure 8-C) and a non-zero ψ_2 concentration all over the biofilm (data not shown), AMX have not yet established in sessile form. This might be due to the very slow growth rate of X_2. The biofilm is dominated by X_1 while X_5 predominate in the inner layer. Substrate trends assume the following configuration: S_1 increases in the bulk liquid due to the lower AOB activity in the outer art of the biofilm where S_5 is totally consumed and its depletion determines the formation of an anoxic zone. Moreover, S_2 represents the main abundant product while S_3 and S_4 keep close to zero all over the biofilm (Figure 8-C). At day 50 (Figures 7-B and 8-D), AMX have colonized the environmental niche which formed at the bottom of the biofilm (Figure 7-B). AOB still dominate the aerobic zone while NOB are confined to the internal layers. S_3 concentration is close to zero as the metabolism of NOB significantly slows down. Note that the availability of S_5 within the biofilm is strictly connected to the penetration depth whose decrease leads to an increasing anoxic zone (Figure 8-D).

Furthermore, AMX grow only where favorable environmental conditions establish despite the biofilm results fully penetrated by the same bacteria in motile/colonizing form ψ_2 for all simulation times (data not shown).
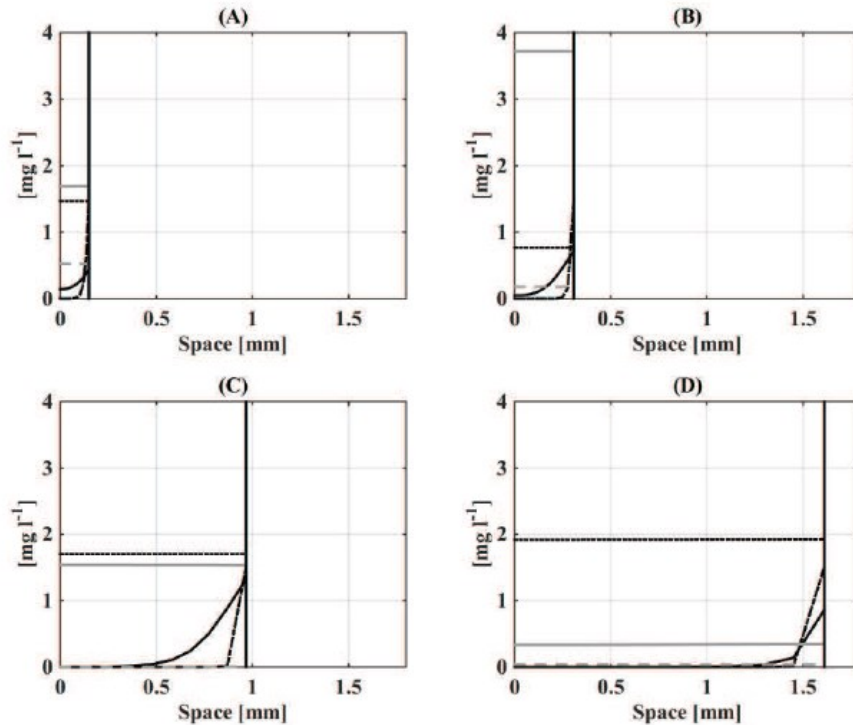
Figure 8. Substrate trends within a multispecies biofilm undergoing ψ_2 colonization after 1(A), 5(B), 20(C) and 50(D) days simulation time. Dotted black line S_1, continuous grey line S_2, dashed grey line S_3, continuous black line S_4, dashed-dotted black line S_5. S_1, S_2, and S_3 concentrations are reduced by a factor of 0.002, 0.005 and 0.005 respectively

AMX invasion is significantly influenced by many parameters such as environmental factors (i.e. pH and temperature) and operational conditions (i.e. dilution rate, C/N ratio, aeration pattern). The main goals for the further computational studies are to determine how the invasion phenomenon is affected by the oxygen and organic carbon availability. For this reason we vary the concentration of oxygen in the bulk liquid S_{5L} and the organic carbon concentration in the inlet S^{in}_4 in the range $[0.5-6]$ and $[120-750]$ respectively. In the following, we will refer to Secs. 4.1.1 and 4.1.2 for the applications with the variable oxygen and organic carbon. We assumed the initial condition reported in Figure 5 for all the simulation studies.

3.4.2.1.1.   Model 1 - Assessment -A- Effect of oxygen concentration
Model outcomes for the simulation studies with variable oxygen are summarized in Figsure 9 and 10 in terms of biomass distribution and substrate concentrations within

the bulk liquid. Four different oxygen levels (0.5-1.5-3-6 mg O_2 L^{-1}) have been tested and the simulations have been run for a target time of 50 days. AMX are strictly inhibited by the oxygen concentration and as expected, their total volume fraction is found to slightly increase when varying the oxygen level from 6 to 1.5. A lower oxygen concentration leads to a decrease in AMX fraction; indeed, under this condition HB reaches the highest fraction competing with AMX and NOB for S_2. The optimal condition for AMX establishment and proliferation within the biofilm occurs at 3 mg O_2 L^{-1}, even if the relative total biofilm fraction is lower with respect to 1.5 mg O_2 L^{-1}. Of course, NOB fraction is higher when the oxygen concentration is equal to 6 mg O_2 L^{-1}. Regarding nitrogen removal, it is possible to note that the S_1 concentration progressively decreases and consequently S_2 increases going from 0.5 to 6 mg O_2 L^{-1}. These substrates show fully penetrated profiles (data not shown) and consequently the AMX can grow for all the cases with their maximum specific growth rate, but only where anoxic conditions are established.
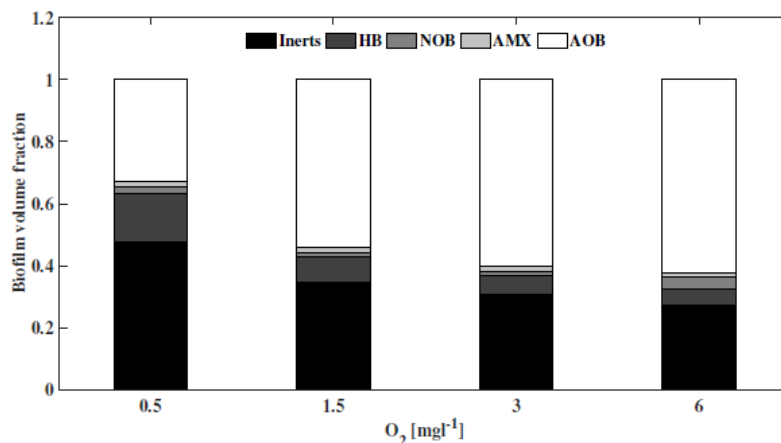
Figure 9. Total biofilm volume fractions at different O_2 concentrations after 50 days simulation time.
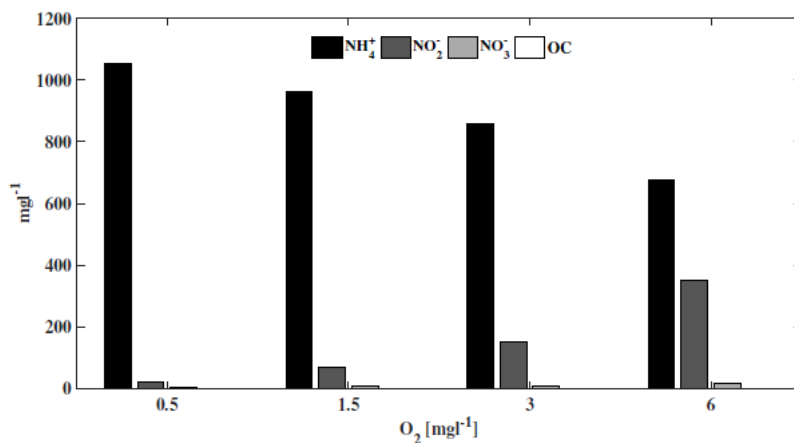
Figure 10. Substrate concentrations within the bulk liquid at different O_2 concentrations after 50 days simulation time.

3.4.2.1.2   Model 1 – Assessment -B- Effect of inlet organic carbon

The second simulation studies investigated the effect of increasing C/N ratios on AMX performances. The oxygen concentration within the bulk liquid has been fixed to 3 mg O_2 L^{-1}. As shown in Figures 11 and 12, four different concentrations of the inlet organic carbon S^{in}_4 have been tested (120-250-500-750 mg O_2 L^{-1}) and all the simulations have been run for 50 days. Figure 11 shows that the AOB volume fraction is prevalent when low organic carbon is available for HB, which compete for oxygen with all the other aerobic species in the external part of the biofilm. AMX invasion and proliferation is favored at $S^{in}_4 = 500$ mg COD L^{-1} since the NOB significantly decrease when increasing the inlet organic carbon concentration. The highest carbon content leads to the highest inerts volume fraction as HB are strongly predominant and out-compete all the other species.
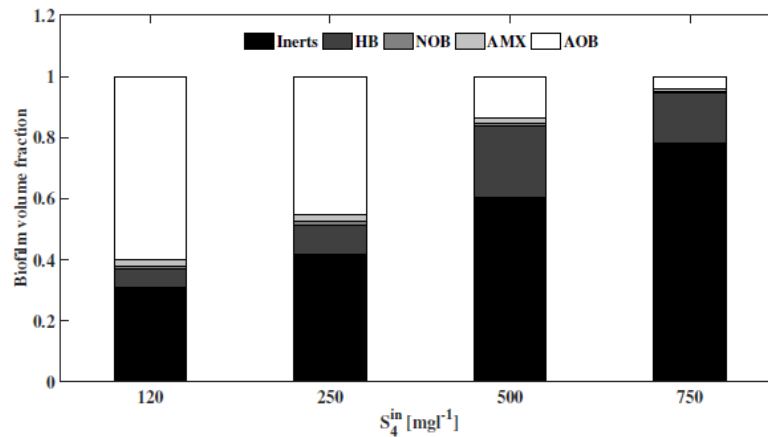
Figure 11. Total biofilm volume fractions at different S^{in}_4 values after 50 days simulation time.

According to the volume fraction distribution, total nitrogen removal is higher when both AMX and AOB can easily perform their metabolisms while NOB activity is inhibited by HB. This particular condition is more evident when the inlet carbon concentration is 250 mg COD L^{-1} and a higher amount of dissolved oxygen is utilized by HB. Ammonium removal is not significant when both AMX and AOB are not prevalent within the biofilm and organic carbon removal starts to be incomplete when increasing S^{in}_4 concentration to 750 mg COD L^{-1}.
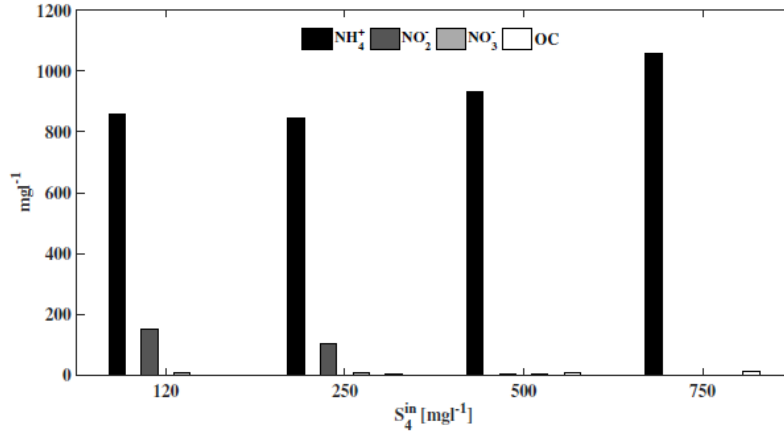
Figure 12. Substrate concentrations within the bulk liquid at different S^{in}_4 values after 50 days simulation time.

3.4.2.2.   Model 2 - Two invading species

In this section, the model was applied to the case of two species invasion, HB and AMX respectively. The microbial species growth is governed by equations (4.1) with the following initial volume fractions

$$f_1(z,0) = 0.7, \ f_2(z,0) = 0, \ f_3(z,0) = 0.3, \ f_4(z,0) = 0, \ f_5(z,0) = 0. \tag{4.26}$$

Only the species X_1 and X_3 are supposed to inhabit the biofilm at $t = 0$. The invasion of the species X_2 and X_4 is simulated. The initial biofilm thickness L_0 is given by (4.3). A representation of the initial microbial distribution is reported in Figure 13.
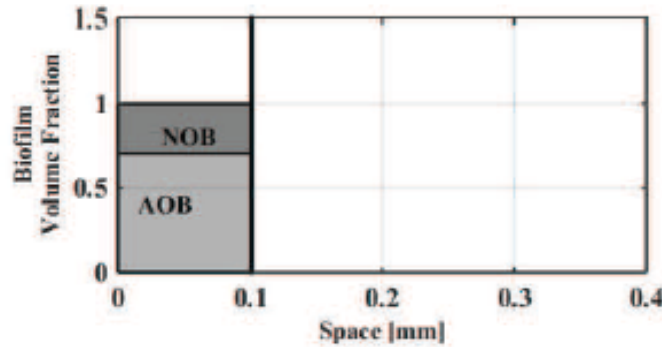
Figure 13. Initial biofilm configuration for Model 2.

The biomass growth rates $r_{M,\ i}$ are the same as Model 1, formulas (4.4)-(4.8). The specific growth rates r_i induced by the switch of the planktonic cells to the sessile mode of growth are defined as

$$r_1 = r_3 = r_5 = 0, \tag{4.27}$$

$$r_2 = k_{col,2} \frac{\Psi_2}{k_{\psi,2}+\Psi_2} \frac{K_{2,5}}{K_{2,5}+S_5} \frac{S_1}{K_{2,1}+S_1} \frac{S_2}{K_{2,2}+S_2}, \tag{4.28}$$

$$r_4 = k_{col,4} \frac{\Psi_4}{k_{\psi,4}+\Psi_4} \left(\frac{S_4}{K_{4,4}+S_4} \frac{S_5}{K_{4,5}+S_5} + \right.$$

$$\left. +\beta_1 \frac{K_{4,5}}{K_{4,5}+S_5} \frac{S_4}{K_{4,4}+S_4} \frac{S_3}{K_{4,3}+S_3} + \beta_2 \frac{K_{4,5}}{K_{4,5}+S_5} \frac{S_4}{K_{4,4}+S_4} \frac{S_2}{K_{4,2}+S_2} \right) \tag{4.29}$$

The growth rate terms r_2 and r_4 for X_2 and X_4, respectively, indicate that the transition of bacteria from planktonic state ψ_2, ψ_4 into the sessile state X_2, X_4 is controlled by the formation of specific environmental niches connected to the local concentration of dissolved substrates. As in Model 1, consider second and fourth equation in (2.8) with $r_{M,2}$ and $r_{M,4}$ given by (4.5) and (4.7), respectively. If it is supposed that $r_2 = r_4 = 0$, then the mentioned equations with initial condition $f_2(z, 0) = f_4(z, 0) = 0$ admit the unique solution $f_2(z, t) = f_4(z, t) = 0$ and the species X_2 and X_4 cannot develop.

The initial-boundary conditions for S_j and net conversion rates of substrates are the same as Model 1, formulas (4.12)-(4.13) and (4.14)-(4.18), respectively. The initial conditions for S^*_j are given by (4.20). The initial-boundary conditions for Ψ_i are same as Model 1, formula (4.23). The initial conditions for ψ^*_i are the following

$$\psi_1^{in} = 0, \ \psi_2^{in} = 1.0 \ mgCOD \ L^{-1}, \ \psi_3^{in} = 0, \psi_4^{in} = 1.2 \ mgCOD \ L^{-1}, \ \psi_5^{in} = 0. \tag{4.30}$$

Note that, by using the same arguments as Model 1, it can be shown that $\Psi_1(z, t) = 0$, $\psi^*_1(t) = 0$, $\Psi_3(z, t) = 0$, $\psi^*_3(t) = 0$, $\Psi_5(z, t) = 0$, $\psi^*_5(t) = 0$,

The operational parameters of the biofilm reactor are the same as Model 1.

In Figures 14 and 15 the simulation results for the multispecies biofilm system with two invading species are reported. Differently from Model 1, the X_4 invasion is very fast and it is already visible after 5 days of simulation time (Figure 14-B). This is due to the different environmental conditions that trigger the invasion of the two microbial species. Indeed the establishment of X_2 is dependent on the formation of an anoxic zone within the biofilm while X_4 are facultative bacteria and can grow in both aerobic and anoxic environments. After 20 days the biofilm configuration is the same of the previous application (Figures 7-A and 15-A) and as we can expect, the further evolution of the system is practically the same for the two cases studied. Simulation results confirm model capability of predicting the invasion phenomenon on time and space. Indeed, the model is able to predict the delays between the X_2 and X_4 colonizations and the location where the two planktonic species establish. To the best of our knowledge, such results cannot be achieved by the existing continuum biofilm models but they might have a significant impact on the developing of new strategies for such biofilm reactors operation.
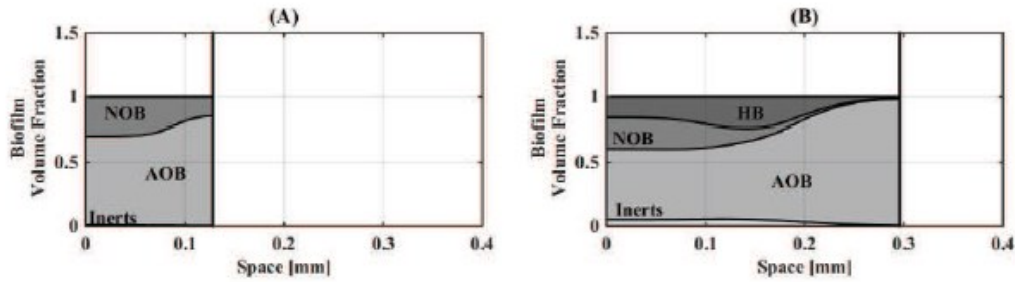
Figure 14. Microbial species distribution of a multispecies biofilm undergoing ψ_2 and ψ_4 colonization after 2(A) and 5(B) days simulation time.
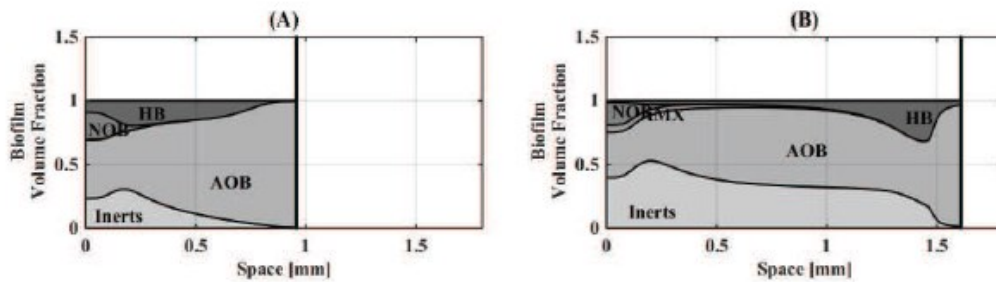
Figure 15. Microbial species distribution of a multispecies biofilm undergoing ψ_2 and ψ_4 colonization after 20(A) and 50(B) days simulation time.

3.5. Conclusions

In this work, the qualitative analysis of the free boundary problem related to the invasion phenomenon in biofilm reactors has been discussed. The model takes into account the dynamics of sessile species, nutrients and microbial products, and planktonic cells, the latter diffusing from the bulk liquid within the biofilm matrix, where they might switch their status from motile to sessile and thus colonize the pre-existing biofilm. The dynamics of bulk liquid have been explicitly modeled by considering two systems of nonlinear ordinary differential equations which derive from mass conservation principles. An existence and uniqueness result has been provided for the related free boundary value problem by using the method of characteristics and the fixed point theorem. It is important to notice that the planktonic species are just provided by the bulk liquid; however, the reverse process which accounts for the switch from sessile to planktonic form of life might occur under specific conditions. This phenomenon could be explicitly taken into account by considering a direct dependence of the free planktonic cell reaction rates on the concentration of the sessile bacteria. The same methodology adopted in this work could be easily adapted to address the existence and uniqueness questions of this new system. Numerical simulations related to a real biofilm systems have been performed. Three specific model applications have been

analyzed. Simulation results demonstrate the underlying conclusion that the invasion model can be effectively used as a predictive tool to develop specific reactor operation strategies. Further developments might be related to the definition of a calibration protocol through experimental data.

References

[1] Boltz, J.P., Smets, B.F., Rittmann, B.E., van Loosdrecht, M.C., Morgenroth, E., Daigger, G.T. 2017. From biofilm ecology to reactors: a focused review. Water Science and Technology, 75, pp.1753-1760.

[2] Mattei, M.R., Frunzo, L., D'Acunto, B., Esposito, G., Pirozzi, F. 2015. Modelling microbial population dynamics in multispecies biofilms including Anammox bacteria. Ecological Modelling, 304, pp.44-58.

[3] Ward, J.P., King, J.R. 2012. Thin-film modelling of biofilm growth and quorum sensing. Journal of Engineering Mathematics, 73, pp.71-92.

[4] D'Acunto, B., Frunzo, L., Klapper, I., Mattei, M.R. 2015. Modeling multispecies biofilms including new bacterial species invasion. Mathematical Biosciences, 259, pp.20-26.

[5] Mašić, A., Eberl, H.J. 2014. A modeling and simulation study of the role of suspended microbial populations in nitrification in a biofilm reactor. Bulletin of Mathematical Biology, 76, pp.27-28.

[6] D'Acunto, B.,Frunzo, L., Mattei, M.R. 2016. Qualitative analysis of the moving boundary problem for a biofilm reactor model. Journal of Mathematical Analysis and Applications, 438(1), pp.474-491.

[7] Frunzo, L., Mattei, M.R. 2017. Qualitative analysis of the invasion free boundary problem in biofilms. Ricerche di Matematica, 66, pp.171-188.

[8] Cresson, R., Escudie, R., Carrere, H., Delgenes, J.P., Bernet, N., 2007. Influence of hydrodynamic conditions on the start-up of methanogenic inverse turbulent bed reactors. Water Research, 41(3), pp.603-612.

[9] Habouzit, F., Hamelin, J., Santa-Catalina, G., Steyer, J.P., Bernet, N., 2014. Biofilm development during the start-up period of anaerobic biofilm reactors: the biofilm archaea community is highly dependent on the support material. Microbial Biotechnology, 7, 257-264.

[10] Cresson, R., Carrere, H., Delgenes, J.P., Bernet, N., 2006. Biofilm formation during the start-up period of an anaerobic biofilm reactor - impact of nutrient complementation. Biochemical Engineering Journal, 30 (1), 55-62.

[11] D'Acunto, B., Esposito, G., Frunzo, L., Mattei, M.R., Pirozzi, F., 2015. Mathematical modeling of heavy metal biosorption in multispecies biofilms. Journal of Environmental Engineering, 142 (9).

[12] Wanner, O., Gujer, W. 1986. A multispecies biofilm model. Biotechnology Bioengineering, 28, pp.314-328.

[13] D'Acunto, B., Esposito, G., Frunzo, L., Pirozzi, F. 2011. Dynamic modeling of sulfate reducing biofilms. Computers Mathematics with Applications, 62, pp.2601-2608.

[14] Cao, Y., van Loosdrecht, M.C., Daigger, G.T. 2017. Mainstream partial nitritation-anammox in municipal wastewater treatment: status, bottlenecks, and further studies. Applied Microbiology and Biotechnology, 101, pp.1365-1383.

[15] Cresson, R., Escudie, R., Steyer, J.P., Delgenes, J.P., Bernet, N., 2008. Competition between planktonic and fixed microorganisms during the start-up of methanogenic biofilm reactors. Water Research, 42 (3), pp.792-800.

[16] Dockery, J., Klapper, I. 2002. Finger formation in biofilm layers. SIAM Journal on Applied Mathematics, 62, pp.853-869.

Chapter 4

Continuous biohydrogen production by thermophilic dark fermentation of cheese whey: use of buffalo manure as buffering agent

Continuous biohydrogen production by thermophilic dark fermentation of cheese whey: use of buffalo manure as buffering agent

Biohydrogen (H_2) production from dark fermentation processes is usually inhibited at low culture pH (< 4.0). This work investigated the culture pH and H_2 production stability during the dark fermentation of cheese whey, supplemented with buffalo manure. The co-fermentation of cheese whey, rich in high carbohydrate but yielding acidic pH, with buffalo manure characterized by a high alkalinity, is promising for continuous H_2 production in dark fermentation. At a cheese whey to buffalo manure ratio of 4 g VS g VS^{-1}, a maximum H_2 yield and production rate of respectively, 152.2 (± 43.9) mL H_2 g VS^{-1} and 215.4 (± 62.1) mL H_2 L^{-1} d^{-1}, were achieved at an organic loading rate of 2.1 g VS L^{-1} d^{-1} of cheese whey at a stable culture pH of 4.8-5.0. The use of buffalo manure improved the H_2 production stability and could replace chemical buffering agents of scaled-up dark fermentation applications.

4.1. Introduction

Activities associated with dairy industries, either related to livestock farming for milk production or processing of milk products such as cheese, generate large amounts of waste [1]. In 2013, out of 144 million tonnes of whole milk collected in the European Union (EU - 28 countries), 36.2% was used for the production of cheese and butter (28.1%), drinking milk (12.1%), cream (12%), milk powder (3.2%) and other uses (8.4%) [2]. Cheese manufacturing industries generate liquid waste byproducts, mainly cheese whey (CHW) [3, 4]. Simultaneously, livestock activities produce large quantities of solid animal manure waste, fodder waste (which generally contains a lignocellulosic fraction) and wastewater which includes urine and faeces. These can pose threats to the atmospheric and aquatic environment due to pathogens and high nitrogen (ammoniacal nitrogen) contents [5]. Dark fermentation (DF) of waste biomass can be a technology that provides environmental credentials from recovery of renewable energy in the form of biohydrogen (H_2), while providing treatment of the organic waste.

Waste biomass rich in carbohydrates is considered to be the most suited for the DF process [6-10]. CHW can be a very suitable feedstock for DF process as it is characterized by high organic loads, comprising mainly of soluble carbohydrates (lactose), proteins and lipids [11-13]. In contrast, animal manure is not considered as a suitable substrate for DF processes as it has a low organic content, i.e. cellulose (28%), hemicelluloses (28%) and

66

lignin (12%) in case of cattle manure and 0.86 g COD g TS^{-1} (Total Solids) for buffalo slurry [14, 15]. The typical H$_2$ yield from animal manure without any pretreatment ranges from 0.7 to 29 mL H$_2$ g VS^{-1} (Volatile Solids) [9]. However, the H$_2$ yields also depend on the storage conditions and time of collection of the animal manure. Considering the fact that at an acidic pH, most of the hydrolytic enzymes do not function optimally [16], animal manure can act as buffering agent to maintain the alkalinity of the digester solids [14, 17]. Indeed, several authors have reported the application of the indigenous buffering capacity of manure for enhanced biogas production in anaerobic fermentation [13, 18, 19]. Moreover, the release of macro and micro nutrients during the DF of substrate can be compromised if protein hydrolysis is inhibited by the low pH. Therefore, animal manure can also provide macro and micronutrients such as NH$_3$, P, K, and trace elements required for bacterial growth [13, 14, 18].

The operational pH plays an important role in the biochemical pathways and the H$_2$ yields of DF. In anaerobic digestion (AD) processes for methane production, the production of acidity from volatile fatty acids (VFAs) generation is balanced by the consumption of VFAs and production of alkalinity from ammonium and bicarbonate [20, 21]. However, in DF processes, the production of VFAs without their consumption and absence of external buffering sources possibly lower the process pH to inhibitory levels. Depending on the type of substrate, often an acidic pH range (5.0-6.0) favors H$_2$ production, while a very low pH (< 4.5) can inhibit the fermentative hydrogen production [10, 22]. DF processes thus require nutrient supplements and adequate pH buffering agents to maintain optimal conditions, which can impede the economic sustainability of the DF process at scaled-up applications [17, 23]. Choi and Ahn [24] suggested the use of substrates with a high pH to replace chemical buffers. A few studies have been carried out using animal manure as a buffering agent and nutrient amendment to obtain higher H$_2$ yields [13, 17, 25]. Marrone et al. [13] optimized the H$_2$ production in co-fermentation with CHW, crude glycerol and buffalo manure (BM) slurry in batch experiments. However, the effect of animal manure addition on long-term continuous H$_2$ production is scarcely reported [17]. To the best of our knowledge, the DF of CHW and BM, both residual by products of dairy-associated industries, have not been reported yet for continuous or semi-continuous H$_2$ production processes. The aim of this work is, therefore, to study the use of BM as a potential co-substrate in continuous H$_2$ production using CHW as the main substrate of a thermophilic (55 °C) DF process. The study also aims at maximizing the H$_2$ yields along with optimal process stability. In addition to the quantity and quality of daily H$_2$

production, the major soluble metabolites, culture pH, alkalinity, and ammonium (NH_4-N) concentrations have been monitored as well to study the DF process.

4.2. Materials and methods

4.2.1. Start-up inoculum and feedstock

The heat shocked anaerobic digested sludge collected from an AD plant described elsewhere [26] was used as start-up inoculum. The TS, VS and NH_4-N content of the inoculum were 29.54 ($\pm$ 0.22) g TS L^{-1}, 18.36 ($\pm$ 0.14) g VS L^{-1} and 283.47 ($\pm$ 10.8) mg NH_4-N L^{-1}, respectively. The pH of the inoculum was 8.3 ($\pm$ 0.1) and the alkalinity was 1437.20 ($\pm$ 14.27) mg $CaCO_3$ L^{-1}. The CHW and BM collected from a cheese factory and buffalo farm in Salerno (Southern Italy) were stored at < 4 °C for further use in the experiments. The composition of CHW and BM used in the study is presented in Table 1.

Table 1. Characteristics of the cheese whey and buffalo manure used in this study.

Characteristics	CHW	BM
pH	4.88 ± 0.01	8.05 ± 0.01
Total solids (%)	6.06 ± 0.03%	5.67 ± 0.04%
Volatile solids (g L^{-1})	50.54 ± 0.22	42.17 ± 1.35
Total Chemical Oxygen Demand (COD) (g L^{-1})	67.02 ± 6	ND
Soluble sugars (g L^{-1})	12.88 ± 0.34	ND
Total Kjeldahl Nitrogen (TKN) (g L^{-1})	0.86 ± 0	1.99 ± 0.1
Lactic acid (g L^{-1})	2.52 ± 0.172	ND
Alkalinity (g L^{-1})	0.5 ± 0	4.37 ± 1

ND- Not Determined

4.2.2. Semi-continuous reactor and operating conditions

A continuously stirred tank reactor of 1.5 L working volume and 0.7 L headspace maintained at a constant thermophilic temperature (55 ± 2 °C) water bath was setup. The reactor was fed manually with CHW and BM and the effluent samples were withdrawn on a daily basis. The produced total volume of gas was measured with a volumetric displacement method using acidic water (1.5% HCl) and the volume of H_2 was confirmed by analysis of the gas composition.

The bioreactor was started with an initial S/X ratio (substrate to inoculum ratio, as g VS substrate / g VS inoculum) of 1.0. The influent feed was diluted with distilled water to obtain the fixed influent rate for maintaining the desired hydraulic retention time (HRT). The CHW:BM ratio presented in Table 2 was obtained for maintaining the suitable indigenous culture pH and stable H_2 production without addition of external chemical

buffering agent. Based on the different BM feeding strategy and DF operational conditions, the reactor operation was divided into seven experimental periods as shown in Table 2. The organic loading rate of CHW was fixed throughout the experimental period, while the BM feed was varied to change their ratios during the course of the experiment.

Table 2. Operational conditions and BM feeding regimes during the experimental runs.

Experimental Periods	Days	CHW:BM (g VS g VS^{-1})	Total OLR (gVS L^{-1} d^{-1})	OLR of CHW (gVS L^{-1} d^{-1})	HRT (d)
I	1 to 10	NA	0.7	0.7	12.0
II	11 to 20	NA	2.1	2.1	12.0
III	21 to 42	1	4.2	2.1	12.0
IV	43 to 72	4	2.6	2.1	12.0
V	73 to 80	4	2.6	2.1	8.0
VI	81 to 91	2	3.2	2.1	8.0
VII	92 to 110	4	2.6	2.1	8.0

NA- Not Applicable

4.2.3. Analytical methods

The biogas composition was quantified by a Varian Star 3400 gas chromatograph equipped with a Shin-Carbon ST 80/100 column and a thermal conductivity detector. The duration of analysis was 14 min. Argon was used as carrier gas with a front and rear end pressure of 20 psi.

The major fermentation products (lactic, acetic, propionic and butyric acids) were quantified by High Pressure Liquid Chromatography (HPLC) (Dionex LC 25 Chromatography Oven) equipped with a Synergi-4u Hydro-RP-80A (size 250 x 4.60 mm) column and UV detector (Dionex AD25 Absorbance Detector) as described by Ghimire et al. [27]. Ethanol was also quantified by HPLC (Aminex HPX-87H column, 300 mm on 7.8 mm, Bio-rad) as described Ghimire et al. [27].

COD was determined according to the method described by Noguerol-Arias et al. [28]. The carbohydrate content was determined by the Dubois method [29]. Total lipids were measured by the Bligh and Dyer chloroform/methanol total lipid extraction method [30]. TS and VS concentrations were determined by the Method 2540 (Part 2000), alkalinity by titration (Method 2320, Part 2000) and TKN by macro-Kjeldahl (Method 4500-N$_{org}$, Part 4000) as described in the Standard Methods [31].

4.2.4. Data analysis

Biohydrogen production rates (HPR) are expressed in mL H_2 L^{-1} d^{-1}, while the H_2 yields (HY) were determined considering the total daily CHW fed to the reactor and expressed as mL H_2 g VS_{added}^{-1}. Average values and corresponding standard deviations were calculated after allowing 3-4 days to achieve steady state. The H_2 Production Stability Index (HPSI) was evaluated by considering the ratio of standard deviation (SD) and average (Avg) HPR, reported previously by Tenca et al. [17] given in Equation (1):

$$HPSI = 1 - \frac{SD_{HPR}}{Avg_{HPR}} \tag{1}$$

A HPSI index closer to 1 represents a stable hydrogen production and larger deviation in average HPR results in less H_2 production stability. The statistical analysis was carried out in R software (OSX version 3.1.3) with the package Rcmdr (OSX version 2.1.7). FactoMineR (version 1.24, more on http://factominer.free.fr/), an extension on R software, was used for multivariate analysis [32]. The metabolite distribution from the different experimental periods in relation to the hydrogen yields and co-relation circles of the major metabolites were generated and plotted.

4.3. Results and discussion

4.3.1. Effect of BM addition on hydrogen production from cheese whey

The HY, HPR and HPSI during the seven experimental periods of the 110 days reactor operation is summarized in Table 3 and Figure 1. The HY during the start-up of the reactor, i.e. during period I was higher (Figure 1a), but the production of H_2 decreased in the following days. H_2 production in experimental period II was not sustained due to the pH drop as a result of VFAs accumulation, possibly because of the increase in OLR (Figure 1b, Table 2). On the addition of buffalo manure, the stability of the H_2 production improved from 0.66 to 0.77 during experimental periods III and IV, respectively (Table 3). Similarly, the HY and HPR increased during the periods III and IV. Nonetheless, the pH showed a slightly decreasing trend during experimental period IV (Figure 1b) which might be attributed to the increase in total metabolite production in the reactor, i.e. from 20.24 mM g VS^{-1} during period III to 35.07 mM g VS^{-1} at period IV (Table 4). One of the best strategies to avoid VFAs accumulation is facilitating their removal from the reactor by decreasing the HRT without washing out the microbial biomass [33].

During experimental period V, the H_2 production decreased further when the HRT of the reactor was decreased from 12 to 8 days. This might be due to biomass wash-out which

was evident by a slight decreased fermentative activity as shown by decreased metabolic by-products yields (30.7 mM g VS^{-1}) (Table 4). Another reason for the low HY can be the sudden decrease in operational pH (4.5 ± 0.1) and increase in lactic acid production, which is not considered as a H_2 yielding DF pathway [27]. Consequently, the BM fraction in the feed was increased (Period VI, Table 2) as a strategy to increase the pH in the reactor. The H_2 production increased for a while, however, it did not last longer than 8-9 days. This might be due to the proliferation of H_2 consumers such as methanogens present in the BM [25, 34]. As a control strategy, the CHW:BM ratio was increased further (Period VII, Table 2) by decreasing the BM in the influent feed. This eventually improved the HY (131.7 ± 44.6 mL H_2 g VS^{-1}) and HPSI (0.66) (Figure 1a).
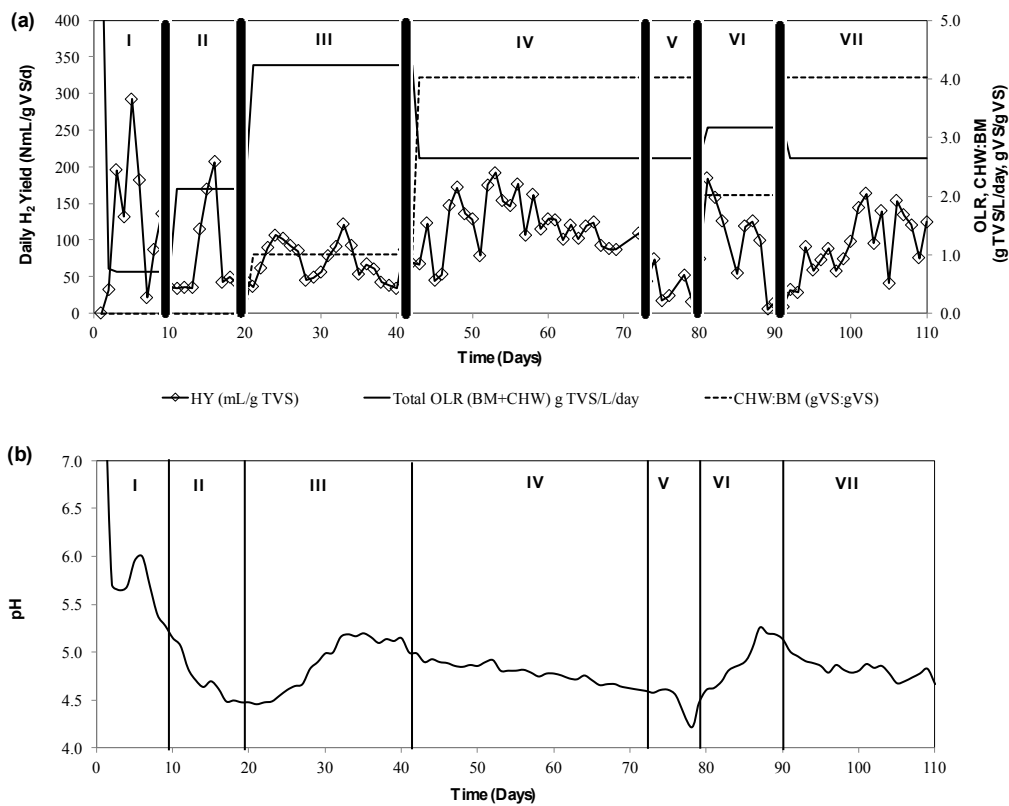
Figure 1. Daily H_2 yields (a) and pH of the reactor mixed liquor (b) during the different buffalo manure feeding strategies in a semi-continuous DF reactor using CHW as main substrate and BM as co-substrate.

Table 3. H_2 production performance during the dark fermentation at different CHW:BM ratios.

Experimental Period	CHW:BM (g VS g VS^{-1})	HY	HPR	HPSI	H_2 (%)	CO_2 (%)
I	NA	123.8 ± 85.1	73.8 ± 45.7	0.38	37.04 ± 7.0	40.13 ± 10.4
II	NA	95.3 ± 64.1	134.9 ± 90.7	0.33	46.69 ± 7.1	40.37 ± 9.6
III	1	139.8 ± 47.8	197.8 ± 67.7	0.66	51.85 ± 9.0	44.43 ± 6.7
IV	4	152.2 ± 43.9	215.4 ± 62.1	0.71	58.01 ± 4.8	39.13 ± 4.6
V	4	51.8 ± 29.3	73.4 ± 41.4	0.44	38.47 ± 12.6	27.80 ± 4.7
VI	2	76.2 ± 76.1	183.0 ± 107.7	0.41	38.38 ± 21.2	37.32 ± 12.0
VII	4	131.7 ± 44.6	186.3 ± 63.7	0.66	51.10 ± 6.3	46.34 ± 6.4

NA- Not Applicable; HY- Hydrogen Yield; HPR- Hydrogen Production Rate; HPSI- Hydrogen Production Stability Index

Table 4. Characteristics of effluents from the DF of CHW with BM as co-substrate during the different experimental periods.

Experimental Period	CHW:BM (g VS g VS^{-1})	Ammonium (mg NH$_4^+$-N L^{-1})	Alkalinity (mg CaCO$_3$ L^{-1})	pH$_{OUT}$	Lactate (mM g VS^{-1})	Ethanol (mM g VS^{-1})	Acetate (mM g VS^{-1})	Propionate (mM g VS^{-1})	Butyrate (mM g VS^{-1})	Hydrogen (mM g VS^{-1})
I	NA	157.9 ± 0.0	1019.3 ± 145.0	5.6 ± 0.3	0.00 ± 0.0	17.27 ± 4.2	21.19 ± 11.6	3.43 ± 2.9	14.80 ± 7.3	7.44 ± 4.5
II	NA	71.8 ± 0.0	337.4 ± 82.9	4.6 ± 0.1	1.42 ± 0.7	2.60 ± 0.1	9.60 ± 11.1	4.09 ± 6.5	8.99 ± 2.7	4.60 ± 3.1
III	1	389.3 ± 59.2	1327.6 ± 388.2	5.0 ± 0.2	0.69 ± 0.8	5.74 ± 1.9	2.61 ± 1.3	0.31 ± 0.2	7.51 ± 2.4	3.38 ± 1.1
IV	4	179.4 ± 34.0	1184.4 ± 373.6	4.8 ± 0.1	0.29 ± 0.5	10.45 ± 3.3	4.18 ± 2.1	0.51 ± 0.4	14.12 ± 6	5.88 ± 1.7
V	4	111.2 ± 3.6	394.5 ± 127.0	4.5 ± 0.1	2.99 ± 1.5	13.70 ± 0.0	2.20 ± 0.9	0.17 ± 0.2	9.64 ± 3.9	2.00 ± 1.1
VI	2	86.1 ± 35.9	878.6 ± 265.8	5.2 ± 0.1	1.18 ± 1.2	8.48 ± 0.8	2.10 ± 1.7	0.10 ± 0.1	6.69 ± 3.7	2.46 ± 2.4
VII	4	81.2 ± 8.2	619.7 ± 152.8	4.8 ± 0.1	1.41 ± 1.4	12.27 ± 1.7	3.28 ± 1.4	0.22 ± 0.2	10.72 ± 3.7	5.09 ± 1.7

NA- Not Applicable

4.3.2. Effect of BM addition on pH, alkalinity and ammonium concentration

The evolution of the alkalinity, ammonium and pH with time during the different BM feeding strategies are presented in Figures 1b and 2. The production of organic acids that follow the DF is responsible for decreases in the culture pH. Figure 2 shows the alkalinity and ammonium concentration during different BM feeding strategies (CHW:BM ratios). Addition of BM to the reactor resulted in an increase in alkalinity, which stabilized the culture pH during the process around 4.8 to 5.0 (Figures 1b and 2). The simultaneous production of VFAs during the two initial experimental periods (Period I and II) resulted in a decrease in culture pH. Therefore, BM was introduced along with CHW (with CHW:BM ratio equivalent to 1 g VS g VS^{-1}). The total alkalinity increased gradually during period III, which resulted in an increase in HPSI. Furthermore, increasing the CHW:BM ratio (from 1 to 4 g VS g VS^{-1}) led to an increase in HY and HPR with slight decrease in the total alkalinity. The results are in agreement with Marone et al. [13] and Tenca et al. [17], who obtained optimal H$_2$ production under the application of BM (25%-54% composition) with the readily degradable substrates, such as CHW and fruit and vegetable wastes.
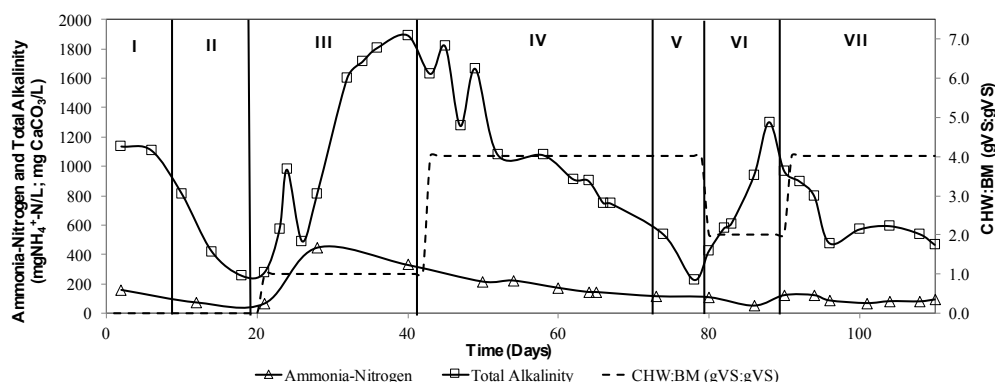
Figure 2. CHW:BM ratio and total alkalinity, and ammonium concentration during the different buffalo manure feeding strategies in the semi-continuous dark fermentation reactor.

The pH of the influent was not adjusted with any chemical buffering agent, therefore, the effluent pH can be related to the endogenous alkalinity provided by the BM. The presence of alkaline components in BM, such as bicarbonate and ammonium, may have contributed to its indigenous buffering capacity. The addition of BM containing ammonium enhances the buffering capacity of the system which can neutralize the VFAs produced [35]. The chemical reaction can be written as follows:

$$C_xH_yCOOH \leftrightarrow C_xH_yCOO^- + H^+ \tag{2}$$

$$NH_3 + H_2O \leftrightarrow NH_4^+ + OH^- \tag{3}$$

where C_xH_yCOOH represents the VFAs. On combining Equations (2) and (3), Equation (4) can be obtained as:

$$C_xH_yCOOH + NH_3 + H_2O \leftrightarrow C_xH_yCOO^- + NH_4^+ + H_2O \tag{4}$$
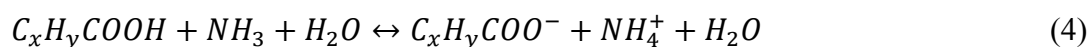
Therefore, more VFAs can be neutralized at higher ammonia concentrations allowing the stabilization of the pH. Similarly, the co-fermentation with BM allows production of VFAs without a sharp decrease in pH. The total organic acids (TAc, sum of all organic acids measured, i.e. lactic, acetic, propionic, butyric, valeric, iso-valeri, caproic, iso-caproic acids) to total alkalinity (TAk) ratio can indicate that the total acids production can be balanced by the alkaline species initially contained in the BM to maintain a suitable pH, and thus a stable H_2 production. Figure 3 gives the relationship between the TAc/TAk ratio with the HPSI. The higher HPSI was obtained at a TAc/TAk ratio of 3-4, suggesting a constant requirement of an alkalinity source to maintain a stable culture pH and H_2 production during the DF process. BM can act as co-substrate in the DF of readily degradable substrate like CHW.

Some studies have linked the improvement in H_2 production during the co-fermentation of animal waste to the maintenance of the TAc and TAk balance during the DF process [13, 17, 25]. Nonetheless, the study done by Zhang et al. [36] attributed the increase in biogas production from sorghum stem upon supplying cow manure to maintaining a suitable Carbon to Nitrogen (C/N) ratio for anaerobic digestion. In another study, Perera and Nirmalakhandan [37] reported that the H_2 production can be enhanced by manure supplementation due to the indigenous H_2 producing microorganisms present in the animal manure.

A limitation in the use of animal manure might be the need for physical or chemical pre-treatment to inhibit methanogenic activities which consume the H_2 [25, 34]. This study did not consider any pre-treatment of the BM prior to its supplementation, in contrast to the study of Marone et al. [13], who sterilized the feed before the DF. The pretreatment can affect the physico-chemical properties of the substrates as well as impact the microbiology of the BM. Another limitation in the use of BM could be the inhibition of the H_2 production due to elevated ammonium concentrations in the BM if used in a higher ratio in relation to the other co-substrate. Generally, animal manures such as swine, poultry and dairy manure have a low C/N ratio (C/N ratio of swine manure: 12.8) [38] and higher levels of ammoniacal nitrogen: cattle slurry contains

1040-1925 mg NH_4^+-N L^{-1} and poultry manure 7000-12.800 mg NH_4^+-N L^{-1} [39], which might cause inhibition of the microbial activity. Cavinato et al. [40] reported the decrease in H_2 production at a total ammoniacal nitrogen concentration higher than 2 g N L^{-1}. However, ammonium levels in this study were lower (80-390 mg NH_4^+-N L^{-1}) than the inhibitory levels reported in the literature. Therefore, ammonium inhibition will not be an issue for dark fermentative H_2 production at higher CHW:BM ratios.
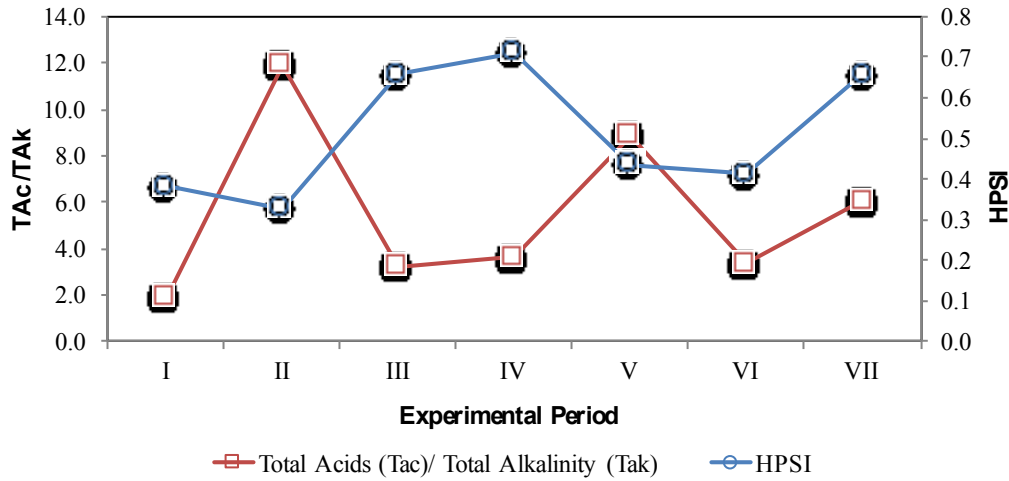
Figure 3. Total acids/Total Alkalinity ratio and HPSI during the operational periods.

4.3.3. Effect of BM addition on metabolite production

Figure 4 shows the plot of correlation circles of the six major metabolites including hydrogen. The principal component analysis of co-relation circles presented in Figure 4 suggests that the H_2 production was mainly due to the butyrate pathway (Equation (6)), which co-related well with the HY. However, the presence of acetate not always gives a good indication of H_2 producing pathways, as homoacetogens can convert the H_2 and CO_2 to acetate [41]. Unsurprisingly, other metabolites such as propionate, lactate or ethanol, which normally do not represent H_2 favorable pathways, were not well correlated. These correlations can be supported by the following equations of DF with glucose as model substrate (Equations. (5)-(9)):

$$C_6H_{12}O_6 + H_2O \rightarrow 2CH_3COOH + 2CO_2 + 4H_2 \tag{5}$$

$$C_6H_{12}O_6 \rightarrow CH_3CH_2CH_2COOH + 2CO_2 + 2H_2 \tag{6}$$

$$C_6H_{12}O_6 + 2H_2 \rightarrow 2CH_3CH_2COOH + 2H_2O \tag{7}$$

$$C_6H_{12}O_6 \rightarrow 2CH_3CH_2OH + 2CO_2 \tag{8}$$

$$C_6H_{12}O_6 \rightarrow 2CH_3CHOHCOOH \tag{9}$$
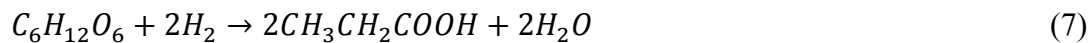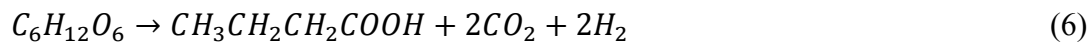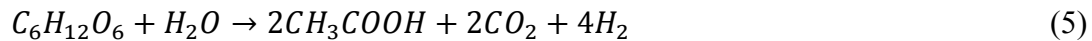
They respectively represent: acetate, butyrate, propionate, ethanol and lactate pathway derived from the theoretical glucose fermentation.

Table 4 gives the major metabolites, such as lactate, acetate, propionate, butyrate and ethanol produced during the different experimental periods. With considering the different concentrations of organic acids and alcohols present in the dark fermentation effluent, H_2 production can be related to more than one biochemical pathway. The culture pH has a profound impact on the selection and growth of fermentative microbial communities and thus their metabolic pathways (H_2 production). Therefore, it is necessary to maintain the culture pH in the DF process above the inhibitory levels of pH 4.5, which favours solventogenesis [22].
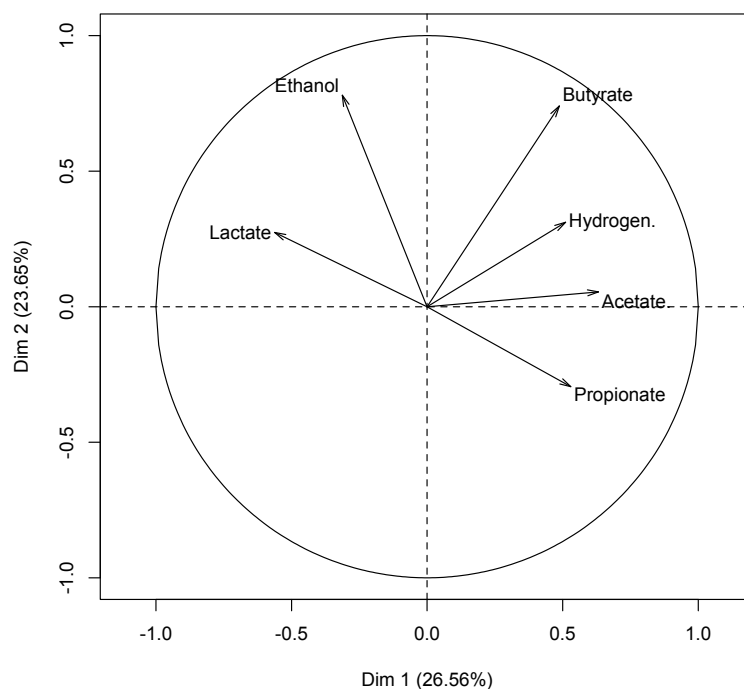
Figure 4. Correlation circle of six metabolites formed by the first two principle components Dim1 and Dim 2, representing 26.56 and 23.65 % of the total variance, respectively.

The addition of BM at experimental period III seems to reduce the propionate yields, which is generally produced at low pH and regarded as H_2 consuming pathway (Equation (7)) (Table 4). Moreover, the presence of H_2 consumers such as methanogens and homoacetogens, which might be present in the BM, can utilize H_2 and thus negatively influence the HY. Nonetheless, the acidic culture pH range applied in this study (4.5-5.6) suggests that this pH range is sufficient to suppress the activity of methanogens, as methane production drops sharply at a pH lower than 6.3 [42]. The addition of BM may thus have influenced the metabolite production in three ways: i) a

buffering action of BM that aided in maintaining a pH that shaped the microbial community of H_2 producers, ii) directly influencing the microbial community in the DF reactor through the microorganisms present in BM and iii) the addition of micro-nutrients (trace elements such as Fe, Zn, Ca) and macro-nutrients (such as Nitrogen-N, phosphorous-P, and potassium-K) that are beneficial to microbial growth and metabolism [10]. Thus, besides being used as buffering agent, BM might also be a source of nutrients for enhancing H_2 production.

4.4. Conclusions

DF of substrates with an acidic pH is challenging due to the sharp pH decrease following the co-production of organic acids during the DF process. Along-term continuous production of H_2 has been demonstrated in this work using the addition of BM to CHW.A HY of 152.2 (± 43.9) mL H_2 g VS^{-1} was obtained with a HPSI of 0.71 when the CHW to BM ratio was 4 g VS g VS^{-1} (Experimental Period IV). BM characterized by a higher alkalinity can be applied as co-substrate for maintaining an operable pH during the DF process around 4.8-5. Therefore, addition of BM can aid in providing stability of the continuous dark fermentative H_2 production and removing the dependency on chemical buffering agents. Hence, co-fermentation of CHW with BM or other locally available feedstock sources can give economic sustainability to scaled-up applications of DF processes.

References

[1] De Gioannis, G., Friargiu, M., Massi, E., Muntoni, A., Polettini, A., Pomi, R., 2014. Biohydrogen production from dark fermentation of cheese whey: influence of pH. International Journal of Hydrogen Energy, 39, pp.20930-20941.

[2] Eurostat. Agricultural products - statistics explained. 2013.

[3] Venetsaneas, N., Antonopoulou, G., Stamatelatou, K., Kornaros, M., Lyberatos, G., 2009. Using cheese whey for hydrogen and methane generation in a two-stage continuous process with alternative pH controlling approaches. Bioresource technology, 100(15), pp.3713-3717.

[4] Carvalho, F., Prazeres, A.R., Rivas, J., 2013. Cheese whey wastewater: characterization and treatment. Science of the Total Environment, 445, pp.385-396.

[5] Cantrell, K.B., Ducey, T., Ro, K.S., Hunt, P.G., 2008. Livestock waste-to-bioenergy generation opportunities. Bioresource Technology, 99(17), pp.7941-7953.

[6] Monlau, F., Barakat, A., Trably, E., Dumas, C., Steyer, J.P., Carrère, H., 2013. Lignocellulosic materials into biohydrogen and biomethane: impact of structural features and pretreatment. Critical Reviews in Environmental Science and Technology, 43(3), pp.260-322.

[7] Yasin, N.H.M., Mumtaz, T., Hassan, M.A., 2013. Food waste and food processing waste for biohydrogen production: a review. Journal of Environmental Management, 130, pp.375-385.

[8] Azwar, M.Y., Hussain, M.A., Abdul-Wahab, A.K., 2014. Development of biohydrogen production by photobiological, fermentation and electrochemical processes: a review. Renewable and Sustainable Energy Reviews, 31, pp.158-173.

[9] Guo, X.M., Trably, E., Latrille, E., Carrere, H., Steyer, J.P., 2010. Hydrogen production from agricultural waste by dark fermentation: a review. International Journal of Hydrogen Energy, 35(19), pp.10660-10673.

[10] Ghimire, A., Frunzo, L., Pirozzi, F., Trably, E., Escudie, R., Lens, P.N.L., Esposito, G., 2015. A review on dark fermentative biohydrogen production from organic biomass: process parameters and use of by-products. Applied Energy, 144, pp.73-95.

[11] Teli, A., Ficara, E., Malpei, F., 2014. Bio-hydrogen production from cheese whey by dark fermentation. Chemical Engineering Transactions, 37, pp.613-618.

[12] Moreno, R., Escapa, A., Cara, J., Carracedo, B., Gómez, X., 2015. A two-stage process for hydrogen production from cheese whey: integration of dark

fermentation and biocatalyzed electrolysis. International Journal of Hydrogen Energy, 40(1), pp.168-175.

[13] Marone, A., Varrone, C., Fiocchetti, F., Giussani, B., Izzo, G., Mentuccia, L., Rosa, S., Signorini, A., 2015. Optimization of substrate composition for biohydrogen production from buffalo slurry co-fermented with cheese whey and crude glycerol, using microbial mixed culture. International Journal of Hydrogen Energy, 40(1), pp.209-218.

[14] Perera, K.R.J., Nirmalakhandan, N., 2011. Evaluation of dairy cattle manure as a supplement to improve net energy gain in fermentative hydrogen production from sucrose. Bioresource Technology, 102(18), pp.8688-8695.

[15] Marone, A., Izzo, G., Mentuccia, L., Massini, G., Paganin, P., Rosa, S., Varrone, C., Signorini, A., 2014. Vegetable waste as substrate and source of suitable microflora for bio-hydrogen production. Renewable Energy, 68, pp.6-13.

[16] Parawira, W., Murto, M., Read, J.S., Mattiasson, B., 2005. Profile of hydrolases and biogas production during two-stage mesophilic anaerobic digestion of solid potato waste. Process Biochemistry, 40(9), pp.2945-2952.

[17] Tenca, A., Schievano, A., Perazzolo, F., Adani, F., Oberti, R., 2011. Biohydrogen from thermophilic co-fermentation of swine manure with fruit and vegetable waste: maximizing stable production without pH control. Bioresource Technology, 102(18), pp.8582-8588.

[18] Lateef, S.A., Beneragama, N., Yamashiro, T., Iwasaki, M., Ying, C., Umetsu, K., 2012. Biohydrogen production from co-digestion of cow manure and waste milk under thermophilic temperature. Bioresource Technology, 110, pp.251-257.

[19] Zhang, Z., Zhang, G., Li, W., Li, C., Xu, G., 2016. Enhanced biogas production from sorghum stem by co-digestion with cow manure. International Journal of Hydrogen Energy, 41(21), pp.9153-9158.

[20] Esposito, G., Frunzo, L., Giordano, A., Liotta, F., Panico, A., Pirozzi, F., 2012. Anaerobic co-digestion of organic wastes. Reviews in Environmental Science and Bio/Technology, 11(4), pp.325-341.

[21] Redzwan, G., Banks, C.J., 2010. Supplementation of ammonium bicarbonates for the treatment of fruit cordial wastewater by anaerobic digestion process. Anaerobe, 16(1), pp.34-37.

[22] Khanal, S.K., Chen, W.H., Li, L., Sung, S., 2004. Biological hydrogen production: effects of pH and intermediate products. International Journal of Hydrogen Energy, 29(11), pp.1123-1131.

[23] Gottardo, M., Cavinato, C., Bolzonella, D., Pavan, P., 2013. Dark fermentation optimization by anaerobic digested sludge recirculation: effects on hydrogen production. Chemical Engineering Transactions, 32, pp.997-1002.

[24] Choi, J., Ahn, Y., 2014. Characteristics of biohydrogen fermentation from various substrates. International Journal of Hydrogen Energy, 39(7), pp.3152-3159.

[25] Wu, X., Zhu, J., Dong, C., Miller, C., Li, Y., Wang, L., Yao, W., 2009. Continuous biohydrogen production from liquid swine manure supplemented with glucose using an anaerobic sequencing batch reactor. International Journal of Hydrogen Energy, 34(16), pp.6636-6645.

[26] Ghimire, A., Frunzo, L., Pontoni, L., d'Antonio, G., Lens, P.N., Esposito, G., Pirozzi, F., 2015. Dark fermentation of complex waste biomass for biohydrogen production by pretreated thermophilic anaerobic digestate. Journal of Environmental Management, 152, pp.43-48.

[27] Ghimire, A., Valentino, S., Frunzo, L., Trably, E., Escudié, R., Pirozzi, F., Lens, P.N.L., Esposito, G., 2015. Biohydrogen production from food waste by coupling semi-continuous dark-photofermentation and residue post-treatment to anaerobic digestion: a synergy for energy recovery. International Journal of Hydrogen Energy, 40(46), pp.16045-16055.

[28] Noguerol-Arias, J., Rodríguez-Abalde, A., Romero-Merino, E., Flotats, X., 2012. Determination of chemical oxygen demand in heterogeneous solid or semisolid samples using a novel method combining solid dilutions as a preparation step followed by optimized closed reflux and colorimetric measurement. Analytical Chemistry, 84(13), pp.5548-5555.

[29] DuBois, M., Gilles, K.A., Hamilton, J.K., Rebers, P.T., Smith, F., 1956. Colorimetric method for determination of sugars and related substances. Analytical Chemistry, 28(3), pp.350-356.

[30] Bligh, E.G., Dyer, W.J., 1959. A rapid method of total lipid extraction and purification. Canadian Journal of Biochemistry and Physiology, 37(8), pp.911-917.

[31] Federation, W.E., American Public Health Association, 2005. Standard methods for the examination of water and wastewater. American Public Health Association (APHA): Washington, DC, USA.

[32] Lê, S., Josse, J., Husson, F., 2008. FactoMineR: an R package for multivariate analysis. Journal of Statistical Software, 25(1), pp.1-18.

[33] Scoma, A., Bertin, L., Fava, F., 2013. Effect of hydraulic retention time on biohydrogen and volatile fatty acids production during acidogenic digestion of dephenolized olive mill wastewaters. Biomass and Bioenergy, 48, pp.51-58.

[34] Cheong, D.Y., Hansen, C.L., 2006. Bacterial stress enrichment enhances anaerobic hydrogen production in cattle manure sludge. Applied Microbiology and Biotechnology, 72(4), p.635.

[35] Zhang, C., Xiao, G., Peng, L., Su, H., Tan, T., 2013. The anaerobic co-digestion of food waste and cattle manure. Bioresource Technology, 129, pp.170-176.

[36] Zhang, Z., Zhang, G., Li, W., Li, C., Xu, G., 2016. Enhanced biogas production from sorghum stem by co-digestion with cow manure. International Journal of Hydrogen Energy, 41(21), pp.9153-9158.

[37] Perera, K.R.J., Ketheesan, B., Gadhamshetty, V., Nirmalakhandan, N., 2010. Fermentative biohydrogen production: evaluation of net energy gain. International Journal of Hydrogen Energy, 35(22), pp.12224-12233.

[38] Yin, D., Liu, W., Zhai, N., Yang, G., Wang, X., Feng, Y., Ren, G., 2014. Anaerobic digestion of pig and dairy manure under photo-dark fermentation condition. Bioresource Technology, 166, pp.373-380.

[39] Callaghan, F.J., Wase, D.A.J., Thayanithy, K., Forster, C.F., 2002. Continuous co-digestion of cattle slurry with fruit and vegetable wastes and chicken manure. Biomass and Bioenergy, 22(1), pp.71-77.

[40] Cavinato, C., Giuliano, A., Bolzonella, D., Pavan, P., Cecchi, F., 2012. Bio-hythane production from food waste by dark fermentation coupled with anaerobic digestion process: a long-term pilot scale experience. International Journal of Hydrogen Energy, 37(15), pp.11549-11555.

[41] Guo, X.M., Trably, E., Latrille, E., Carrere, H., Steyer, J.P., 2014. Predictive and explicative models of fermentative hydrogen production from solid organic waste: role of butyrate and lactate pathways. International Journal of Hydrogen Energy, 39(14), pp.7476-7485.

[42] Li, C., Fang, H.H., 2007. Fermentative hydrogen production from wastewater and solid wastes by mixed cultures. Critical Reviews in Environmental Science and Technology, 37(1), pp.1-39.

Chapter 5

Preliminary study on the adoption of dark fermentation as pretreatment for a sustainable hydrothermal denaturation of cement-asbestos composites

Preliminary study on the adoption of dark fermentation as pretreatment for a sustainable hydrothermal denaturation of cement-asbestos composites

A harmless cement conglomerate reinforced with glass fibers (GFC), simulating a cement-asbestos composite (CAC), was dissolved into dark fermentation (DF) synthetic and real effluents. The experimental campaign carried out with synthetic DF effluents showed a strong diffusional resistance to volatile fatty acids (VFAs) migration through GFC. However, at the end of the dissolution phase in real DF effluents, a complete dissolution of the GFC cement phase and a final pH equal to 4.71 were achieved by the use of GFC grain size lower than 1.0 mm, GFC load equal to $5.0 \cdot 10^3$ ppm, and glucose as biodegradable substrate. Moreover, during the DF process a whole production of 284 mmol H_2 L_{sol}^{-1} was obtained.

This investigation represents a preliminary study on the denaturation of CAC, by a DF and hydrothermal treatment train, as promising alternative to the landfilling. Indeed, hydrothermal denaturation of CAC requires, as reported in previous studies, severe and expensive operational conditions and remarkable acid consumption to dissolve the cement matrix. On the other hand, the DF of bio-degradable compounds results in the production of rich in VFAs solutions, which could be used for CAC pretreatment leading to the cement matrix dissolution, and generates bio-hydrogen as a renewable energy source for the hydrothermal phase.

5.1. Introduction

CAC have been widely used in the last decades in the construction industry because of the low thermal conductivity, high mechanical strength and low cost [1]. However, strong concern about health hazards associated with asbestos were described since the 1960s [2]. For this reason, the management of asbestos-containing waste (ACW) is a topic that is increasingly concerned with the scientific community [3, 4]. In Italy, the amount of ACW is approximately $30 \cdot 10^6$ t, i.e. $18 \cdot 10^6$ m^3, of which ~$8 \cdot 10^6$ m^3 are asbestos [5]. Since ACWs induce unacceptable sanitary risk, the Italian legislation [6] considers all ACW as hazardous materials and requires their encapsulation before disposal in agreement with the European Waste Catalogue code 170605 [7].

On the other hand, asbestos contained in ACW is persistent. As a result, if a controlled landfill gets damaged, asbestos fibers may be released in the environment with a

consequent contamination of superficial and deep waters and the surrounding atmosphere [8]. Moreover, the reduction of waste to be landfilled is generally accepted [9, 10]. For this reason, recent studies have been devoted to alternative ACW treatments aimed to the denaturation of the asbestos fibers or their conversion in non-harmful compounds. Specifically, high energy milling operations [11] or thermal treatments at temperatures leading to composites vitrification [12, 13] have been proposed. In particular, the treatment of ACWs is already carried out in industrial plants, as Inertam and GeoMelt®, through processes which lead to the asbestos vitrification by means of plasma guns or Joule vitrification. The Inertam, installed in France, treats about $7 \cdot 10^3$ t ACW per year with a cost ranging between $1.0 \cdot 10^3$ -$2.5 \cdot 10^3$ € t^{-1}, not including removal and transportation costs, and produces $4 \cdot 10^3$-$6 \cdot 10^3$ t of a stony material (Cofalit) per year. The latter is sold for 10 € t^{-1} as a substitute of quartz and basalt in building materials [14, 15]. Moreover, the GeoMelt® treatment plant, built in Japan, effectively destroys the asbestos fibers and reduces the volume by approximately 80% with respect to the initial ACW volume (consequently, the landfilling of the end-product is cheaper and more sustainable). In particular, 3 t of ACW were treated within 44 h with a max melt temperature of 1565 °C and a process efficiency equal to 0.91 kW kg^{-1} [16]. However, the drawback that makes these processes economically disadvantageous to landfilling consists in the high energy consumption because the vitrification of these wastes occurs at 1600 °C. In alternative, some treatments, which require lower temperatures, were proposed [17, 18, 19]. For instance, it has been reported that chrysotile fibers deriving from a Greek mine were successfully converted into crystals of forsterite and silicates (1) within 3.0 h of hydrothermal treatment carried out at 700 °C and 2.25 MPa [20].

$$2Mg_3Si_2O_5(OH)_4 \rightarrow 3Mg_2SiO_4 + 2SiO_2 + 4H_2O \tag{1}$$
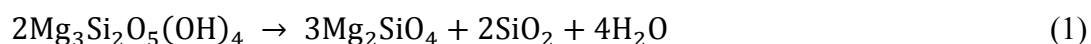
Forsterite crystals were also obtained after 13 min microwave treatment of pure serpentine asbestos used for building insulation [8]. Similarly, it was reported that a 12 min microwave treatment at temperature exceeding 1000 °C succeeded in asbestos fibers denaturing [21]. The main drawback related to these processes is their energetic demand. Consequently, hydrothermal treatments carried-out at low temperature (100 °C) in presence of an aqueous phase containing 5.0 N sulfuric acid have been proposed for the treatment of cement-asbestos composites (CAC) [22]. In this context, it was reported that the thermo-chemical digestion of the chrysotile phase by sulfuric acid

occurs by diffusion of hydrogen ions, followed by crystal surface attack. As a result, magnesium ions and silica are extracted from asbestos structure (2) [23, 24, 25].

$$Mg_3Si_2O_5(OH)_4 + 3H_2SO_4 \rightarrow 3Mg^{2+} + 3SO_4^{2-} + 2SiO_2 + 5H_2O \qquad (2)$$
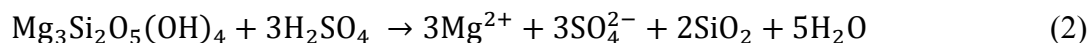
Higher sulfuric acid consumption occurs in asbestos cement composites as respect to stoichiometric reaction. Indeed, these conglomerates are rich in portlandite (Ca(OH)$_2$), calcium carbonate (CaCO$_3$) (3) and calcium silicates which may compete with asbestos in the reaction with sulfuric acid [26].

$$CaCO_3 + H_2SO_4 \rightarrow Ca^{2+} + SO_4^{2-} + CO_2 + H_2O \qquad (3)$$
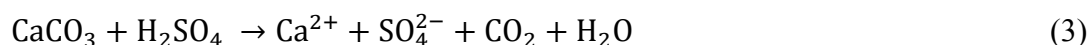
In order to limit the consumption of expensive acids, an innovative bio-chemical process has been recently proposed [27]. By this treatment, a strong dissolution of the CAC cement phase is obtained due to the lactic acid deriving from the metabolic activity of *Lactobacillus casei* and/or *Lactobacillus plantarum* on exhausted milk whey, thus achieving a pH close to the optimal conditions (1< pH < 3) for further hydrothermal treatment. This process is still economically disadvantageous as compared to the disposal of CAC in controlled landfills although: a) a waste material is used (exhausted milk whey); b) very small amounts of organic acids (lactic or oxalic acid) need to be added at the end of the fermentative phase; c) the by-products of the process are reusable and marketable. In fact, even if the operating conditions of the hydrothermal phase are mild (T = 120-150 °C, P = 5-20 bar), most of the costs is still due to energy consumption.

The biological phase of the above mentioned process could be substituted by DF of carbon rich waste biomasses, which is an innovative anaerobic biological treatment leading to the prevalent production of bio-hydrogen and organic acids [28, 29]. The acidity resulting in the effluents from DF process is due to the conversion of the bio-degradable organic compounds in volatile fatty acids (VFAs), such as acetic, propionic and butyric acid [30, 31]. As shown before, the hydrothermal treatments of CAC have been already studied and have proved their effectiveness in treating these wastes by consuming large amount of acids and energy.

The aim of this study is to investigate the dissolution of the cement matrix of a glass-fiber conglomerate (GFC), simulating a CAC, by the use of DF synthetic and real effluents. Specifically, the influence of different operational conditions as GFC grain size range and load, VFAs type and concentration and temperature was investigated

with DF synthetic effluents. Afterwards, a real DF process for glucose conversion was carried out with the aim of using the effluents to dissolve the cement matrix of GFC and quantify the H_2 produced during the whole process. This investigation represents a preliminary study on the denaturation of CAC, by a combined DF and hydrothermal treatment system, as alternative to the disposal in controlled landfills. Specifically, in order to reduce the costs of CAC hydrothermal denaturation, the DF of bio-degradable waste biomasses in presence of CAC could be adopted as a promising pretreatment. Indeed, it produces an acidic liquid effluent useful for the dissolution of the CAC cement matrix, leading to a reduction of the costs related to the acid consumption, and contextually generates bio-hydrogen which could be used during the hydrothermal phase as a renewable, cheap and clean energy source (Figure 1). Moreover, the effluent of the hydrothermal phase, rich in VFAs, could be stabilized and valorized by other biological processes such as photofermentation [32], microbial electrolysis cells [33] or anaerobic digestion [34], generating a secondary source of biogas containing CH_4 or H_2.
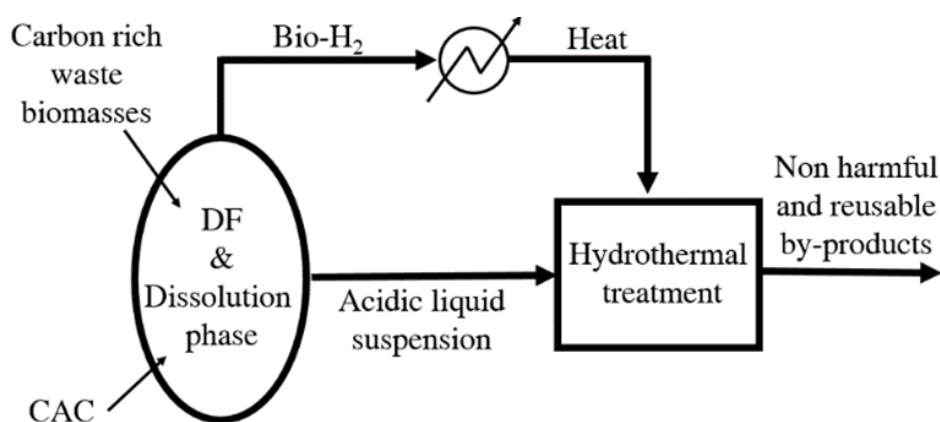
Figure 1. Scheme of the proposed process.

5.2. Materials and methods

5.2.1. Materials

CEM II A-LL 42.5 R, a Portland cement with limestone and high early strength, provided by Buzzi Unicem [35] was used for the preparation of cement conglomerates. The main constituents are: 80-94% clinker, 6-20% limestone LL (< 0.2% organic carbon), gypsum (0-5%), and minor additional constituents. The soda-lime glass fibers

used for the preparation of GFC were obtained from a glass wool roll and are characterized by a diameter and the length in the range of 1-10 μm and 10^2-10^3 μm.

HPLC grade methanol and acetonitrile were purchased from Carlo Erba (www.carloerbareagents.com/en/). H_2SO_4 (98%), anhydrous glucose (99.5%), acetic acid (> 99.7%), propionic acid (> 99.5%), butyric acid (> 99%) were purchased from Sigma Aldrich (www.sigmaaldrich.com). In particular, both Carlo Erba and Sigma Aldrich are specialized in the sales of chemical laboratory reagents. All reagents and organic solvents were used as received.

In all the experiments, distilled water was used as solvent.

In accordance with the study of Yeshanew et al. [36], the digestate used for the preparation of DF inoculum was collected from the mesophilic wet anaerobic digestion (AD) plant of the dairy farm "Davide Colangelo" located in Capaccio (Salerno, Italy). In particular, the total solids (TS), volatile solids (VS) and the pH of the AD sludge were equal to 50.75 g L^{-1}, 27.90 g L^{-1} and 7.7 respectively. The Ca^{2+} concentration was equal to 824 ppm, and no VFAs were detected.

5.2.2. Preparation of cement-glass composite and control

70 g of soda-lime glass wool were dipped in 2.0 L of distilled water. The resulting suspension was whipped with the aim of reducing the size of the glass fibers in order to improve the mixing with the cement. Then, it was filtered and placed in oven for 12 h at 108 °C. Afterwards, the glass fibers (approximately 67.3 g) were added to 650 g of cement and introduced into a vessel with hermetic closure; after 15 min shaking, the mixture was added to 325 mL of water and mixed with the Hobart normalized mixer (USA) [6]. The fibers were added to mortar formulation ($10\%_{w/w}$) as total replacement of asbestos fibers, which represent the 8-16%$_{w/w}$ of a conventional CAC [37]. For comparison, a cement paste specimen was prepared as control with the aim of quantify the final concentration of the glass fiber in the aged GFC. Tap water was used and the water/cement ratio was kept constant at 0.5.

Samples were shaped in the form of cylinders (diameter = 150 mm; height = 10 mm) and aged for 28 d at T = 20 ± 2 °C and relative humidity exceeding 90%, followed by final stabilization at room temperature. The dried material was successively crushed and sieved in granulometric classes in order to study the influence of the grain size on the dissolution phase. In this context, the grains were classified as follows:

- C1: d < 1.0 mm;

- C2: 1.0 mm < d < 1.4 mm;

- C3: 1.4 mm < d < 2.0 mm;

- C4: d > 2.0 mm.

5.2.3. Experimental set-up

5.2.3.1.   GFC dissolution experimental apparatus

A six position magnetic stirrer with integrated thermostat probes was used for the experimental campaign. To the purpose, different loads of GFC were suspended in 250 mL aqueous solutions of acetic acid (AcA), propionic acid (PrA), and butyric acid (BrA), then stirred at 370 rpm. The GFC suspensions were placed into a 300 mL flasks. The cap of each flask was perforated to introduce a thermostat probe and a 2.0 mm Teflon tube for the withdrawal, at different reaction times, of the samples through a 5 mL syringe. The liquid samples were filtered with a 0.22 μm regenerate cellulose syringe filters (Whatman) and rapidly analyzed to determinate the Ca^{2+} ion concentrations.

5.2.3.2.   AFBR configuration and operation

The inoculum of DF tests was obtained after a thermal pretreatment phase of the anaerobic digestion sludge. The inhibition of methanogenic bacteria was obtained by treating the digestate in oven for 1 h at 105 °C [38].

200 mL of inoculum, 200 mL distilled water and 14 g of glucose (35 g L^{-1}) were added into an air tight 500 mL transparent borosilicate glass bottle GL 45 (Shott Duran, Germany). By this way, the substrate to inoculum ratio (F/M) was close to 2.6 (g COD substrate/g VS inoculum). This procedure was applied to five different DF reactors and, before closing the bottles, 0.5 h nitrogen purge was carried out with the aim of ensuring anaerobic conditions. Afterwards, the batch reactors were quickly closed with air tight caps equipped with two sampling pipes for the collection of liquid and gaseous samples. Specifically, the gas-sampling pipe of each batch bioreactor was connected to a 2 L eudiometer, which allowed for the measurement of the biogas volume and the withdrawal of gaseous samples. Each batch bioreactor was immersed into a thermostatic bath at 35 ± 1 °C and magnetically stirred at 370 rpm. Once the production

of hydrogen reached the plateau, the caps were removed and, under nitrogen atmosphere, GFC samples and glucose were suspended into the solutions.

5.2.4. Analytical methods

The concentration of Ca^{2+} ions dissolved in water was evaluated through atomic adsorption spectrometry (AAS) using a Varian Model 55B SpectrAA (F-AAS) equipped with a flame (acetylene/air) and a deuterium lamp for background correction. Biogas composition was characterized by a Varian Star 3400 gas chromatograph equipped with Shin-Carbon ST 80/100 column and a thermal conductivity detector. Argon was used as carrier gas with 1.4 bar front and rear end pressure. The analysis lasted 15 min.

The VFA concentrations were quantified by high pressure liquid chromatography (HPLC) (Dionex LC 25 Chromatography Oven) equipped with a Synergi 4u Hydro-RP 80A (size 250 x 4.60 mm) column and UV detector (Dionex AD25 Absorbance Detector). According to Luongo et al. [39], the isocratic elution consisting of 20% methanol and 10% acetonitrile in 5 mM H_2SO_4 solution was pumped at a rate of 0.9 mL min^{-1} by the use of a Dionex GP 50 Gradient pump. The elution time was 18.5 min. Cement-based conglomerates were characterized by scanning electron microscope (SEM), energy dispersive X-ray (EDX), thermogravimetric (TGA), and X-ray diffraction (XRD) analysis. Specifically, in the case of SEM and EDX analysis, used to have magnified images and the elemental composition of the samples, an electron microscope FESEM-EDX Carl Zeiss Sigma 300 VP was used. The samples were fixed on aluminum stubs and then sputtered with gold by the use of a Sputter Quorum Q150. TGA analysis were carried-out by the use of a Perkin-Elmer Pyris 1 thermogravimetric analyzer, which has been used to characterize the samples composition through analysis of characteristic thermal decomposition patterns. Specifically, the samples were heated under air streaming (30 ml min^{-1}) from 50 °C to 800 °C at a rate of 10 °C min^{-1}. XRD analysis, used for determining the atomic and molecular structure of the crystals in the samples as function of the diffraction of incident X-rays into specific directions. XRD analysis were performed with a Philips PW1710 diffractometer operating in the range of 5 °2θ - 60 °2θ with a Cu Kα radiation (λ = 1.54056 nm).

Total solids and volatile solids were measured according to standard methods [40]. The pH of the solution was monitored with a Hanna Instruments HI 98190 pH/ORP pH-meter.

5.3. Results and discussion

5.3.1. Characterization of the cement conglomerates

Scanning Electron Microscope (SEM) micrographs of the cement conglomerates and bare aggregates are reported in figure 2. Specifically, figure 2 (a, b) shows cement paste features, figure 2 (c, d) shows the glass fibers structure, while GFC morphology can be observed in figure 2 (e, f). The latter images are very similar to those of an asbestos containing cement composite although it can be observed a more fibrous appearance of chrysotile which leads to sanitary risk in all natural compartments including man [18].
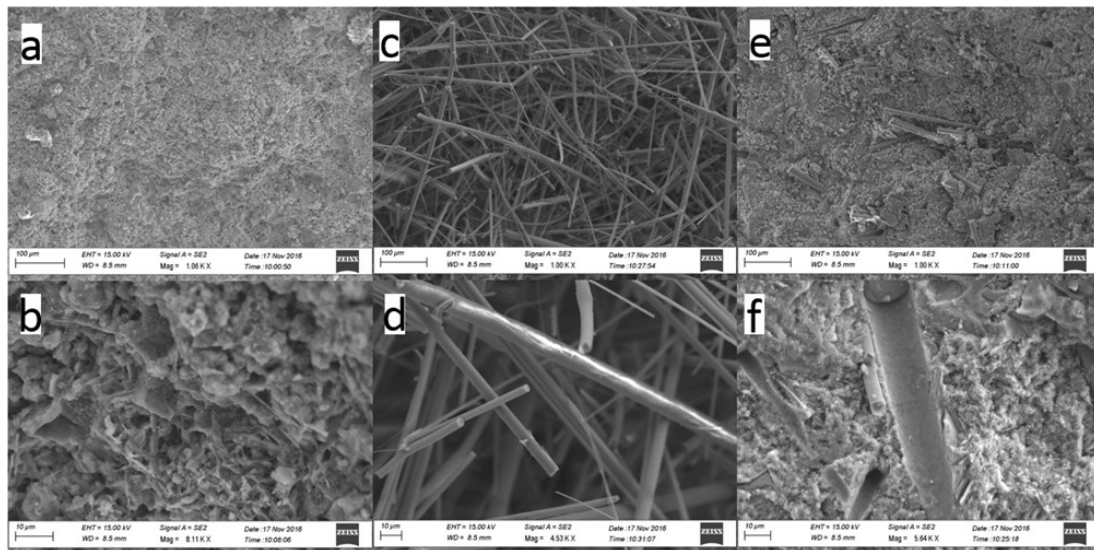
Figure 2. SEM images of: cement paste (a, b), glass fibers (c, d), and GFC (e, f).

EDX analysis of the cement specimens and glass fibers were also carried-out (Table 1). Cement paste and GFC show a prevalence of elements such as oxygen, calcium, silicon and carbon because of the high content of hydrated calcium silicates (C-S-H), portlandite ($Ca(OH)_2$) and calcium carbonate ($CaCO_3$). Specifically, it can be observed that GFC shows a decrease of calcium concentration, approximately $8\%_{w/w}$. Considering that the content of calcium present in the glass fibers is about $5.2\%_{w/w}$, it is possible to state that the content of glass fibers in the GFC is approximately $10\%_{w/w}$, result confirmed by the ratio between glass fibers (67.3 g) and cement (650 g) adopted during the preparation of the sample. This consideration is also supported by an increase of silicon concentration in GFC with respect to the cement paste. In addition, an increase of the sodium concentration in the GFC was observed. This result is ascribed to sodium oxide (Na_2O) present in the glass fibers, obtained by thermal decomposition of sodium carbonate (Na_2CO_3) as glass raw material.

Table 1. EDX analysis of the cement paste, glass fibers and GFC.

Element	Cement paste (g kg^{-1})	Glass fibers (g kg^{-1})	GFC (g kg^{-1})	Solid residue (g kg^{-1})
C	55	-	50	-
O	495	554	502	474
Na	6	77	12	33
Mg	5	16	6	6
Al	14	8	12	-
Si	52	319	77	446
K	9	2	3	2
Ca	353	52	322	19
Fe	10	-	13	11
Br	2	-	4	10
Mn	-	2	-	-

The diffractograms of cement paste and composite (Figure 3a) show the presence of portlandite (18 °2θ; 29 °2θ; 34 °2θ; 47.5 °2θ; 51 °2θ), calcium carbonate (29.5 °2θ) and alite and/or belite (32.1 °2θ; 32.8 °2θ, 40 °2θ). The presence of these compounds, confirmed by EDX analysis, is in agreement with the results obtained by Kontoleontos et al. [41].

The results of the thermogravimetric analysis show three distinct weight losses (Figure 3b). The first, between 45 °C and 150 °C, is ascribed to water evaporation. The second weight loss, approximately 1.1%$_{w/w}$ and 1.7%$_{w/w}$ for the cement paste and the GFC, is observed at 425°C and is due to portlandite dehydration (4).

$$Ca(OH)_2 \rightarrow CaO + H_2O \tag{4}$$

The third and final weight loss (450-700 °C), approximately 19.7%$_{w/w}$ and 14.9%$_{w/w}$ for the cement paste and the GFC, is ascribed to the slow thermal decomposition of calcium carbonate into calcium oxide and CO_2 (5).

$$CO_3 \rightarrow CaO + CO_2 \tag{5}$$
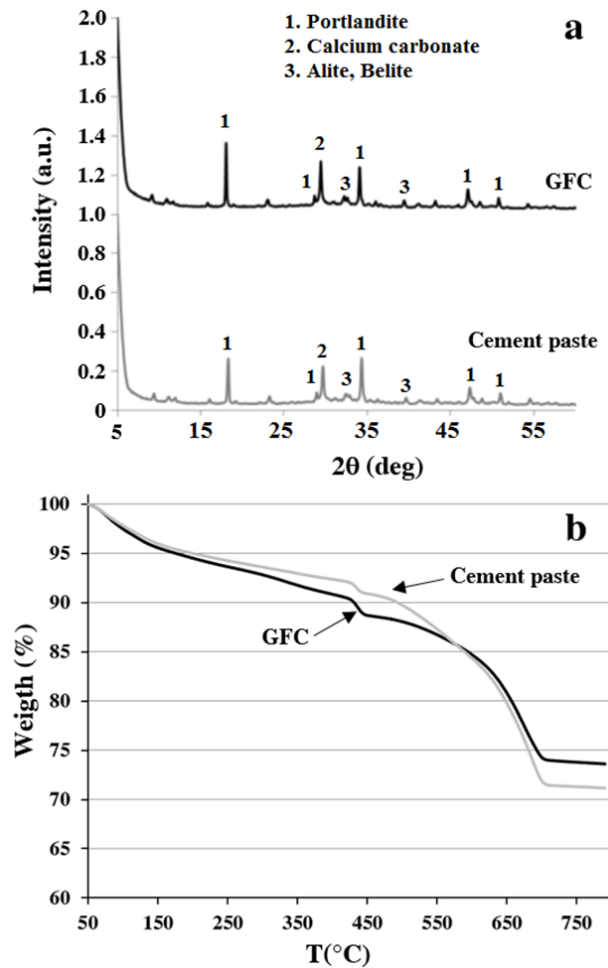
Figure 3. XRD (a) and TGA (b) analysis of the cement paste and GFC.

These results, according to what previously reported [42], confirm XRD analysis about the presence of portlandite and calcium carbonate.

For this reasons, GFC can be considered a good succedaneum of a CAC containing 10%$_{w/w}$ of asbestos fibers, such as Eternit, in terms of preparation protocol and chemico-mineralogical characteristics [37].

5.3.2. Dissolution of GFC by DF simulated solutions

Ca^{2+} equilibrium concentrations ($[Ca^{2+}]_{eq}$), normalized to Ca^{2+} theoretical concentrations ($[Ca^{2+}]_t$), were analyzed in presence of different single VFAs at increasing concentrations. Specifically, 1200 ppm of GFC (d <1.0 mm) were suspended into the acidic solutions. By considering the calcium amount in GFC (32%$_{w/w}$), the $[Ca^{2+}]_t$ added in each solutions was equal to 9.6 mM. Once the equilibrium was attained, after 48 h contact time, an increase of VFAs initial concentration resulted in an increase of $[Ca^{2+}]_{eq}$ normalized concentration. In particular, for the specific VFA concentrations

(AcA, PrA and BuA) close to 20 mM, more than 90% of the calcium contained in the GFC was released in the solution. On the other hand, VFA concentrations exceeding 25 mM resulted in a complete calcium dissolution. Consequently, it can be concluded that calcium is present in solution as acetate, propionate and butyrate, as described by the following equilibria:

$$CH_3COOH_L \leftrightarrow CH_3COO_L^- + H^+ \tag{6}$$

$$CH_3CH_2COOH_L \leftrightarrow CH_3CH_2COO_L^- + H^+ \tag{7}$$

$$CH_3CH_2CH_2COOH_L \leftrightarrow CH_3CH_2CH_2COO_L^- + H^+ \tag{8}$$

$$Ca_S^{2+} + 2CH_3COO_L^- \leftrightarrow Ca(CH_3COO)_{2,L} \tag{9}$$

$$Ca_S^{2+} + 2CH_3CH_2COO_L^- \leftrightarrow Ca(CH_3CH_2COO)_{2,L} \tag{10}$$

$$Ca_S^{2+} + 2CH_3CH_2CH_2COO_L^- \leftrightarrow Ca(CH_3CH_2CH_2COO)_{2,L} \tag{11}$$
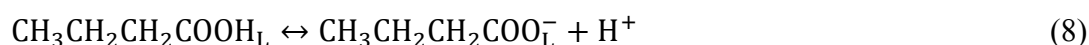
As reported in equilibria 9-11, the stoichiometric concentration of the VFAs for a complete dissolution of calcium present in 1200 ppm of GFC was approximately 19.2 mM. This value is very close to what experimentally determined.

Figure 4 shows the effect of GFC load in the range of 0–4800 ppm, constant VFA concentration (63 mM). When GFC was added to the VFA solutions at the load of 4800 ppm ($[Ca^{2+}]_t$ = 38.4 mM), the highest dissolved calcium concentration was approximately 30 mM. On the other hand, all the calcium was dissolved within 48 h for GFC loads lower than 3600 ppm. These results confirmed the stoichiometry of equilibria 9-11, but evidenced the highest dissolution rate operated by AcA. The differences among the tested VFAs in the calcium dissolution rates may be ascribed to the different dimensions of the acids. In fact, the BuA and AcA show the highest and lowest steric hindrance. Consequently, AcA tends to penetrate into the GFC smallest pores faster than BuA, with a resulting best performance in terms of calcium dissolution.
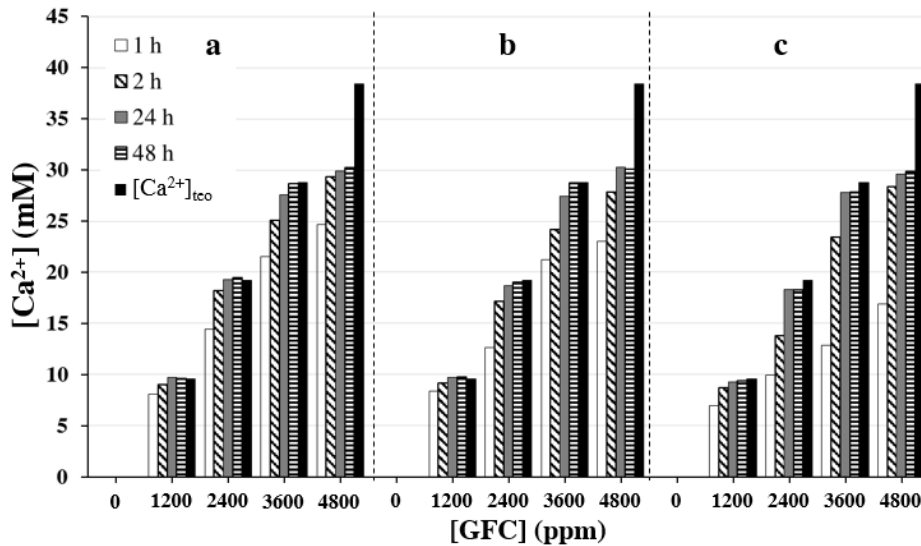
Figure 4. Calcium dissolution as a function of GFC load, contact time and VFA type:
(a) AcA, (b) PrA, (c) BuA; [VFA] = 63 mM; d < 1.0 mm; T=25 °C.

The effect of GFC grain size on the calcium dissolution rate was investigated with the selected VFAs. As reported in figure 5, an increase of GFC particle dimensions resulted in a decrease of calcium dissolution rate for all the VFAs. In fact, in the case of C4 class (d > 2.0 mm), only 86.4%, 85.7%, and 85.0% of GFC calcium was dissolved in presence of AcA, PrA and BuA solutions respectively, after 48 h of contact time. This result can be explained by a decrease of the exposed surface area associated to an increase of GFC particle size.
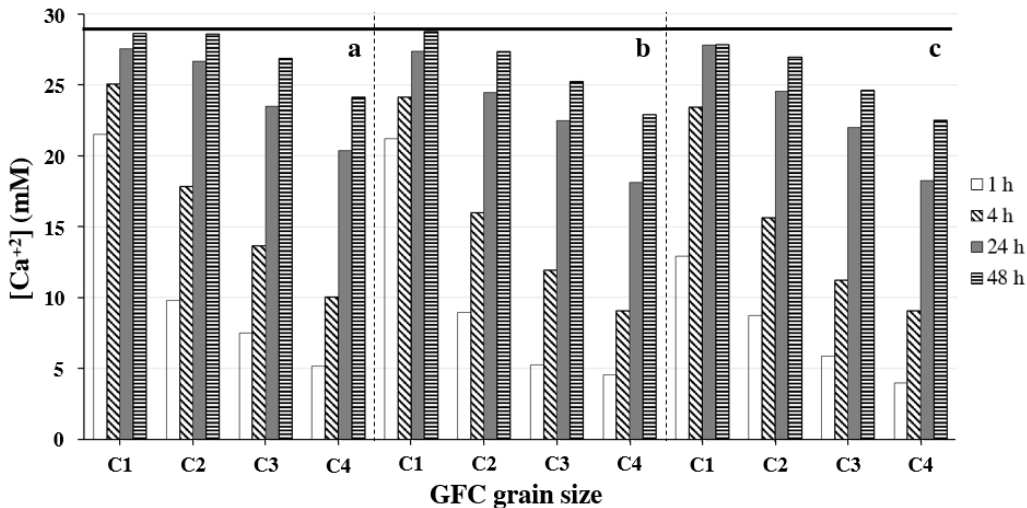
Figure 5. Calcium dissolution as a function of GFC grain size, contact time and VFA type: (a) AcA, (b) PrA, (c) BuA; [VFA] = 63 mM; [GFC] = 3600 ppm; $[Ca^{2+}]_t = 28.8$ mM; T=25 °C. The bold continuous line represents the calcium theoretical concentration.

Figure 6 shows the effect of temperature on the calcium dissolution rates, constant VFA concentrations (63 mM), GFC load (3600 ppm), and particle size (d < 1.0 mm). A strong

temperature influence on the calcium dissolution rates in BuA solutions was observed at the early stage of the tests. In fact, the increase of the temperature from 25 °C to 40 °C resulted in a calcium concentration raise within the first hour contact time equal to 7%, 8% and 72 % in AcA, PrA, and BuA solutions respectively.
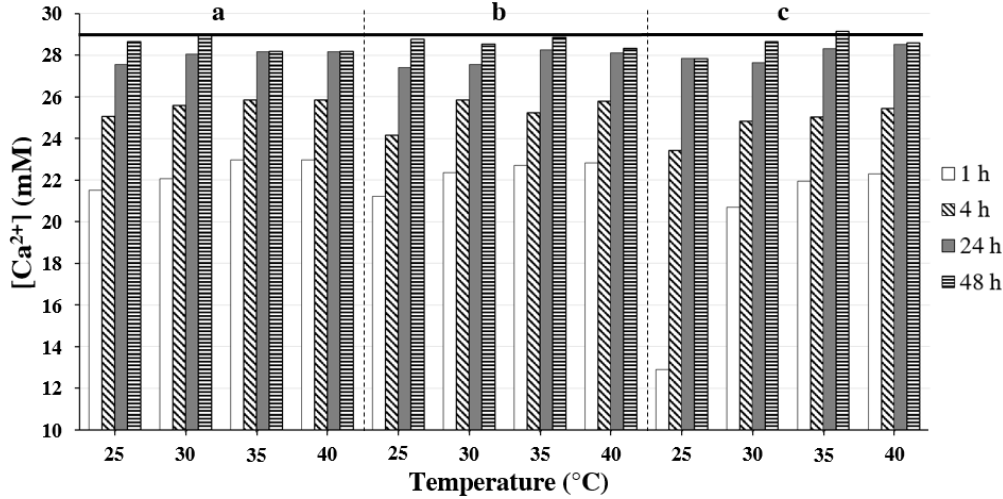
Figure 6. Calcium dissolution as a function of temperature, contact time and VFA type: (a) AcA, (b) PrA, (c) BuA; [VFA] = 63 mM; [GFC] = 3600 ppm; $[Ca^{2+}]_t$ = 28.8 mM; d < 1.0 mm. The bold continuous line represents the calcium theoretical concentration.

On these premises, the diffusional resistance to chemicals migrations through the solid phase may play a relevant role as rate determining step of the overall kinetic process. In fact, the general kinetic equation, relating to the concentration of species of equilibria 9-11 along the spatial coordinate (r) and time (t), could be obtained after integration of the second Fick's law under infinite solution volume boundary conditions [43]:

$$U(t) = \frac{[Ca^{2+}]_{t\,(l)}}{[Ca^{2+}]_{\infty\,(l)}} = 1 - \frac{6}{\pi^2} \sum_{n=1}^{\infty} \frac{1}{n^2} \exp\left(-\frac{Dt\pi^2 n^2}{r_0^2}\right) \quad (n = 1, 2, 3, \ldots) \tag{12}$$

where U(t) is the fractional attainment of equilibrium, r_0 the solid particle size, and D the diffusion coefficient of interdiffusing chemicals in and out of the solid phase. In particular, all the phenomena observed in this investigation could be explained by imposing the Knudsen diffusion coefficient in equation 12. In fact, the Knudsen diffusion coefficient ($D_{K,A}$) is expressed as a function of temperature (T), molecular weight (PM_A) of the interdiffusing species (such as the VFAs or their calcium soluble salts) and pore size (d_p) [44]:

$$D_{K,A} = 4850 \cdot d_p \cdot \sqrt{\frac{T}{PM_A}} \tag{13}$$

Finally, at the end of a test carried out with 3600 ppm of C2 GFC (1.0 mm<d<1.4 mm) suspended in a 63 mM AcA solution (see Figure 5), a characterization of the remaining suspended solids was carried out by SEM (Figure 7) and EDX (Table 1) analysis. In particular, SEM analysis show a large quantity of free glass fibers (Figure 4a) and the presence of particles (Figure 4b) which are probably formed of insoluble compounds such as silicates deriving from the GFC cement matrix. In fact, the EDX analysis revealed very high concentrations of silicon ($44.6\%_{w/w}$) and oxygen ($47.4\%_{w/w}$). Moreover, in agreement with the experimental results, the calcium concentration in the solid phase ($1.9\%_{w/w}$) indicates an almost complete dissolution of the GFC cement matrix.
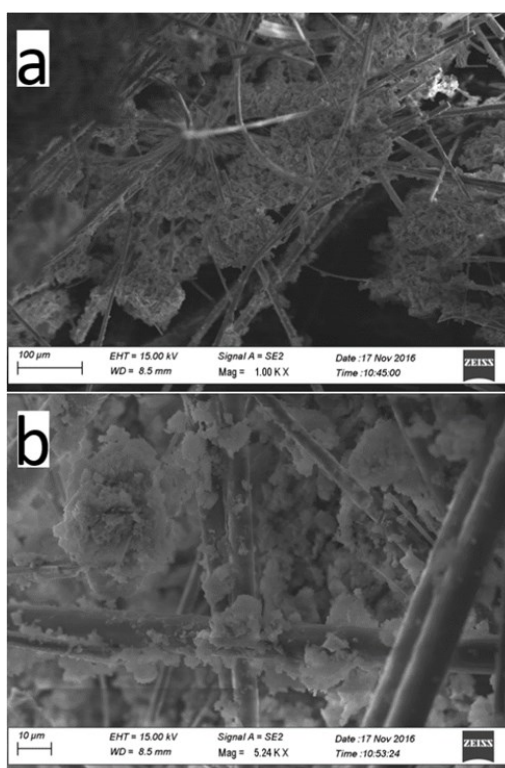
Figure 7. SEM images of the suspended solids at the end of the dissolution phase.

5.3.3. Dissolution of GFC by real DF effluents

The average cumulative production of bio-hydrogen during the DF experiments and VFA concentrations after 43 h were reported in Figure 8. After 41 h, the H_2 production reached a plateau and a final production equal to 127 mmol H2 L_{sol}^{-1} (Figure 8a). The halt in H_2 production was probably due to the reached pH values of 4.87 ± 0.04 in the liquid bulk. These results were confirmed by the analysis of the liquid samples which revealed high accumulation of organic acids, such as VFAs (Figure 8b). Specifically,

the low concentrations of PrA could be due to the absence of propionate producing saccharolytic clostridia which trigger hydrogen consuming pathway [30]. The presence of high concentrations of lactic acid ($1.6 \cdot 10^3$ ppm) indicates that the glucose degradation was not completed. Indeed, the H_2 yield (indicated as mol H_2 mol hexose^{-1}) resulted to be 0.66. This value is small if compared to other mesophilic experiments with hydrogen yields between 1.7-1.9 mol H_2 mol hexose^{-1} [45]. On the other hand, the presence of lactic acid (LaA) could favor the dissolution of GFC cement matrix.
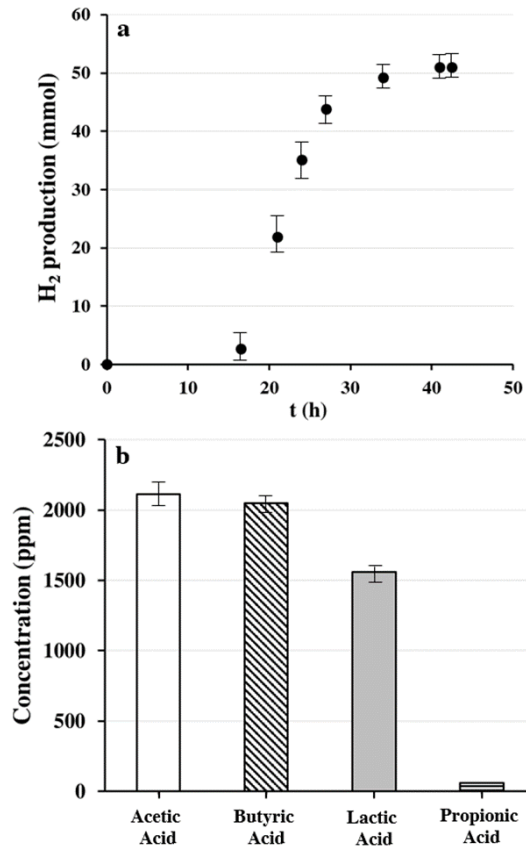
Figure 8. H_2 (a) and VFA (b) production during and after the DF treatment of glucose. T = 35 °C; 370 rpm; $[C_6H_{12}O_6] = 35 \cdot 10^3$ ppm; F/M ≈ 1.3.

At the end of this first phase, the reactors were fed with other 14 g of glucose and different amount of GFC. In particular, considering the results reported in the previous paragraph, class C1 GFC samples were suspended with loads equal to 0 ppm, $2.5 \cdot 10^3$ ppm, $5.0 \cdot 10^3$ ppm, $10 \cdot 10^3$ ppm, and $20 \cdot 10^3$ ppm. After 2 h (t = 45 h), as result of GFC cement matrix dissolution, the pH raised in all the experiments as reported in table 2, except in the case in which GFC was not added. Moreover, as shown in figure 9a, after 12 h from the adding of GFC and glucose, the H_2 production resumed. In particular, after 52 h (t = 95) the highest H_2 production of 62.5 mmol was obtained in

the case of $5.0 \cdot 10^3$ ppm of GFC suspended into the solution. In this condition, a complete dissolution of the GFC cement phase was reached (Figure 9b).
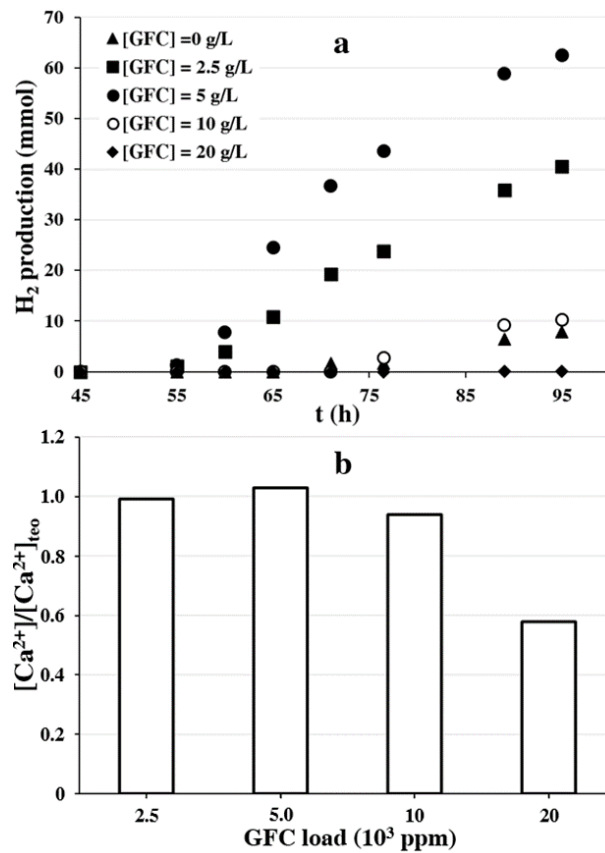
Figure 9. H_2 productions (a) and normalized dissolved Ca^{2+} concentrations (b) at varying GFC load. T = 35 °C; 370 rpm, d < 1.0 mm.

These results show the importance of the optimal GFC load. Indeed, in the case of the test carried out with $10 \cdot 10^3$ ppm GFC load, $2.9 \cdot 10^3$ ppm of Ca^{2+} (which correspond to almost 90% of the theoretic Ca^{2+}) were dissolved, but also 10.2 mmol of H_2 were produced. A higher amount of Ca^{2+} was dissolved in the presence of $20 \cdot 10^3$ of GFC, but lower efficiencies were obtained in terms of both cement phase dissolution (only 58% of the theoretical Ca^{2+}) and H_2 production. Moreover, in these cases, lower global VFA concentrations were obtained (Table 2).

Table 2. pH values and VFA concentrations at the end of the experimental runs.

GFC load (10^3 ppm)	pH at t = 45 h	pH at t = 95 h	[AcA] at t = 95 h (10^3 ppm)	[BuA] at t = 95 h (10^3 ppm)	[LaA] at t = 95 h (10^3 ppm)	[PrA] at t = 95 h (ppm)
0	4.89	4.64	2.2	2.4	1.9	63
2.5	5.31	4.69	2.4	5.8	2.3	78
5.0	6.06	4.71	2.9	7.9	3.7	68
10	7.22	5.08	3.1	4.1	3.9	61
20	9.88	5.81	2.5	2.5	7.9	84

These results are probably associated to an excessive increase in salinity, which can inhibit hydrogen production and microbial activity [46]. On the other hand, when only $2.5 \cdot 10^3$ ppm of GFC were suspended, a complete dissolution of the cement phase was observed, but the process led to the production of an intermediate H_2 cumulative volume (40.2 mmol), since a too acidic pH was faster reached. In addition, the final pH reached at the end of the dark fermentation stage represents a crucial parameter to take into account for the further hydrothermal process. In fact, since it has been reported that the optimal operative pH for the hydrothermal phase should be in the range 1.0 - 3.0 [27], at the end of the dissolution phase a strong acidity of the effluent is desirable to minimize the cost of reagents. As a result, it can be stated that the optimal GFC load corresponds to $5.0 \cdot 10^3$ ppm. In this context, the use of mathematical modelling, once suitably modified, might be further helpful in testing a large variation of environmental and operational conditions affecting the whole process [47, 48]. Moreover, if the effluents of the hydrothermal treatments, rich in VFAs, undergo to an anaerobic digestion process, the energetic balance of the whole treatment could be further improved.

5.3.4. Main benefits of the proposed process

The first advantage of the proposed process consists in the decrease of the acid consumption related to the hydrothermal phase. Indeed, since the chrysotile fiber concentrations in a CAC are approximately in the range of 8-16%w/w [37], the amounts of calcium and magnesium to be dissolved are almost 30-35%w/w and 3-4%w/w respectively. Consequently, by considering the stoichiometry of the reactions (2) and (3), the amount of sulfuric acid to be added during the hydrothermal treatment should decrease by 71-79% compared to what reported by Nam et al. [22], because the calcium present in the cement matrix could be completely dissolved by the VFAs produced during the DF pretreatment. Another important advantage of the proposed process

consists in the production of hydrogen during due to the DF process. Moreover, the effluents of the hydrothermal treatment, rich in VFAs, could undergo to an AD process, which can lead to the generation of methane. At this purpose, it has been demonstrated that coupling DF and AD processes could lead to a net energy yield ranging between the 250 kJ L_{sol}^{-1} and 300 kJ L_{sol}^{-1} [49]. Similarly, the effluents of the hydrothermal phase could be allocated in a microbial fuel cell with a consequent production of electricity. In this case, the net energy production may be higher than that resulting from the final adoption of AD [50]. In this way, the energy generated during the two biological processes may be used to heat the solution during the hydrothermal phase, which should be carried out at 100 °C for 24 h [22].

Finally, both the production of VFAs and the production of energy could derive from the biodegradation of a carbon rich waste biomass, which could be represented by agro-food wastes, such as the molasses deriving from sugar refinery [51] and the exhaust cheese whey deriving from dairies [52]. Consequently, the proposed process, in line with the green economy principles, could be performed by the use of a non-marketable agro-food waste to decrease the costs related to the hydrothermal treatment of CAC.

5.4. Conclusions

The present study represents a preliminary investigation on an innovative combined system based on a DF and a hydrothermal treatment stages aimed to obtain an effective and cheaper CAC denaturation. Indeed, the DF step has been successfully applied to dissolve the cementitious phase of a composite, simulating a CAC, and to produce a renewable source of energy, the bio-H_2, supporting the hydrothermal phase. Indeed, even if now it is not possible to make a balance between the produced and the consumed energy, the proposed process should be able to decrease the acid consumption and the energy costs during the hydrothermal phase.

In particular, Synthetic DF effluents were used to evaluate the best operative conditions for GFC dissolution. At this purpose, the results revealed a strong diffusional resistance to VFAs migration through GFC. Specifically, all the phenomena observed in this investigation could be explained by imposing the Knudsen diffusion coefficient into the integrated second Fick's law.

The liquid DF effluents resulted effective for the dissolution of CAC simulating conglomerates. In fact, in the case of $5.0 \cdot 10^3$ ppm GFC load, the cement matrix was completely dissolved into a real solution deriving from the DF of glucose. Moreover,

this process resulted in a H$_2$ production equal to 284 mmolH$_2$ L$_{sol}^{-1}$, which could be used as energy source during the hydrothermal treatment, and in a final pH of the suspension equal to 4.71, which is close to the best conditions for the asbestos fiber denaturation. In particular, the adoption of different GFC loads resulted in lower hydrogen productions and/or dissolution efficiencies.

Compared to the other results reported in the literature, the H$_2$ yields were low since too acidic pH were reached. Nevertheless, the acidity of the solution was necessary for the dissolution of CAC cement matrix. On the other hand, if the effluents of the hydrothermal treatments, rich in VFAs and lactic acid, undergo to other biological processes, such as microbial fuel cells or anaerobic digestion, the energetic balance of the whole treatment could be further improved due to the final CH$_4$ and H$_2$ production. The results obtained in this manuscript represent a starting point for future investigations on the proposed treatment train. Indeed, as future steps of this investigation, it will be carried out the dissolution of the cement matrix of a real CAC during the DF process and the subsequent hydrothermal treatment of these effluents, rich in asbestos fibers. Moreover, the adoption of real biodegradable wastes instead of glucose together with the treatment and valorization of the effluents deriving from the hydrothermal phase will be considered for scaled-up applications of the proposed system. After these mandatory steps, a life cycle assessment of the whole treatment train could be carried out.

References

[1]   Dellisanti, F., Rossi, P.L., Valdrè, G., 2009. Remediation of asbestos containing materials by Joule heating vitrification performed in a pre-pilot apparatus. International Journal of Mineral Processing, 91, pp.61-67.

[2]   Newhouse, M.L., Thompson, H., 1965. Mesothelioma of pleura and peritoneum fol- lowing exposure to asbestos in the London area. British Journal of Industrial Medicine, 22, pp.261-269.

[3]   Baek, S.C., Kim, Y.C., Choi, J.H., Hong, W.H., 2016. Determination of the essential activity elements of an asbestos management system in the event of a disaster and their prioritization. Journal of Cleaner Production, 137, pp.414-426.

[4]   Zhang, Y.L., Kim, Y.C., Hong, W.H., 2016. Visualizing distribution of naturally discharged asbestos fibers in Korea through analysis of thickness changes in asbestos cement slates. Journal of Cleaner Production, 112, pp.607-619.

[5]   Plescia, P., Gizzi, D., Benedetti, S., Camilucci, L., Fanizza, C., De Simone, P., Paglietti, F., 2003. Mechanochemical treatment to recycling asbestos containing waste. Waste Management, 23, pp.209-218.

[6]   Italian Organization for Standardization (UNI) (2005). Methods of testing cement-Part 1: determination of strength, UNI, Milan, Italy, EN 196-1.

[7]   EU Council Decision 94/904/EC establishing a list of hazardous waste pursuant to Article 1(4) of Council Directive 91/689/EEC on hazardous waste.

[8]   Leonelli, C., Veronesi, P., Boccaccini, D.N., Rivasi, M.R., Barbieri, L., Andreola, F., Lancellotti, I., Rabitti, D., Pellacani, G.C., 2006. Microwave thermal inertisation of asbestos containing waste and its recycling in traditional ceramics. Journal of Hazardous Materials, B135, pp.149-155.

[9]   Finnveden, G., Johansson, J., Lind, P., Moberg, A., 2005. Life cycle assessment of energy from solid waste-part 1: general methodology and results. Journal of Cleaner Production, 13(3), pp.213-229.

[10] Mober, A., Finnveden, G., Johansson, J., Lind, P., 2005. Life cycle assessment of energy from solid waste—part 2: landfilling compared to other treatment methods. Journal of Cleaner Production, 13(3), pp.231-240.

[11] Colangelo, F., Cioffi, R., Lavorgna, M., Verdolotti, L., De Stefano, L., 2011. Treatment and recycling of asbestos-cement containing waste. Journal of Hazardous Materials, 195, pp.391-397.

[12] Bernardo, E., Esposito, L., Rambaldi, E., Tucci, A., 2011. Sintered glass ceramic articles from plasma vitrified asbestos containing waste. Advances in Applied Ceramics, 110(6), pp.346-352.

[13] Chan, Y.M., Agamuthu, P., Mahalingam, R., 2000. Solidification and stabilization of asbestos waste from an automobile brake manufacturing facility using cement. Journal of Hazardous Materials, B77, pp.209-226.

[14] Bernardo, E., Scarinci, G., Edme, E., Michon, U., Planty, N., 2009. Fast-sintered gehlenite glass–ceramics from plasma-vitrified municipal solid waste incinerator fly ashes. Journal of the American Ceramic Society, 92(2), pp.528-530.

[15] OVAM, 2016. State of the art: asbestos - Possible treatment methods in Flanders: constraints and opportunities.

[16] Finucane, K.G., Thompson, L.E., Abuku, T., Nakauchi, H., 2008. Treatment of asbestos waste using the Geomelt Vitrification Process. WM2008 Conference, February 24-28, Phoenix, AZ, Abstract #8261, pp.1-10.

[17] Kusiorowski, R., Zaremba, T., Piotrowski, J., 2016. Influence of the type of pre-calcined asbestos containing wastes on the properties of sintered ceramics. Construction and Building Materials, 106, pp.422-429.

[18] Kusiorowski, R., Zaremba, T., Piotrowski, J., Gerle, A., 2013. Thermal decomposition of asbestos-containing materials. Journal of Thermal Analysis and Calorimetry, 113, pp.179-188.

[19] Giantomassi, F., Gualtieri, A.F., Santarelli, L., Tomasetti, M., Lusvardi, G., Lucarini, G., Governa, M., Pugnaloni, A., 2010. Biological effects and comparative cytotoxicity of thermal transformed asbestos-containing materials in a human alveolar epithelial cell line. Toxicology in Vitro, 24(6), pp.1521-1531.

[20] Anastasiadou, K., Axiotis, D., Gidarakos, E., 2010. Hydrothermal conversion of chrysotile asbestos using near supercritical conditions. Journal of Hazardous Materials, 179, pp.926-932.

[21] Yoshikawa, N., Kashimura, K., Hashiguchi, M., Sato, M., Horikoshi, S., Mitani, T., Shinohara, N., 2015. Detoxification mechanism of asbestos materials by microwave treatment. Journal of Hazardous Materials, 284, pp.201-206.

[22] Nam, S.M., Jeong, S., Lim, H., 2014. Thermochemical destruction of asbestos-containing roofing slate and the feasibility of using recycled waste sulfuric acid. Journal of Hazardous Materials, 65, pp.151-157.

[23] Alexander, G., Maroto-Valer, M., Gafarova-Aksoy, P., 2007. Evaluation of reaction variables in the dissolution of serpentine for mineral carbonation. Fuel, 86, pp.273-281.

[24] Tier, S., Revitzer, H., Eloneva, S., Fogelholm, C.J., Zevenhoven, R., 2007. Dissolution of natural serpentinite in mineral and organic acids, International Journal of Mineral Processing, 83, pp.36-46.

[25] Fujishige, M., Sato, R., Kuribara, A., Karasawa, I., Kojima, A., 2006. $CaCl_2$ addition effect and melt formation in low-temperature decomposition of chrysotile with $CaCO_3$. Journal of the Ceramic Society of Japan, 114(10), pp.844-848.

[26] Beddoe, R.E., Dorner, H.W., 2005. Modelling acid attack on concrete: Part I. The essential mechanisms. Cement Concrete Research, 35, pp.2333-2339.

[27] Balducci, G., Foresti, E., Lelli, M., Lesci, I.G., Marchetti, M., Pierini, F., Roveri, N., inventors. Process for treating an asbestos containing material. EU patent: EP2428254 B1. 2013 March 27.

[28] Hawkes, F., Hussy, I., Kyazze, G., Dinsdale, R., Hawkes, D., 2007. Continuous dark fermentative hydrogen production by mesophilic microflora: principles and progress. International Journal of Hydrogen Energy, 32, pp.172-184.

[29] Ghimire, A., Frunzo, L., Pirozzi, F., Trably, E., Escudie, R, Lens, P.N.L., Esposito, G., 2015. A review on dark fermentative biohydrogen production from organic biomass: Process parameters and use of by-products. Applied Energy, 144, pp.73-95.

[30] Khanal, S., Chen, W.H., Li, L., Sung, S., 2003. Biological hydrogen production: effects of pH and intermediate products. International Journal of Hydrogen Energy, 29, pp.1123-1131.

[31] Ghimire, A., Luongo, V., Frunzo, L., Pirozzi, F., Lens, P.N.L., Esposito, G., 2017. Continuous biohydrogen production by thermophilic dark fermentation of cheese whey: use of buffalo manure as buffering agent. International Journal of Hydrogen Energy, 42(8), pp.4861-4869.

[32] Özgür, E., Afsara, N., de Vrije, T., Yücel, M., Gündüz, U., Claassen, P.A.M., Eroglu, I., 2010. Potential use of thermophilic dark fermentation effluents in photofermentative hydrogen production by *Rhodobacter capsulatus*. Journal of Cleaner Production, 18(1), pp.S23-S28.

[33] Liu, W., Huang, S., Zhou, A., Zhou, G., Ren, N., Wang, A., 2012. Hydrogen generation in microbial electrolysis cell feeding with fermentation liquid of waste activated sludge. International Journal of Hydrogen Energy, 37, pp.13859-13864.

[34] Lin, J., Zuo, J., Ji, R., Chen, X., Liu, F., Wang, K., Yang, Y., 2012. Methanogenic community dynamics in anaerobic co-digestion of fruit and vegetable waste and food waste. Journal of Environmental Sciences, 24(7), pp.1288-1294.

[35] Italian Organization for Standardization (UNI) (2011). Cement composition, specifications and conformity criteria for common cements, UNI, Milan, Italy, EN 197-1.

[36] Yeshanew M.M., Frunzo L., Luongo V., Pirozzi F., Lens P.N.L., Esposito G., 2016. Start-up of an anaerobic fluidized bed reactor treating synthetic

carbohydrate rich wastewater. Journal of Environmental Management, 184, pp-456-464.

[37] Hansen, T.C., Radjy, F., Sellevold, E.J., 1973. Cement paste and concrete. Annual Review of Materials Science, 3, pp.233-268.

[38] Ghimire, A., Frunzo, L., Pontoni, L., d'Antonio G., Lens P.N.L., Esposito G., Pirozzi F., 2015. Dark fermentation of complex waste biomass for biohydrogen production by pretreated thermophilic anaerobic digestate. Journal of Environmental Management, 152, pp.43-48.

[39] Luongo, V., Ghimire, A., Frunzo, L., Fabbricino, M., d'Antonio, G., Pirozzi, F., Esposito, G., 2017. Photofermentative production of hydrogen and poly-β-hydroxybutyrate from dark fermentation products. Bioresource Technology, 228, pp.171-175.

[40] APHA. 1998. Standard Methods for the Examination of Water and Wastewater, 20th ed. American Public Health Association/American Water Works Association/Water Environment Federation, Washington DC, USA.

[41] Kontoleontos, F., Tsakiridis, P., Marinos, A., Katsiotis, N., Kaloidas, V., Katsioti, M., 2013. Dry-grinded ultrafine cements hydration. Physicochemical and microstructural characterization. Materials Research, 16(2), pp.404-416.

[42] Ye, G., Liu, X., De Schutter, G., Taerwe, L., Vandevelde, P., 2007. Phase distribution and microstructural changes of self-compacting cement paste at elevated temperature. Cement and Concrete Research, 37, pp.978-987.

[43] Petruzzelli, D., Petrella, M., Boghetich, G., Clabrese, P., Petruzzelli, V., Petrella, A., 2009. Neutralization of acidic wastewater by the use of waste limestone from the marble industry. Mechanistic aspects and mass transfer phenomenon of the acid-base reaction at the liquid-solid interface. Industrial & Engineering Chemistry Research, 48, pp.399-405.

[44] Mu, D., Liu, Z.S., Huang, C., Djilali, N., 2008. Determination of the effective diffusion coefficient in porous media including Knudsen effects. Microfluidics and Nanofluidics, 4, pp.257-260.

[45] Haroun, B.M., Hafez, H., Nakhla, G., Nasr, F.A., 2017. Response of acclimatized mesophilic biohydrogen cultures to feed changes. Chemical Engineering Journal, 314, pp.358-367.

[46] Lee, M.J., Kim, T.H., Min, B., Hwang, S.J., 2012. Sodium (Na^+) concentration effects on metabolic pathway and estimation of ATP use in dark fermentation hydrogen production through stoichiometric analysis. Journal of Environmental Management, 108, pp.22-26.

[47] Mattei, M.R., Frunzo, L., D'Acunto, B., Esposito, G., Pirozzi, F., 2015. Modelling microbial population dynamics in multispecies biofilms including Anammox bacteria. Ecological Modelling, 304, pp.44-58.

[48] D'Acunto, B., Frunzo, L., Mattei, M.R., 2016. Qualitative analysis of the moving boundary problem for a biofilm reactor model. Journal of Mathematical Analysis and Applications, 438(1), pp.474-491.

[49] Ruggeri, B., Tommasi, T., Sassi, G., 2010. Energy balance of dark anaerobic fermentation as a tool for sustainability analysis. International Journal of Hydrogen Energy, 35(19), pp.10202-10211.

[50] Perera, K.R.J., Ketheesan, B., Gadhamshetty, V., Nirmalakhandan, N., 2010. Fermentative biohydrogen production: evaluation of net energy gain. International Journal of Hydrogen Energy, 35(22), pp.12224-12233.

[51] Yan, D., Lu, Y., Chen, Y. F., Wu, Q., 2011. Waste molasses alone displaces glucose-based medium for microalgal fermentation towards cost-saving biodiesel production. Bioresource Technology, 102(11), pp.6487-6493.

[52] Dębowski, M., Korzeniewska, E., Filipkowska, Z., Zieliński, M., Kwiatkowski, R., 2014. Possibility of hydrogen production during cheese whey fermentation process by different strains of psychrophilic bacteria. International Journal of Hydrogen Energy, 39(5), pp.1972-1978.

Chapter 6

Engineering strategies for enhancing photofermentative biohydrogen production by purple non-sulfur bacteria using dark fermentation effluents

Engineering strategies for enhancing photofermentative biohydrogen production by purple non-sulfur bacteria using dark fermentation effluent

This chapter aims to summarize the state of the art of Photo Fermentation (PF) processes for hydrogen (H_2) production by overviewing existing understanding of the microbiology of the PF process, different photobioreactor (PBR) design, conversion efficiencies of different purple non-sulphur bacteria (PNSB) strains, process operational parameters such as pH, temperature, nutrient requirements. This competence can be applied for the valorisation of DF effluents (DFE) and wastewater through H_2 and PHB production. In addition, this work presents current approaches of the mathematical modeling of PF as well as highlights the economics of the process.

6.1. Introduction

6.1.1. Hydrogen production processes

Most energy fuels, chemicals and raw materials in our daily lives are derived from petroleum based refineries. However, depleting fossil fuel reserves and increasing greenhouse gas emissions and severe pollution problems as the consequence of by-products from fossil fuel utilization is driving interests towards biorefineries for the production of energy and useful chemicals [1, 2]. In the energy and environmental sector, hydrogen (H_2) has gained considerable interests owing to its higher specific energy content (122 MJ/kg) as well as water and energy being the sole oxidative reaction by-products [3]. At present, H_2 production for industrial applications is mainly derived from thermo-catalytic and gasification processes, which are highly dependent on fossil fuels. In comparison to the energy intensive physico-chemical routes for H_2 production, biological processes can be operated at ambient conditions and are advantageous as they can utilize renewable biomass [4, 5].

Based on the light dependency as an energy source for the biochemical reactions, biological H_2 production pathways can be broadly categorized into light dependent and independent processes [6, 7]. The light dependent photo-hydrogen production systems can be further classified into i) direct photolysis, where water is broken down into H_2 and O_2 gas by algae and cyanobacteria, ii) indirect photolysis in which cyanobacteria (or cyanophytes) synthesize H_2 in the presence of light and inorganic carbon, and iii) photofermentation (PF), carried out by photosynthetic bacteria where photodecomposition of organic compounds occurs. The light independent

processes include i) dark fermentation (DF), which involves fermentative hydrogen production from carbohydrate rich organic biomass, and ii) H_2 from bio-electrochemical systems or microbial electrolysis cells.

6.1.2. Light independent H_2 production

DF is a well studied biological route for the production of hydrogen from organic biomass, including waste, due to its higher H_2 production rates than light dependent processes [4]. However, due to the thermodynamic constraints, dark fermentative conversion of carbohydrate rich organic biomass offers lower H_2 yields and gives incomplete conversion of organic biomass, i.e. organic acids and alcohols remain as major fermentation by-products. On the brighter side, the PF processes can convert these dark fermentative by-products to biohydrogen. Moreover, PF processes have higher H_2 yields and generate less residues compared to DF processes [8, 9]. A dual system can integrate the conversion of carbohydrates to organic acids in the first stage (DF) and the utilization of its by-products in the second stage (PF) [10].

6.1.3. Light dependent H_2 production

Using light as a source of energy, purple non-sulfur bacteria (PNSB) synthesize H_2 by carrying out an anaerobic photosynthesis. In PNSB, this takes place in the presence of the nitrogenase enzyme and light, with reduced carbon sources such as organic acids. In addition, under certain operating conditions, PNSB also synthesize cell reserve materials or biopolymers, i.e. polyhydroxybutyrate (PHB) molecules [11, 12].

An example of PF is the conversion of acetic acid to biohydrogen and/or biopolymers. It can be expressed by the following equations (Equations 1 and 2):

$$2\,CH_3COOH + 4\,H_2O \xrightarrow{Light\ energy} 8\,H_2 + 4\,CO_2 \tag{1}$$

$$2\,CH_3COOH + 2\,[H] \xrightarrow{Light\ energy} PHB_{monomer} + H_2O \tag{2}$$

$$C_6H_{12}O_6 + 2\,H_2O \longrightarrow 2\,CH_3COOH + 2\,CO_2 + 4\,H_2 \tag{3}$$
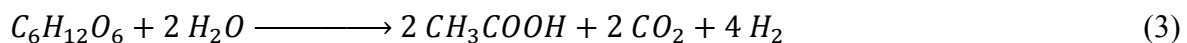
Photofermentative H_2 production systems are attractive because of their higher H_2 yield potential, i.e. 66.67 mmol H_2 g COD^{-1} (Equation 1) from PF systems compared to only 22.22 mmol H_2 g COD^{-1} from the DF process with acetate as sole by-product (Equation 3). Moreover, the biopolymer production can add an economic value to the PF process. However, photofermentative production of H_2 and PHB are competing processes [11, 13]. Nonetheless, a

concomitant production of H_2 and PHB is also possible, as shown in a study by Montiel-Corona et al. [14]. The photofermentative H_2 and PHB production depends on several operating conditions, such as nutrients availability (carbon to nitrogen ratio (C/N) ratio), PNSB strain (mixed or pure culture), pH, light intensity and presence of physical-chemical stress, for example the presence of inhibitors of H_2 formation such as ammonium in the culture medium [8, 15, 16]. The ability of PNSB to convert reduced carbon sources such as organic acids and alcohols to H_2 and PHB makes PNSB based PF a good post treatment process for dark fermentation effluents (DFE) [17, 18, 19, 20, 21]. Moreover, the potential of the PF process to be operated as stand alone system for wastewater treatment has also been reported [8, 22, 23]. With the increasing application of DF processes for H_2 production, the integrated DF-PF process can enhance H_2 yields, thus providing sustainability to scaled-up biohydrogen production processes. Likewise, the potential of PF processes for the production of biopolymers can give further economic gain.

6.2. Microbiology and phototrophic metabolism of PNSB

6.2.1. Bacterial photosynthesis

Bacterial photosynthesis can be divided into two types depending on the presence or absence of oxygen for the metabolism of bacteriochlorophyll, a bacterial photosynthetic pigment. Oxygenic photosynthesis is carried out by cyanobacteria and prochlorophytes, whereas anoxygenic photosynthesis can be generally mediated by purple bacteria, green sulfur bacteria, heliobacteria and others [24]. Photosynthetic anoxygenic bacteria are a very diverse groups of bacteria which carry out bacteriochlorophyll dependent photosynthesis as a metabolic process [25]. The anoxygenic phototrophic bacteria can be broadly grouped into different classes (Figure 1), based on their photosynthetic pigments and electron donors [24, 25]. Depending on the electron donors used, purple bacteria can be further divided into purple sulfur bacteria (use sulfur compounds as electron donors) and non-sulfur bacteria (use organic substances as electron donor).

Some drawbacks of this photofermentative system as pointed by Hellenbeck and Benemann [26] include inherent high energy demand associated with the nitrogenase enzyme, lower photo conversion efficiencies and economic issues of anaerobic photobioreactors covering large areas. These drawbacks can be overcome by effective design and operation of the photobioreactors (PBRs) and selecting proper strains or enrichment of PNSB for an efficient conversion to photo-H_2.
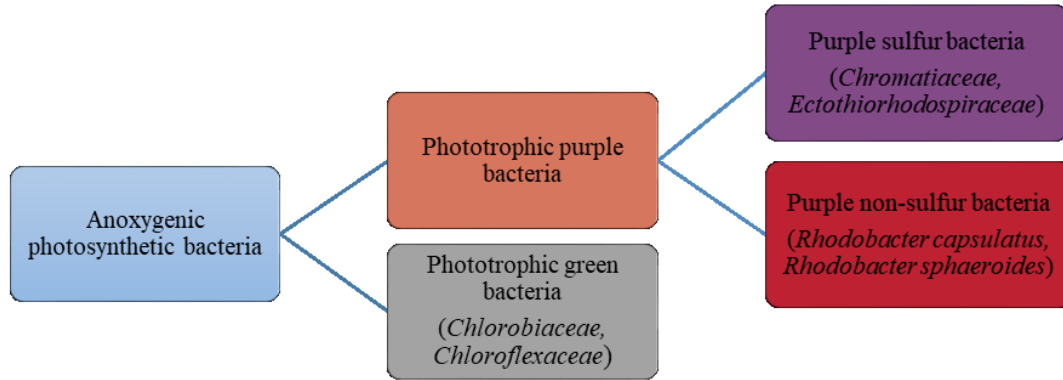
Figure 1. Classification of anoxygenic photosynthetic bacteria.

6.2.2. Purple non-sulfur bacteria (PNSB)

Among the anoxygenic bacteria, the PNSB exhibit very diverse morphological, biochemical and metabolic properties [27]. PNSB are gram-negative photo-heterotrophs, which normally carry out photosynthesis under anaerobic conditions. Although PNSB are facultative anaerobes, they can also grow chemotropically under oxygenic conditions using oxygen as electron acceptor [25]. Different from purple sulfur bacteria, which use elemental sulfur as the electron donor, PNSB typically use organic electron donors such as organic acids, however, they can also use hydrogen gas as electron donor [24].

PNSB can utilize various types of carbon sources such as short-chain organic acids and glucose. The theoretical photofermentative conversion of different organic acids, typically present in DFE, to H_2 can be expressed by the following reactions (Equations 4-7) [12, 28, 29]:

Lactate:
$$C_3H_6O_3 + 3\,H_2O \rightarrow 6\,H_2 + 3\,CO_2 \tag{4}$$

Acetate:
$$CH_3COOH + 2\,H_2O \rightarrow 4\,H_2 + 2\,CO_2 \tag{5}$$

Propionate:
$$C_3H_6O_2 + 4\,H_2O \rightarrow 7\,H_2 + 3\,CO_2 \tag{6}$$
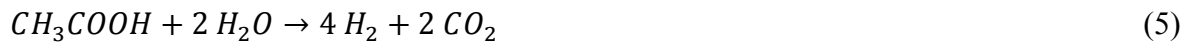
Butyrate:
$$C_4H_8O_2 + 6\,H_2O \rightarrow 10\,H_2 + 4CO_2 \tag{7}$$

However, the conversion ability of different PNSB for different substrates varies [29, 30]. Some species prefer a certain sole carbon source, while H_2 yields seem to be higher with mixed sources of carbon [28]. The variation in H_2 production from different carbon sources can be explained

by differences in their reduction states and the associated metabolism for the assimilation of different carbon sources [28, 31, 32]. Similarly, when the carbon source is acetate, most of the reducing power of the PNSB is utilized for the synthesis of PHB rather than H_2 [31, 33].

6.2.3. Photosystem of PNSB

The photosynthetic apparatus of PNSB is simple as it contains only one photosystem (PS), unlike the two PS in algae and cyanobacteria. PNS bacterial cells contain bacteriochlorophyll α or β located on cytoplasmic membrane. The PS of PNSB contains the light harvesting complexes that absorb photons initiating a charge (electron-hole) separation through excitation (Figure 2). Electrons that are liberated from organic acids are transported around through a number of electron carriers, i.e. the cytochrome C_2 complex, cytochrome bc_1 complex (Cyt bc_1) and quinone Q (Figure 2). The transfer of electrons across the membranes creates a large proton gradient which drives the synthesis of ATP from ADP by ATP synthase (Figure 2) [34, 35]. The extra energy in the form of ATP will be used to reduce ferredoxin-fd. Then, the ATP and reduced ferredoxin drives the proton reduction to hydrogen by nitrogenase [6]. Thus, as a result of anoxygenic photosynthesis, conversion of organic substances into H_2 takes place.
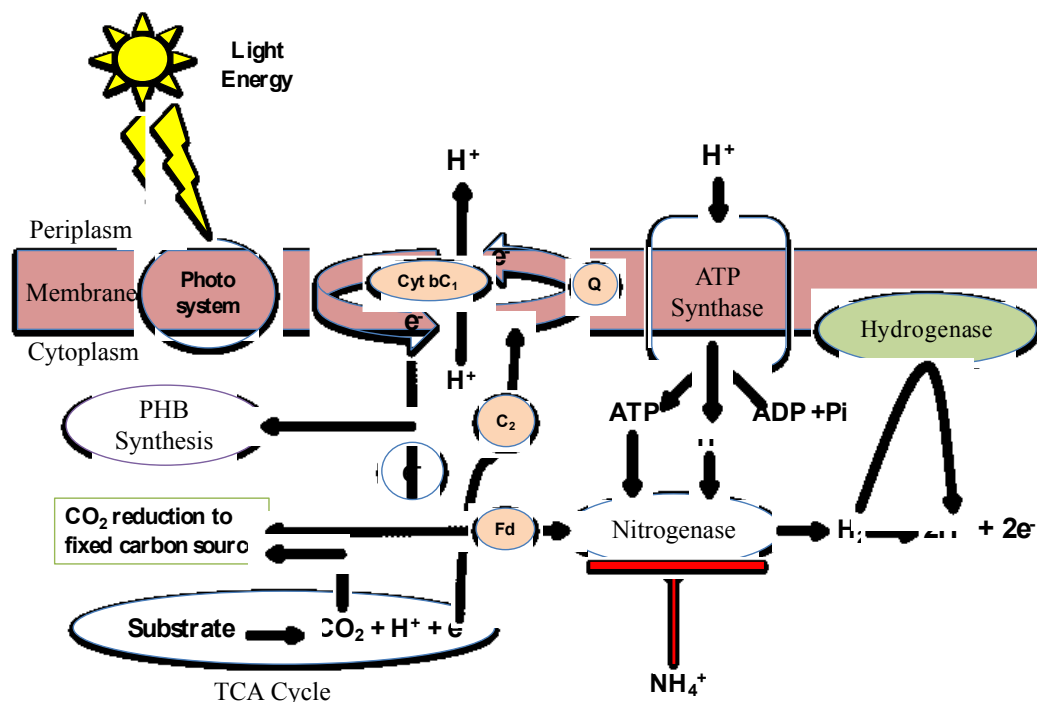
Figure 2. Schematic representation of mechanisms of photofermentative H_2 and PHB production in PNSB (adapted and modified from [15, 31, 35]).

Nitrogenase and hydrogenase are the two enzymes that strongly influence hydrogen production: nitrogenase promotes its production, whereas hydrogenase consumes hydrogen (Figure 2). Besides the light conditions, the PF culture medium should be under nitrogen limitation and oxygen should be absent, as their presence inhibits the nitrogenase activity [8, 31, 36]. The activity of the nitrogenase enzyme is of fundamental importance for efficient photo-H_2 production [26]. Equations 8 and 9 explain the effect of N_2 on the metabolism of PNSB [5]:

With dinitrogen:
$$N_2 + 8\,H^+ + 8\,e^- + 16\,ATP \rightarrow 2\,NH_3 + H_2 + 16\,ADP + 16\,P_i \tag{8}$$

Without dinitrogen:
$$8\,H^+ + 8e^- + 16\,ATP \rightarrow 4\,H_2 + 16\,ADP + 16\,P_i \tag{9}$$
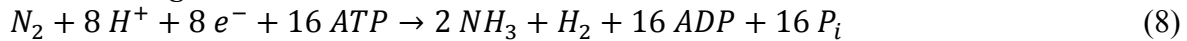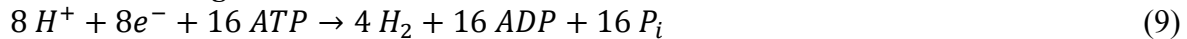
The presence of nitrogen, either in gaseous form or in the culture medium, can thus inhibit the activity of the nitrogenase enzyme that synthesizes molecular H_2. Therefore, substrates with a high C/N ratio are more suitable for H_2 conversion in these systems. Thus, the nitrogen content in the substrate (e.g. DFE) should be considered when coupling PF to dark fermentation.

6.2.4. PHB accumulation by PNSB

PNSB accumulate poly-β-hydroxybutyrate (PHB), an intracellular storage of carbon and energy formed under physiological stress, particularly, at high carbon to nitrogen (C/N) ratio, higher ammonia concentration or sulphur deprived conditions [11, 37, 38]. The production of PHB and H_2 functions as the way to dissipating the excess reducing power and the PHB synthesis competes with the H_2 production (Figure 2). Thus, depending on the aim of the process, the PF can be directed towards H_2 production by suppressing the PHB synthesis through genetic engineering of the PNSB [39]. Kars and Gündüz [31] reviewed the different genetic manipulation strategies to improve photofermentative biohydrogen production. They proposed to modify the acetate assimilation pathways that share the common biosynthetic route of PHB.

After the deletion of the PHB producing gene from *R. sphaeroides* KD131, the H_2 production rate was increased from 36.1 mL H_2 L^{-1} h^{-1} to 43.8 mL H_2 L^{-1} h^{-1} [39], in accordance with the study of Hustede et al. [33] who observed an increase in cell growth and H_2 production when eliminating the gene for PHB synthesis in *Rhodobacter sphaeroides*.

In addition, PNSB produce light harvesting bacterial pigments (bacteriochlorophylls and carotenoids) that can be of commercial interests [40]. This ability of PNSB has been highlighted in a few older studies and need to be explored again [41, 42].

6.3. Photo-hydrogen conversion efficiencies

Akkerman et al. (2002) suggested three parameters to evaluate the photo-H_2 production process: H_2 production yield, the yield coefficient of H_2 produced relative to the carbon source consumed and the photochemical efficiency (PE). Table 1 compares PF and DF systems in terms of H_2 yields from substrate conversion and production rate. PF systems are superior in terms of substrate to H_2 conversion, while they have slower H_2 production kinetics than DF systems. Considering the theoretical conversion of substrate to H_2 from Equations 4-7 and the experimental results reported in past studies (Table 1), PNSB have a very versatile metabolism and high substrate to H_2 conversion efficiency [25, 30, 43]. Their PF system lacks oxygen sensitivity issues that are encountered in biophotolysis. Moreover, their light utilization proficiency is high, as PNSB can absorb and utilize both visible (400-700 nm) and near infrared (700-900 nm) light. Also, PNSB use a wide variety of substrates [37]. The application of PNSB can be promising for PF systems, as they not only give a higher substrate to product conversion and higher H_2 yield, but also benefit in their capability to reduce pollution loads, e.g. treatment of effluents (organic acids) from DF, with the added economic benefit in the form of PHB production, a valuable biopolymer.

Table 1. Comparison of photo and dark fermentation systems for H_2 production.

Bio H_2 systems (*Microorganisms*)	Carbon source	H_2 production rate mL H_2 L^{-1} h^{-1}	H_2 Yield mL H_2 g COD^{-1a}	Reference
Photofermentation				
R. palustris WP3-5	DFE	25.2	235.1	[44]
R. sphaeroides RV	Succinate	16.5	158.7	[28]
Mixed culture	DFE	5.7	568.5	[14]
Dark fermentation				
Kitchen waste compost	Vegetable waste	1000	38	[45]
Clostridium thermocellum 7072	Corn stalks	740	140	[46]
Klebsiella sp. TR17	Glycerol	48	128.6[b]	[20]

[a]mL H_2 g COD^{-1} is calculated from the data provided in the publications

[b]mL H_2 g COD^{-1} consumed

The photofermentative H_2 production efficiency can also be measured as photochemical efficiency (PE), which is an efficiency parameter with which the light is utilized to produce

energy stored as hydrogen in a PF process. The PE depends on the photosynthetically active radiation (PAR) range, which determines the light energy absorbed by the photofermentative species. For example, green algae have a PAR range of 400-700 nm, while the range for PNSB is 400-950 nm (Figure 3). Akkerman et al. [35] reported that the PE values vary between 3 to 10% in green algae. Redwood et al. [47] achieved a 71% increase in combined photosynthetic activity by illuminating both *Rhodobacter sphaeroides* and *Arthrospira (Spirulina) platensis* by dividing a single beam of simulated sunlight using a dichroic mirror.
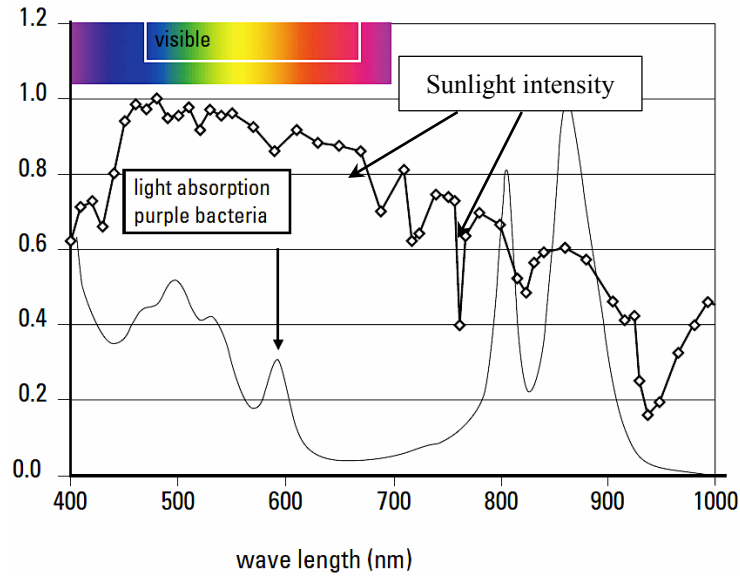
Figure 3. Sunlight and light absorption by purple bacteria [35].

In addition to H_2 yield and the other parameters mentioned before, the performance of a PF process can be evaluated by the light conversion efficiency. Light or solar energy conversion efficiency can be calculated as the ratio of total energy produced, i.e. stored in the form of H_2, to the total energy input to the bioreactor (energy as photons in case of solar conversion efficiencies). The light conversion efficiency (η) can be calculated with an empirical formula, i.e. the ratio of the total energy (heat of combustion) value of hydrogen to energy input to the PBR by solar radiation [36]. The η can be evaluated as:

$$\eta\,(\%) = \frac{[33.61 \cdot \rho_{H_2} \cdot V_{H_2}]}{[I \cdot A \cdot t]} \cdot 100 \qquad\qquad (10)$$

Where:

V_{H2} is the volume of produced H_2 in L;
ρ_{H2} is the density of the produced hydrogen gas in g L^{-1};
I is the light intensity in W m^2;
A is the irradiated area in m^2;

t is the duration of hydrogen production in hours.

Koku et al. (2002) reported a varying range of light conversion efficiencies between 1-5% on the average for different strains of *Rhodobacter sphaeroides*. According to the best of knowledge of the authors, a PE higher than 10% has not been reported so far. However, a wide range of approaches to increase the PE has been suggested in the literature, including the design of efficient PBR and improving lighting conditions [15, 16], genetic modifications of PNSB for enhancing nitrogenase activity [48], reduction of the pigment content for higher light uptake [49], deletion or inactivation of the genes responsible for PHB synthesis [39, 50] and developing hydrogenase deficient (*hup*⁻) mutant PNSB strains responsible for H_2 uptake [50, 51].

6.4 Operating conditions of photobioreactors for H_2 production

6.4.1. PNSB inoculum

PNSB are widely distributed in nature and prefer aquatic environments with low oxygen concentrations, significant amounts of soluble organic matter, moderate temperatures and weak as well as stronger light conditions [52]. Besides freshwater, members of the PNSB group can also be found in marine and hypersaline environments and even in sediments that are exposed to light. These organisms can also thrive in thermal springs and alkaline soda lakes [52]. An eutrophic lake is an example of a favorable habitat for members of these genera [30, 52].

Rhodopseudomonas palustris, *Rhodobacter sphaeroides*, *Rhodobacter capsulatus* and others are the most studied PNSB stains. However, PNSB strains capable of utilizing the substrates and light at higher conversion efficiencies are of research interest. Many studies have successfully isolated H_2 producing PNSB strains from different mixed consortia. Some examples of isolated H_2 producing PNSB and their H_2 yields and production rates are presented in Table 2.

Afsar et al. [53] carried out PF studies using different PNSB strains, which showed the PF efficiency highly depends on the effluent composition and bacterial strain used. The PF was carried out using the effluents from the thermophilic DF of glucose and potato steam peel hydrolysate as carbon source under indoor batch conditions. The PNS strains, such as *Rhodobacter capsulatus* (DSM1710), *Rhodobacter capsulatus* hup⁻ (YO3), *Rhodobacter sphaeroides* O.U.001 (DSM5864), *Rhodobacter sphaeroides* O.U.001 hup⁻ and *Rhodopseudomonas palustris*, were used in the study. The results showed that *R. sphaeroides* gave the highest amount of hydrogen from PF of glucose dark fermentation effluents, while *R.*

capsulatus produced better results on effluents from the dark fermentation of potato steam peels hydrolysate.

However, the use of pure cultures of bacterial strains demands maintenance of sterile conditions in the bioreactors. The varying PF efficiencies of different PNS bacterial strains on different substrates suggests, for substrates such as DFEs which contain mixed organic acids, the use of mixed consortia of PNSB bacteria in order to exploit the substrate utilization capacity of different PNS bacterial strains. In a study by Montiel-Corona et al. [14], the H_2 yields from enriched mixed PNSB cultures was higher (1478 ± 17 mL H_2 L^{-1}) than from pure *R. capsulatus* cultures (1252 ± 20 mL H_2 L^{-1}).

6.4.1.1.   Inoculum age

The selection of inoculum culture age can be critical to obtain a higher performance of PF systems. It has been found that the PNSB inoculum from the exponential phase of the growth curve is suitable for better performance of PBRs for biohydrogen production [54]. Koku et al. [55] found vast differences in total H_2 production, H_2 production rates and the overall substrate conversion rates when *Rhodobacter sphaeroides* O.U. 001 of two different inoculum ages were used in the PF of malic acid. The inoculum harvested from the mid-exponential phase gave a higher total gas production (357 mL H_2), gas production rate (0.009 mL H_2 L^{-1} h^{-1}) and overall substrate conversion rate (35%) than from an inoculum harvested at the stationary phase, which gave a lower total gas production (236 mL H_2), gas production rate (0.003 mL H_2 L^{-1} h^{-1}) and overall substrate conversion rate (24%).

In a study by Sasikala et al. (1991) on the effect of culture age on the photo-production of hydrogen by *R. sphaeroides* O.U. 001, the inoculum with a 20 hour culture period gave the highest H_2 evolution (60 mL H_2 L^{-1} reactor), while it was lower for a short (4 h) or long (38 h) culture period. A range of optimal inoculum ages has been reported in the literature. Akroum-Amrouche et al. [57] reported an optimum inoculum age of 36-48 hours in PF using *Rhodobacter sphaeroides* CIP 60.6, while Liu et al. [58] reported an inoculum age of 24 hours for *Rhodopseudomonas faecalis* RLD-53 as optimum.

The aged inoculum can give poor performance in terms of H_2 production and large retention times may shift the metabolic pathways to accumulation of PHB [55]. They also reported that a repeated culture of PNSB might lead to loss of H_2 production capacity due to a decline in the activity of the electron carrier ferredoxin.

6.4.1.2.   Cell immobilization

Studies have used different cell immobilization techniques in order to have the advantage of operating the PF process in the exponential growth phase for an infinite period of time and protect the culture strains from the inhibitory effects of chemicals which might be present in influent [58, 59, 60, 61]. However, a major limitation in cell immobilized PF systems is the penetration and transmission of light through the immobilization media. Also, the cell immobilization technology might not be practical when the PNSB cells are required to be harvested for PHB production.

Zhu et al. [61] used cationic polyelectrolytes, such as chitosan, poly-L-lysine (PLL), polyethyleneimine (PEI) and trimethylammonium glycol chitosan iodide (TGCI), to entrap *Rhodobacter sphaeroides* in order to prevent the inhibitory effect of NH_4^+ on H_2 production. In another study by Chen and Chang [59], a small amount of solid carrier, e.g. activated carbon, silica gel, or clay, was used for immobilization of *Rhodopseudomonas palustris* WP3-5 cells. The results of the study showed 67.2-50.9% and 37.2-32.5% increases in H_2 production rate and H_2 yield, respectively, when clay and silica gel were used. Similarly, Zhu et al. [60] demonstrated that the immobilization in agar gels could protect the PNS strains from inhibitory effects of the ammonium ion in photofermentative hydrogen production from tofu wastewater using *Rhodobacter sphaeroides*.

Table 2. Comparison of photo-H_2 production by different isolated and mixed PNSB strains from various inoculum sources.

Microbial inoculum sources	Isolated PNSB members	Highest H_2 producing stain	Main carbon source	Temp. (°C)	pH	Light intensity (Lux)	Maximum H_2 yield (mL H_2 g COD^{-1})[a]	Maximum H_2 production rate (mL H_2 L^{-1} h^{-1})	Reference
Pig dung	Not reported	*Rhodopseudomonas palustris*	Acetate	30	7	5,000	171.8	-	[62]
Wastewater ponds	*Rhodobacter sps.*	*Rhodobacter sphaeroides* ZX-5	Butyrate	30	6.0-9.0	4,000 (Tungsten lamps)	-	118	[63]
Water and lake bed samples	Not reported	Unidentified PNSB strain TN1	Acetate	30	-	3,000	647.5	43	[64]
Freshwater pond sludge	Not reported	*Rhodopseudomonas faecalis* strain RLD-53	Malate	35	7	4,000 (Incandescent lamp)	1242.5	25	[65]
Lake water and sediment samples	*Rb. Capsulatus, Rs. rubrum, Rb. Sphaeroides, R. palustris* stain AV33	*Rhodopseudomonas palustris* stain AV33	Lactate	30	6.8	200 µmol (photons) m^2/s (Incandescent lamp)	-	50.7	[30]
Activated sludge	*R. palustris*	Unidentified PNSB mixed culture	DFE of starch wastewater	31	5.5	48[b] (equivalent to 190 W/m^2 of tungsten lamp)	970.0	120.8 ± 7	[66]
Activated sludge	Not reported	Unidentified enriched IZT PNSB	DFE	30	7.0	3000 (LEDs and halogen lamps)	321.3 ± 3.7	5.7	[14]
Silt sewage, pig manure, and cow dung	Not reported	Unidentified PNSB mixed culture	Enzymatic hydralysate of corncob	30	7.0	4000 (LED lamps)	-	165	[67]

[a] COD values are calculated from theoretical oxygen demand of main carbon sources

[b] Calculated using the available data and conversion values from the URL: http://www.egc.com/useful_info_lighting.php

6.4.2. Carbon and nutrient sources

The substrate types and their concentration used in PF can influence the H_2 production rates and yields. Han et al. [28] studied the effect of different carbon sources and their concentrations on the photo-H_2 production using a batch culture of *Rhodobacter sphaeroides* RV. The substrates used were either individual substrates such as acetate, propionate, butyrate, lactate, malate, succinate, ethanol, glucose, citrate or sodium carbonate or mixed carbon sources such as malate and succinate, or lactate and succinate. The results of the study showed that the H_2 production for the mixed substrates is higher (794 mmol H_2 mol^{-1} substrate for 2.02 g L^{-1} lactate and 2.0 g L^{-1} succinate) than using a single substrate (424 mmol H_2 mol^{-1} substrate for 0.8 g L^{-1} sodium propionate). This makes PF prominent for the application in the treatment of DFE that typically contains more than one organic acid [17, 18].

6.4.2.1. Effect of organic loading rate and hydraulic retention time

The Organic Loading Rate (OLR) and the Hydraulic Retention Time (HRT) strongly affect the performance of PBRs as they determine the substrate degradation efficiency and the hydrogen production rate. Venkata Mohan et al. [68] studied the effect of different OLRs on photo-H_2 production and substrate degradation efficiency. The synthetic wastewater gave the maximum substrate degradation efficiency (1.4 kg COD m^{-3} day^{-1}) at an OLR of 2.45 kg COD m^{-3} day^{-1}, while higher specific H_2 production (19.29 mol H_2 kg $COD_{removed}^{-1}$) was achieved at an OLR of 1.4 kg COD m^{-3} day^{-1} with 45% COD removal. In another study, Tawfik et al. [66] studied the effect of varying OLR (3.2 to 16 kg COD m^{-3} day^{-1}) using mixed PNSB cultures, which resulted in maximum H_2 production at an OLR of 6.4 kg COD m^{-3} day^{-1}. Increasing OLR caused VFAs accumulation, which might inhibit the PNSB. Therefore, inhibition of the nitrogenase activity resulted in decreasing H_2 production when the OLR was higher than 6.4 kg COD m^{-3} day^{-1} [66]. This is supported by another PF study carried out with acid hydrolyzed wheat starch and a pure culture of *Rhodobacter sp.* [69]. The results of the study showed that, upon increasing the initial sugar concentration from 2.2 to 13.0 g L^{-1}, the H_2 yield (H_2Y) increased, with a maximum H_2Y achieved at 5 g L^{-1} (143.5 mL H_2 g COD^{-1}).

A range of optimum HRT, varying from 2.5 h [66] to 3 days [70] has been reported in the literature for achieving higher photo-H_2 production in a continuous reactor. Tawfik et al. [66] found an optimum HRT at 2.5 h (0.97 ± 0.12 LH_2 $gCOD_{removed}^{-1}$ d^{-1}), when studying a range of

HRT from 0.9 to 4.0 h. They also observed the improvement in removal efficiency of butyrate and lactate when the HRT was increased. Similarly, another study carried out with mixed PNSB by Zhang et al. [67] showed that varying HRTs from 12 to 72 h significantly affected the H_2Y with the highest H_2Y of 482.4 mmol H_2 L^{-1} obtained at a HRT of 36 h. In contrast, Ozmihci and Kargi [70] obtained the highest H_2Y and production rate at an HRT of 72 h during PF of DFE using *Rhodobacter sphaeroides*. The differences in optimum HRT may be attributed to differences in PNSB strains, substrate concentration, carbon to nitrogen ratio (C/N) and other operating conditions such as pH, temperature and light intensity.

6.4.2.2.   Effect of C/N ratio

The carbon to nitrogen ratio plays an important role in the growth of PNSB, photo-H_2 and PHB production. However, higher levels of nitrogen inhibit H_2 production while higher C/N ratios enhance the production of PHB [38, 55, 71, 72]. A low C/N ratio can result in the accumulation of ammonia, which inhibits the nitrogenase and thus the H_2 production process. Therefore, it is always desirable to have nitrogen-limited conditions in the PBR. Due to the nitrogen requirements for bacterial photosynthetic metabolism and inhibition of nitrogenase at higher ammonium concentrations, there is a tradeoff between the minimum amount of nitrogen for bacterial growth and non-inhibiting levels.

A range of C/N ratios has been reported in the literature, i.e. from as low as 8 to as high as 120. Eroglu et al. [71] reported the optimum C/N ratio of 30 with 15 mM to 2 mM (malic acid to glutamic acid) for the maximum hydrogen production rate. In another study, Boran et al. [73] reported a C/N ratio of 38.6 with 40 mM of acetic acid and 2 mM of sodium glutamate in PF by *Rhodobacter capsulatus* in a solar tubular photobioreactor under outdoor conditions. Similarly, Argun et al. [72] reported the optimum total VFAs and NH^+_4-N concentrations of 2350 mg L^{-1} and 47 mg L^{-1}, respectively, for increasing the H_2 production by *Rhodobacter sphaeroides* strains. In another study [74], the highest H_2 production potential of 19.9 m^3 H_2 m^{-3} was obtained from olive mill wastewater with the highest C/N molar ratio of 73.8.

Waligórska et al. [38] found that accumulation of PHB increased by 30 fold when the C/N ratio increased from 6 to 120 in *R. sphaeroides*. However, the amount of PHB accumulation mainly depends on the PNSB strains and the other process operational conditions [12, 14]. As PHB biosynthesis is a H_2 competing pathway, its concomitant production with H_2 could raise future

interests, as PHB possesses economic value as a biodegradable polymer [36]. Some of the results from previous studies on H_2 and PHB production in PF processes are summarized in Table 3.

6.4.2.3. Micronutrients

Microorganisms need different micronutrients such as iron and nickel for their metabolism and growth. The PF process relies on the photosynthetic electron transport systems from which bacteria obtain their energy (Figure 2). The constituents of the electron transport systems such as cytochromes are Fe protein complexes and PNSB strains have 24 Fe atoms in each nitrogenase [75]. Another electron carrier, ferrodoxin, also contains Fe. Thus, Fe limitation can influence the metabolism of PNSB and production of H_2.

Uyar et al. [76] found that the hydrogen yield increases from 0.3 to 1.0 L $L_{culture}^{-1}$ when iron was added to micronutrient. They suggested 0.1 mM of ferric citrate as optimum concentration for hydrogen production. Similarly, Zhu et al. [75] studied the effect of ferrous ion (0-3.2 mg L^{-1}) on PF using *Rhodobacter sphaeroides* and found that the photo-H_2 production was significantly suppressed when Fe^{2+} was limited. The H_2 production increased when increasing the Fe^{2+} concentration and reached the maximum at the concentration of 2.4 mg L^{-1}. In another study, Rai et al. [77] studied the effects of Ni^{2+}, Fe^{2+} and Mg^{2+} on the PF of cheese whey for H_2 production, and showed significant effects of Ni^{2+} and Fe^{2+} supplementation on H_2 yields. However, the presence of nickel might also enhance the hydrogenase activity, which takes up the H_2 produced by the nitrogenase activity, thus decreasing the net H_2 production yield [8].

6.4.2.4. Presence of bicarbonate

Some studies have shown that addition of bicarbonate and carbonate ions enhances the H_2 production in PF [14, 78]. Bicarbonate and carbonate function as electron acceptors and enhance the utilization of butyric and propionic acids, while their absence unbalances the oxidation-reduction potential resulting in decreased H_2 production. Takabatake et al. [78] reported that the presence of carbonate improves assimilation of ammonium (NH_4^+) and VFAs. They also observed that the uptake of 1 mM acetate releases 0.37-0.40 carbonate. However, this internal production of carbonate was not enough to promote butyrate and propionate consumption, which are more reductive than bacterial cells. For PNSB growth on butyrate, each mole of butyrate requires 0.7 mol of CO_2 [14].

Table 3. Comparison of hydrogen and PHB production by different isolated strains and enriched mixed cultures of PNS via photofermentation of various carbon sources.

Microbial inoculum sources	Main carbon and nitrogen source (COD in g L⁻¹)ᵃ	C/N ratio	Light intensity	PHB (% dry cell weight)	Volumetric H₂ Yield (mL H₂ L⁻¹)	Reference
Rhodobacter sphaeroides 17023 (wild type)	30 mM acetate and 7 mM glutamic acid (1.9)	8.6	1500 (Incandescent light)	70.0	0	[33]
Rhodobacter sphaeroides 17023 (wild type)	30 mM lactate and 7 mM glutamic acid (2.8)	12.86	1500 (Incandescent light)	24.0	2310	[33]
Enriched photoheterotrophic culture	DFE (11.61 g/L butyric, 1.76 g/L propionic and 1.01 g/L acetic acid and 0.78 g/L total ammonia (24.8)	10.63	3000 (LED and halogen lamps)	5.0	1478 ± 17	[14]
Rhodobacter capsulatus				29.0	1252 ± 20	[14]
Rhodobacter sphaeroides O.U. 001 (DSM 5648)	0.54 g/L malic acid and 0.8 g/L sodium glutamate in sugar refinery wastewater (30% v/v in medium) (NAᵇ)	-	200 W/m²	70.4	648	[79]
Rhodobacter sphaeroides **AV1a**	DFE of food waste (3.5)	-	40000	32.5 ± 3	914.1 ± 8	[80]
Rhodobacter sphaeroides strain RV	40 mM Acetate only with nitrogen limitation (1.9)	-	5000 (Incandescent light)	38.0	0	[11]

ᵃ COD values are calculated from theoretical oxygen demand of main carbon sources
– Data not available

6.4.3. Environmental conditions

6.4.3.1. Effect of light intensity and wavelength

The light conversion efficiency (η) varies for different PNSB strains because of their different light harvesting antenna pigments, thus they have a different photosynthetically active radiation (PAR) range. However, η also depends on the light intensity, illuminated area of the PBR, reactor design and other operational conditions of the PF process. Generally, the intensity of light has a positive influence on the H₂ production. There are some studies dedicated to assess the effect of the light intensity on growth and H₂ production by PNSB [36, 81–84].

Uyar et al. [81] studied the effect of intensity of light, light wavelength and illumination protocol on the growth and H₂ production by *Rhodobacter sphaeroides* O.U. 001 in photobioreactors

(Figure 4). The hydrogen production increased with increasing the light intensity and the highest production was reached at 270 W m^{-2}. The results also showed the decrease in photo-production of hydrogen by 39% when there is a lack of infrared light (750-950 nm wavelength). The substrate conversion efficiency was increased and hydrogen production was stimulated when the light was illuminated after inoculation and no hydrogen was produced during the dark periods.
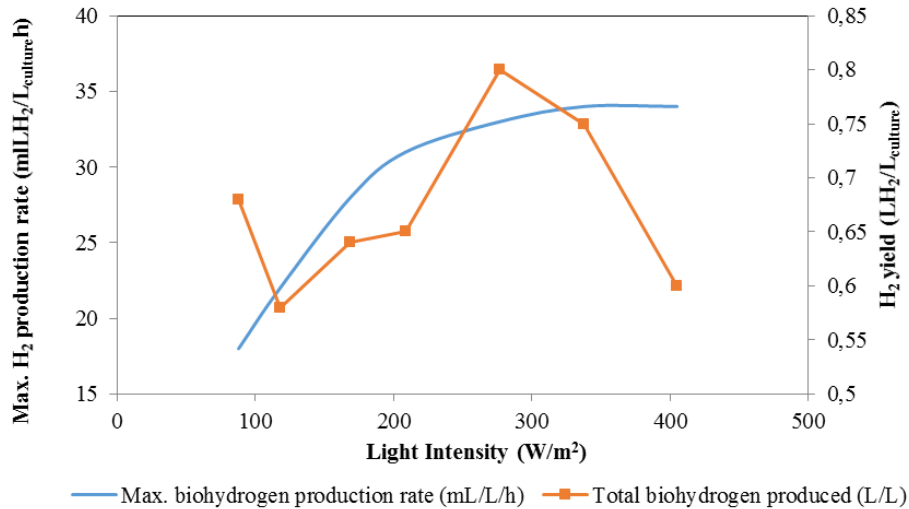
Figure 4. Effect of light intensity on biohydrogen production by *Rhodobacter sphaeroides* O.U. 001 (based on the data obtained from [81]).

Sevinç et al. [82] studied the effect of temperature (20, 30 and 38 °C) and light intensity (1500, 2000, 3000, 4000 and 5000 lux) on the kinetic parameters and hydrogen production in PF of acetic and lactic acid using *Rhodobacter capsulatus*. The results of the study reported the maximum hydrogen production at 5000 lux for 20 °C and 3000 lux for 30 and 38 °C. In a more recent study, Androga et al. [84] established an optimal light intensity and temperature of 287 W m^{-2} (4247.6 Lux) and 27.5 °C, respectively, in PF tests carried out using *R. capsulatus* DSM 1710 in a medium containing acetate, lactate and glutamate. In accordance, Akman et al. [83] reported an optimum light intensity of 263.6 W m^{-2} (3955 lux) in a PF study carried out with acetate as the carbon source and *R. capsulatus*.

Future development of PF systems requires an economical solution to provide the sources of light, so that outdoor systems utilizing natural sunlight become a practical option. Therefore, research interests have been growing to exploit the natural sunlight in PF processes [14, 85–87]. Even though sunlight cannot ensure continuous light conditions, there are some studies that have shown that the dark and light cycles might not have significant effects on photo-H$_2$ production [88] or have positive effects on H$_2$ production depending on the exposure duration of the light

and dark conditions [89]. Montiel-Corona et al. [14] reported a 40.25% reduction in H_2 yields during PF using mixed PNSB in comparison to indoor conditions. However, H_2 yields obtained from outdoor reactors can be comparable to those under indoor conditions [87]. In addition to the type of light source, photofermentative H_2 production also depends on other operating conditions of the PBRs, such as mixing conditions that affects the distribution of light, culture temperature and pH. Furthermore, harnessing the natural light in upscale applications of PF might reduce the cost of long-term PBRs operation.

6.4.3.2.　　　Culture temperature and pH

The operating temperature of a culture is one of the important parameters that affects the bacterial metabolism or metabolic pathways as well as substrate conversion efficiency and thus H_2 production. Basak and Das [54] reported 31 to 36 °C as optimum temperature for *Rhodobacter sp.*, while Androga et al. [84] reported 26.8 °C as optimum culture temperature for a higher H_2 yield. Moreover, culture pH affects the biochemical reactions as it determines the ionic form of the active sites for enzymatic activity [16]. PF studies have been carried out in the pH range varying between 5.5 to 7.5 (Table 2 and 4). Akroum-Amrouche et al. [57] reported an optimum pH of 7.5 (± 0.1) for the H_2 production by *Rhodobacter sphaeroides,* while Nath and Das [90] reported an optimum H_2 production at pH 6.5 for the same PNSB species. This difference of change in optimum pH can be attributed to the difference in substrate type used in PF experiments as lactate was used as a sole carbon source in the former, while DF spent medium was used in the latter study. In another study, Koku et al. [36] reported an optimum pH of 7.1-7.3 for the activity of the nitrogenase enzyme, while the range of 6.5 to 7.5 is optimum for the activity of the hydrogenase enzyme.

During most of the PF tests, pH has shown an increasing trend which could be due to PHB production [11, 90]. Eroglu et al. [71] reported a slight decrease in pH during the bacterial growth phase and pH increase during H_2 production. The effluents from DF are generally in the acidic pH range [4], and are required to be adjusted to a pH range 6.5-7.5 to ensure the optimum operating conditions in the PF process. However, the range of optimum pH seems to be dependent on the PNSB species. Some other studies [66, 63] have shown the feasibility of H_2 production by mixed PNSB at pH 5.5-6.0, which is generally an ideal pH range of DFE obtained from DF processes.

6.4.3.3.   Effect of mixing

Mixing is required in PBRs to keep the PNSB biomass suspended and uniformly distribute the substrates and nutrients in the culture medium. Moreover, since, the light source is non mobile, mixing would only ensures the uniform distribution of light for the suspended microorganisms throughout the PBRs, thus, avoiding light gradients. It also helps to maintain sufficient mass transfer, which generally includes the exchange of gases, i.e. H_2 and CO_2. Akroum-Amrouche et al. [57] found unstable H_2 production with a 13.0% and 60.8% reduction of the average and maximum H_2 production rate when mixing was stopped during the exponential phase of PF. In another study, Li et al. [88] reported that mixing during the H_2 production phase of the PNSB stationary growth phase as vital for higher H_2 yields than during the exponential cell growth phase. Moreover, the type of mixing system may also affect the photo-H_2 production performance. Zhang et al. [67] showed that baffled PBRs can outperform magnetic-stirred PBRs as supported by higher H_2 yields as well as faster cell growth and substrate conversion. This higher H_2 production can be attributed to enhanced gas transfer and distribution of light in the PBRs due to well mixing conditions.

6.4.3.4.   Inhibition of photo-H_2 production

Nitrogenase plays an important role in the hydrogen generation. Thus, the presence of chemical substances that disrupt the nitrogenase activity decreases the photo-H_2 production. Koku et al. [36] reported that the presence of N_2 and NH_4^+ inhibit the H_2 production. Also CO, EDTA and O_2 are likely to inhibit the nitrogenase activities. Similarly, an elevated level of CO_2 inside the reactor inhibits the photo-H_2 production, while lower levels (4-18% w/v) favour the growth phase of PNSB and thus H_2 production (See section 6.4.2). Furthermore, a lower C/N ratio does not favour photo-H_2 production as it could result in the accumulation of ammonium and inhibition of nitrogenase in a PF process for H_2 production.

Table 4. Variation of different operational parameters in PF studies.

PNS strains	Carbon (& nitrogen) source	Culture Reactor type)	Culture Temp. °C	pH	Light intensity (Lux if not specified)	Maximum H$_2$ yield mL H$_2$ g COD^{-1} [b]	Maximum H$_2$ Production Rate mL H$_2$ L^{-1} h^{-1}	Reference
R. sphaeroides O.U.001 (DSM586)	DFE of glucose	Batch	30	6.4	38-50[a] (Tungsten lamp)	-	26.4	[53]
R. capsulatus (DSM1710)	DFE of potato steam peels hydrolysate	Batch	30	6.4	38-50[a] (Tungsten lamp)	-	12.3	[53]
R. capsulatus (hup⁻)	Acetic acid (glutamate)	Continuous Tubular PBR	< 40	< 8.0	Natural sunlight	122.5	8.9	[91]
R. sphaeroides CIP 60.6	Lactate (glutamate)	Batch	30	7.0	4500-8500 (Tungsten lamp)	-	39.8	[57]
R. capsulatus YO3(hup⁻)	Acetate (glutamate)	Fed-batch panel PBR	35	7.0	Natural sunlight	-	11.4	[87]
Rhodopseudomonas palustris WP 3-5	Formic, acetic, butyric, lactic acid (glutamate)	Continuous Column PBR	28-35	6.8	4000-7000	-	13.2	[92]
R. sphaeroides O.U.001	Malate (glutamate)	Batch annular PBR	32	6.8	15 W m^{-2} equivalent	1050	6.5	[93]
Mixed culture	Acetate & glucose (glutamate)	Batch	34	6-7	4000 (Fluorescent light)	78.6[c]	-	[94]
	Butyrate & glucose (glutamate)					74.5[c]	-	
R. capsulatus (DSM 155)	Dark fermented effluents	Batch	30-33	6.6-6.8	4000	-	19.0	[76]
R. sphaeroides O.U.001 (DSM 5864)	Malate	Flat panel PBR	32	6.8	50[a] (Tungsten lamp)	1073.3	10.0	[95]
Rhodopseudomonas palustris WP3-5	Butyrate (glutamic acid)	Batch	32	7.1	10,000 (Tungsten lamp)	803.6	24.9	[96]

[a] Calculated using the available data and conversion values from the URL: http://www.egc.com/useful_info_lighting.php
[b] COD values are calculated from theoretical oxygen demand of main carbon sources
[c] mL H2 g COD^{-1} d^{-1}
- Data not available

6.5. PBR systems

6.5.1. PBR reactor configurations

The design considerations of PBRs for photo-H_2 production are similar to those of PBRs for algal biomass production. However, anaerobic conditions are required for the PF process using PNSB. Most of the published reviews on the design of PBRs for biohydrogen production are based on bioreactors for algal biomass production [35, 97, 98]. In some more recent works [15, 16] the authors summarized the knowledge on the design, illumination and culture strategies of PBR systems aimed at enhancing photo-H_2 production with PNSB.

The most common reactor types reported in the literature are presented in Figure 8.5. More insight has been provided in the performance of different reactors with more elaboration on tubular and flat panel reactors, as these reactors configurations have been the subject of major interest because of their practicability in scaled-up PF processes.

A   B

C   D
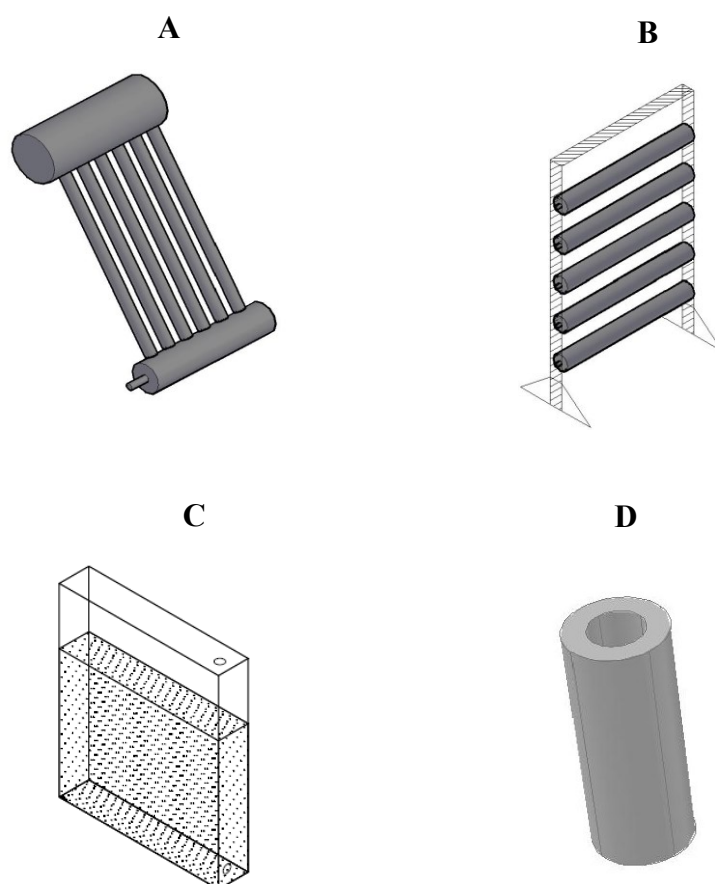
Figure 5. Schematic representation of PBRs. A) nearly horizontal tubular PBR; B) Tubular
(Fence type); C) Flat panel PBR; D) Anular type PBR.

6.5.1.1.   Plate reactors

Plate reactors are flat panels which consist of a rectangular transparent box with a depth vary between 1-5 cm [35]. These reactors have received research attention for photo-H_2 production because of their large illumination area and possibilities of scaling up and suitability in outdoor conditions. Flat plate PBRs are constructed with cheap materials, which are generally transparent to achieve the maximum utilization and conversion of solar energy.

Eroglu et al. [95] investigated the performance of an 8 L flat plate PBR under outdoor operating conditions using a culture of *Rhodobacter sphaeroides* O.U.001. Among the different carbon sources such as malate, lactate, acetate and olive mill wastewater used in the PF, the highest hydrogen production rate (10 mL H_2 L^{-1} h^{-1}) was reached with malate as carbon source and formate was found to be the dominant end product. Ugwu et al. [99] reported the following potential problems that flat plate systems can face during scale up: i) requirement of many compartments and support materials, ii) difficulty in operational temperature control, and iii) wall growth resulting in reduced light penetration.

6.5.1.2.   Tubolar reactors

Tubular PBRs contain a long transparent tube with a length ranging from 10 to 100 meters and diameters ranging from 3 to 6 cm [35]. These PBRs are one of the most suitable reactors for outdoor conditions. Generally, tubular PBRs are constructed with transparent glass or plastic tubes. The culture is recirculated with a mixing system (such as a pump) to provide efficient mass transfer and equal light distribution.

Boran et al. [73] successfully developed and demonstrated a pilot scale (80 L) tubular PBR for photofermentation of acetate using *Rhodobacter capsulatus* in outdoor operating conditions (during winter seasons) in Ankara (Turkey). The PBR gave an average molar productivity of 0.31 mol H_2 m^{-3} h^{-1} during daylight hours and the gas contained 99% hydrogen and 1% carbon dioxide by volume. The system provided an overall hydrogen yield of 0.6 mol H_2 mol^{-1} acetate and the H_2 production with respect to the total illuminated surface area amounted to 0.112 mol H_2 m^{-2} d^{-1}.

Ugwu et al. [99] reported some limitations that tubular PBRs face during scale up: i) difficulty in operational temperature control, ii) fouling and growth on the walls of the tubes, and iii) large space requirements.

One of the major problems during the scaling up of tubular PBRs is the decrease in illumination surface to volume ratio because of the increase in diameter of the tube. This causes a decrease in light intensity (light shading effect) for the cells at the lower part of the tube, which

negatively affects the cell growth. However, a good mixing system provides also an efficient light distribution [100].

6.5.1.3.   Vertical-column reactors

Vertical-column reactors have been subject of research for algal biomass production as they are compact, have low cost and are easy to operate [99]. Bubble columns, airlift reactors and annular column reactors are common vertical-column PBR configurations [101]. Bubble column reactors have a larger diameter than tubular reactors and are frequently used indoor (at a larger lab scale) or outdoor. Because of the larger diameters in these reactors, darker zones are created at the center of the column, which might be disadvantageous for photosynthetic bacterial growth. Besides these three major reactors types, laboratory scale PF research has been carried out in internally illuminated reactors [44]. Dasgupta et al. [97] have briefed the possibility of using different configurations such as torus shaped and helical reactors.

The concept of an annular column reactor aims to overcome the problem associated with the central darker zones in bubble column reactors [101]. The major advantages of this reactor configuration are high mass transfer rate, good mixing conditions with less shear on bacterial cells, low energy consumption and potential for industrial application. However, the small illumination surface makes this configuration less competitive than other counterparts.

6.5.1.4.   Comparison between panel and tubular PBRs

Table 4 compares studies done in various configurations of PBRs. Flat panel and tubular reactors have the highest theoretical efficiencies and have been used at pilot scale under outdoor conditions [73, 95, 102, 103]. These studies opened perspectives for scaling up of these two promising PBRs for photo-H_2 production using PNSB cultures. In some lab scale studies, higher H_2 productivities were obtained with flat panel PBRs, while some studies with tubular PBRs have shown good performance under outdoor light conditions. Moreover, tubular PBRs are easier to manage and scale-up.

Photo-H_2 production through PF can be a promising technology for clean energy recovery. In addition, recovery of PHB can be of further interest. To establish PF as post treatment of DFE, more research needs to be performed for improving the system efficiency through optimization of different operating parameters. The system efficiency can be improved by providing optimum culture conditions and bioreactor design. The PF systems have been presented as the bottlenecks in the integrated DF-PF process because of their higher production cost. Thus, innovative low-cost mixing, heating and cooling systems need to be explored and PBR designs

for improving the surface area to volume (A/V) ratio require future research. Moreover, PHB can add economic value to the PF process. Using mixed PNSB to utilize the conversion efficiencies of different microbial consortia can give an economic advantage by the reducing cost of H_2 production.

Table 5. Comparison of tubular and plate PBRs under outdoor conditions.

PNS strains	Carbon source	PBR type	Volume in liters (Dimension)	Operations conditions	Maximum H_2 yield	Maximum H_2 production rate L H_2 m^{-3} h^{-1}	Productivity per illuminated surface area L H_2 $m^{-2} \cdot d^{-1}$	Productivity per ground area L H_2 $m^{-2} \cdot d^{-1}$)	Light conversion efficiency[a] (%)	Reference
Rhodobacter capsulatus DSM155	Acetate, sodium lactate and glutamate	Flat-panel	4×25 L	Summer (Aachen, Germany)	-	12.3	3.69	29.52	0.20%	[103]
Rhodobacter capsulatus DSM156	Acetate, sodium lactate and glutamate	Tubular	60 L (0.12 m dia. & 0.65 m length)	Summer (Aachen, Germany)	-	6.3	3.35	3.35	0.19%	[103]
Rhodobacter capsulatus DSM 1710	Acetate, lactate and glutamate	Tubular	80 L	Winter (Ankara, Turkey)	15%	6.9	2.46	1.74	1%	[73]
Rhodobacter capsulatus YO3 (Hup⁻)	Acetate and glutamate	Flat-panel	4 L	Summer (Ankara, Turkey)	53%	11.4	1.5	4.93	-	[87]
Rhodobacter capsulatus YO3 (Hup⁻)	Acetate and glutamate	Tubular	90 L	Outdoor Conditions (Ankara, Turkey)	35%	8.9	9.6	6.7	0.20%	[91]
Arthrospira platensis M2 (cyanobacteria)	CO_2	Tubular	34 L	Summer (Florence, Italy)	-	1176.0	738.0	-	5.6% [b]	[104]
Arthrospira platensis M2 (cyanobacteria)	CO_2	Flat-panel	5.4 L	Summer (Florence, Italy)	-	1017.3	686.6	-	4.8% [b]	[104]

[a] Light conversion efficiency was calculated using Equation 10. [b] Efficiency of the cultures was calculated by multiplying the reactor productivity by the mean enthalpy value of the biomass of *A. platensis* M2 cultivated outdoors (21.56 kJ g^{-1}) and divided by the mean visible solar energy input on the PBR surface (14.08 MJ d^{-1}).

6.5.2. Design considerations for PBRs

In addition to the physical parameters such as quantity of light penetrating into the bioreactor, a good PBR design should consider various physico-chemical parameters such as pH, temperature, dissolved oxygen and CO_2, shear due to agitation, C/N ratio, carbon sources and availability of nutrients. As mentioned earlier, these parameters influence various biochemical pathways and ultimately the H_2 production in PBRs.

A general consideration to achieve a good design of PBRs as reported by Dasgupta et al. [97] includes the following physicochemical parameters which affect the performance of PBRs: i) high light penetration into PBRs, ii) high surface area to volume ratio (higher illumination area), iii) temperature and pH control, iv) good mixing system, v) better gas exchange or mass transfer, and vi) transparency and durability of the materials.

6.5.2.1. Surface area to volume (A/V) ratio

The amount of light absorbed by a reactor system is a limiting factor in PBR systems. Surface area to volume ratio is one of the important parameters to be considered during the design of PBRs as it determines the amount of light entering into the system. The higher the A/V ratio, the larger will be the surface area for receiving light for growth and metabolism. Therefore, the A/V ratio can be directly co-related with cell concentration and the volumetric productivity of the system [97].

Gebicki et al. [102] compared hydrogen productivities of a flat panel (A/V ratio of 20 m^{-1}) and an inclined horizontal tubular (A/V ratio of 15.38 m^{-1}) PBR with respect to illuminated surface area and ground area occupied by the reactor. The mean hydrogen productivity of the flat panel reactor was 1250 mL H_2 $m_{illuminated\ surface}^{-2}$ d^{-1}, while that of the tubular reactor was 1100 mL H_2 $m_{illuminated\ surface}^{-2}$ d^{-1}. The illuminated area per unit ground area occupied by the panel reactor was 8.9 times higher than that of the tubular reactor, which gives the economic edge of the comparison. However, a fenced type tubular PBR (Figure 5) could be a research interest in the future as this reactor configuration occupies less space compared to inclined horizontal tubular PBRs.

6.5.2.2. Mixing system

Mixing systems in PBRs could include pumping, mechanical stirring and airlift mixers. Ugwu et al. [100] proposed a static mixer for tubular bioreactors. The selection of the

type of mixing system is important as the pumps used for mixing or recirculation exert shear forces that might be harmful to PNSB. Another disadvantage of the mixing system is the additional cost due to the required energy for its operation.

6.5.2.3.   Construction materials

Selection of materials during the construction of PBRs not only determines the economy, but also the performance of the system. Several factors should be considered while selecting the construction materials. PBRs can be constructed from glass, polyvinyl chloride (PVC) material, low-density polyethylene (LDPE), poly-methyl methacrylate (PMMA) and fiberglass. Dasgupta et al. [97] reported the following properties for the selection of the construction material for PBRs: i) high transparency, ii) durable and low cost, iii) non-toxic to PNS strains and resistant to chemicals and metabolites produced by the PNS strains, and iv) high weathering resistant and easiness in cleaning.

The results of the Net Energy Analysis (NER) of three different materials, viz. glass, LDPE and PMMA, done by Gebicki et al. [103] suggests the use of LDPE for the construction of tubular and panel PBRs.

6.6. Mathematical modeling of growth and product kinetics of PNSB

Knowledge on the kinetics of the biological process becomes vital to have a better design and control of the process. The strong influence of operational parameters such light intensity and substrate concentrations on photofermentative H_2 and PHB synthesis has been demonstrated [13, 28, 33, 81, 84]. However, very limited work has been done on the kinetic analysis of the photofermentation process [36, 105, 106].

6.6.1. Biomass growth

Few mathematical models have been proposed to study growth kinetics of PNSB cultures. A theoretical cell growth rate can be expressed as:

$$\frac{dX}{dt} = \mu X - mX \tag{11}$$

Where: X is the cell dry weight concentration (g L^{-1}), m is maintenance coefficient for biomass (decay rate) and μ is the specific growth rate (h^{-1}). Gadhamshetty et al. [105] proposed the Monod equation to provide the expression for μ to model the growth curve in a batch PBRs with the assumptions that sufficient light and optimal C/N ratio is

available under stressful nitrogen concentrations. The proposed model simulates the biomass growth under substrate-limited conditions as:

$$\frac{dX}{dt} = \mu X = \left(\frac{\mu_m\,S}{K_s+S}\right)X \tag{12}$$

where: the specific growth rate μ (h^{-1}) depends on both maximum specific growth rate μ_m (h^{-1}) and the half saturation constant K_S (mg L^{-1}).

However, the growth curve obtained for *R. sphaeroides* O.U. 001 deviated from the Monod model [55]. The Equation 12 needs to include the substrate inhibition and inhibition due to higher biomass concentration. Moreover, the inhibition from higher substrate levels could be due to osmotic stress and/or the presence of one or more unknown inhibitors such as pigments [105]. Besides higher biomass concentration reduces the light intensity inside the PBR, causes self-shading effects and limits the substrate diffusion, which in turn affects the hydrogen production. Thus, the specific growth rate (μ) in Equation 12 is modified in Equation 13 to include the two inhibitory effects:

$$\mu = \frac{\mu_m S}{K_s+S+\frac{S^2}{K_{Xi}}}\left(1-\frac{X}{X_m}\right) \tag{13}$$

The inhibitory effect due to biomass concentration is provided by a Logistic model. The term "X_m" is the maximum cell dry mass concentration at which growth will cease. The specific growth rate in the Equation 13 is further modified to include the effect of the light exposure on PNSB. The modification included the declining effect of excess light on biomass growth as the surplus absorbed light energy may results in damage and degradation of the reaction center involved in the photosynthetic process. The final equation is expressed as:

$$\mu = \frac{\mu_m S}{K_s+S+\frac{S^2}{K_{Xi}}}\left(1-\frac{X}{X_m}\right)\left(\frac{I}{K_{XI}+I+K_I I^2}\right) \tag{14}$$

where, K_I is light inhibition constant of cell formation (m^2 W^{-1}), K_{XI} is light saturation constant of cell formation (W m^{-2}), K_{Xi} is substrate inhibition constant of cell formation (g L^{-1}) which depends on type of substrate and PNSB strains or culture. The smaller the value of K_I, the larger is the inhibition effect of light on PNSB growth.

6.6.2.   Consumption of substrate

The Contois model can be used to describe the consumption of the substrate.

$$\frac{dS}{dt} = -\frac{\mu_m S}{Y(S+K_S X)} X \tag{15}$$

$$\frac{dS}{dt} = \frac{1}{Y_{\frac{X}{S}}} \mu X \tag{16}$$

6.6.3.   Relation between biomass growth and product formation

Mu et al. [107] used the Modified Luedeking-Piret model to establish the relationship
product (P_i) formation, substrate (S) degradation and biomass (X) growth for the DF
hydrogen production by mixed anaerobic cultures. The following Luedeking-Piret
model could be used to describe the relationship between three parameters. The
Luedeking–Piret model and its modified form can describe the relationship between
formation of H_2 and PHB as products and biomass:

$$\frac{dP_i}{dt} = -Y_{\frac{Pi}{X}}\frac{dX}{dt} + \beta X \tag{17}$$

$$\frac{dP_i}{dt} = -Y_{\frac{P_i}{X}}\frac{dX}{dt} \tag{18}$$

where: 'P_i' is the concentration of the product 'i' and '$Y_{Pi/X}$' is the yield of product 'i'
with respect to biomass 'X'.

Similarly, the formation of products with respect to consumption of substrate can be
written as:

$$\frac{dP_i}{dt} = -Y_{\frac{P_i}{S}}\frac{dS}{dt} \tag{19}$$

where: 'P_i' is the concentration of the product 'i' and '$Y_{pi/s}$' is the yield of product 'i'
with respect to substrate 'S'.

The growth of biomass can be expressed in relation to the substrate consumption as:

$$\frac{dX}{dt} = -Y_{\frac{X}{S}}\frac{dS}{dt} \tag{20}$$

where: 'X' is the concentration of the biomass and '$Y_{X/s}$' is the yield of biomass with
respect to the substrate 'S'.

On integrating Equation 20 from initial concentration (S_0) to final substrate
concentration (S) and product (from initial concentration of 0 to final product
concentration Pi), it is possible to write the following equations:

$$dP_i = -Y_{P_i}dS$$

$$\int_0^{P_i} dP_i = -Y_{P_i} \int_{S_o}^{S} dS \tag{21}$$

$$P_i = -Y_{P_i}(S_0 - S) \tag{20}$$

with i = H$_2$ and PHB.

These relationships can be applied to model the kinetics of substrate consumption, PNSB growth and products formation (H$_2$ and PHB) in the PF process. Some reported values of kinetics parameters established in different PF processes are presented in the following Table.

Table 6. Some reported values of kinetic model parameters.

S.N.	Kinetic Parameters	Values	Reference
1.	μ_m (h^{-1})	0.17	[105]
2.	K_S (g L^{-1})	0.0912	[105]
3.	$Y_{\frac{X}{S}}$ (g g^{-1})	3.7	[71]
4.	K_I (m^2 W^{-1})	0.0975	[56]
5.	K_{XI} (W m^{-2})	22	[105]
6.	K_{Xi} (g L^{-1})	7	[105]

6.7. Future perspectives

6.7.1. Economics

There are very few studies aimed at determining the economics of photo-H$_2$ production [108, 109]. Benemann [108] presented an economic analysis of a conceptual two-stage process where microalgae are used to produce a carbohydrate rich biomass cultivated in large open ponds and hydrogen will be produced in tubular photobioreactors. The paper reported the estimated overall total hydrogen production costs of 9.5 $ GJ^{-1}. Another study [109] conducted a cost analysis of integrated thermophilic DF followed by PF process with 60 kg H$_2$ h^{-1} (2 MW thermal power equivalent) production capacity, operating for 8000 hours per year (PF operating for 10 h per day and 3000 h annually). In this integrated concept, the cost per kilogram of biohydrogen is 56 € (~75.15 $), with 47 € kg H$_2^{-1}$ for tubular PBR based PF process. This cost of production is much higher than that of hydrogen from coal (0.36-1.83 $ kg H$_2^{-1}$) and natural gas (2.48-3.17 $ kg H$_2^{-1}$) [109–111]. However, it has been reported a costs of 21 € kg H$_2^{-1}$ for standalone

thermophilic DF system, which is lower than the production cost of combined system (i.e. 56 € kg H_2^{-1}), thus the PF process needs improvement to lower the unit production cost of H_2.

The light conversion efficiencies of the PF play an important role in determining the economics of photo-hydrogen production. In addition, the substrates and the PNSB strains are also crucial factors. The selection of PBRs also influences the capital and operational cost and in the end, the unit cost of the photo-hydrogen production [109].

6.7.2   Integration with dark fermentation process

PF can be applied as a post treatment stage on DFE, which mostly contains organic acids and alcohols (Figure 6). The integrated DF-PF process has been demonstrated by several studies [17, 66, 112]. DF has the unique capability to utilize a wide range of complex waste biomass that can ensure the future supply of feestock, and combining the two processes (DF + PF) can provide the complete conversion of organic substrate in addition to enhanced H_2 yields. Typical chemical reactions of conversion of organic acids produced in mixed type fermentation to photo-H_2 are presented in Equations 4-7. Redwood et al. [10] reviewed different possible integration strategies for coupling DF-PF processes. In general, DF-PF systems can be integrated in three possible ways; i) utilizing DFE produced in PF systems, ii) cultivating dark and photofermentative microorganisms in one reactor system [113, 114] or iii) separating the two systems by a physical barrier such as a membrane [115, 116]. DF followed by photo-H_2 production is well studied by many researchers [4].

Depending on the process operating parameters such as pH, substrate loading and substrate type, DFE generally has an acidic pH (< 6.0) and inhibiting levels of ammonia and organic acids. Therefore, the DFE requires pre-treatment such pH adjustment, dilution and removal of ammonia before feeding into a PF process. Ammonia concentrations exceeding 2-5 mM inhibit the photo-H_2 production [72, 92]. Therefore, substrates with a higher C/N ratio are usually preferred for PF. Depending on the DFE requirements, several ammonia removal strategies such as stripping, treatment with natural zeolites and membrane processes can be applied [117, 118]. However, most continuous dark fermentative processes lack high ammonia levels due to incomplete conversion of proteins or amino acids present in the substrates, making them ideal substrates for the PF processes.
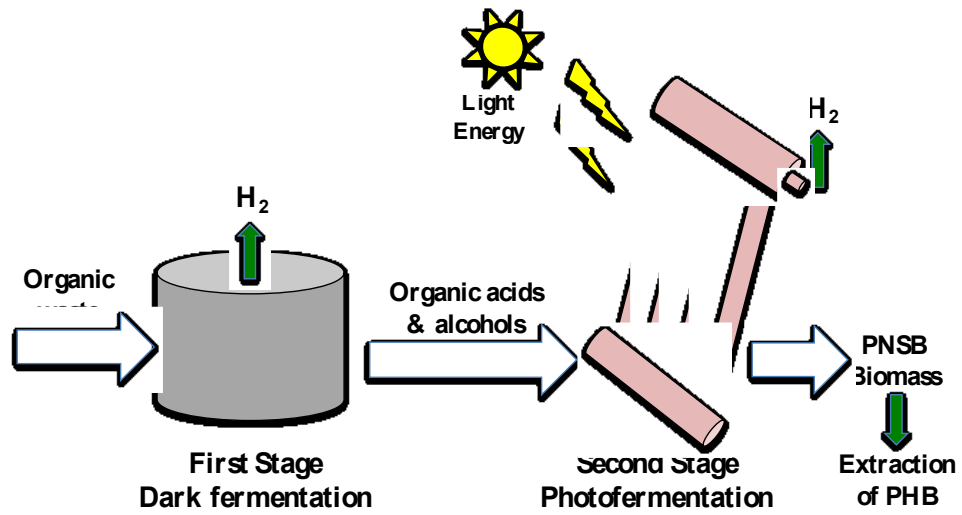
Figure 6. Sequential DF-PF processes for production of H$_2$ and PHB.

References

[1]   Cherubini, F. 2010. The biorefinery concept: Using biomass instead of oil for producing energy and chemicals. Energy Conversion and Management, 51(7), pp.1412-1421.

[2]   Menon, V., Rao, M. 2012. Trends in bioconversion of lignocellulose: Biofuels, platform chemicals & biorefinery concept. Progress in Energy and Combustion Science, 38(4), pp.522-550.

[3]   Balat, H., Kırtay, E. 2010. Hydrogen from biomass - Present scenario and future prospects. International Journal of Hydrogen Energy, 35(14), pp.7416-7426.

[4]   Ghimire, A., Frunzo, L., Pirozzi, F., Trably, E., Escudie, R., Lens, P.N.L., Esposito, G. 2015. A review on dark fermentative biohydrogen production from organic biomass: process parameters and use of by-products. Applied Energy, 144, pp.73-95.

[5]   Das, D., Veziroglu, T.N. 2001. Hydrogen production by biological processes : a survey of literature. International Journal of Hydrogen Energy, 26, pp.13-28.

[6]   Hallenbeck, P.C., Ghosh, D. 2009. Advances in fermentative biohydrogen production: the way forward? Trends in Biotechnology, 27(5), pp.287-97.

[7]   Das, D., Veziroglu, T.N. 2008. Advances in biological hydrogen production processes. International Journal of Hydrogen Energy, 33(21), pp.6046-6057.

[8]   Li, R.Y., Fang, H.H.P. 2009. Heterotrophic photo fermentative hydrogen production. Critical Reviews in Environmental Science and Technology, 39(12), pp.1081-1108.

[9]   Lo, Y.C., Chen, C.Y., Lee, C.M., Chang, J.S. 2010. Sequential dark–photo fermentation and autotrophic microalgal growth for high-yield and CO_2-free biohydrogen production. International Journal of Hydrogen Energy, 35(20), pp.10944-10953.

[10] Redwood, M.D., Paterson-Beedle, M., Macaskie, L.E. 2008. Integrating dark and light bio-hydrogen production strategies: towards the hydrogen economy. Reviews in Environmental Science and Bio/Technology, 8(2), pp.149-185.

[11] Khatipov, E., Miyake, M., Miyake, J., Asada, Y. 1998. Accumulation of poly-beta-hydroxybutyrate by *Rhodobacter sphaeroides* on various carbon and nitrogen substrates. FEMS Microbiology Letter, 162(1), pp.39-45.

[12] De Philippis, R., Ena, A., Guastini, M., Sili, C., Vincenzini, M. 1992. Factors affecting poly-β-hydroxybutyrate accumulation in cyanobacteria and in purple non-sulfur bacteria. FEMS Microbiological Reviews, 103, pp.187-194.

[13] Wu, S.C., Liou, S.Z., Lee, C.M. 2012. Correlation between bio-hydrogen

production and polyhydroxybutyrate (PHB) synthesis by *Rhodopseudomonas palustris* WP3-5. Bioresource Technology, 113, pp.44-50.

[14] Montiel-Corona, V., Revah, S., Morales, M. 2015. Hydrogen production by an enriched photoheterotrophic culture using dark fermentation effluent as substrate: Effect of flushing method, bicarbonate addition, and outdoor-indoor conditions. International Journal of Hydrogen Energy, 40(30), pp.9096-9105.

[15] Adessi, A., De Philippis, R. 2014. Photobioreactor design and illumination systems for H_2 production with anoxygenic photosynthetic bacteria: a review. International Journal of Hydrogen Energy, 39(7), pp.3127-3141.

[16] Chen, C.Y., Liu, C.H., Lo, Y.C., Chang, J.S. 2011. Perspectives on cultivation strategies and photobioreactor designs for photo-fermentative hydrogen production. Bioresource technology, 102(18), pp.8484-8492.

[17] Rai, P.K., Singh, S.P., Asthana, R.K. 2014. Biohydrogen production from sugarcane bagasse by integrating dark- and photo-fermentation. Bioresource Technology, 152, pp.140-146.

[18] Nasr, M., Tawfik, A., Ookawara, S., Suzuki, M., Kumari, S., Bux, F. 2014. Continuous biohydrogen production from starch wastewater via sequential dark-photo fermentation with emphasize on maghemite nanoparticles. Journal of Industrial and Engineering Chemistry, 21, pp.500-506

[19] Cheng, J., Ding, L., Xia, A., Lin, R., Li, Y., Zhou, J., Cen, K. 2015. Hydrogen production using amino acids obtained by protein degradation in waste biomass by combined dark- and photo-fermentation. Bioresource Technology, 179, pp.13-19.

[20] Chookaew, T., O-thong, S., Prasertsan, P. 2015. Biohydrogen production from crude glycerol by two stage of dark and photo fermentation. International Journal of Hydrogen Energy, 40(24), pp.2-7.

[21] Dipasquale, L., Adessi, A., d'Ippolito, G., Rossi, F., Fontana, A., De Philippis, R. 2015. Introducing capnophilic lactic fermentation in a combined dark-photo fermentation process: a route to unparalleled H_2 yields. Applied Microbiology and Biotechnology, 99(2), pp.1001–1010.

[22] Eroğlu, E., Eroğlu, I., Gündüz, U., Yücel, M. 2008. Effect of clay pretreatment on photofermentative hydrogen production from olive mill wastewater. Bioresource Technology, 99(15), pp.6799-808.

[23] Hülsen, T., Batstone, D.J., Keller, J. 2014. Phototrophic bacteria for nutrient recovery from domestic wastewater. Water Research, 50, pp.18-26.

[24] Kim, B.H., Gadd, G.M. 2008. *Bacterial Physiology and Metabolism*. Cambridge University Press.

[25] McEwan, A.G. 1994. Photosynthetic electron transport and anaerobic metabolism in purple non-sulfur phototrophic bacteria. Antonie van Leeuwenhoek, 66(1-3), pp.151–64.

[26] Hallenbeck, P.C., Benemann, J.R. 2002. Biological hydrogen production; fundamentals and limiting processes. International Journal of Hydrogen Energy, 27(11), pp.1185-1193.

[27] Imhoff, J.F., Truper, H.G., Pfennig, N. 1984. Rearrangement of the species and genera of the phototrophic purple nonsulfur bacteria. International Journal of Systematic Biology, 34(3), pp.340-343.

[28] Han, H., Liu, B., Yang, H., Shen, J. 2012. Effect of carbon sources on the photobiological production of hydrogen using *Rhodobacter sphaeroides* RV. International Journal of Hydrogen Energy, 37(17), pp.12167-12174.

[29] Barbosa, M.J., Rocha, J.M., Tramper, J., Wijffels, R.H. 2001. Acetate as a carbon source for hydrogen production by photosynthetic bacteria. Journal of Biotechnology, 85(1), pp.25-33.

[30] Bianchi, L., Mannelli, F., Viti, C., Adessi, A., De Philippis, R. 2010. Hydrogen-producing purple non-sulfur bacteria isolated from the trophic lake Averno (Naples, Italy). International Journal of Hydrogen Energy, 35(22), pp.12216-12223.

[31] Kars, G., Gündüz, U. 2010. Towards a super H_2 producer: improvements in photofermentative biohydrogen production by genetic manipulations. International Journal of Hydrogen Energy, 35(13), pp.6646-6656.

[32] Wang, R., Cui, C., Jin, Y., Liu, B., Xing, D., Xie, G., Ren, N. 2014. Photo-fermentative hydrogen production from mixed substrate by mixed bacteria. International Journal of Hydrogen Energy, 39(25), pp.1-5.

[33] Hustede, E., Steinbüchel, A., Schlegel, H.G. 1993. Relationship between the photoproduction of hydrogen and the accumulation of PHB in non-sulphur purple bacteria. Applied Microbiology and Biotechnology, 39, pp.87-93.

[34] Hu, X., Ritz, T., Damjanović, A., Autenrieth, F., Schulten, K. 2002. *Photosynthetic apparatus of purple bacteria*. Quarterly reviews of biophysics (Vol. 35).

[35] Akkerman, I., Janssen, M., Rocha, J., Wijffels, R.H. 2002. Photobiological hydrogen production: photochemical efficiency and bioreactor design. International Association of Hydrogen Energy, 27, pp.1195-1208.

[36] Koku, H., Eroglu, I., Gunduz, U., Yucel, M., Turker, L. 2002. Aspects of the metabolism of hydrogen production by *Rhodobacter sphaeroides*. International Journal of Hydrogen Energy, 27(11-12), pp.1315-1329.

[37] Eroglu, E., Melis, A. 2011. Photobiological hydrogen production: recent advances and state of the art. Bioresource Technology, 102(18), pp.8403-8413.

[38] Waligórska, M., Seifert, K., Górecki, K., Moritz, M., Laniecki, M. 2009. Kinetic model of hydrogen generation by *Rhodobacter sphaeroides* in the presence of NH_4^+ ions. Journal of Applied Microbiology, 107(4), pp.1308-1318.

[39] Kim, M.S., Kim, D.H., Son, H.N., Ten, L.N., Lee, J.K. 2011. Enhancing photo-fermentative hydrogen production by *Rhodobacter sphaeroides* KD131 and its PHB synthase deleted-mutant from acetate and butyrate. International Journal of Hydrogen Energy, 36(21), pp.13964-13971.

[40] Venil, C.K., Zakaria, Z.A., Ahmad, W.A. 2013. Bacterial pigments and their applications. Process Biochemistry, 48(7), pp.1065-1079.

[41] Schmidt, K. 1971. Carotenoids of purple nonsulfur bacteria. Archives of Microbiology, 77(3), pp.231-238.

[42] Cohen-Bazire, G., Sistrom, W.R., Stanier, R.Y. 1965. Kinetic studies of pigment synthesis by non-sulfur purple bacteria. Journal of Cellular and Comparative Physiology, 49(1), pp.25-68.

[43] Rupprecht, J., Hankamer, B., Mussgnug, J.H., Ananyev, G., Dismukes, C., Kruse, O. 2006. Perspectives and advances of biological H_2 production in microorganisms. Applied Microbiology and Biotechnology, 72(3), pp.442-449.

[44] Chen, C., Yeh, K., Lo, Y., Wang, H., Chang, J. 2010. Engineering strategies for the enhanced photo-H_2 production using effluents of dark fermentation processes as substrate. International Journal of Hydrogen Energy, 35(24), pp.13356-13364.

[45] Lee, Z.K., Li, S.L., Kuo, P.C., Chen, I.C., Tien, Y.M., Huang, Y.J., Chuang, C.P., Wong, S.C., Cheng, S.-S. 2010. Thermophilic bio-energy process study on hydrogen fermentation with vegetable kitchen waste. International Journal of Hydrogen Energy, 35(24), pp.13458-13466.

[46] Cheng, X.Y., Liu, C.Z. 2011. Hydrogen Production via Thermophilic Fermentation of Cornstalk by Clostridium thermocellum. Energy & Fuels, 25(4), pp.1714-1720.

[47] Redwood, M.D., Dhillon, R., Orozco, R.L., Zhang, X., Binks, D.J., Dickinson, M., Macaskie, L.E. 2012. Enhanced photosynthetic output via dichroic beam-sharing. Biotechnology Letters, 34(12), pp.2229-2234.

[48] Ozturk, Y., Yucel, M., Daldal, F., Mandaci, S., Gunduz, U., Turker, L., Eroglu, I. 2006. Hydrogen production by using *Rhodobacter capsulatus* mutants with genetically modified electron transfer chains. International Journal of Hydrogen Energy, 31(11), pp.1545-1552.

[49] Kondo, T., Arakawa, M., Hirai, T., Wakayama, T., Hara, M., Miyake, J. 2002.

Enhancement of hydrogen production by a photosynthetic bacterium mutant with reduced pigment. Journal of Bioscience and Bioengineering, 93(2), pp.145-150.

[50] Franchi, E., Tosi, C., Scolla, G., Della Penna, G., Rodriguez, F., Pedroni, P. M. 2005. Metabolically engineered *Rhodobacter sphaeroides* RV strains for improved biohydrogen photoproduction combined with disposal of food wastes. Marine Biotechnology, 6(6), pp.552-565.

[51] Uyar, B., Gürgan, M., Özgür, E., Gündüz, U., Yücel, M., Eroglu, I. 2015. Hydrogen production by hup− mutant and wild-type strains of *Rhodobacter capsulatus* from dark fermentation effluent of sugar beet thick juice in batch and continuous photobioreactors. Bioprocess and Biosystems Engineering, 38(10), pp.1935-1942.

[52] Imhoff, J. F., Hiraishi, A., Suling, J. 2005. Anoxygenic Phototrophic Purple Bacteria. In Bergey's Manual® of Systematic Bacteriology of Systematic Bacteriology (pp. 119-132). Springer US.

[53] Afsar, N., Özgür, E., Gürgan, M., Akköse, S., Yücel, M., Gündüz, U., Eroglu, I. 2011. Hydrogen productivity of photosynthetic bacteria on dark fermenter effluent of potato steam peels hydrolysate. International Journal of Hydrogen Energy, 36(1), pp.432-438.

[54] Basak, N., Das, D. 2007. The Prospect of purple non-sulfur (PNS) photosynthetic bacteria for hydrogen production: The Present State of the Art. World Journal of Microbiology and Biotechnology, 23(1), pp.31-42.

[55] Koku, H., Eroglu, I., Gunduz, U., Yucel, M., Turker, L. 2003. Kinetics of biological hydrogen production by the photosynthetic bacterium *Rhodobacter sphaeroides* O.U. 001. International Journal of Hydrogen Energy, 28(4), pp.381-388.

[56] Sasikala, K., Ramana, C.V., Roa, P.R. 1991. Environmental regulation for optimal biomass yield and photoreduction of hydrogen by *Rhodobacter sphaeroides* O.U.001. International Journal of Hydrogen Energy, 16(9), pp.597-601.

[57] Akroum-Amrouche, D., Abdi, N., Lounici, H., Mameri, N. 2011. Effect of physico-chemical parameters on biohydrogen production and growth characteristics by batch culture of *Rhodobacter sphaeroides* CIP 60.6. Applied Energy, 88(6), pp.2130-2135.

[58] Liu, B.F., Xie, G.J., Ding, J., Ren, N.Q. 2011. Optimization of photo-hydrogen production by immobilized *Rhodopseudomonas Faecalis* RLD-53. Natural Resources, 2(1), pp.1-7.

[59] Chen, C.Y., Chang, J.S. 2006. Enhancing phototropic hydrogen production by solid-carrier assisted fermentation and internal optical-fiber illumination. Process Biochemistry, 41(9), pp.2041-2049.

[60] Zhu, H., Suzuki, T., Tsygankov, A.A., Asada, Y., Miyake, J. 1999. Hydrogen production from tofu wastewater by *Rhodobacter sphaeroides* immobilized in agar gels. International Journal of Hydrogen Energy, 24(4), pp.305-310.

[61] Zhu, H., Wakayama, T., Suzuki, T., Asada, Y., Miyake, J. 1999. Entrapment of *Rhodobacter sphaeroides* RV in cationic polymer/agar gels for hydrogen production in the presence of NH_4^+. Journal of Bioscience and Bioengineering, 88(5), pp.507-512.

[62] Yanling, Y., Zhenmei, L.V, Hang, M.I.N., Jun, C. 2008. Dynamic changes of microbial community diversity in a photohydrogen producing reactor monitored by PCR-DGGE. Journal of Environmental Science, 20, pp.1118-1125.

[63] Tao, Y., Yangling, H., Wu, Y., Liu, F., Li, X., Zong, W., Zhou, Z. 2008. Characteristics of a new photosynthetic bacterial strain for hydrogen production and its application in wastewater treatment. International Journal of Hydrogen Energy, 33(3), pp.963-973.

[64] Suwansaard, M., Choorit, W., Zeilstra-Ryalls, J.H., Prasertsan, P. 2009. Isolation of anoxygenic photosynthetic bacteria from Songkhla Lake for use in a two-staged biohydrogen production process from palm oil mill effluent. International Journal of Hydrogen Energy, 34(17), pp.7523-7529.

[65] Ren, N.Q., Liu, B.F., Ding, J., Xie, G.J. 2009. Hydrogen production with *R. faecalis* RLD-53 isolated from freshwater pond sludge. Bioresource Technology, 100(1), pp.484-487.

[66] Tawfik, A., El-Bery, H., Kumari, S., Bux, F. 2014. Use of mixed culture bacteria for photofermentive hydrogen of dark fermentation effluent. Bioresource Technology, 168, pp.119-126.

[67] Zhang, Z., Wang, Y., Hu, J., Wu, Q., Zhang, Q. 2015. Influence of mixing method and hydraulic retention time on hydrogen production through photo-fermentation with mixed strains. International Journal of Hydrogen Energy, 40(20), pp.6521-6529.

[68] Venkata Mohan, S., Srikanth, S., Dinakar, P., Sarma, P.N. 2008. Photo-biological hydrogen production by the adopted mixed culture: data enveloping analysis. International Journal of Hydrogen Energy, 33(2), pp.559-569.

[69] Kapdan, I.K., Kargi, F., Oztekin, R., Argun, H. 2009. Bio-hydrogen production from acid hydrolyzed wheat starch by photo-fermentation using different *Rhodobacter* sp. International Journal of Hydrogen Energy, 34(5), pp.2201-2207.

[70] Ozmihci, S., Kargi, F. 2010. Bio-hydrogen production by photo-fermentation of dark fermentation effluent with intermittent feeding and effluent removal. International Journal of Hydrogen Energy, 35(13), pp.6674-6680.

[71] Eroglu, I., Aslan, K., Gu, U. 1999. Substrate consumption rates for hydrogen production by *Rhodobacter sphaeroides* in a column photobioreactor, 70, pp.103-113.

[72] Argun, H., Kargi, F., Kapdan, I. 2008. Light fermentation of dark fermentation effluent for bio-hydrogen production by different *Rhodobacter* species at different initial volatile fatty acid (VFA) concentrations. International Journal of Hydrogen Energy, 33(24), pp.7405-7412.

[73] Boran, E., Özgür, E., van der Burg, J., Yücel, M., Gündüz, U., Eroglu, I. 2010. Biological hydrogen production by *Rhodobacter capsulatus* in solar tubular photo bioreactor. Journal of Cleaner Production, 18, pp.S29-S35.

[74] Eroğlu, E., Eroğlu, İ., Gündüz, U., Yücel, M. 2009. Comparison of physicochemical characteristics and photofermentative hydrogen production potential of wastewaters produced from different olive oil mills in Western-Anatolia, Turkey. Biomass and Bioenergy, 33(4), pp.706-711.

[75] Zhu, H., Fang, H., Zhang, T., Beaudette, L. 2007. Effect of ferrous ion on photo heterotrophic hydrogen production by *Rhodobacter sphaeroides*. International Journal of Hydrogen Energy, 32(17), pp.4112-4118.

[76] Uyar, B., Schumacher, M., Gebicki, J., Modigell, M. 2009. Photoproduction of hydrogen by *Rhodobacter capsulatus* from thermophilic fermentation effluent. Bioprocess and Biosystems Engineering, 32(5), pp.603-606.

[77] Rai, P.K., Asthana, R.K., Singh, S.P. 2014. Optimization of photo-hydrogen production based on cheese whey spent medium. International Journal of Hydrogen Energy, 39(14), pp.7597-7603.

[78] Takabatake, H., Suzuki, K., Ko, I.B., Noike, T. 2004. Characteristics of anaerobic ammonia removal by a mixed culture of hydrogen producing photosynthetic bacteria. Bioresource Technology, 95(2), pp.151-158.

[79] Yiğit, D.Ö., Gündüz, U., Türker, L., Yücel, M., Eroğlu, N. 1999. Identification of by-products in hydrogen producing bacteria; *Rhodobacter sphaeroides* O.U. 001 grown in the waste water of a sugar refinery. Progress in Industrial Microbiology, 35(C), pp.125-131.

[80] Ghimire, A., Valentino, S., Frunzo, L., Pirozzi, F., Lens, P.N.L., Esposito, G. 2016. Concomitant biohydrogen and poly-β-hydroxybutyrate production from dark fermentation effluents by adapted *Rhodobacter sphaeroides* and mixed photofermentative cultures. Bioresource Technology, 217, pp.157-164.

[81] Uyar, B., Eroglu, I., Yucel, M., Gunduz, U., Turker, L. 2007. Effect of light intensity, wavelength and illumination protocol on hydrogen production in photobioreactors. International Journal of Hydrogen Energy, 32(18), pp.4670-4677.

[82] Sevinç, P., Gündüz, U., Eroglu, I., Yücel, M. 2012. Kinetic analysis of photosynthetic growth, hydrogen production and dual substrate utilization by *Rhodobacter capsulatus*. International Journal of Hydrogen Energy, 37(21), pp.16430-16436.

[83] Akman, M.C., Erguder, T.H., Gündüz, U., Eroğlu, İ. 2015. Investigation of the effects of initial substrate and biomass concentrations and light intensity on photofermentative hydrogen gas production by Response Surface Methodology. International Journal of Hydrogen Energy, 40(15), pp.1-8.

[84] Androga, D.D., Sevinç, P., Koku, H., Yücel, M., Gündüz, U., Eroglu, I. 2014. Optimization of temperature and light intensity for improved photofermentative hydrogen production using *Rhodobacter capsulatus* DSM 1710. International Journal of Hydrogen Energy, 39(6), pp.2472-2480.

[85] Androga, D.D., Özgür, E., Eroglu, I., Gündüz, U., Yücel, M. 2012. Photofermentative Hydrogen Production in Outdoor Conditions. In Hydrogen Energy-Challenges and Perspectives. InTech.

[86] Avcioglu, S.G., Ozgur, E., Eroglu, I., Yucel, M., Gunduz, U. 2011. Biohydrogen production in an outdoor panel photobioreactor on dark fermentation effluent of molasses. International Journal of Hydrogen Energy, 36(17), pp.11360-11368.

[87] Androga, D.D., Ozgur, E., Gunduz, U., Yucel, M., Eroglu, I. 2011. Factors affecting the longterm stability of biomass and hydrogen productivity in outdoor photofermentation. International Journal of Hydrogen Energy, 36(17), pp.11369-11378.

[88] Li, X., Wang, Y., Zhang, S., Chu, J., Zhang, M., Huang, M., Zhuang, Y. 2011. Effects of light/dark cycle, mixing pattern and partial pressure of H_2 on biohydrogen production by *Rhodobacter sphaeroides* ZX-5. Bioresource Technology, 102(2), pp.1142-1148.

[89] Sargsyan, H., Gabrielyan, L., Hakobyan, L., Trchounian, A. 2015. Light–dark duration alternation effects on *Rhodobacter sphaeroides* growth, membrane properties and bio-hydrogen production in batch culture. International Journal of Hydrogen Energy, 40(11), pp.4084-4091.

[90] Nath, K., Das, D. 2009. Effect of light intensity and initial pH during hydrogen production by an integrated dark and photofermentation process. International Journal of Hydrogen Energy, 34(17), pp.7497-7501.

[91] Boran, E., Ozgur, E., Yucel, M., Gunduz, U., Eroglu, I. 2012. Biohydrogen production by *Rhodobacter capsulatus* Hup− mutant in pilot solar tubular photobioreactor. International Journal of Hydrogen Energy, 37, pp.16437-16445.

[92] Lee, C.M., Hung, G.J., Yang, C.F. 2011. Hydrogen production by *Rhodopseudomonas palustris* WP 3-5 in a serial photobioreactor fed with

147

hydrogen fermentation effluent. Bioresource Technology, 102(18), pp.8350-8356.

[93] Basak, N., Das, D. 2009. Photofermentative hydrogen production using purple non-sulfur bacteria *Rhodobacter sphaeroides* O.U.001 in an annular photobioreactor: a case study. Biomass and Bioenergy, 33(6-7), pp.911-919.

[94] Srikanth, S., Venkata Mohan, S., Prathima Devi, M., Peri, D., Sarma, P.N. 2009. Acetate and butyrate as substrates for hydrogen production through photo-fermentation: Process optimization and combined performance evaluation. International Journal of Hydrogen Energy, 34(17), pp.7513-7522.

[95] Eroglu, I., Tabanoglu, A., Gunduz, U., Eroglu, E., Yucel, M. 2008. Hydrogen production by *Rhodobacter sphaeroides* O.U.001 in a flat plate solar bioreactor. International Journal of Hydrogen Energy, 33(2), pp.531-541.

[96] Chen, C., Lu, W., Wu, J., Chang, J. 2007. Enhancing phototrophic hydrogen production of *Rhodopseudomonas palustris* via statistical experimental design. International Journal of Hydrogen Energy, 32(8), pp.940-949.

[97] Dasgupta, C.N., Gilbert, J.J., Lindblad, P., Heidorn, T., Borgvang, S.A., Skjanes, K., Das, D. 2010. Recent trends on the development of photobiological processes and photobioreactors for the improvement of hydrogen production. International Journal of Hydrogen Energy, 35(19), pp.10218-10238.

[98] Carvalho, A.P., Meireles, L.A., Malcata, F.X. 2006. Microalgal reactors: a review of enclosed system designs and performances. Biotechnology Progress, 22(6), pp.1490-1506.

[99] Ugwu, C.U., Aoyagi, H., Uchiyama, H. 2008. Photobioreactors for mass cultivation of algae. Bioresource technology, 99(10), pp.4021-4028.

[100] Ugwu, C.U., Ogbonna, J.C., Tanaka, H. 2003. Design of static mixers for inclined tubular photobioreactors. Journal of Applied Phycology, 15(2/3), pp.217-223.

[101] Posten, C. 2009. Design principles of photo-bioreactors for cultivation of microalgae. Engineering in Life Sciences, 9(3), pp.165-177.

[102] Gebicki, J., Modigell, M., Schumacher M., Burg, J.V.D., Roebroeck, E. 2009. Development of photobioreactors for anoxygenic production of hydrogen by purple bacteria. Chemical Engineering Transactions, 18, pp.363-366.

[103] Gebicki, J., Modigell, M., Schumacher, M., van der Burg, J., Roebroeck, E. 2010. Comparison of two reactor concepts for anoxygenic H_2 production by *Rhodobacter capsulatus*. Journal of Cleaner Production, 18, pp.S36-S42.

[104] Tredici, M.R., Zittelli, G.C. 1998. Efficiency of Sunlight Utilization : Tubular Versus Flat Photobioreactors Biotechnology and Bioengineering, 57(2), pp.187-197.

[105]   Gadhamshetty, V., Sukumaran, A., Nirmalakhandan, N., Theinmyint, M. 2008. Photofermentation of malate for biohydrogen production— a modeling approach. International Journal of Hydrogen Energy, 33(9), pp.2138-2146.

[106]   Zhang, D., Dechatiwongse, P., del Rio-Chanona, E.A., Maitland, G.C., Hellgardt, K., Vassiliadis, V.S. 2015. Modelling of light and temperature influences on cyanobacterial growth and biohydrogen production. Algal Research, 9, pp.263-274.

[107]   Mu, Y., Wang, G., Yu, H.Q. 2006. Kinetic modeling of batch hydrogen production process by mixed anaerobic cultures. Bioresource technology, 97(11), pp.1302-1307.

[108]   Benemann, J.R. 1997. Feasibility analysis of photobiological hydrogen production. International Association of Hydrogen Energy, 22, pp.979-987.

[109]   HYVOLUTION. 2011. *Non-thermal production of pure hydrogen-Final Activity Report*. Wageningen, The Netherlands.

[110]   Bartels, J.R., Pate, M.B., Olson, N.K. 2010. An economic survey of hydrogen production from conventional and alternative energy sources. International Journal of Hydrogen Energy, 35(16), pp.8371-8384.

[111]   Claassen, P.A., de Vrije, T., Koukios, E., van Niel, E., Eroglu, I., Modigell, M., Friedl, A., Wukovits, W., Ahrer, W., 2010. Non-thermal production of pure hydrogen from biomass: HYVOLUTION. Journal of Cleaner Production, 18, pp.S4-S8.

[112]   Yang, H., Shi, B., Ma, H., Guo, L. 2015. Enhanced hydrogen production from cornstalk by dark- and photo-fermentation with diluted alkali-cellulase two-step hydrolysis. International Journal of Hydrogen Energy, 40(36), pp.1–8.

[113]   Chandra, R., Nikhil, G., Mohan, S. 2015. Single-stage operation of hybrid dark-photo fermentation to enhance biohydrogen production through regulation of system redox condition: evaluation with real-field wastewater. International Journal of Molecular Sciences, 16(5), pp.9540-9556.

[114]   Liu, B.F., Ren, N.Q., Tang, J., Ding, J., Liu, W.Z., Xu, J.F., Cao, G.L., Guo, W.Q. and Xie, G.J., 2010. Bio-hydrogen production by mixed culture of photo- and dark-fermentation bacteria. International Journal of Hydrogen Energy, 35(7), pp.2858-2862.

[115]   Redwood, M.D., Orozco, R.L., Majewski, A., Macaskie, L.E. 2011. Biohydrogen production by extractive fermentation and photofermentation, pp.2–7.

[116]   Liu, B.F., Xie, G.J., Wang, R.Q., Xing, D.F., Ding, J., Zhou, X., Ren, H.Y., Ma, C. and Ren, N.Q., 2015. Simultaneous hydrogen and ethanol production from

cascade utilization of mono-substrate in integrated dark and photo-fermentative reactor. Biotechnology for Biofuels, 8(1), p.8.

[117] Androga, D.D., Özgür, E., Eroglu, I., Gündüz, U., Yücel, M. 2012. Amelioration of photofermentative hydrogen production from molasses dark fermenter effluent by zeolite-based removal of ammonium ion. International Journal of Hydrogen Energy, 37(21), pp.16421-16429.

[118] Redwood, M.D., Orozco, R.L., Majewski, A.J., Macaskie, L.E. 2012. An integrated biohydrogen refinery: Synergy of photofermentation, extractive fermentation and hydrothermal hydrolysis of food wastes. Bioresource Technology, 119, pp.384-392.

Chapter 7

Photofermentative Production of Hydrogen and Poly-β-hydroxybutyrate from Dark Fermentation Products

Photofermentative Production of Hydrogen and
Poly-β-hydroxybutyrate from Dark Fermentation Products

The aim of this work is to investigate the hydrogen and poly-β-hydroxybutyrate (PHB) production during the photofermentative treatment of the effluent from a dark fermentation reactor fed with the organic fraction of municipal solid waste. Two different inocula, an adapted culture of *Rhodobacter sphaeroides* AV1b and a mixed consortium of purple non sulphur bacteria have been investigated under the same operational conditions. Different hydrogen productivities of 364 and 559 N mL H_2 L^{-1} were observed for the *Rhodobacter sphaeroides* and the mixed culture consortium tests, respectively: the consortium of PNSB resulted 1.5 fold more productive than the pure culture. On the other hand, *Rhodobacter sphaeroides* culture showed a higher PHB productivity (155 mg PHB g COD^{-1}) than the mixed culture (55 mg PHB g COD^{-1}). In all the tests, the concomitant H_2 and PHB production was associated to a dissolved COD removal higher than 80%.

7.1. Introduction

In energy and environmental field, hydrogen (H_2) has gained considerable interests due to its higher specific energy content (122 MJ kg^{-1}), clean combustion [1] and environmental friendliness in production and use [2, 3, 4].

At present, the production of H_2 for industrial applications comes mainly from thermo-catalytic and gasification processes, which in turn are fossil fuels dependent. In comparison to these energy intensive physico-chemical routes for H_2 production, biological processes represent a valid alternative as they can utilize renewable biomasses [4]. However, one of the main challenges arising from the use of low value organic biomass for hydrogen production lies in the maximization of hydrogen yields. The dark fermentation (DF) of waste biomass represents the most explored biological route for the biohydrogen production. However, dark fermentative degradation of carbohydrate rich organic biomass normally leads to incomplete substrate conversion and low H_2 yields due to thermodynamic constrains and accumulation of organic acids and alcohols as by-products [5, 6]. These different types of carbon can be used as a reducing energy source by other microbial species to perform diverse biochemical reactions [7]. Therefore, combining the DF with other processes such as

photo fermentation (PF) or bioelectrochemical systems could lead to higher H_2 yields and enhance the waste biomass valorization [8].

Under anaerobic conditions, Purple Non-Sulphur Bacteria (PNSB) carry out an anaerobic photosynthesis using light and reduced carbon sources, such as organic acids and alcohols, to produce H_2. This ability could be exploited for treating dark fermentation effluents (DFE) [9, 10]. Indeed, the combined DF - PF process not only results in a higher hydrogen production (e. g. 4 extra H_2 moles for each mole of acetic acid), but also in the possibility of synthetizing poly-β-hydroxybutyrate, which is a biopolymer precursor of economic interest [11].

In photofermentative bacteria, PHB is often produced under nutrient starvation and accumulated in the cytoplasm as intracellular carbon and energy storage compounds. Several studies have been conducted on PHB or, generally, on poly-hydroxyalkalonates (PHA) bio-accumulation [12, 13], as the optimization of the biological production of plastic material may be seen as the way to overpass the environmental and recycling issues deriving from the wide utilization of petrochemical-derived plastic materials. However, their extraction and production procedures do not allow the commercial application due to the high costs required.

H_2 and PHB production strongly depend on the Volatile Fatty Acids (VFAs) present in the DFE used as feedstock for the PF. Based on the type and concentration of VFAs in the culture media, PNSB can differently convert organic sources in biological H_2 by several pathways [14, 15]. Moreover, the structures of these copolymers directly affect their mechanical properties and thus their feasible applications [16].

Several studies report that the synthesis of PHB competes with the H_2 production, as both functions constitute the way to dissipate the excess reducing power [17]. Nonetheless, a concomitant production of H_2 and PHB is possible, as shown by other studies [11, 14], but it depends on several operating conditions, such as nutrients availability (carbon to nitrogen (C/N) ratio), PNSB strains (mixed and pure culture), pH, light intensity and presence of physico-chemical stress, e.g. major H_2 inhibitor, ammonium in the culture medium, sulphur deprived conditions [18, 19, 20, 21]. Depending on the aim of the process, PF can be directed towards H_2 production, suppressing the PHB synthesis by genetic modifications of the PNSB [22] or towards PHB accumulation in photosynthetic bacteria by controlling acetate and nitrogen availability in the growth medium.

153

The majority of the studies on both photofermentative H_2 production and PHB accumulation involved the use of pure cultures and simple organic substrates. While the use of pure strains usually results metabolically advantageous, one of the main drawbacks in the scale-up of the PF process relies on the presence of inhibitory compounds or competitive species that can affect the purity of the cultures, reducing the efficiency of the system [23]. These problems could be addressed by the use of mixed cultures, as the synergic interactions of the H_2 producing PNSB in the consortium might enhance the efficiency and the effectiveness of PF in terms of H_2 production.

In this work, the ability of PNSB to produce H_2 and PHB from DFE obtained from the thermophilic DF of the organic fraction of municipal solid wastes (OFMSW) has been investigated. In particular, two different inocula, i.e. *Rhodobacter sphaeroides* AV1b and an enriched mixed culture of PNSB obtained from an anaerobic digestate, were tested under different operating conditions in order to examine the parameters affecting H_2 and PHB productivities. The performances of the different inocula were evaluated in terms of H_2 and PHB production and removal of soluble organic compounds.

7.2. Materials and methods

7.2.1. Dark Fermentation Effluent

The DFE utilized in this study was collected after 110 working days from a thermophilic semi-batch continuous stirred tank reactor with a 0.7 L working volume, a 300 mL headspace and an operating pH of 5.0 (± 0.3). The H_2 yields and production rates were 105 (± 28) N mL H_2 g VS^{-1} and 205 (± 40) N mL H_2 L^{-1} d^{-1} at organic loading rate of 2 g VS L^{-1} d^{-1} and hydraulic retention time of 4 days. The DFE was characterized in terms of total Kjeldhal nitrogen (211 ± 4.0 mg L^{-1}), nitrogen ammonium concentration (1.89 ± 0.3), COD (4672 ± 136 mg L^{-1}) and organic acids concentration (acetic acid 575.90 mg L^{-1}, butyric acid 1117.32 mg L^{-1}, propionic acid 477.90 mg L^{-1} and lactic acid 36.11 mg L^{-1}).

In order to separate the liquid fraction, rich in organic acids, DFE was settled for 30 min, centrifuged at 4500 rpm for 20 min and finally diluted 1:2 with distilled water to obtain a clear medium for PF tests. This enhances the light penetration and reduces

the potential hydrolysis of particulate organic materials which might occur otherwise during PF tests.

7.2.2. Inoculum

Two different cultures were compared in this study: an adapted culture of *Rhodobacter sphaeroides* AV1b (RS) isolated from the Averno Lake (Naples, Italy) and a mixed consortium (MC) of PNSB enriched in a lab-scale reactor under continuous illumination. In particular, the mixed culture (MC) was obtained from the digestate of an anaerobic digestion full-scale plant treating buffalo manure as main substrate for methane production. After the clarification procedure, the digestate was inoculated in synthetic VFAs medium under continuous illumination to stimulate the selection of the PNSB species.

The experiments were carried out in triplicate by using 500 mL reactors with a 400 mL working volume, operated in batch conditions. The reactors were equipped with thin tubing on the top for sampling and gas extraction. The light was continuously provided through fluorescent lamps with constant illumination of 4000 lx according to other studies investigating the light effects on growth and H_2 production of photofermentative bacteria [24, 25, 26, 27]. The stirring conditions were fixed to 300 rpm through IKA RT 5 stirrer stations [25, 26]. The experiments were executed at fixed room temperature (25°C), flushing the headspace of the reactors with argon gas for different times (0, 10 and 20 min). The PF reactors were fed with the real DFE previously defined or with a synthetic culture medium (preliminary tests only) reproducing the same characteristics of the real DFE. The pH of the medium culture for all the PF tests was initially adjusted to 6.0 with 1 M NaOH to prevent any low pH inhibition due to the presence of organic acids as substrates [20, 28]. Total dissolved nitrogen concentration was kept low by removing the particulate organic components from the DFE. In this way, the protein hydrolysis and further release of ammonium, which usually occurs at high pH values, was limited to avoid nitrogen inhibition on PNSB activity [29]. Moreover, high C/N ratios have been found to enhance the production of PHB [30, 31]. In addition, the initial VFA concentrations from the DFE were not in the inhibiting range as reported by Han et al. [32].

The samples were collected every 2-5 days and H_2 production was quantified through water displacement. The measurement system consisted in an acidic water (1.5% HCl) column where the biogas was forced to pass through; specifically, the volume of

gas produced was quantified as the volume of water displaced by the overpressure of the reactor headspace. The H_2 production was calculated by considering the total biogas composition under normal conditions.

7.2.3. Analytical methods

Hydrogen was quantified by a Varian Star 3400 gas chromatograph equipped with ShinCarbon ST 80/100 column and a thermal conductivity detector. Argon was utilized as carrier gas with 20 psi front and rear end pressure. The duration of analysis was 15 min. The VFAs were quantified by high pressure liquid chromatography (HPLC) (Dionex LC 25 Chromatography Oven) equipped with a Synergi 4u Hydro RP 80A (size 250 x 4.60 mm) column and UV detector (Dionex AD25 Absorbance Detector). The isocratic elution consisted of 20% methanol and 10% acetonitrile in 5 mM H_2SO_4, pumped at a rate of 0.9 mL min^{-1} by using a Dionex GP 50 Gradient Pump. The elution time was 18.5 min. For PHB analysis, the samples were lyophilized and the polymers were extracted according to Oehmen et al. [33]. PHB concentration was quantified by a gas chromatograph (GC) equipped with a mass spectrometer (MS) and ZB Semi Volatiles (Zebron) column using helium as carrier gas. The light intensity was measured with a lux meter (Lutron-LX-107). The COD was determined by the Closed Reflux method and total Kjeldahl nitrogen by macro-Kjeldahl in accordance to Standard Methods [34]. Biomass growth was quantified by spectrophotometric measurements of the Optical Density at 660 nm (OD660) (Photolab Spektral, WTW, Germany). Total Suspended Solids (TSS) were quantified after filtering 20 mL of PNSB culture samples on 0.45 μm filters dried at 105 °C for 24 h. Total suspended solids (TSS) were correlated to the OD660 measurements using a specific calibration curve for each culture (OD660 = 3.4534*TSS (R^2 = 0.99845) and OD660 = 3.2413*TSS (R^2 = 0.99837), respectively, for *R. sphaeroides* AV1b and mixed PNSB cultures.).

7.3. Results and discussion

In all the experiments, the initial TSS content was kept low (< 0.05 g L^{-1}) in order to favour light penetration and diffusion in the bulk liquid.
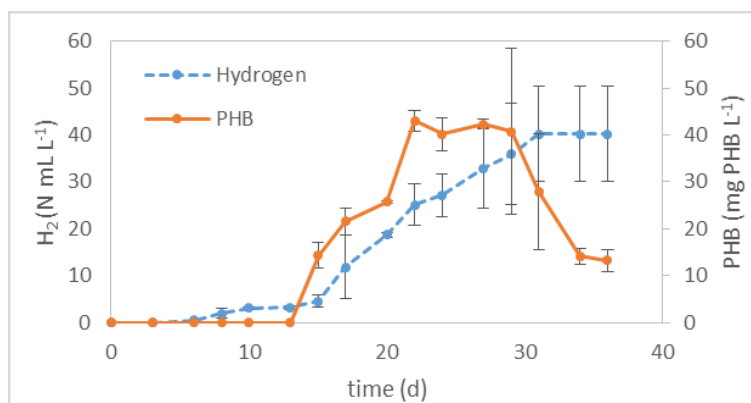
Figure 1. Cumulative H_2 production and PHB trend from synthetic DFE with 10 min
argon flushed test.
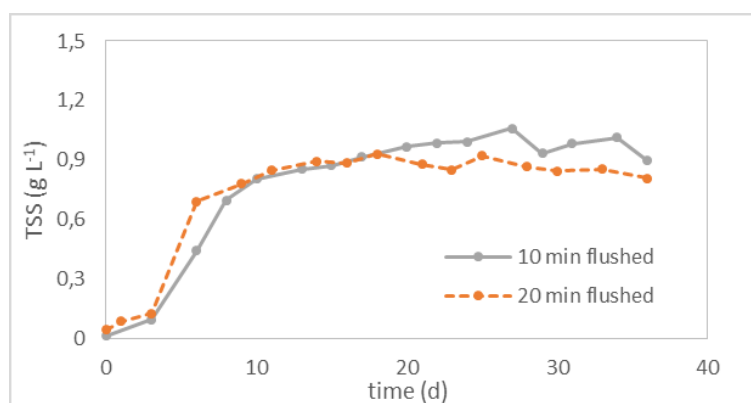
Figure 2. Biomass growth trends of MC under different operational conditions (10
and 20 min argon flushed reactors).

A preliminary set of experiments was conducted with the MC in order to evaluate the
effect of argon flushing on the reactor performance. To this aim, a synthetic culture
medium reproducing the features of the real DFE in terms of VFAs (acetic acid
563.70 mg L^{-1}, butyric acid 1088.90 mg L^{-1}and propionic acid 448.20 mg L^{-1}) was
used as feeding solution to the photofermentative batch reactors. The serum bottles
were flushed with argon for different times (0 and 10 min) which correspond to the
following residual nitrogen percentages (79 and 60) in the reactor headspace. The
experimental results showed that the high nitrogen concentration in the headspace
observed for a 10 min flushing exerts a negative effect on the cumulative H_2
production and PHB accumulation as the mixed culture was affected by a long lag
phase (Fig. 1). Moreover, neither H_2 production [24, 35] nor PHB accumulation was
detected in the PF tests without argon flushing (data not shown). This may be related
to the functioning of nitrogenase and hydrogenase enzymes, which can induce the
conversion of dinitrogen gas and protons to ammonia and the H_2 re-oxidization into
protons and electron [14, 17, 36, 37]. Indeed, the presence of N_2 promotes nitrogen

157

fixation rather than H_2 production and inhibits the structural genes for the three key enzymes of PHB synthesis from acetyl coenzyme A [38, 39]. Moreover, it can be noted that biomass growth trends were not affected by the initial nitrogen content in the headspace (Fig. 2). Indeed, the TSS concentration in tests with 0 and 10 min argon flushing was comparable to the other tests with 20 min argon flushed reactors fed with synthetic and / or real DFE (Fig. 2). Increasing flushing time (from 10 to 20 min) and progressing from a synthetic to a real DFE, which might be rich in other micronutrients such as iron or molybdenum [40], led to higher H_2 and PHB productivity (Fig. 3).
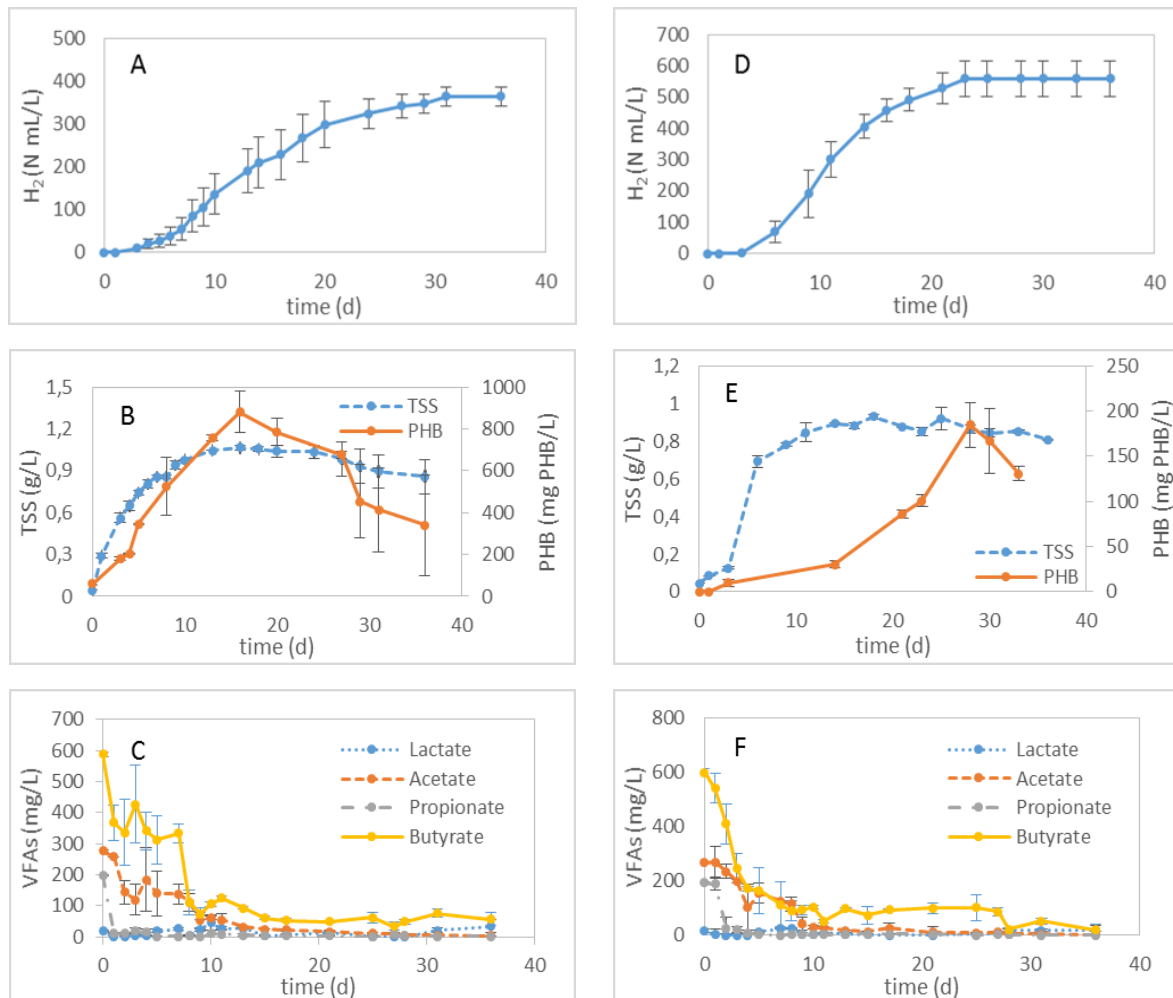
Figure 3. Cumulative H_2 production (A, D), biomass and PHB trends (B, E) and organic acids depletion in RS (A, B, C) and MC (D, E, F) tests.

Based on the results achieved in these preliminary tests, two sets of experiments were conducted by using RS and MC photofermentative reactors flushed for 20 min with argon and fed with the real DFE. The H_2 production (Figs. 3A and 3D), the concomitant biomass growth in terms of TSS and PHB accumulation (Figs. 3B and

3E), and the depletion of organic acids (Figs. 3C and 3F) have been reported. The maximum pH value of 7.3 was reached during the MC tests. For each reactor, similar pH trends were observed with a slight increase during the exponential growth phase and a further stabilization to the not inhibiting value of 7 [41, 42, 43].

After 36 days of incubation, the cumulative volumetric yields of 364 ($\pm$ 9) N mL H_2 L^{-1} and 559 ($\pm$ 58) N mL H_2 L^{-1} were obtained for the RS and MC reactors, respectively. The cumulative H_2 production from RS and MC tests was comparable to the maximum H_2 production of around 1000 N mL H_2 L^{-1} from DFE obtained by Uyar et al. [44]. During the first days, VFA concentrations decreased faster in MC than in RS and the final concentrations observed at the end of the experiments were lower in MC; in particular, the residual butyrate concentration in RS resulted higher than 50 mg L^{-1} at day 36. The concomitant PHB accumulation was observed in both the experiments (Figs. 3B and 3E). RS test led to the maximum PHB concentration of 882 ($\pm$99) mg PHB L^{-1} after 16 days whereas the lower value of 185 ($\pm$ 25) mg PHB L^{-1} was obtained at day 28 in the MC test. According to the past studies by Johnson et al. [45] and James et al. [46], a characteristic decrease in PHB concentration during the last days of incubation was observed. PHB represents an intracellular storage of carbon and energy that bacteria are able to use when VFAs start to be depleted or almost completely used (Figs. 3B and 3E). During the RS test, the PHB consumption was associated to a concomitant enhancement of H_2 cumulative production (Fig. 3A). On the contrary, during the MC experiments, the maximum value for hydrogen production was reached at day 25 and remained constant even after the decrease in PHB concentration (Fig. 3D).

The maximum biomass concentration of 1.06 ($\pm$ 0.02) g TSS L^{-1} and 0.93 ($\pm$ 0.01) g TSS L^{-1} were observed during the RS and MC tests, respectively (Figs. 3B and 3E). The characteristic exponential phase in bacterial growth was probably limited by the self-shading from light irradiance [14, 25].

The mixed PNSB culture led to higher H_2 yields in comparison to the pure *R. sphaeroides* AV1b culture. This can be attributed to the adaptation of the mixed PNSB inoculum to H_2 production, confirmed in a study by Montiel-Corona et al. [11] who obtained higher H_2 production from mixed PNSB consortia compared to a pure culture. On the contrary, PHB productivity in MC, that might not be rich in PHB producing species, was very low comparing with the RS tests, remarking the importance of pure cultures in PHB production.

159

A slight difference in COD removal was observed: RS tests reached 82% (± 1.5%) of conversion while MC degraded 90% (± 1.1%) of the initial soluble COD, indicating that the type of PNSB strain can affect the COD removal. This can be due to the presence of several microbial species in the mixed PNSB culture, which could utilize the different carbon sources present in DFE leading to a higher process robustness. Indeed, the synergies established among the different H_2 producing species might enhance the conversion of the organic substrates to H_2 and play a crucial role in the establishment of a less sensitive system to the operational conditions (e.g. pH and temperature).

In this context, the use of mathematical modelling might be crucially helpful in testing a large variation of environmental and operational conditions affecting the process [47, 48].

7.4. Conclusions

The results demonstrate the possibility of adapting a mixed PNSB culture for higher hydrogen production compared to the pure cultures. However, higher PHB yields was obtained with pure cultures of *R. sphaeroides* AV1b than the mixed culture. Nonetheless, the use of mixed cultures could be promising in the scale-up application of the PF systems for the treatment of DFE, as it provides a higher COD removal efficiency and saves the asepsis costs increasing process robustness. Conversely, pure *R. sphaeroides* cultures could be specifically applied for PHB production as a value added products from PF process.

References

 [1] Balat, H., Kırtay, E., 2010. Hydrogen from biomass - Present scenario and future prospects. International Journal of Hydrogen Energy 35, pp.7416-7426.

 [2] Lin, C.S.K., Koutinas, A.A., Stamatelatou, K., Mubofu, E.B., Matharu, A.S., Kopsahelis, N., Pfaltzgraff, L.A., Clark, J.H., Papanikolaou, S., Kwan, T.H., Luque, R., 2014. Current and future trends in food waste valorization for the production of chemicals, materials and fuels: a global perspective. Biofuels, Bioproducts and Biorefining, 8(5), pp.686-715.

 [3] Andreottola, G., Ragazzi, M., Foladori, P., Villa, R., Langone, M., Rada, E.C., 2012. The unit intregrated approch for OFMSW treatment. University "Politehnica" of Bucharest Scientific Bulletin, Series C: Electrical Engineering, 74(1), pp.19-26.

 [4] Ghimire, A., Frunzo, L., Pirozzi, F., Trably, E., Escudie, R., Lens, P.N.L., Esposito, G., 2015. A review on dark fermentative biohydrogen production from organic biomass: process parameters and use of by-products. Applied Energy 144, pp.73-95.

 [5] De Gioannis, G., Muntoni, A., Polettini, A., Pomi, R., 2013. A review of dark fermentative hydrogen production from biodegradable municipal waste fractions. Waste Management, 33, pp.1345-1361.

 [6] Urbaniec, K., Bakker, R.R., 2015. Biomass residues as raw material for dark hydrogen fermentation - a review. International Journal of Hydrogen Energy, 40, pp.3648-3658.

 [7] Mattei, M.R., D'Acunto, B., Esposito, G., Frunzo, L., Pirozzi, F., 2015. Mathematical modeling of competition and coexistence of sulfate-reducing bacteria, acetogens, and methanogens in multispecies biofilms. Desalination and Water Treatments, 55(3), pp.740-748.

 [8] Bastidas-Oyanedel, J.R., Bonk, F., Thomsen, M.H., Schmidt, J.E., 2015. Dark fermentation biorefinery in the present and future (bio)chemical industry. Reviews in Environmental Science and Bio/Technology, 14, pp.473-498.

 [9] Cheng, J., Ding, L., Xia, A., Lin, R., Li, Y., Zhou, J., Cen, K., 2015. Hydrogen production using amino acids obtained by protein degradation in waste biomass by combined dark- and photo-fermentation. Bioresource Technology, 179, pp.13-19.

[10] Rai, P.K., Singh, S.P., Asthana, R.K., 2014. Biohydrogen production from sugarcane bagasse by integrating dark- and photo-fermentation. Bioresource Technology, 152, pp.140-6.

[11] Montiel-Corona, V., Revah, S., Morales, M., 2015. Hydrogen production by an enriched photoheterotrophic culture using dark fermentation effluent as substrate: effect of flushing method, bicarbonate addition, and outdoor-indoor conditions. International Journal of Hydrogen Energy, 40, pp.9096-9105.

[12] Kumar, P., Ray, S., Kalia, V.C., 2016. Production of co-polymers of polyhydroxyalkanoates by regulating the hydrolysis of biowastes. Bioresource Technology, 200, pp.413-419.

[13] Korkakaki, E., Mulders, M., Veeken, A., Rozendal, R., van Loosdrecht, M.C.M., Kleerebezem, R., 2016. PHA production from the organic fraction of municipal solid waste (OFMSW): overcoming the inhibitory matrix. Water Research, 96, pp.74-83.

[14] Ghimire, A., Valentino, S., Frunzo, L., Pirozzi, F., Lens, P.N.L., Esposito, G., 2016. Concomitant biohydrogen and poly-β-hydroxybutyrate production from dark fermentation effluents by adapted *Rhodobacter sphaeroides* and mixed photofermentative cultures. Bioresource Technology, 217, pp.157-164.

[15] Kemavongse, K., Prasertsan, P., Upaichit, A., Methacanon, P., 2007. Effect of co-substrate on production of poly-beta-hydroxybutyrate (PHB) and copolymer PHBV from newly identified mutant *Rhodobacter sphaeroides* U7 cultivated under aerobic-dark condition. Songklanakarin Journal of Science and Technology, 29, pp.1101-1113.

[16] Reddy, C.S.K., Ghai, R., Kalia, R.V.C., 2003. Polyhydroxyalkalonates: an overview. Bioresource Technology, 87, pp.137-146.

[17] Wu, S.C., Liou, S.Z., Lee, C.M., 2012. Correlation between bio-hydrogen production and polyhydroxybutyrate (PHB) synthesis by *Rhodopseudomonas palustris* WP3-5. Bioresource Technology, 113, pp.44-50.

[18] Eroglu, E., Melis, A., 2011. Photobiological hydrogen production: Recent advances and state of the art. Bioresource Technology, 102, pp.8403-13.

[19] Adessi, A., De Philippis, R., 2014. Photobioreactor design and illumination systems for H_2 production with anoxygenic photosynthetic bacteria: a review. International Journal of Hydrogen Energy, 39, pp.3127-3141.

[20] Chen, C.Y., Liu, C.H., Lo, Y.C., Chang, J.S., 2011. Perspectives on cultivation strategies and photobioreactor designs for photo-fermentative hydrogen production. Bioresource Technology, 102, pp.8484-92.

[21] Fermoso, F.G., Van Hullebusch, E.D., Guibaud, G., Collins, G., Svensson, B.H., Carliell-Marquet, C., Vink, J.P.M., Esposito, G., Frunzo, L., 2015. Fate of trace metals in anaerobic digestion. Biogas Science and Technology, Springer International Publishing, pp.171-95.

[22] Kim, M.S., Kim, D.H., Son, H.N., Ten, L.N., Lee, J.K., 2011. Enhancing photo-fermentative hydrogen production by *Rhodobacter sphaeroides* KD131 and its PHB synthase deleted-mutant from acetate and butyrate. International Journal of Hydrogen Energy, 36, pp.13964-13971.

[23] Ghosh, S., Dairkee, U.K., Chowdhury, R., Bhattacharya, P., 2017. Hydrogen from food processing wastes via photofermentation using Purple Non-sulfur Bacteria (PNSB)-A review. Energy Conversion and Management, 141, pp.299-314.

[24] Koku, H., Eroglu, I., Gunduz, U., Yucel, M., Turker, L., 2002. Aspects of the metabolism of hydrogen production by *Rhodobacter sphaeroides*. International Journal of Hydrogen Energy, 27, pp.1315-1329.

[25] Sevinç, P., Gündüz, U., Eroglu, I., Yücel, M., 2012. Kinetic analysis of photosynthetic growth, hydrogen production and dual substrate utilization by *Rhodobacter capsulatus*. International Journal of Hydrogen Energy, 37, pp.16430-16436.

[26] Androga, D.D., Sevinç, P., Koku, H., Yücel, M., Gündüz, U., Eroglu, I., 2014. Optimization of temperature and light intensity for improved photofermentative hydrogen production using *Rhodobacter capsulatus* DSM 1710. International Journal of Hydrogen Energy, 39, pp.2472-2480.

[27] Akman, M.C., Erguder, T.H., Gündüz, U., Eroğlu, İ., 2015. Investigation of the effects of initial substrate and biomass concentrations and light intensity on photofermentative hydrogen gas production by Response Surface Methodology. International Journal of Hydrogen Energy, 40, pp.5042-5049.

[28] Akroum-Amrouche, D., Abdi, N., Lounici, H., Mameri, N., 2011. Effect of physico-chemical parameters on biohydrogen production and growth characteristics by batch culture of *Rhodobacter sphaeroides* CIP 60.6. Applied Energy, 88, pp.2130-2135.

[29] Keskin, T., Abo-Hashesh, M., Hallenbeck, P.C., 2011. Photofermentative hydrogen production from wastes. Bioresource Technology, 102, pp.8557-8568.

[30] Koku, H., Eroglu, I., Gunduz, U., Yucel, M., Turker, L., 2003. Kinetics of biological hydrogen production by the photosynthetic bacterium *Rhodobacter sphaeroides* O.U. 001. International Journal of Hydrogen Energy, 28, pp.381-388.

[31] Argun, H., Kargi, F., Kapdan, I., 2008. Light fermentation of dark fermentation effluent for bio-hydrogen production by different *Rhodobacter* species at different initial volatile fatty acid (VFA) concentrations. International Journal of Hydrogen Energy, 33, pp.7405-7412.

[32] Han, H., Liu, B., Yang, H., Shen, J., 2012. Effect of carbon sources on the photobiological production of hydrogen using *Rhodobacter sphaeroides* RV. International Journal of Hydrogen Energy, 37, pp.12167-12174.

[33] Oehmen, A., Zeng, R.J., Yuan, Z., Keller, J., 2005. Anaerobic metabolism of propionate by polyphosphate-accumulating organisms in enhanced biological phosphorus removal systems. Biotechnology and Bioengineering, 91, pp.43-53.

[34] Federation, W.E., American Public Health Association, 2005. Standard methods for the examination of water and wastewater. American Public Health Association (APHA): Washington, DC, USA.

[35] Sasikala, K., Ramana, C.V., Rao, P.R. and Subrahmanyam, M., 1990. Effect of gas phase on the photoproduction of hydrogen and substrate conversion efficiency in the photosynthetic bacterium *Rhodobacter sphaeroides* OU 001. International Journal of Hydrogen Energy, 15(11), pp.795-797.

[36] Liu, B.F., Ren, N.Q., Ding, J., Xie, G.J., Cao, G.L., 2008. Enhanced photo-H_2 production of *R. faecalis* RLD-53 by separation of CO_2 from reaction system. Bioresource Technology, 100, pp.1501-1504.

[37] Varley, J.B., Wang, Y., Chan, K., Studt, F., Norskov, J.K., 2015. Mechanistic insights into nitrogen fixation by nitrogenase enzymes. Physical Chemistry Chemical Physics, 17, pp.29541-29547.

[38] Brown, K.A., Harris, D.F., Wilker, M.B. Rasmussen, A., Khadka, N., Hamby, H., Keable, S., Dukovic, G., Peters, J.W., Seefeldt, L.C., King, P.W., 2016. Light-driven dinitrogen reduction catalyzed by a CdS:nitrogenase MoFe protein biohybrid. Science, 352, pp.448-450.

[39] Lee, S.Y., 1995. Bacterial Polyhydroxyalkanoates. Biotechnology and Bioengineering, 49, pp.1-14.

[40] Özgür, E., Mars, A.E., Peksel, B., Louwerse, A., Yücel, M., Gündüz, U., Claassen, P.A.M., Eroglu, I., 2010. Biohydrogen production from beet molasses by sequential dark and photofermentation. International Journal of Hydrogen Energy, 35, pp.511-517.

[41] Tao, Y., He, Y., Wu, Y., Liu, F., Li, X., Zong, W., Zhou, Z., 2008. Characteristics of a new photosynthetic bacterial strain for hydrogen production and its application in wastewater treatment. International Journal of Hydrogen Energy, 33, pp.963-973.

[42] Tawfik, A., El-Bery, H., Kumari, S., Bux, F., 2014. Use of mixed culture bacteria for photofermentive hydrogen of dark fermentation effluent. Bioresource Technology, 168, pp.119-126.

[43] Boran, E., Özgür, E., Yücel, M., Gündüz, U., Eroglu, I., 2012. Biohydrogen production by *Rhodobacter capsulatus* Hup⁻ mutant in pilot solar tubular photobioreactor. International Journal of Hydrogen Energy, 37, pp.16437-16445.

[44] Uyar, B., Schumacher, M., Gebicki, J., Modigell, M., 2009. Photoproduction of Hydrogen by *Rhodobacter Capsulatus* from Thermophilic Fermentation Effluent. Bioprocess and Biosystems Engineering, 32, pp.603-606.

[45] James, B.W., Mauchline, W.S., Dennis, P.J., Keevil, C.W., Wait, R., 1999. Poly-3-hydroxybutyrate in *Legionella pneumophila*, an energy source for survival in low-nutrient environments. Applied and Environmental Microbiology, 65(2), pp.822-827.

[46] Johnson, K., Jiang, Y., Kleerebezem, R., Muyzer, G., van Loosdrecht, M.C., 2009. Enrichment of a mixed bacterial culture with a high polyhydroxyalkanoate storage capacity. Biomacromolecules, 10(4), pp.670-676.

[47] Mattei, M.R., Frunzo, L., D'Acunto, B., Esposito, G., Pirozzi, F., 2015. Modelling microbial population dynamics in multispecies biofilms including Anammox bacteria. Ecological Modelling, 304, pp.44-58.

[48] D'Acunto, B., Frunzo, L., Mattei, M.R., 2016. Qualitative analysis of the moving boundary problem for a biofilm reactor model. Journal of Mathematical Analysis and Applications, 438, pp.474-491.

Chapter 8

Bio-hythane production from microalgae biomass: key challenges and potential opportunities for algal bio-refineries

Bio-hythane production from microalgae biomass: key challenges and potential opportunities for algal bio-refineries

The interest in microalgae for wastewater treatment and liquid bio-fuels production (i.e biodiesel and bioethanol) is steadily increasing. The associated biomass and by-product residues generated from these processes can be utilized as a feedstock in anaerobic fermentation for the production of gaseous bio-fuels. In this context, dark fermentation coupled with anaerobic digestion can be a potential technology for the production of hydrogen and methane from these residual algal biomasses. The mixture of these gaseous bio-fuels, known as hythane, has superior characteristics and is increasingly regarded as an alternative to fossil fuels. This chapter reviews the current developments achieved in the conversion of algal biomass to bio-hythane (H_2 + CH_4).

8.1. Introduction

"Make hay while the sun shines": here mankind started to envision the future in a sustainable manner. In recent years, waste to wealth concept is growing rapidly: waste biomass is valuable to be discarded. Increased scientific and commercial interest has triggered the development of viable biorefining concepts in order to convert raw cellulose wastes into bio-fuels, chemicals and industrial products due to environmental concerns, depletion of fossil fuel resources and public awareness. Up to date, there has been also an increasing trend towards a more efficient utilization of agro-industrial/wastewater/cellulose waste residues for the conversion to hydrogen (H_2) and methane (CH_4) [1].

Environmentalists have started to focus on green energy when the globe started to face problems like global warming and fossil fuel depletion. Utilization of organic wastes for CH_4 production has already been commercialized. However, biological hydrogen production utilizing waste biomass is a new and promising approach to meet the increasing demand for green energy. Biohydrogen (H_2) could eventually replace a part of our fossil fuels need in day-to-day life due to its perceived environmental benefits and potential availability from organic wastes. H_2 is an effective energy carrier when compared with petrol/natural gas, the energy released per unit mass being at least twice that of traditional fuels. However, the density of H_2 is lower (0.08988 g L^{-1} at 0 °C and 101.325 kPa) than that of all the other fossil fuels, which emphasizes the need for efficient storage. H_2 is an ideal fuel that releases only water upon combustion and may

be converted into electricity *via* fuel cells or directly used in internal combustion engines. It can also be used for the synthesis of ammonia, alcohols and aldehydes, as well as for the hydrogenation of edible oil, petroleum, coal and shale oil. Among the wide portfolio of feedstocks available for H_2 production, algal biomass has recently received considerable attention due to its high carbohydrate content [2, 3].

CH_4 and H_2 have been hailed as most important energy carrier due to their various commercial uses [4, 5]. When mixed together in the so-called hythane or enriched methane (5-25% H_2), this mixture can be better exploited during combustion. Moreover, the addition of H_2 to methane increases tis H/C ratio, which helps in the reduction of greenhouse gas (GHG) emission, widens the narrow flammability range of methane eventually increasing fuel efficiency and increases flame speed, thus reducing combustion duration and improving heat efficiency [4, 5, 6]. In this context, hythane has recently attracted attention due to its versatile uses as transportation fuel in countries like USA and India [6]. Although the production of CH_4 from renewable waste biomass has been already commercialized, most of the H_2 that has been produced for commercial uses is based on fossil fuels. Therefore, production of hydrogen from renewable sources is the major bottle-neck in the sustainable production of hythane.

Biological processes have been proposed as a promising approach for cleaner and sustainable production of hythane (H_2 and CH_4). In contrast to physical-chemical hydrogen and CH_4-producing techniques, biological technologies can be engineered to produce hydrogen or CH_4 utilizing renewable feedstocks under mild operating conditions without generating any harmful by-products. Some even predict that a new economy empowered by hydrogen will fundamentally change the nature of our market and political and social institutions just as coal did in the 19th century and petroleum in the 20th century [7].

The concept of zero waste has been widely explored as "a process of building that has a closed waste loop, where all outputs are used again as inputs and no waste is created". Algal blooms are abundant and have not been exploited, so they could be used for bioenergy production and the remnants have various biorefining applications. Increasing interest in microalgal biodiesel production and its associated generation of residues as by-products offers the possibility of bioconverting these by-products into valuable resources *via* anaerobic fermentation technologies. Moreover, recent investigations on the potential of microalgae for wastewater treatment have shown the potential of algal-bacterial symbiosis to support the generation of large amounts of

biomass potentially used as a feedstock for bio-fuel production. Thus, an algal biomass is emerging as an attractive and sustainable feedstock source compared to conventional biomass such as agricultural residues, agro-industrial organic waste, food crops and organic fraction of municipal solid waste (OFMSW).

This work aims to provide an updated overview of the recent advances in bio-hythane (H_2 + CH_4) production *via* dark fermentation (DF) and anaerobic digestion (AD) of microalgal biomass. This chapter provides an extended overview of bio-hythane production and the future challenges and prospects for its scaled-up applications. The main parameters influencing a sustainable generation of microalgal biomass and its application to bio-hythane production are discussed. Finally, the role of different operational and environmental parameters such as pH, temperature, organic loading rate (OLR) and hydraulic retention time (HRT) in bio-hythane production are also reviewed.

8.2. Microalgal biomass

Microalgae are unicellular or multi-cellular photosynthetic organisms which are normally ubiquitous in fresh as well as saline water. These organisms can convert inorganic carbon or simpler organic carbon molecules into higher organic compounds *via* photosynthesis and heterotrophic metabolism, respectively. Microalgae can be broadly classified into i) prokaryotic microalgae (cyanobacteria) ii) eukaryotic green microalgae (*chlorophyta*), eukaryotic red microalgae (*Rhodophyta*), iv) diatoms (*Bacillariophyceae*) and v) golden algae (*Chrysophyceae*). Microalgae exhibit an excellent carbon dioxide fixation potential and can grow under a variety of natural and engineered conditions, i.e. in open ponds (raceway) or closed photobioreactors (PBRs) besides in their natural habitats.

The interest on algal biomass as a feedstock for bio-fuels production has gradually increased over the past decade [8]. Microalgae-based bio-fuels offer several benefits when compared to first generation bio-fuels: in addition to their higher abundance, easiness in feedstock cultivation and storage along with their cost-effectiveness. Microalgae also offer numerous interesting advantages as a feedstock source such as high biomass productivities, year-round cultivation, use of non-arable/unfertile land, easiness to control species-dependent accumulation of components like lipids, carbohydrates, proteins and others. Algal biomass can be used for production of high value added products such as fatty acid methyl esters (FAMEs) and proteins, thereby

creating a high capital commercial venture. Biomass and oil areal productivities of algae are higher than that of vascular plants under optimal culture conditions. The average maximum specific growth rate of microalgae is equivalent to 1 day^{-1} compared to 0.1 day^{-1} for higher plants [8]. The photosynthetic efficiency (PE) of terrestrial plants is 1–2% of the impinging solar irradiation, whereas microalgae in engineered systems can achieve PEs of 4–5% [9]. Moreover, microalgae can be cultivated in wastewater/industrial effluents/discharged liquids as growth media by utilizing their residual N, P and trace elements. In addition, microalgae can utilize the CO_2 present in flue gases and biogas as a carbon source, thereby contributing to a significant CO_2 emissions mitigation [10].

8.2.1. Growth and metabolism of microalgae

Microalgae are often cultivated using inorganic carbon as a carbon source and light as a source of energy. However, several microalgae strains are also capable of utilizing organic compounds as a source of carbon and energy (Table 1), which makes microalgae one of the most versatile organisms in Earth. The different metabolisms involved in microalgae growth are represented in equations (1-3) [11].

Photoautotrophic:
$$4\,H_2O + HCO_3^- \xrightarrow{\text{Light energy}} C(biomass) + 0.5\,O_2 + 3\,OH^- \tag{1}$$

Heterotrophic:
$$(1+a)C_2HO + O_2 \xrightarrow{\text{Light energy}} C(biomass) + a\,CO_2 + (1+a)H_2O \tag{2}$$

Mixotrophic:
$$b\,HCO_3 + c\,CH_2O \xrightarrow{\text{Light energy}} [b + (c-a)]C(biomass) + 3\,OH^- + a\,CO_2 \tag{3}$$
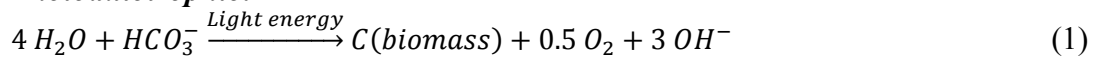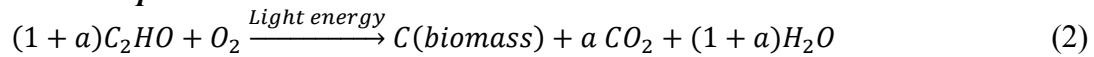
As a result of microalgal metabolism, the biochemical properties of the culture medium might change. The pH of the cultivation broth increases during photoautotrophic growth, in heterotrophy pH decreases, while during mixotrophic growth pH changes are not noteworthy.

Table 1. Different modes of algal biomass cultivation (adapted from [11, 12, 13]).

Modes of cultivation	Carbon source	Energy source	Biomass and lipid productivity
Photoautotrophic	Inorganic	Light	Low
Heterotrophic (Photo)	Organic	Light	High
Heterotrophic (Chemo)	Organic	Organic	High
Mixotrophic	Organic and inorganic	Light and organic	High

The composition and growth characteristics of microalgae strongly depend on the cultivation conditions [11, 12]. Typically, microalgal biomass is composed of carbohydrates (5-23%), proteins (6-52%) and lipids (7-23%) [15]. The biochemical composition of different microalgal strains, which directly impacts on the bio-fuel production potential [2, 13], is presented in Table 2. Besides these major components, microalgae contain cell constituents such as phosphorous, sulphur and other micronutrients (iron, cobalt, zinc among others) which are known to enhance the activity of biological biofuel production processes such as methanogenesis, DF and other microbial fermentation processes [15]. Some studies have demonstrated the positive as well as negative impacts of bacterial population on microalgal culture [16]. The presence of bacteria can be an issue especially during heterotrophic and mixotrophic culture of microalgae. The microalgal growth can be affected by the competition with bacteria for the uptake of nutrients or carbon source from the culture medium.

Table 2. Biochemical composition of different microalgae species (adapted from [13, 91, 92, 93].

Species	Proteins (%)	Lipids (%)	Carbohydrates (%)
Arthrospira maxima	60-71	6-7	13-16
Chaetoceros sp.	43	19	1
Chlamydomonas reinhardtii	48	21	17
Chlorella pyrenoidosa	57	2	26
Chlorella vulgaris	51-58	14-22	12-17
Dunaliella salina	26-57	6-16	25-32
Euglena gracilis	39–61	14-20	14-18
Rhodomonas sp.	29	19	9
Spirulina maxima	60-71	6-7	13-16
Spirulina platensis	46-64	4-9	8-25
Scenedesmus obliquus	50-56	12-14	10-17

8.2.3. Microalgae production and harvesting systems

The competitiveness of bio-fuel production from microalgae with fossil fuels still remains its major challenge. Microalgae require substantial amounts of nitrogen and phosphorous as essential nutrients for their growth and metabolisms. Therefore, the most common technologies for mass production of algal biomass demand large amount of chemical fertilizers, which are based on fossil fuels and require huge amounts of energy for their synthesis and extraction [8]. Chisti and Yan [20] suggested the development of genetically engineered microalgae capable of atmospheric nitrogen fixation. A promising alternative to reduce the costs of microalgae production is based on the use of wastewaters as a source of nutrients during microalgae cultivation. Table 3 presents the different microalgae cultivation modes and their productivities.

Table 3. Typical microalgae cultivation modes and productivities.

Microalgae species	Type of cultivation (based on carbon sources)	Productivity ($g L^{-1} d^{-1}$)	References
Scenedesmus obliquus	Phototrophic (air)	0.06	[21]
Scenedesmus obliquus	Mixotrophic (Glucose)	0.1- 0.51	[21]
Chlorella protothecoides CCAP 211/8D	Phototrophic (CO_2)	0.002-0.02	[22]
Chlorella protothecoides	Heterotrophic (Glucose)	2.2-7.4	[23]
Chlorella vulgaris #259	Phototrophic (CO_2)	0.01	[24]
Chlorella vulgaris #259	Heterotrophic (Glucose and acetate)	0.08-0.015	[24]
Chlorella vulgaris #259	Mixotrophic (Glucose and glycerol)	0.09-0.25	[24]
Chlorella pyrenoidosa	Mixotrophic (Anaerobic digestate)	0.63	[25]
Freshwater microalgal mixture dominated by *Scenedesmus sp.*	Mixotrophic (Anaerobic digestate)	2.60[a]	[26]
Chlorella sorokiniana	Heterotrophic (DF effluents)	0.33[a]	[27]

[a] $g L^{-1}$

Life cycle assessment (LCA) studies have consistently shown that fertilizers consumption, microalgae harvesting and oil extraction from algae entail the highest energy demands for algal bio-fuel production [16, 17, 18]. AD of algal biomass can by-

pass the concentration and oil extraction steps, thus reducing the total energy consumption and operating costs [13, 19]. Moreover, the recycling of the nutrients released from the anaerobic digestion of algal biomass could increase the environmental sustainability of the process. Closed PBRs have higher investment costs compared to open systems such as raceway ponds. However, PBRs can produce a highly concentrated microalgal biomass, which can significantly reduce the costs of biomass downstream. The net energy ratio (NER) for the biofuel generated from the algal biomass cultivated in raceway ponds, which correlates the energy input to the energy produced, is higher than that of PBRs. Moreover, the operating costs of PBRs are one order of magnitude higher than those of raceway ponds [31].

Harvesting is one of the most important operation unit processes in microalgae based bio-fuel production as it can account for 20-30% of the bio-fuel production cost [2, 28]. Several harvesting technologies available in pharmaceutical, biotechnological and environmental engineering applications such as centrifugation, filtration, flocculation and flotation, are commonly used for microalgae separation from the cultivation broth [32]. The choice of the harvesting method is often based on the end use of the microalgal biomass. Low cost harvesting techniques like gravity settling through enhanced flocculation are required when low added value products like bio-fuels are targeted. However, the effect of the use of chemical flocculants on bio-fuel production should be considered, since traces of these chemicals might have inhibitory effects on microbial activity during anaerobic fermentation.

Liquid bio-fuels (biodiesel and/or bioethanol) production from microalgae generates approximately 60-70% of residual biomass as by-product. Several studies have highlighted the potential of such a residual by-product for the production of biohydrogen and/or biomethane [9, 13, 20, 21, 22, 23, 24, 25]. In addition, the residual digestate from anaerobic fermentation can be utilized directly as a source of nutrients for algal biomass production [19, 26, 27]. Therefore, liquid bio-fuels production processes from algal biomass can be coupled with anaerobic fermentation for the production of both biohydrogen and biomethane. In addition, part of the energy generated from biogas combustion can be used to process the algal biomass for biodiesel production, thus increasing the sustainability of microalgae biorefineries.

8.3. Conversion technologies of microalgae to bio-fuels via biorefinery concept

The microalgal biorefinery concept is based on the application of different technologies in the conversion of algal biomass into value-added products, bio-fuels and chemicals. Nowadays, there are several technologies available for the conversion of microalgal biomass to bio-fuels such as biodiesel, ethanol, biohydrogen, biogas, etc. The recovery of various bio-fuels and chemicals from microalgae depends on the biochemical composition of harvested biomass and selection of the appropriate technology. For instance, the recovery of biodiesel from microalgae depends on their lipid content, i.e. triacylglycerols which are the substrate to produce biodiesel. For an algal lipid content lower than 40%, the energy consumption and economic cost of the energy recovered as biodiesel is not attractive due to the high energy intensity of microalgae harvesting and biodiesel production [15]. These two processes usually represent the bottleneck of full-scale biodiesel production from microalgae, due to the technical limitations reaching high concentration levels of dry biomass and a cost effective lipid extraction. In this context, the recovery of energy directly through the applications of technologies such as AD would be economically feasible based on the absence of biomass concentration and oil extraction steps of this technology. Therefore, tailoring the technologies to achieve the production of economically viable fuels and chemicals depending upon the nature of the harvested biomass (i.e. biochemical properties) is of utmost need. Under both scenarios, with/without biodiesel production (Figure 1), the biomass residues recovered can be converted to valuable chemicals like organic acids, biohydrogen and the residual by-products to methane in combined dark fermentation and biomethanation processes.
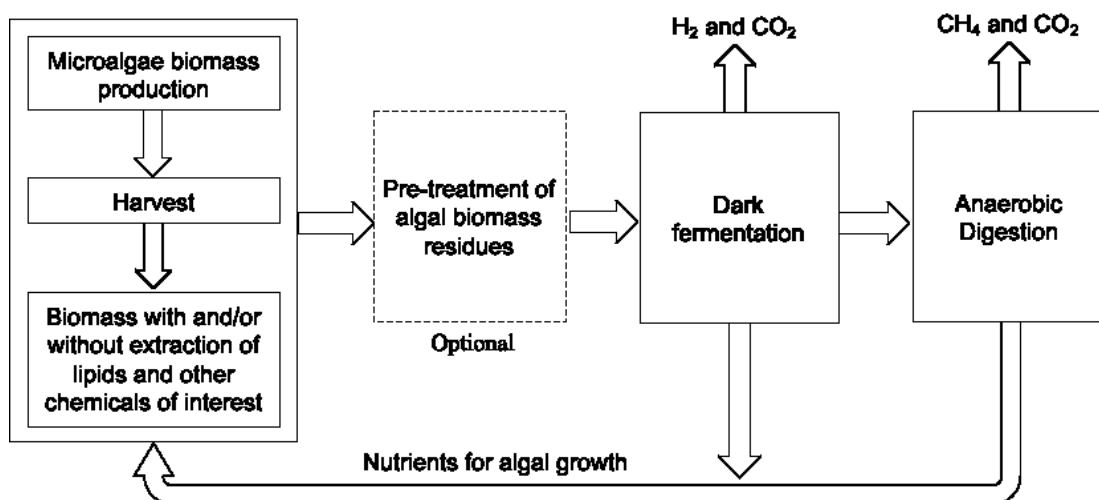
Figure 1. Biorefinery approach for bio-hythane production

8.3.1. Fermentative H$_2$ production

DF is one of the ideal technologies for H$_2$ production because of its high productivities, the potential to treat a large variety of organic wastes and the concomitant production of volatile acids that can be used as building blocks [41], [42]. Thus, DF exhibits the unique capability to utilize low cost organic waste biomass such as microalgal biomass as a feedstock. In DF processes, the carbohydrate-rich substrates above mentioned are broken down anaerobically by hydrogen-producing bacteria (HPB) and molecular hydrogen is produced released in the process of disposing the excess electrons through the activity of the hydrogenase present in HPB. HPB may include strict anaerobes (*Clostridia*, rumen bacteria, etc.), facultative anaerobes (e.g. *Escherichia coli*, *Enterobacter*, *Citrobacter*) and even aerobes (*Alcaligenes, Bacillus,* etc) [43]. Mixed cultures can yield 4 mol and 2 mol of molecular hydrogen per mol of carbohydrate *via* the acetate and butyrate pathways (reactions 1.4 and 1.5), respectively [43]. Pure cultures can yield up to 3.5-3.8 mol of H$_2$ per mol of substrate [2].

The metabolic pathways (Embden–Meyerhof) for the production of fermentative hydrogen *via* biodegradation of microalgal simple carbohydrates involve two biochemical pathways under anaerobic environments, which are shown in Figure 2. Another possible biochemical pathway is based on the transformation of pyruvate into acetyl-CoA and formate in a reaction catalyzed by the enzyme formate hydrogen lyase (FHL) present in certain facultative anaerobes like *Escherichia coli* [44]. In conclusion, 2–4 mol of hydrogen per mole of carbohydrate can be produced. The yield depends on the metabolic pathway, which in turn depends on the hydrogen partial pressure inside the reactor [45]. Acetate involves NADH oxidation to yield 4 mol of biohydrogen per mol of carbohydrate, while buytrate utilizes NADH and produces 2 mols of hydrogen per 1 mol of carbohydrate. Hence, the yield of 2-4 mol of bio molecular hydrogen per mol of carbohydrate depends on the hydrogenases *viz* NADH-dependent and Fd-dependent with ferredoxin reduced either through the NFOR (NADH-ferredoxin oxidoreductase) or through the NADH-Fd dependent hydrogenase [2]. A fraction of pyruvate is used in both enzymatic pathways to yield ATP and then biohydrogen. Moreover, the PFOR pathway can be considered as more favorable since it yields 4 mol of biohydrogen per mol of carbohydrate [46].
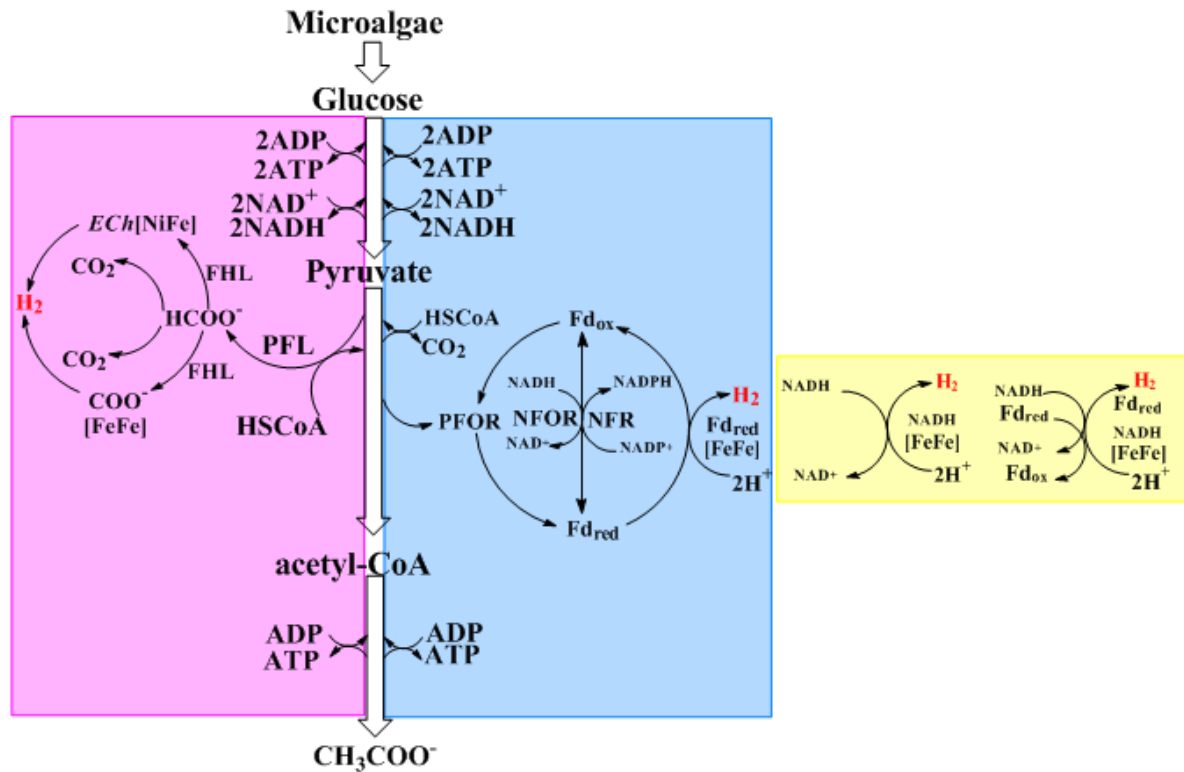
Figure 2. Metabolic pathways for the production of fermentative hydrogen from microalgal carbohydrates

The high carbohydrate content of microalgal biomass (Table 2) makes them an attractive substrate for DF [2], [3], [47]. The carbohydrate content determines the suitability of a substrate for dark fermentative H_2 production, high levels of carbohydrate content being normally correlated with high H_2 productivities [48]. Table 4 presents biohydrogen production yields obtained from various microalgae species. DF of microalgal biomass has been reported by many researchers [37], [49], [50] in three different scenarios (Table 4), i) lipid extracted, ii) pre-treated iii) raw microalgal biomass. These scenarios influence the biohydrogen or biomethane yields as microalgae have chemical barriers that limit their biodegradability during the DF or AD [51]. Sambusiti et al. [2] reported an experimental biodegradability of the microalgal biomass < 36%. The biodegradability of microalgal biomass during DF was calculated as the ratio of experimental to theoretical biohydrogen production. Microalgal biodegradability can be enhanced by the application of different pre-treatment methods.

Table 4. Bio-hythane production from microalgae biomass in a biorefinery concept.

Microalgae culture	Pre-treatment	Systems type	H_2 yield (mL H_2 g VS^{-1})	CH_4 yield (mL CH_4 g VS^{-1})	Reference
Lipid extracted *Scenedesmus* biomass	-	DF	30.00	-	[37]
Lipid extracted *Scenedesmus* biomass	4% (w/w) were pre-treated with 8 g L^{-1} NaOH at 100 °C for 8 h	DF + AD	46.00 ± 2.40	393.60±19.50	[38]
Dunaliella tertiolecta	-	Stand alone DF and AD	12.60	24.00	[52]
Chlorella vulgaris	-	Stand alone DF and AD	10.80	286.00	[52]
Chlorella pyrenoidosa	Steam heating with dilute H_2SO_4	DF + PF[b] + AD	75.60 in DF and 122.70 in PF	186.20	[53]
Arthrospira platensis	microwave-assisted dilute H_2SO_4	DF + PF	96.60[a] from DF and 240.40 [a] from PF	-	[54]
Chlorella vulgaris	-	DF	31.20	-	[55]
Chlorella pyrenoidosa supplemented with cassava starch	Steam heating with dilute H_2SO_4	DF + PF[b] + AD	276.20 from DF and 664 from PF	126.00	[56]
Nanofrustulum sp.	Lipid extraction (methyl pentane as solvent)	AD	-	304.00 ± 5.00	[57]
	No lipid extraction	AD	-	507.00 ± 5.00	[57]

[a] mLH_2 g^{-1} dry weight, [b] PF - photo fermentation

8.3.2. Anaerobic digestion for CH_4 production

AD is a well-established technology that supports the production of biogas (methane - CH_4 and carbon dioxide - CO_2) from diverse biomass sources such as OFMSW, animal manure, agricultural residues, industrial and municipal wastewater. AD is a complex biochemical process which involves four steps, namely hydrolysis, acidogenesis, acetogenesis and methanogenesis. The symbiosis and interaction between different complex groups of microorganisms and processes makes AD sensitive to various factors such as inoculum type, substrates and operational parameters *viz* pH, temperature, OLR and HRT.

The two stage AD process, where hydrolysis − acidogenesis and acetogenesis - methanogenesis in the absence of molecular oxygen (so the route must take place in a highly redox environment of −200 to −400 mV) are separately carried in two reactors, offers several benefits in-terms of higher OLR and biogas productivities when compared to the conventional single stage AD process. The use of microalgae as feedstock for AD is very promising since this process can support the conversion of the carbon remaining in the lipid-extracted microalgal biomass to CH_4.

The stoichiometry of coupling methanogenesis with ADP phosphorylation depends on the hydrogen concentration. Methanogens can utilize sulphur as a terminal electron acceptor because they can re-oxidize the reduced sulphur with CO_2, one of the other methanogenic carbon substrates which in sequence simultaneously reduce to methane gas. AD does not need substrate drying because it can occurs in both wet and dry conditions depending on the reactor configuration. Microalgae AD is typically applied in wet continuous stirred tank reactors (CSTR), which reduces the overall energy consumption of the process.

Two stage operation provides AD with operational flexibility for a wide range of OLRs and substrate types, and higher biogas production rates [5]. Thus, AD can also be applied as a side-stream process for the conversion of the by-products from DF (organic acids and alcohols) and the residues obtained from the pre-treatment of algal biomass. [37] compared one-stage and two-stage AD in terms of biogas production potential and energy efficiency using *Scenedesmus* biomass. The two-stage process supported 46 ± 2 mL H_2 g VS^{-1} in DF and 394 ± 19 mL CH_4 g VS^{-1} in the subsequent AD stage. The authors found that the methane yield was 22% higher and the energy efficiency increased from 51% to 65% compared to one-stage AD. Likewise, [58] reported a

theoretical maximum H_2 and CH_4 yields of 318 mL H_2 g DW^{-1} (dried weight) and 262 mL CH_4 g DW^{-1}, respectively, for *Artrosphira maxima* [58]. The authors calculated an increase in the theoretical energy conversion efficiency from 16.6% when considering exclusively H_2 to 61.9% when combining H_2 and CH_4 production. Therefore, the integration of AD and DF significantly enhance the sustainability of microalgae-to-biofuel conversion by increasing the energy yields.

A major limitation during AD of microalgal biomass is the potential process inhibition due to ammonia toxicity. This is a function of the carbon to nitrogen ratio in the biomass (i.e. carbohydrate to protein content), microalgae concentration and pH of the anaerobic broth. The high protein content of the algal biomass during the digestion of high microalgae concentrations can lead to high ammonium-nitrogen concentrations in the anaerobic digestion bioreactor, which poses toxicity effects on the methanogenic population and ultimately prevents the consumption of VFA and thus AD process.

8.3.3. Operational conditions enhancing H_2 and CH_4 production

Anaerobic fermentation of microalgal biomass is still challenging due to constraints such as the low concentration of biodegradable substrates, recalcitrant microalgae cell constituents inducing a low biodegradability, low C/N ratios, ammonia toxicity and effects from salinity (in the case of microalgae cultivated in saline water) and metal ions [9]. The H_2 and CH_4 productivities from microalgae strongly depend on their biochemical composition, which in turn depends on the microalgae species and culture conditions (Table 4). In this context, several operating parameters such as pH, temperature, OLR, HRT as well as inoculum enrichment and immobilization influence the yield and production rates of biohydrogen or biomethane (Figure 3). Similarly, pretreatment of algal biomass influences on substrate utilization and their conversion in biohythane.
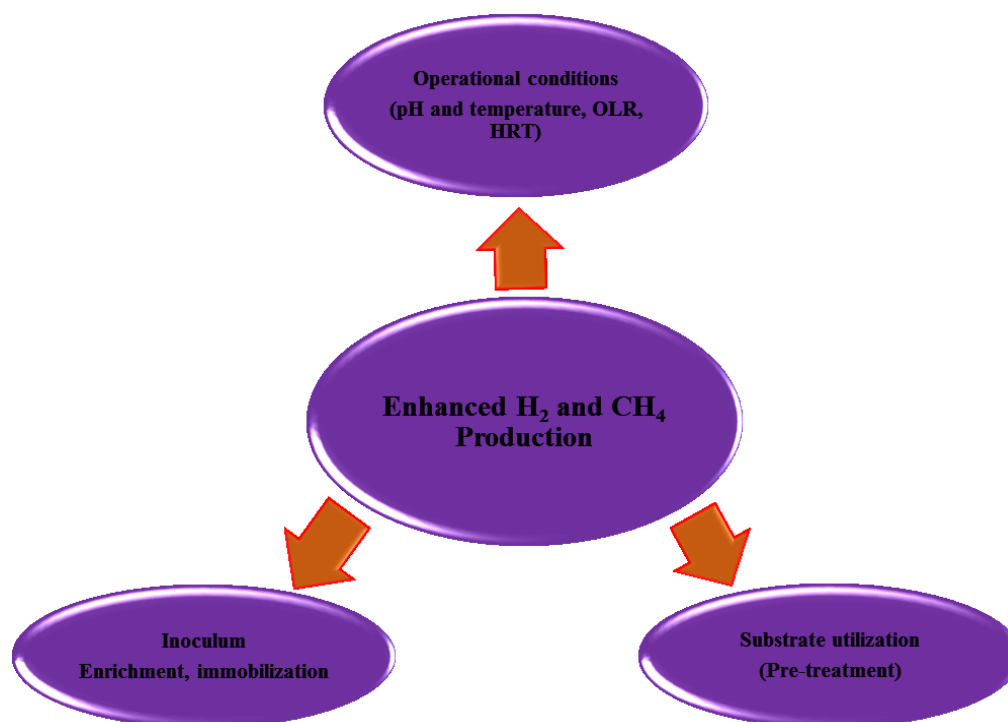
Figure 3. Different strategies to enhance bio-hythane production (adapted and modified from Ghimire et al., 2015a).

Mixed culture fermentation provides more flexibility and robustness for the treatment of a wide range of waste biomasses and varying operational conditions (temperature, pH, organic loading rates), and offers an economic advantage derived from avoiding sterilization cost. H_2 synthesizing bacteria are ubiquitous in soil, wastewater sludge, compost, cow dung, municipal solid waste, *etc.* and can be used as seed inocula for DF [31, 41, 42]. The type of hydrogen synthesizing seed inocula or culture is very important for the startup and performance of the hydrogen production process. Several past investigations for DF processes have been carried out with various species of *Clostridia* and *Enterobacter* as pure cultures [61]. Likewise, mixed culture have been used for the dark fermentative H_2 production from wide range of complex substrates [42]. In this regard, the enrichment of mixed cultures becomes necessary to enhance H_2 production and promote the inhibition of H_2 consumers such as methanogens and homoacetogens. Commonly used inoculum pre-treatment methods to inhibit the methanogenic communities include the use of acid, base, aeration, chloroform, iodopropane, sodium 2-bromoethasulfonic acid (BESA), heat shock, freezing and thawing [42]. However, these inoculum pre-treatment methods seem to be more effective during batch DF compared to continuous processes, where operational parameters play a more vital role in both the efficiency and the stability of the process.

The operational temperature and pH rank among the most crucial parameters determining the optimum metabolic pathway of hydrogen synthesis, as well as the inhibition of hydrogen consumption. pH plays a crucial role in dark fermentative H_2 production in mixed cultures. In particular, acidic pH inhibits the activity of H_2 consumers such as methanogens and homoacetogens, and most importantly, it positively affects the activity of the hydrogenase enzyme and the metabolic pathways in DF, thus influencing the total H_2 yields. A broad range of optimal pH (4.0 – 8.0) has been reported for DF. [37] studied the effect of pH in the range 5.0 – 7.0 during the DF of lipid-extracted microalgal biomass residues without any pre-treatment. The study showed that the highest H_2 yield (20.8 mL g VS^{-1}) was obtained at an initial pH of 6.0. Similarly, pH plays an important role in AD, with a range of 7.0–8.0 typically considered as the optimum pH for AD and pH values lower than 6.5 inhibiting methanogenic populations. In this regard, the high amount of chemical buffering agents needed to maintain an acidic pH (higher than 4.5 – 5.5) in the DF reactor negatively impacts on the operational cost of DF. However, the coupling of DF and AD with recycling of digestate from the AD stage to DF represents an ideal solution to maintain the culture pH during DF. Past studies have shown the technical feasibility of two stage DF and AD processes with digestate recycling [44, 45, 46].

Thermophilic temperatures typically favor the dark fermentative H_2 yield and anaerobic digestion of microalgae, which might be attributed to an enhanced hydrolysis of microalgal biomass. Kinnunen et al. [47] reported a thermophilic (55 ºC) semi-continuous reactor supporting a 48% higher methane yield (220 mL CH_4 g VS^{-1}) than a mesophilic reactor (35 ºC) (149 mL CH_4 g VS^{-1}) during the digestion of dry extracted *Nannochloropsis* sp. residue from biodiesel production. Similarly, the OLRs applied in the reactors directly affects the H_2 and CH_4 production rates and total yields, which are also a function of the microalgae species i.e. biochemical composition. The same author [65] reported an inhibition of methane production due to ammonia-nitrogen at an OLR of 2 g VS L^{-1} d^{-1} and a HRT of 46 d, while a mesophilic reactor out-performed at an OLR of 3 g VS L^{-1} d^{-1} and a HRT of 30 d. This was due to the enhanced microalgae hydrolysis under thermophilic conditions. Moreover, the effect of ammonia toxicity during AD is influenced by the pH and temperature, which are the main parameters determining the equilibrium established between un-ionized ammonia (NH_3-N) and ammonium ions (NH_4-N). Overall, HRTs of ≈ 2–6 days have been reported as the

optimum range for DF of FW in a CSTR process [30, 48], which are similar to the HRTs to the first stage of two-stage AD of FW [67].

8.4. Bio-hythane production: innovative approach

Figure 4 summarizes the two-stage fermentation involved in the production of bio-hythane. In the first stage, H_2 production is controlled by a complex population of hydrolytic and acidogenic bacteria, where as in the second stage methanogenic archaea control methane generation [54]. Fermentative hydrogen production via DF coupled with AD constitutes an attractive alternative to thermo-chemical processes through an integrated production of a distinctive mixture of H_2 (5-25%) and CH_4 (75-95%) named bio-hythane. This eco-friendly gaseous bio-fuel can be produced in a two-stage process consisting of a DF reactor integrated with an AD reactor [67]. The coupled DF-AD process involves a further conversion of the microbial metabolites produced during DF into CH_4 in AD, i.e. the industrially viable total energy recovery via the production of bio-hythane under strict AD bio-pathways. Therefore, coupling DF-AD processes can ensure the production of a versatile gaseous bio-fuel and high biomass conversion efficiencies in a more sustainable biorefinery concept. Moreover, the nutrient rich digestate from DF and AD can be further used to produce algal biomass in photobioreactors (Table 1). The emission of combustion pollutants viz CO, unburned HCs and NO_x are considerably reduced by the addition of a small amount of hydrogen to natural gas [68]. Varde and Frame [69] and Villante and Genevese [70] demonstrated that the use of a mixture of hydrogen and methane in fueled-vehicles and high-temperature fuel cells significantly improved their energy efficiency and environmental sustainability by reducing CO_2 emissions when compared to the combustion of methane [53, 54, 55].
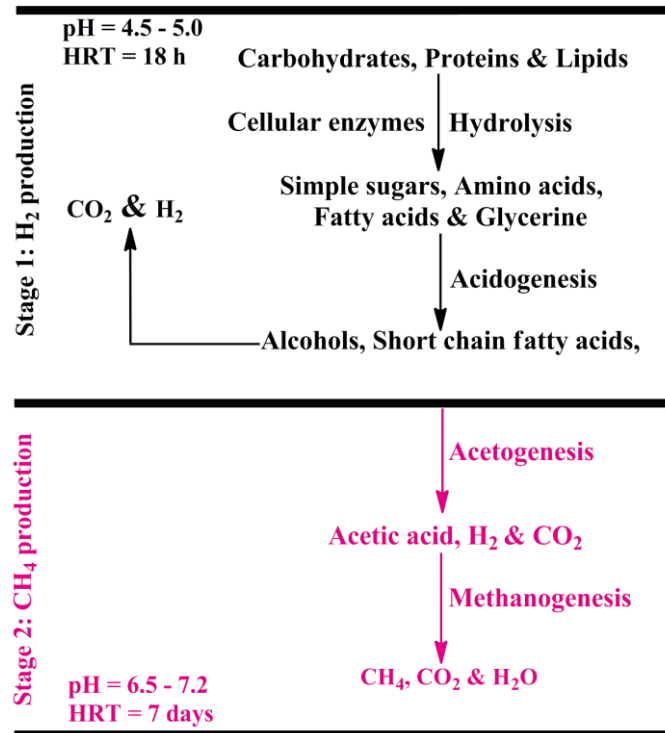
Figure 4. Two-stage anaerobic digestion process.

Industrial AD plants involve hydrolytic/acidogenic reactors in which the hydrolysis of complex organic compounds into simpler compounds occurs, and where these intermediates are further converted to organic acids and then to methane in a second methanogenic reactor (Figure 4) [74]. The two-stage process for the production of bio-hythane will possibly support the same substrate degradation efficiency brought about by the hydrolysis step prior to the methanogenic step. Two-stage processes have been shown to support a better stability and robustness of the methanogenic step and to be able to cope with higher organic loading rates when compared to conventional one-stage methanogenic processes [75]. The optimization of the process parameters can be conducted by the physical separation of the hydrogen and methane producing reactors to maximize and control their production. The yield and productivity of bio-hythane depend on the substrate characteristics, pH, temperature, HRT, OLR and the operational mode [76].

The bio-hythane approach via two-stage fermentation is influenced by the diversion of the microbial metabolic intermediates formed during anaerobic fermentation. The prevalent end-products and metabolism varied with hydrogen and methane generation. Hence, a careful process optimization is required to control the hydrogen and methane content in the biogas mixture. For instance, sugar rich substrates experience a faster hydrolysis/acidogenesis and support higher H_2 production rates and therefore high

H_2/CH_4 ratios. On the other hand, hydrolysis is the rate-limiting process during the degradation of complex substrates, which results in lower H_2 production rates and high methane contents due to the complexity of the microbial ecosystem involved. Thus, a careful control of the microbial ecosystems and process operation during bio-hythane production is essential for upgrading this technology in a commercial scale.

Gaseous bio-fuels such as H_2 and CH_4 offer several benefits over ethanol or biodiesel. The net energy gain from the gaseous bio-fuels is superior compared to their liquid counterparts. In fact, the energy input to microalgal biodiesel production can be up to 6 six times higher than the energy output [3]. This is due to the energy requirement to remove the water from the harvested micro algal biomass prior to trans-esterification. On the other hand, anaerobic fermentation for H_2 and CH_4 production can be conducted at multiple microalgae concentrations. In addition, particle emissions from gaseous bio-fuels combustion are significantly lower than those of liquid bio-fuels [3].

8.4.1. Operational conditions for bio-hythane production

Contamination of DF by methanogens can be avoided by maintaining the HRT at 69 to 86% of the HRT in conventional methanogenic reactors to promote the wash-out of methanogens under continuous operation, taking advantage of the slow growth of methanogens as compared to fermentative bacteria. The HRT plays a key role in the AD of algal biomass, differing from those used for readily degradable FW. Hence, Bohutskyi et al. [77] reported that CH_4 production occurred in the first 20-30 days for all the five microalgal species tested, this production depending on the lipid content rather than the carbohydrate and protein content of the algal biomass. The optimum HRT depends on the physical and biochemical characteristics of microalgae: strain, macromolecular composition, pre-treatment, lipid-extraction, concentration and type of cultivation mode in which algal biomass is grown. Venkata Subhash and Venkata Mohan [33] and Xia [47] reported 3 days of incubation for maximum cumulative H_2 production for acid pre-treated lipid extracted and un-extracted microalgal biomass, respectively. Most of the studies of DF of algal biomass have been conducted in batch mode. The most important operating conditions along with the yields and productivities of bio-hythane are compiled in Table 5. Typical bio-hythane productivities in the two stage DF-AD varies depending upon the type of substrate used and the reactor operating conditions (Tables 4 and 5). A pH of 4.9-6.0 favors hydrogen production as well as the growth of acidogenic H_2-producing microorganisms, while preventing the growth of

methanogens. Guo et al. [48] reported that a high pH of 7.5 favors methanogens contamination in the first stage fermenter. The integrated dark fermentation-methanogenesis may need pH control under some particular scenarios. Liu et al. [78] and Kobayashi et al. [79] obtained methane yields of ~500 L CH_4 kg VS^{-1} from OFMSW in continuous stirred tank reactors of 8 and 40 L (first and second stage, respectively) at 55°C and a low pH of 5.5. The authors concluded that sludge recirculation from AD to DF enhanced both hydrogen production and the degradation of carbohydrate compared with a two-stage process with no sludge recirculation.

Liu et al. [78] observed a 21% higher methane yield in a two-stage process (hydrolysis/acidogenesis in one stage and acetogenesis/methanogenesis in second) when compared to a one-stage process under mesophilic conditions using household solid waste substrate. Similarly, Luo et al. [80] and Nasr et al. [81] reported that a two-stage process yielded 11% and 18.5% more gaseous bio-fuels ($H_2 + CH_4$), respectively, when compared to conventional anaerobic digestion using a biodiesel industrial waste and raw thin stillage, respectively. Patterson et al. [82] estimated the environmental impact of a single-stage methane and two-stage bio-hythane processes using a LCA approach in accordance with European guidance [83]. The analysis involved food waste and wheat feed/straw substrates using diesel fossil fuels as a reference scenario. The study concluded that two-stage processes considerably diminish the environmental carcinogens and eco-toxicity when compared to single-stage processes. Above all, there is of utmost need to demonstrate the stable long-term operation of two-stage processes, reduce the cost of operation and monitoring procedures, and reduce the impact of inhibitory effects derived from the accumulation of nitrogen in the second stage. These areas require further research and development for scale-up application of two-stage processes.

Table 5. Two-stage hydrogen and methane fermentation from biomass.

Substrate	H₂			CH₄			$H_2 (H_2 + CH_4)^{-1}$ (v/v)
	Inoculum	Operation	Yield	Inoculum	Operation	Yield	
Ethanol stillage, cake and glycerol waste	Anaerobic digested manure	CSTR, C	48.00 L kg VS^{-1}	Anaerobic digested manure	CSTR, C	344 L kg VS^{-1}	0.12
Glucose	AS	Chemostat, C	1.38 mol mol hexose^{-1}	AS	Up-flow reactor, C	NA	NA
		CSTR, C	0.34 mol mol hexose^{-1}		CSTR, C	0.12 mol mol hexose^{-1}	0.74
		CSTR, B	2.33 mol mol hexose^{-1}	ACS	CSTR, B	0.8 mol mol hexose^{-1}	0.75
	ACS		2.75 mol mol hexose^{-1}			2.13 mol mol hexose^{-1}	0.56
	AS from UASB	SBBR, SC	2.12 mol mol hexose^{-1}	AS from UASB	SBBR, SC	3.09 mol mol hexose^{-1}	0.41
	GS from UASB	SB, B	185 L kg COD^{-1}	GS from UASB	SB, B	267 L kg COD^{-1}	
Glucose and AcOH	AS	CSTR, C	3.21 mol mol hexose^{-1}	AS	CSTR, C	3.63 mol mol^{-1}	0.47
Lactose		CSTR, B	100 L kg COD^{-1}		CSTR, B	303 L kg COD^{-1}	0.25
		SB, B	46 L kg VS^{-1}		SB, B	394 L kg VS^{-1}	0.10
Sucrose		CSTR, B	1.62 mol mol hexose^{-1}	AS	Up-flow anaerobic filter, C	2.75 mol mol hexose^{-1}	0.37

AcOH = Acetic acid; AS: Anaerobic digester sludge; ACS: Activated sludge; UASB: Up-flow anaerobic sludge blanket; GS: Granular sludge; C: Continuous; CSTR = H₂ continuous stirred tank reactor; B: batch; SBBR: Sequencing batch bioreactor; SB: Serum bottle; SC: Semi-continuous; NA: Not available; COD: Chemical oxygen demand; VS: Volatile solid.
(The gas yield was displayed based on the added concentration of the substrate in VS / COD / mol), Modified from Liu et al. (2013)

8.5. Potential and challenges towards bio-hythane production scale-up

The integrated bio-hythane production concept has cross the threshold of commercial demonstration phase in a few companies. Since 2013, Sapporo Breweries Limited (Japan) is operating a pre-commercial plant for bio-hythane production from vegetables and crops wastes. China ranks top in the world in the production of bio-hythane due to i) the fast development of large-scale biogas fermentation technologies (which ultimately constitute an outstanding platform for the endorsement in the development of CNG/hythane vehicles), ii) the availability of huge amounts of agricultural waste biomass (0.7 & 4 billion tons year^{-1} of plant residues & livestock manure, respectively), iii) the pressure to reduce GHG emissions and iv) the need to develop a clean and sustainable production [84] with a subsequent increasing demand for gaseous fuels due to recent shortages in gasoline and diesel [67, 68]. The plant and manure bio-wastes above mentioned could be theoretically converted into about 200 and 100 billion m^3 of H$_2$ and CH$_4$ (300 billion m^3 of bio-hythane), respectively, via the two-stage dark fermentation processes, which is equivalent to over four times the total amount of natural gas consumption in China [87]. Nearly more than ten large-scale biomethane projects of > 10000 m^3 digester volume have been built throughout the past three years in China for the valorisation of biomass, which offer a platform to boost bio-hythane generation. The scale-up of bio-hythane production process could also be started with existing biogas facilities by necessary retrofitting. Bio-hythane can be further upgraded by eliminating carbon dioxide and utilized as a vehicle fuel. In this context, it can be anticipated that bio-hythane will successfully compete with biomethane as a second-generation clean gas bio-fuel.

The upscale of the HyMeTek technology (Innovative Hydrogenation & Methanation Technology) involved the construction of two feedstock storage tanks used as a carbon source reservoir, two feedstock tanks for nutrient medium, a hydrogen production fermenter and a methane digester with respective volumes of 0.75 m^3, 0.75 m^3, 0.4 m^3 and 2.5 m^3. The stainless steel bio-hythane reactors were designed based on an up-flow anaerobic UASB reactor equipped with a warm-water jacket and a control system panel to maintain the temperature at 35 °C and pH at optimum values. Maximum H$_2$ and CH$_4$ productivities of 2.97 and 0.86 m^3 m^{-3} d^{-1} with yields of 1-5 mol H$_2$ mol COD^{-1} and 27-56 CH$_4$ mL g COD^{-1}, respectively, were achieved at a HRT of 9 h using food industrial wastewater of 60 g COD L^{-1} and a NaOH scubber for biogas purification. Another two-

stage system for bio-hythane production has been succesfully scaled up 10 times in Dobrzelin Sugar Factory (Poland) with the support of a grant of the National Centre for Research and Development (PBS1/B9/9/2012). Another advanced two-phase HyMeTek bio-hythane production system has been constructed by Feng Chia University (Taiwan).

The lipid extraction methods during microalgae downstream influence biohydrogen or biomethane production. Thus, the chloroform/methanol mixture used during solvent extraction resulted in a complete inhibition of methane production [51]. Literature has also consistently reported [70, 71, 72] the inhibition of bio-hythane production at ammonia concentrations > 800 mg L^{-1} [73, 74]. The acclimation of anaerobic microbial communities to high NH_3 concentrations is well documented in literature [79]. For instance, Velsen et al. [93] recorded methane production at concentrations of ammonium ranging from 700 to 5000 mg NH_4^+ L^{-1} using seed inoculum adapted to ammonium concentration of 815 mg L^{-1}. Nitrogen removal has been effectively conducted via stripping [94], natural zeolites adsorption, membrane separation [95] and microbial removal processes such as Annamox [96] or nitrification/denitrification [97]. For instance, Liu et al. [89] achieved > 97% ammonia removal from pig manure by air-recirculated stripping at 36 °C at a pH of 12.4.

Figure 5 summarizes the major constraints of bio-hythane production along with potential design and operational strategies to overcome these limitations. The major disadvantages of AD could overcome during bio-hythane production since the acidogenic H_2 fermentation supports an enhance hydrolysis, which ultimately makes microalgae more amenable to the methanogenic archaea to enhance the biogas production performance.
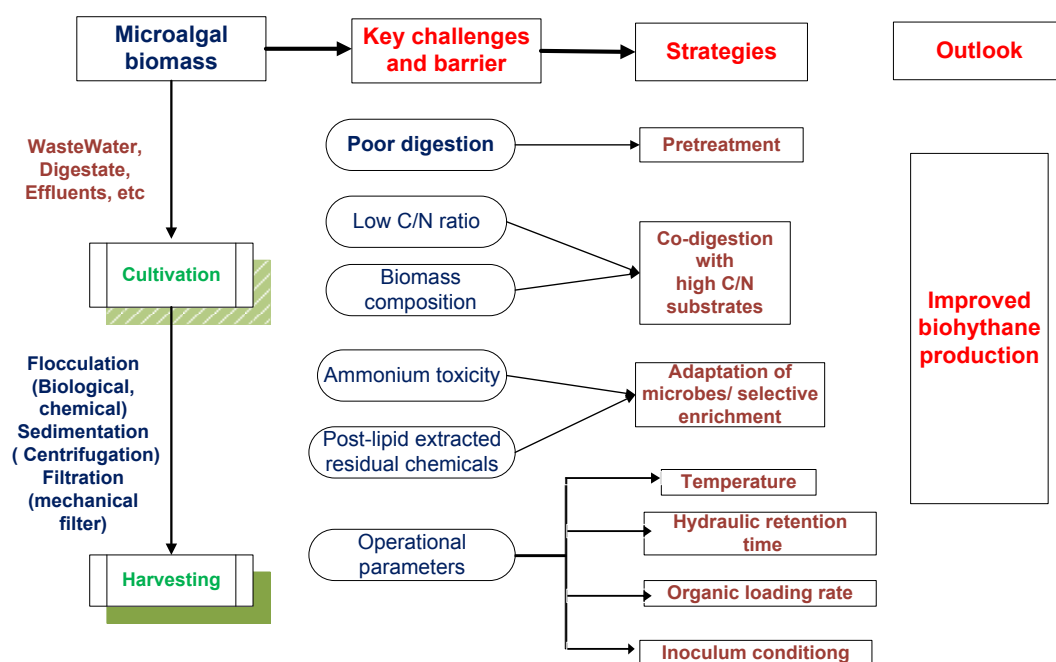
Figure 5. Overview of enhanced bio-hythane production from microalgal biomass.

8.6. Key issues and future perspectives

Availability of CO_2, supply of nutrients (especially nitrogen and phosphorous), water foot print, technology and cost of production and harvesting are one of the major constraints for the production of algal biomass based biofuels. The sustainable production of algal biomass can be achieved from the coupling the biomass production systems with treatment of wastewater and anaerobic digestate which can mitigate the need for the supply of macro and micronutrients for their growth and metabolism. Microalgae can be effectively cultivated either in open ponds or closed PBRs. Microalgae culture contamination by fungi, virus or protozoa represents an unresolved challenge during microalgae cultivation in open ponds [98]. On the other hand, microalgae growth inhibition has been reported at pH value over 11, which are typically achieved in carbon limited cultures [80, 81]. High microalgae productivities in open ponds under long-term operation have been only achieved with algal strains *viz Dunaliella*, *Spirulina* and *Chlorella* sp., whose cultivation is characterized by harsh culture environments like high salinity, alkalinity and nutrient restrictions [100]. Closed PBRs offer a higher degree of protection against culture contamination and higher biomass productivities than their open counterparts. Nonetheless, closed PBRs exhibit higher energy consumptions and investment costs, which limits the use of this technology for the cultivation of microalgae for bio-fuel applications.

LCAs of microalgae bio-fuels typically reveal negative energy gains and environmental impacts [101]. LCA debate has been mainly focused on life-cycle impacts of the usage of water, energy, inorganic salts and phosphorous-nitrogen fertilizers, methanol utilization for transesterification and glycerol by-product production. Microalgae require high inputs of nitrogen for their cultivation, which are responsible for a noteworthy indirect emission of GHGs [102]. Likewise, microalgae harvesting is another major challenge due to the high energy requirements in harvesting processes [103]. In this context, cross-flow membrane filtration, ultrasonic harvesting and electro-coagulation/electrolytic aggregation have emerged as low-cost harvesting methods [104]. For the reduction of energy consumption during microalgae-based bio-fuel production, further strategies need to be explored. In the particular context of bio-hythane production from microalgae and waste biomass, a number of emerging techniques have been proposed, although few limitations must be overcome in order to achieve a sustainable gaseous bio-fuel production process.

The first key issue to achieve an effective and robust bio-hythane production is the consistent design and rational control of the microbial consortium governing hydrogen fermentation. Indigenous consortia present in mixed culture during DF are less efficient compared to pure culture of H_2 producers. Therefore, a designed (microbial augmentation through addition of potential strains of H_2 producers) or acclimated consortium should be used, which requires a fundamental understanding of the microbial mechanisms involved in DF-AD. If microbial consortia are sensibly designed and controlled, the direct bioprocess could be inexpensive and commercially feasible. In this regard, a cost-competitive production of bio-hythane eventually depends on the efficient integration of the two-stage process, where innovative quality control algorithms can be applied to support a more effective biohydrogen and biomethane production.

Furthermore, the recycling of digestate in two-stage processes represents another innovative strategy to improve the performance of DF. This strategy involves the recycling and mixing of the digestate with the dilute feedstock in order to provide a buffering effect. However, the recycling of the digestate to the first-stage hydrogen production will likely entail a deleterious consortium contamination by methane-producing microorganisms. In such case, innovative solutions comprise the implementation of a membrane filtration module prior to digestate recirculation [105],

temperature-phased processes [106], HPB bioaugmentation and the increase in the OLR in the DF reactor [80].

Moreover, the key issue on the bio-hythane product chain mainly includes the DF process control to produce the bio-hydrogen, an appropriate mixture of H_2 and CH_4. The carbon dioxide is excluded from this process to achieve a suitable bio-hythane composition i.e., a H_2 $(H_2 + CH_4)^{-1}$ of 0.01-0.75. A sustainable supply of bio-hythane with a controlled H_2/CH_4 ratio could be achieve by engineering the anaerobic biopathways. The two-stage process can be regulated by the controlling the pH, retention time, recycling ratio, etc. For instance, an increase in the H_2/CH_4 ratio can be achieved by increasing the recirculation rate to the biomethane reactor if a reflex ratio is suitably applied as a regulator. The H_2/CH_4 ratio can be reduced by supplying a fraction of the H_2 produced in first DF stage to the methanogenic stage in order to boost CO_2 reduction to CH_4. The integrated bio-hythane production using microalgae can improve the C:N ratio through effluent recycling and increase the production of gaseous bio-fuels, which can also be utilized for electrical/thermal energy production while the mass cultivation photobioreactors can also be employed for biogas upgrading. The resulting digestate can be ideal nutrient sources for the cost-competitive and sustainable production of algal biomass. A detailed knowledge of the growth and characteristics of both raw microalgae and their biofuel-associated residues, along with the optimization of the two-stage DF-AD process, will be crucial to establish sustainable biomass based refinery for clean energy.

8.7. Conclusion

The present chapter focused on the generation of bio-hythane from microalgae via two-stage dark fermentation, with special emphasis on key issues influencing bio-hythane production and future perspectives. The expected strong demand for hythane fuel and the severe necessity of biomass waste management worldwide, the concept of concurrent high-value bio-hythane production was proposed. The integrated hydrogen and methane production from microalgae and waste biomass would be a profitable clean energy solution, which would make bio-hythane production sustainable. Several crucial factors to be considered prior to technology scale up to boost hydrogen production from DF have been discussed in this chapter.

References

[1]   Kumar, G., Bakonyi, P., Periyasamy, S., Kim, S.H., Nemestóthy, N., Bélafi-Bakó, K., 2015. Lignocellulose biohydrogen: practical challenges and recent progress. Renewable and Sustainable Energy Reviews, 44, pp.728-737.

[2]   Sambusiti, C., Bellucci, M., Zabaniotou, A., Beneduce, L., Monlau, F., 2015. Algae as promising feedstocks for fermentative biohydrogen production according to a biorefinery approach: a comprehensive review. Renewable and Sustainable Energy Reviews, 44, pp.20-36.

[3]   Xia, A., Herrmann, C., Murphy, J.D., 2015. How do we optimize third-generation algal biofuels?. Biofuels, Bioproducts and Biorefining, 9, pp.358-367.

[4]   Roy, S., Das, D., 2015. Biohythane production from organic wastes: present state of art. Environmental Science and Pollution Research, 23, pp.9391-9410.

[5]   Liu, Z., Zhang, C., Lu, Y., Wu, X., Wang, L.L., Han, B., Xing, X.H., 2013. States and challenges for high-value biohythane production from waste biomass by dark fermentation technology. Bioresource Technology, 135, pp.292-303.

[6]   Cavinato, C., Bolzonella, D., Pavan, P., Cecchi, F., 2016. Two-phase anaerobic digestion of food wastes for hydrogen and methane production. In Enriched Methane - First Step Towards the Hydrogen Economy, Springer International Publishing, pp.75-90.

[7]   Ekins, P., Hughes, N., 2010. The prospects for a hydrogen economy (2): hydrogen transitions. Technology Analysis & Strategic Management, 22, pp.1-17.

[8]   Chisti, Y., 2010. Fuels from microalgae. Biofuels, 1, pp.233-235.

[9]   Ward, A.J., Lewis, D.M., Green, F.B., 2014. Anaerobic digestion of algae biomass: a review. Algal Research, 5, pp.204-214.

[10]   Bahr, M., Díaz, I., Dominguez, A., González Sánchez, A., Muñoz, R., 2014. Microalgal-biotechnology as a platform for an integral biogas upgrading and nutrient removal from anaerobic effluents. Environmental Science and Technology, 48, pp.573-581.

[11]   Chojnacka, K., Marquez-Rocha, F.J., 2004. Kinetic and stoichiometric relationships of the energy and carbon metabolism in the culture of microalgae.

Biotechnology, 3, pp.21-34.

[12]   Xia, A., Murphy, J.D., 2016. Microalgal cultivation in treating liquid digestate from biogas systems. Trends in Biotechnology, 34(4), pp.264-275.

[13]   Wang, J., Yang, H., Wang, F., 2014. Mixotrophic cultivation of microalgae for biodiesel production: status and prospects. Applied Biochemistry and Biotechnology, 172, pp.3307-3329.

[14]   Chen, C.Y., Yeh, K.L., Aisyah, R., Lee, D.J., Chang, J.S., 2011. Cultivation, photobioreactor design and harvesting of microalgae for biodiesel production: a critical review. Bioresource Technology, 102, pp.71-81.

[15]   Sialve, B., Bernet, N., Bernard, O., 2009. Anaerobic digestion of microalgae as a necessary step to make microalgal biodiesel sustainable. Biotechnology Advances, 27, pp.409-416.

[16]   Lakaniemi, A.M., Intihar, V.M., Tuovinen, O.H., Puhakka, J.A., 2012. Growth of *Chlorella vulgaris* and associated bacteria in photobioreactors. Microbial Biotechnology, 5, pp.69-78.

[17]   Chacón-Lee, T.L., González-Mariño, G.E., 2010. Microalgae for "Healthy" foods-possibilities and challenges. Comprehensive Reviews in Food Science and Food Safety, 9, pp.655-675.

[18]   Martínez-Fernández, E., Acosta-Salmón, H., Southgate, P.C., 2006. The nutritional value of seven species of tropical microalgae for black-lip pearl oyster (*Pinctada margaritifera*, L.) larvae. Aquaculture, 257, pp.491-503.

[19]   Renaud, S.M., Thinh, L. V., Parrry, D.L., 1999. The gross chemicl composition and fatty acid composition of 18 species of tropical Australian microalgae for possible use im mariculture. Aquaculture, 170, pp.147-159.

[20]   Chisti, Y., Yan, J., 2011. Energy from algae: current status and future trends. Applied Energy, 88, pp.3277-3279.

[21]   Mandal, S., Mallick, N., 2009. Microalga *Scenedesmus obliquus* as a potential source for biodiesel production. Applied Microbiology and Biotechnology, 84, pp.281-291.

[22]   Illman, A.M., Scragg, A.H., Shales, S.W., 2000. Increase in *Chlorella* strains calorific values when grown in low nitrogen medium. Enzyme and Microbial Technology, 27, pp.631-635.

[23]   Xiong, W., Li, X., Xiang, J., Wu, Q., 2008. High-density fermentation of microalga *Chlorella protothecoides* in bioreactor for microbio-diesel

production. Applied Microbiology and Biotechnology, 78, pp.29-36.

[24]   Liang, Y., Sarkany, N., Cui, Y., 2009. Biomass and lipid productivities of
Chlorella vulgaris under autotrophic, heterotrophic and mixotrophic growth
conditions. Biotechnology Letters, 31, pp.1043-1049.

[25]   Tan, X., Chu, H., Zhang, Y., Yang, L., Zhao, F., Zhou, X., 2014. *Chlorella
pyrenoidosa* cultivation using anaerobic digested starch processing wastewater
in an airlift circulation photobioreactor. Bioresource Technology, 170, pp.538-
548.

[26]   Uggetti, E., Sialve, B., Latrille, E., Steyer, J.P., 2014. Anaerobic digestate as
substrate for microalgae culture: the role of ammonium concentration on the
microalgae productivity. Bioresource Technology, 152, pp.437-443.

[27]   Turon, V., Trably, E., Fayet, A., Fouilland, E., Steyer, J.P., 2015. Raw dark
fermentation effluent to support heterotrophic microalgae growth: microalgae
successfully outcompete bacteria for acetate. Algal Research, 12, pp.119-125.

[28]   Chiaramonti, D., Maniatis, K., Tredici, M.R., Verdelho, V., Yan, J., 2015. Life
Cycle Assessment of algae biofuels: needs and challenges. Applied Energy,
154, pp.1049-1051.

[29]   Stephenson, A.L., Kazamia, E., Dennis, J.S., Howe, C.J., Scott, S.A., Smith,
A.G., 2010. Life-Cycle Assessment of potential algal biodiesel production in
the united kingdom: a comparison of raceways and air-lift tubular bioreactors.
Energy and Fuels, 24, pp.4062-4077.

[30]   Collet, P., Hélias, A., Lardon, L., Steyer, J.P., Bernard, O., 2015.
Recommendations for Life Cycle Assessment of algal fuels. Applied Energy,
154, pp.1089-1102.

[31]   Collet, P., Hélias Arnaud, A., Lardon, L., Ras, M., Goy, R.A., Steyer, J.P.,
2011. Life-Cycle Assessment of microalgae culture coupled to biogas
production. Bioresource Technology, 102, pp.207-214.

[32]   Barros, A.I., Gonçalves, A.L., Simões, M., Pires, J.C.M., 2015. Harvesting
techniques applied to microalgae: a review, Renewable and Sustainable Energy
Reviews, 41, pp.1489-1500.

[33]   Venkata Subhash, G., Venkata Mohan, S., 2014. Deoiled algal cake as
feedstock for dark fermentative biohydrogen production: an integrated
biorefinery approach. International Journal of Hydrogen Energy, 39, pp.9573-
9579.

[34]   Varrone, C., Izzo, G., Massini, G., Marone, A., Signorini, A., Wang, A., 2015.
Linking biodiesel and biohydrogen production through the dark fermentation of
crude glycerol: applying the biorefinery concept. pp.2-3.

[35]   Ehimen, E.A., Sun, Z.F., Carrington, C.G., Birch, E.J., Eaton-Rye, J.J., 2011.
Anaerobic digestion of microalgae residues resulting from the biodiesel
production process. Applied Energy, 88, pp.3454-3463.

[36]   Clomburg, J.M., Gonzalez, R., 2013. Anaerobic fermentation of glycerol: a
platform for renewable fuels and chemicals. Trends in Biotechnology, 31,
pp.20-28.

[37]   Yang, Z., Guo, R., Xu, X., Fan, X., Luo, S., 2011. Fermentative hydrogen
production from lipid-extracted microalgal biomass residues. Applied Energy,
88, pp.3468-3472.

[38]   Yang, Z., Guo, R., Xu, X., Fan, X., Luo, S., 2011. Hydrogen and methane
production from lipid-extracted microalgal biomass residues. International
Journal of Hydrogen Energy, 36, pp.3465-3470.

[39]   Prajapati, S.K., Kumar, P., Malik, A., Vijay, V.K., 2014. Bioconversion of
algae to methane and subsequent utilization of digestate for algae cultivation: a
closed loop bioenergy generation process. Bioresource Technology, 158,
pp.174-180.

[40]   Turon, V., Baroukh, C., Trably, E., Latrille, E., Fouilland, E., Steyer, J. P.,
2015. Use of fermentative metabolites for heterotrophic microalgae growth:
yields and kinetics. Bioresource Technology, 175, pp.342-349.

[41]   Das, D., Khanna, N., Veziroglu, T.N., 2008. Recent developmens in biological
hydrogen production process. Chemicak Industry and Chemical Engineering
Quaterly, 14, pp.57-67.

[42]   Ghimire, A., Frunzo, L., Pirozzi, F., Trably, E., Escudie, R., Lens, P.N.L.,
Esposito, G., 2015. A review on dark fermentative biohydrogen production
from organic biomass: process parameters and use of by-products. Applied
Energy, 144, pp.73–95.

[43]   Li, C., Fang, H.H.P., 2007. Fermentative hydrogen production from wastewater
and solid wastes by mixed Cultures. Critical Reviews in Environmental
Science and Technology, 37, pp.1-39.

[44]   Cai, G., Jin, B., Monis, P., Saint, C., 2011. Metabolic flux network and analysis
of fermentative hydrogen production. Biotechnology Advances, 29, pp.375-

387.

[45]   Hallenbeck, P.C., Abo-Hashesh, M., Ghosh, D., 2012. Strategies for improving biological hydrogen production. Bioresource Technology, 110, pp.1-9.

[46]   Abo-Hashesh, M., Wang, R., Hallenbeck, P.C., 2011. Metabolic engineering in dark fermentative hydrogen production; theory and practice. Bioresource Technology, 102, pp.8414-8422.

[47]   Xia, A., Jacob, A., Rizwan, M., Herrmann, C., Murphy, J.D., 2016. Production of hydrogen, ethanol and volatile fatty acids through co-fermentation of macro- and micro-algae. Bioresource Technology, 205, pp.118-125.

[48]   Guo, X.M., Trably, E., Latrille, E., Carrere, H., Steyer, J.P., 2014. Predictive and explicative models of fermentative hydrogen production from solid organic waste: role of butyrate and lactate pathways. International Journal of Hydrogen Energy, 39, pp.7476-7485.

[49]   Cai, J., Chen, M., Wang, G., Pan, G., Yu, P., 2015. Fermentative hydrogen and polyhydroxybutyrate production from pretreated cyanobacterial blooms. Algal Research, 12, pp.295-299.

[50]   Chandra, R., Venkata Mohan, S., 2011. Microalgal community and their growth conditions influence biohydrogen production during integration of dark-fermentation and photo-fermentation processes. International Journal of Hydrogen Energy, 36, pp.12211–12219.

[51]   Neves, V.T.D.C., Andrade, E., Perelo, L.W., 2016. Influence of lipid extraction methods as pre-treatment of microalgal biomass for biogas production. Renewable and Sustainable Energy Reviews, 59, pp.160-165.

[52]   Lakaniemi, A.-M., Hulatt, C.J., Thomas, D.N., Tuovinen, O.H., Puhakka, J.A., 2011. Biogenic hydrogen and methane production from *Chlorella vulgaris* and *Dunaliella tertiolecta* biomass. Biotechnology for Biofuels, 4, pp.34.

[53]   Xia, A., Cheng, J., Ding, L., Lin, R., Huang, R., Zhou, J., Cen, K., 2013. Improvement of the energy conversion efficiency of *Chlorella pyrenoidosa* biomass by a three-stage process comprising dark fermentation, photofermentation, and methanogenesis. Bioresource Technology, 146, pp.436-443.

[54]   Cheng, J., Xia, A., Liu, Y., Lin, R., Zhou, J., Cen, K., 2012. Combination of dark- and photo-fermentation to improve hydrogen production from *Arthrospira platensis* wet biomass with ammonium removal by zeolite.

International Journal of Hydrogen Energy, 37, pp.13330-13337.

[55]   Yun, Y.M., Jung, K.W., Kim, D.H., Oh, Y.K., Shin, H.S., 2012. Microalgal
biomass as a feedstock for bio-hydrogen production. International Journal of
Hydrogen Energy, 37, pp.15533-15539.

[56]   Xia, A., Cheng, J., Ding, L., Lin, R., Song, W., Zhou, J., Cen, K., 2014.
Enhancement of energy production efficiency from mixed biomass of
Chlorella pyrenoidosa and cassava starch through combined hydrogen
fermentation and methanogenesis. Applied Energy, 120, pp.23-30.

[57]   Zhao, B., Ma, J., Zhao, Q., Laurens, L., Jarvis, E., Chen, S., Frear, C., 2014.
Efficient anaerobic digestion of whole microalgae and lipid-extracted
microalgae residues for methane energy production. Bioresource Technology,
161, pp.423-430.

[58]   Cheng, J., Zhang, M., Song, W., Xia, A., Zhou, J., Cen, K., 2011. Cogeneration
of hydrogen and methane from *Arthrospira maxima* biomass with bacteria
domestication and enzymatic hydrolysis. International Journal of Hydrogen
Energy, 36, pp.1474-1481.

[59]   Wong, Y.M., Wu, T.Y., Juan, J.C., 2014. A review of sustainable hydrogen
production using seed sludge via dark fermentation. Renewable and
Sustainable Energy Reviews, 34, pp.471-482.

[60]   Kumar, G., Lay, C.H., Chu, C.Y., Wu, J.H., Lee, S.C., Lin, C.Y., 2012. Seed
inocula for biohydrogen production from biodiesel solid residues. International
Journal of Hydrogen Energy, 37, pp.15489-15495.

[61]   Elsharnouby, O., Hafez, H., Nakhla, G., El Naggar, M.H., 2013. A critical
literature review on biohydrogen production by pure cultures. International
Journal of Hydrogen Energy, 38, pp.4945-4966.

[62]   Gottardo, M., Cavinato, C., Bolzonella, D., Pavan, P., 2013. Dark fermentation
optimization by anaerobic digested sludge recirculation: effects on hydrogen
production, Chemical Engineering Transactions, 32, pp.997-1002.

[63]   Cavinato, C., Bolzonella, D., Fatone, F., Cecchi, F., Pavan, P., 2011.
Optimization of two-phase thermophilic anaerobic digestion of biowaste for
hydrogen and methane production through reject water recirculation.,
Bioresource Technology, 102, pp.8605-8611.

[64]   Yeshanew, M.M., Frunzo, L., Pirozzi, F., Lens, P.N.L., Esposito, G., 2016.
Production of biohythane from food waste via an integrated system of

continuously stirred tank and anaerobic fixed bed reactors. Bioresource Technology, Bioresource Technology, 220, pp.312-322.

[65]   Kinnunen, H. V., Koskinen, P.E.P., Rintala, J., 2014. Mesophilic and thermophilic anaerobic laboratory-scale digestion of *Nannochloropsis* microalga residues. Bioresource Technology, 155, pp.314-322.

[66]   Ghimire, A., Valentino, S., Frunzo, L., Trably, E., Escudié, R., Pirozzi, F., Lens, P.N.L., Esposito, G., 2015. Biohydrogen production from food waste by coupling semi-continuous dark-photofermentation and residue post-treatment to anaerobic digestion: a synergy for energy recovery. International Journal of Hydrogen Energy, 40(46), pp.16045-16055.

[67]   Aslanzadeh, S., Rajendran, K., Taherzadeh, M.J., 2014. A comparative study between single- and two-stage anaerobic digestion processes: effects of organic loading rate and hydraulic retention time. International Biodeterioration & Biodegradation, 95, pp.1-8.

[68]   Jamal, Y., Wyszynski, M.L., 1994. On-board generation of hydrogen-rich gaseous fuels - a review. International Journal of Hydrogen Energy, 19, pp.557-572.

[69]   Varde, K.S., Frame, G.M., 1984. A study of combustion and engine performance using electronic hydrogen fuel injection. International Journal of Hydrogen Energy, 9, pp.327-332.

[70]   Villante, C., Genovese, A., 2012. Hydromethane: a bridge towards the hydrogen economy or an unsustainable promise?. International Journal of Hydrogen Energy, 37, pp.11541-11548.

[71]   Das, L., 2000. A comparative evaluation of the performance characteristics of a spark ignition engine using hydrogen and compressed natural gas as alternative fuels. International Journal of Hydrogen Energy, 25, pp.783-793.

[72]   Nikooyeh, K., Jeje, A.A., Hill, J.M., 2007. 3D modeling of anode-supported planar SOFC with internal reforming of methane. Journal of Power Sources, 171, pp.601-609.

[73]   De Saint Jean, M., Baurens, P., Bouallou, C., Couturier, K., 2015. Economic assessment of a power-to-substitute-natural-gas process including high-temperature steam electrolysis. International Journal of Hydrogen Energy, 40, pp.6487-6500.

[74]   Willquist, K., Nkemka, V.N., Svensson, H., Pawar, S., Ljunggren, M.,

Karlsson, H., Murto, M., Hulteberg, C., van Niel, E.W.J., Liden, G., 2012. Design of a novel biohythane process with high H_2 and CH_4 production rates. International Journal of Hydrogen Energy, 37, pp.17749-17762.

[75]   Ke, S., Shi, Z., 2005. Applications of two-phase anaerobic digestion for industrial wastewater treatment. International Journal of Environmental Pollution, 23, pp.65-80.

[76]   Cavinato, C., Giuliano, A., Bolzonella, D., Pavan, P., Cecchi, F., 2012. Bio-hythane production from food waste by dark fermentation coupled with anaerobic digestion process: a long-term pilot scale experience. International Journal of Hydrogen Energy, 37, pp.11549-11555.

[77]   Bohutskyi, P., Betenbaugh, M.J., Bouwer, E.J., 2014. The effects of alternative pretreatment strategies on anaerobic digestion and methane production from different algal strains. Bioresource Technology, 155, pp.366-372.

[78]   Liu, D., Liu, D., Zeng, R.J., Angelidaki, I., 2006. Hydrogen and methane production from household solid waste in the two-stage fermentation process. Water research, 40, pp.2230-2236.

[79]   Kobayashi, T., Xu, K.Q., Li, Y.Y., Inamori, Y., 2012. Effect of sludge recirculation on characteristics of hydrogen production in a two-stage hydrogen-methane fermentation process treating food wastes. International Journal of Hydrogen Energy, 37, pp.5602-5611.

[80]   Luo, G., Xie, L., Zhou, Q., Angelidaki, I., 2011. Enhancement of bioenergy production from organic wastes by two-stage anaerobic hydrogen and methane production process. Bioresource Technology, 102, pp.8700-8706.

[81]   Nasr, N., Elbeshbishy, E., Hafez, H., Nakhla, G., Hesham El Naggar, M., 2012. Comparative assessment of single-stage and two-stage anaerobic digestion for the treatment of thin stillage. Bioresource Technology, 111, pp.122-126.

[82]   Patterson, T., Esteves, S., Dinsdale, R., Guwy, A., Maddy, J., 2013. Life Cycle Assessment of biohydrogen and biomethane production and utilisation as a vehicle fuel. Bioresource Technology, 131, pp.235-245.

[83]   Pottering, H.G., Necas, P., 2009. Promotion of the use of energy from renewable sources and amending and subsequently repleaing Directives 2001/77/EC and 2003/30/EC. Official Journal of the European Union, 140, pp.16-62.

[84]   Ou, X., Zhang, X., Chang, S., 2010. Alternative fuel buses currently in use in

China: life-cycle fossil energy use, GHG emissions and policy recommendations. Energy Policy, 38, pp.406-418.

[85] Liu, G. Shen, L., 2007. Quantitive appraisal of biomass energy and its geographical distribution in China. Journal of Natural Resources, 22(1), pp.9-19.

[86] Tan, T., Shang, F., Zhang, X., 2010. Current development of biorefinery in China. Biotechnology Advances, 28, pp.543-555.

[87] Higashi, N., 2009. Natural gas in China. Energy markets and security/2009.

[88] Walker, M., Iyer, K., Heaven, S., Banks, C.J., 2011. Ammonia removal in anaerobic digestion by biogas stripping: an evaluation of process alternatives using a first order rate model based on experimental findings. Chemical Engineering Journal, 178, pp.138-145.

[89] Liu, L., Pang, C., Wu, S., Dong, R., 2015. Optimization and evaluation of an air-recirculated stripping for ammonia removal from the anaerobic digestate of pig manure. Process Safety and Environmental Protection, 94, pp.350-357.

[90] Rajagopal, R., Massé, D.I., Singh, G., 2013. A critical review on inhibition of anaerobic digestion process by excess ammonia. Bioresource Technology, 143, pp.632-641.

[91] Nielsen, H.B., Angelidaki, I., 2008. Strategies for optimizing recovery of the biogas process following ammonia inhibition. Bioresource Technology, 99, pp.7995-8001.

[92] Salerno, M.B., Park, W., Zuo, Y., Logan, B.E., 2006. Inhibition of biohydrogen production by ammonia. Water research, 40, pp.1167-1172.

[93] van Velsen, A.F.M., 1979. Adaptation of methanogenic sludge to high ammonia-nitrogen concentrations. Water Research, 13, pp.995-999.

[94] Serna-Maza, A., Heaven, S., Banks, C.J., 2014. Ammonia removal in food waste anaerobic digestion using a side-stream stripping process. Bioresource Technology, 152, pp.307-315.

[95] Montalvo, S., Guerrero, L., Borja, R., Sánchez, E., Milán, Z., Cortés, I., Angeles de la la Rubia, M., 2012. Application of natural zeolites in anaerobic digestion processes: a review. Applied Clay Science, 58, pp.125-133.

[96] Sri Shalini, S., Joseph, K., 2013. Start-up of the SHARON and ANAMMOX process in landfill bioreactors using aerobic and anaerobic ammonium oxidising biomass. Bioresource Technology, 149, pp.474-485.

200

[97]   Malamis, S., Katsou, E., Di Fabio, S., Bolzonella, D., Fatone, F., 2014.
Biological nutrients removal from the supernatant originating from the
anaerobic digestion of the organic fraction of municipal solid waste. Critical
Reviews in Biotechnology, 34(3), pp.244-257.

[98]   Rawat, I., Ranjith Kumar, R., Mutanda, T., Bux, F., 2013. Biodiesel from
microalgae: a critical evaluation from laboratory to large scale production.
Applied Energy, 103, pp.444-467.

[99]   Park, J.B.K., Craggs, R.J., Shilton, A.N., 2011. Wastewater treatment high rate
algal ponds for biofuel production. Bioresource Technology, 102, pp.35-32.

[100]   Harun, R., Singh, M., Forde, G.M., Danquah, M.K., 2010. Bioprocess
engineering of microalgae to produce a variety of consumer products.
Renewable and Sustainable Energy Reviews, 14(3), pp.1037-1047.

[101]   Pfromm, P.H., Amanor-Boadu, V., Nelson, R., 2011. Sustainability of algae
derived biodiesel: a mass balance approach. Bioresource Technology, 102(2),
pp.1185-1193.

[102]   Handler, R.M., Canter, C.E., Kalnes, T.N., Lupton, F.S., Kholiqov, O.,
Shonnard, D.R., Blowers, P., 2012. Evaluation of environmental impacts from
microalgae cultivation in open-air raceway ponds: analysis of the prior
literature and investigation of wide variance in predicted impacts. Algal
Research, 1, pp.83-92.

[103]   Xu, L., Wim Brilman, D.W.F., Withag, J.A.M., Brem, G., Kersten, S., 2011.
Assessment of a dry and a wet route for the production of biofuels from
microalgae: energy balance analysis. Bioresource Technology, 102(8),
pp.5113-5122.

[104]   NAABB, 2013. National Alliance for Advanced Biofuels and Bio-products
Report.

[105]   Kraemer, J.T., Bagley, D.M., 2005. Continuous fermentative hydrogen
production using a two-phase reactor system with recycle. Environmental
Science & Technology, 39(10), pp.3819-3825.

[106]   Chu, C.-F., Li, Y.-Y., Xu, K.-Q., Ebie, Y., Inamori, Y., Kong, H.-N., 2008. A
pH- and temperature-phased two-stage process for hydrogen and methane
production from food waste. International Journal of Hydrogen Energy, 33(18),
pp.4739-4746.

Chapter 9

Lactic acid recovery from a simplified mimic of *Thermotoga neapolitana* fermentation broth using ion exchange resins in batch and fixed-bed reactors

Lactic acid recovery from a simplified mimic of *Thermotoga neapolitana* fermentation broth using ion exchange resins in batch and fixed-bed reactors

This study focused on the integration of the lactic acid adsorption and desorption onto commercially available resins in batch reactors with consequent scale-up in fixed-bed reactors. Four anionic resins (Amberlite® IRA-900, IRA-400, IRA-96 and IRA-67) were used as adsorbents for lactic acid recovery from solutions that mimic the fermentation broth of *Thermotoga neapolitana*. The effects of the initial pH, resin pre-treatment, temperature and initial lactic acid concentration on the adsorption capacity of resins were investigated in batch experiments. The best weak (IRA-67) and strong (IRA-400) anionic resins were further tested in batch experiments to assess the adsorption kinetics and to develop a complete adsorption-desorption system over 13 cycles. Amberlite® IRA-67 was selective for lactic acid (removal efficiency > 91%) with a good desorption efficiency (49%). Therefore, it was chosen for a scale-up test in fixed-bed reactor experiments in order to evaluate the effect of variation of the influent flow rate on the adsorption phase and its stability over 6 sequential adsorption-desorption cycles. The use of 0.5 M NaOH as a regenerating solution during the desorption step achieved high lactic acid concentrations (25.4 g L^{-1}) with a low amount of eluent employed (3 bed volumes).

9.1. Introduction

Increasing fossil fuel prices along with a major attention on environmental issues and sustainable development based on renewable resources push the transition from a traditional petrochemical-based to a biotechnological-based production of valuable chemicals such as lactic acid [1, 2]. Lactic acid (2-hydroxypropionic acid) is a common carboxylic acid that can occur in two separated stereoisomers, i.e. L (+) and D (-), or in a racemic mixture. Although this compound is conventionally produced by chemical synthesis, about 90% of the annual worldwide lactic acid production directly derives from fermentation of carbohydrates, such as glucose, sucrose, lactose and starch [3, 4]. In order to reduce the overall cost of biotechnological lactic acid production, it is important to optimize the fermentation phase in terms of feeding conditions, pH, temperature, mixing conditions, nutrient supply, type and initial substrate concentration [5, 6]. Depending on the specific lactic acid-producing microorganisms involved, many hexose or pentose sugars can be utilized for lactic

acid production by fermentation and different food waste materials, e.g. molasses [3], milk whey [7] or date juice [8]. Moreover, starchy and lignocellulosic materials, e.g. starches from potato [9], rice [10], wheat and pineapple [11], *Eucaliptus* wood [12], wheat straw [13] and corncobs [14], were found as proper and cheap starting substrates for lactic acid production.

The L (+) form is preferred by industry due to the presence of L-lactate dehydrogenase inside the human body [15] that enables its application in four main categories: food, cosmetic, pharmaceutical and chemical applications [16]. Recently, the global lactic acid consumption considerably increased due to its relevant application as a monomer in the production of biodegradable polylactic acid (PLA), which is a well-known sustainable bioplastic material [17]. Noticeably, high purity lactic acid for high crystallinity PLA production is required [18].

The recovery and purification of lactic acid from dilute and complex aqueous solutions, such as fermentation broths, is still a challenging operation in terms of efficiency and cost. Indeed, the recovery and purification steps account for about 50% of the overall lactic acid production costs [19]. Nowadays, different downstream processing techniques for lactic acid recovery are available [20, 21], including calcium lactate crystallization, adsorption, ion exchange, reactive extraction, membrane extraction, electro dialysis, esterification and reactive distillation. Among these techniques, adsorption by polymeric anionic resins is promising for lactic acid recovery from biological processes, such as dark fermentation (DF) and capnophilic lactic fermentation (CLF), that yield relatively low (< 5 g L^{-1}) lactic acid concentration in the spent broth [19, 22, 23, 24, 25]. Adsorption can be highly selective for the targeted chemical, by varying the functional groups and support matrices of the resins employed. Moreover, they can be directly used in the fermenter for *in situ* recovery, as the resins are non-toxic to microorganisms [26].

The sorption of lactic acid on polymeric anionic resins can be ascribed to two different phenomena that happen simultaneously: adsorption and ion exchange [4]. Adsorption mainly occurs at pH values lower than the pKa (3.86), where lactic acid is in its non-dissociated molecular form, while ion exchange occurs at higher pH values as lactate is in the charged ionic form. The adsorption capacity and removal efficiency are influenced by various factors such as properties of the anionic resin (e.g. matrix, structure, functional group and porosity), lactic acid (polarity, molecular weight, structure and solute concentration) and operating conditions (contact time, pH,

temperature and mixing conditions) [27, 28]. Therefore, based on the results achieved in another study with solely batch adsorption experiments [29], as a screening step, four anionic exchange resins (Amberlite® IRA-900, IRA-400, IRA-96 and IRA-67) were tested in batch conditions to characterize their behaviour for lactic acid recovery from solutions that mimic the concentrations of *T. neapolitana* fermentation broth. Later, the lactic acid adsorption performance of the best strong (IRA-400) and weak (IRA-96) anionic resin was further tested by changing the contact time, the eluent concentration and the volume in the desorbing step. In fact, the ease of regeneration, the desorption efficiency and a highly concentrated and pure eluent represent additional requirements for the selection of a suitable anionic resin [30, 31, 32]. Therefore, we used low concentration solutions of HCl and NaOH for, respectively, the strong and the weak resins tested. Finally, a continuous fixed-bed reactor (FBR) was operated for lactic acid adsorption at different flow rates, investigating the stability of IRA-96 in several adsorption-desorption cycles.

9.2. Materials and methods

9.2.1. Model *T. neapolitana* fermentation broth

A synthetic *T. neapolitana* fermentation broth was prepared from an analytical grade lactic acid stock solution (88% purity) and demineralized water as described in [29]. Due to the high complexity of the spent fermentation broth [33], this study focused on simpler solutions constituted by lactic acid at concentrations close to those achievable by *T. neapolitana* growth on sugars. The broth was heated near the boiling point to both mimic the culture conditions (80 °C and above) and completely hydrolyse the lactic anhydride present, reaching a final concentration of 4.5 g L^{-1}. All the samples were stored at 4°C and their lactic acid concentration was checked prior to use. Prior to each experiment, pH was adjusted at 6.5 in order to imitate the final pH occurring during CLF due to CO_2 sparging [23, 24, 25].

9.2.2. Resin selection

Four anionic exchange resins were tested for lactic acid recovery from a model *T. neapolitana* fermentation broth: i) Amberlite® IRA-900 (Cl⁻) referred as IRA-900, ii) Amberlite® IRA-400 (Cl⁻) referred as IRA-400, iii) Amberlite® IRA-96 (free base) referred as IRA-96, and iv) Amberlite® IRA-67 (free base) referred as IRA-67. The

main characteristics are reported in Table 1. The analytical grade anionic resins were purchased from Sigma-Aldrich (Milan, Italy).

Table 1. Physico-Chemical properties of the strongly basic (IRA-900 and IRA-400) and weakly basic (IRA-96 and IRA-67) anionic resins.

Resin	Matrix	Functional group (+)	Form	Particle size (diameter)	Moisture content (%)
IRA-900	Styrene-divinylbenzene (macroporous)	Benzyltriethyl-ammonium	Cl⁻	650-820 μm	58-64
IRA-400	Styrene-divinylbenzene (gel)	Quaternary ammonium	Cl⁻	600-750 μm	40-47
IRA-96	Styrene-divinylbenzene (macroporous)	Tertiary amine (at least 85%)	Free base	550-750 μm	57-63
IRA-67	Acrylic (gel)	Polyamine	Free base	500-750 μm	~60

9.2.3. Resin characterization

The surface morphology of the anionic exchange resins was investigated using a JSM-6010LA, Jeol (Tokyo, Japan) scanning electron microscope (SEM). Figure 1 (a-d) shows the initial conditions of the fresh anionic resins. Before the observations, all the samples were sputter-coated with gold with an auto fine coater (JFC-1300, Jeol, Tokyo, Japan). The coater is a complementary equipment to the SEM and provides necessary preparation of non-metallic non-conductive samples for use in SEM.

The specific number of active sites of the tested anionic resins was checked by potentiometric acid-base titration using an automatic titrator (848 Titrino Plus, Metrohm AG, Herisau, Switzerland), as described by Lützenkirchen et al. [34]. This technique is based on the differences between titrations of resin samples and blanks using HCl as the titrant. Solid samples (or blanks) and titrant were preliminary flushed with a low nitrogen flow overnight and for 1 h, respectively. During the potentiometric acid-base titration, 50 μL of HCl was added to the samples through a burette tip, once every five minutes until a pre-set end-point (same pH or same added volume of titrant in blank and sample titrations) was reached. Samples were

continuously mixed using a magnetic stirrer (801 Stirrer, Metrohm AG, Herisau, Switzerland) in the presence of continuously blowing nitrogen gas. In all the phases, nitrogen purging was done to prevent carbon dioxide uptake from ambient air and related reduction-oxidation reactions that can affect pH measurements.
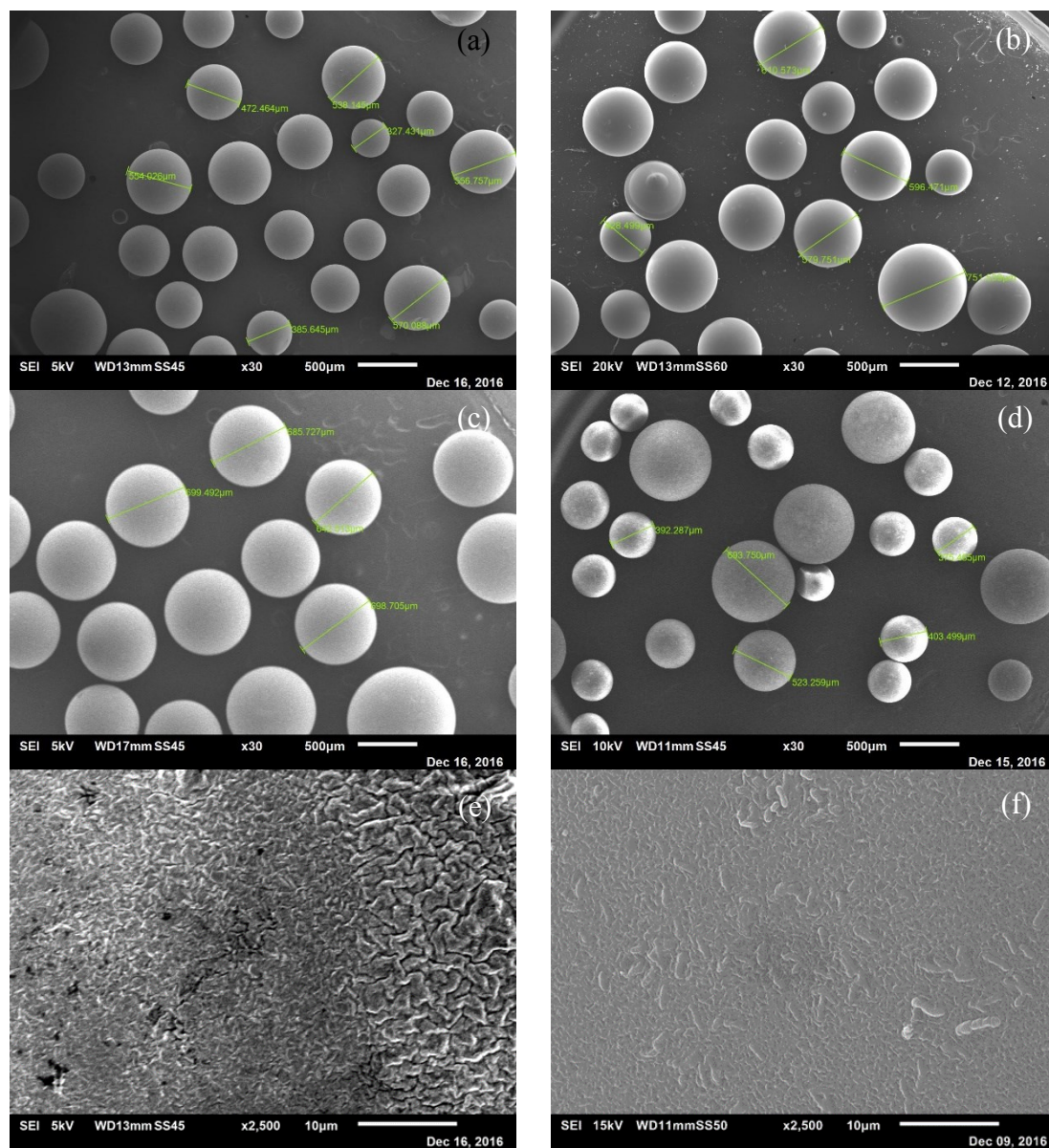
Figure 1. Low magnification SEM images of fresh anionic resins: (a) IRA-900, (b) IRA-400, (c) IRA-96, and (d) IRA-67 and high magnification SEM micrographs of IRA-67 (e) before, and (f) after six adsorption-desorption cycles during column experiments.

9.2.4. Resin pre-treatment

When specified, a resin preparation procedure was adopted to enhance the performance of the resin investigated. The strong anionic resins (IRA-900 and IRA-400) were pre-treated with a specific sequential washing procedure as outlined by

Moldes et al. [4]: (i) 1 N HCl solution, (ii) demineralized water, (iii) 1 N NaOH solution, (iv) demineralized water, (v) 1 N HCl solution and thereafter with (vi) demineralized water until pH 7.0 was reached. According to the same study [4], weak anionic resins (IRA-96 and IRA-67) were pre-treated with the following washing steps: (i) 1 NaOH solution, (ii) demineralized water, (iii) 1 N HCl solution, (iv) demineralized water, (v) 1 N NaOH solution, and then with (vi) demineralized water until pH 7.0 was reached.

9.2.5. Batch experiments

The preliminary batch studies for lactic acid recovery included different experiments investigating the effect of several process parameters: (i) initial pH and pre-treatment of the anionic resins, (ii) initial lactic acid concentration and working temperature, (iii) kinetic behaviour and contact time, and (iv) combined adsorption-desorption cycles. All the batch experiments were conducted in a temperature-controlled environment, either on an orbital shaker (INNOVA 2100, New Brunswick Scientific, New Jersey, USA) or in a shaking thermostatic water bath (GFL1083, Burgwedel, Germany) at a speed of 180 rpm for up to 4 h as recommended in Dethe et al. [35]. Serum bottles (30 mL) with screw cap containing 0.5 g of anionic resin (10% *w/v*) and 5.0 mL of bulk solution were used for all the batch adsorption studies, unless stated otherwise. All the batch adsorption experiments were performed in duplicate by employing sacrificial serum bottles for each data point.

The initial pH (2.0-6.5) of the samples mimicking *T. neapolitana* fermentation broth was adjusted by either adding 3.0 M NaOH or 1 M HCl. The behaviour of the resins was compared using fresh (untreated) or pre-treated resins as described in 2.4. The effect of temperature (30°C and 80°C) and initial lactic acid concentration (1.4, 2.3, 4.5, 9.0, 13.5 and 18.0 g L^{-1}) were investigated on the pre-treated strong and weak anionic resins. The adsorption performances for these experiments were analysed at a fixed pH: 5.0 for IRA-400 and 900 and 2.0 for IRA-67 and 96.

Kinetic batch experiments were carried out at the most effective conditions, i.e. 30°C and an initial pH of 5.0 and 2.0 for, respectively, the weak and strong resin. Samples were withdrawn at regular time intervals (10, 20, 40, 60 min and 24 h) for lactic acid measurements.

Combined adsorption-desorption batch studies were performed at 30°C using 2 g of fresh anionic resins IRA-400 or IRA-67 (40% *w/v*) contacted with 5 mL fermentation

broth. The model *T. neapolitana* fermentation broth with an initial lactic acid concentration of 4.5 g L^{-1} was periodically added at the start of each 10 min cycle. The initial pH was adjusted to 5.0 (for IRA-400) or 2.0 (for IRA-67) and each cycle was made up of the following sequential stages: (i) pre-washing with demineralized water, (ii) adsorption, (iii) desorption (HCl and NaOH for, respectively, the strong and the weak resin), (iv) washing with demineralized water, and (v) final adjustment until pH 7.0 was reached. For the first 5 cycles, the desorption phase was performed using 2 mL of 1 M NaOH or 1 M HCl solutions, while the concentration and volume of the eluents were reduced to 0.5 M and 1 mL, respectively, for the remaining cycles. According to the batch kinetic studies, each of the 13 adsorption and desorption cycles was carried out with a contact time of 10 min.

9.2.6. Fed-batch experiments

The fed-batch experiments were carried out in a temperature-controlled (30°C) environment on an orbital shaker at 180 rpm as described in the previous section. Serum bottles (30 mL) with screw caps were filled with 0.5 g of fresh anionic resins IRA-400 and IRA-67 (10% *w/v*), and made in contact with 5 mL of model solutions having an initial lactic acid concentration of 4.5 g L^{-1}. The initial pH was adjusted to 5.0 (for IRA-400) or 2.0 (for IRA-67) by adding 3.0 M NaOH and 1 M HCl, respectively.

The constant working volume of the fed-batch system was maintained by withdrawing a certain volume of sample compensated by feeding the same volume of fresh model broth. In particular, the exhausted fermentation broth (4 mL) were withdrawn every hour with the subsequent addition of fresh fermentation broth (4 mL). This procedure was repeated for 6 h. These experiments were designed to get preliminary information on the adsorption of lactic acid using anionic resins in a fixed-bed reactor (FBR).

9.2.7. Column experiments in continuous FBR

A glass column (i.d. 2.6 cm, o.d. 2.9 cm, length 17.9 cm) was loaded with 10 g fresh resin IRA-67 (bed height 3.5 cm, bed volume BV 18.6 cm^3). A glass wool layer, previously washed with demineralized water, was placed between the bottom of the column and the resin. The acidified samples mimicking *T. neapolitana* fermentation broth (pH 2.0) as well as demineralized water were pumped continuously to the FBR

in down flow mode (avoiding bed fluidization) using a peristaltic pump (7528-30 Masterflex, Cole-Parmer, Vernon Hills, Illinois, USA) fitted with silicone tubing ($3x5$ mm). An additional peristaltic pump (7528-30 Masterflex, Cole-Parmer, Vernon Hills, Illinois, USA) was used to control the outlet flow rate.

An initial set of column experiments was carried out to investigate the effect of the flow rate variation on the adsorption of lactic acid. In this phase, the critical loading rate (LA_{clr}), which represents the volumetric loading rate at which the lactic acid removal efficiency decreases, was experimentally evaluated.

The effect of flow rate variation was explored during the second set of experiments, in which 5 adsorption-desorption cycles with 5 different flow rates (2.5, 3.5, 5.0, 8.0, and 10.0 mL min^{-1}) were tested. Finally, several column experiments were carried out with 6 adsorption-desorption cycles by applying an adsorption phase of 5 h, at a flow rate of 3.5 mL min^{-1}, to further check the stability of the IRA-67 resin for lactic acid recovery from the fermentation broth.

9.2.8. Analytical methods

Lactic acid concentrations were determined in duplicate by ionic chromatography (IC) analysis using an ICS-1100 (Dionex, Thermo Fisher Scientific Inc., USA) as described by Pradan et al. [29]. The mobile phase was 1.7 mM NaHCO$_3$ and 1.8 mM Na$_2$CO$_3$ with a flow rate of 0.5 mL min^{-1}. Prior to analysis, the pH of all the samples was adjusted in the range of 5.0 to 8.0 by using 0.1 M NaOH or 0.05 M HCl. The pH was measured by a Prazisions pH-meter E510 (Metrohm AG, Herisau, Switzerland) provided with a multi-parameter probe and calibrated with commercial buffers.

9.3. Results

9.3.1 Batch tests for lactic acid adsorption

Depending on the initial pH used, the lactic acid removal efficiency for the two strong anionic resins tested (IRA-900 and IRA 400) showed a similar trend (Figure 2). Both resins were effective at a pH above the pKa (3.86) of lactic acid. At pH 5.0 (Figure 2c), the highest lactic acid removal efficiency was 43.6% (w/p - with pre-treatment or pre-treated) and 46.8% (n/p – not pre-treated or fresh) for IRA-900 and 49.2% (pre-treated) and 50.0% (fresh) for IRA-400, respectively. The lactic acid removal efficiency did not change significantly for pH > 5.0 and the effect of the pre-treatment

was negligible for both strong anionic resins (Figure 2). On the other hand, the weak anionic resins (IRA-96 and IRA-67) showed high selectivity at a pH below the lactic acid pKa, reaching the highest removal efficiency for the pre-treated resins (99.2% for IRA-96 and 99.3% for IRA-67) at pH 2.0 (Figure 2a).
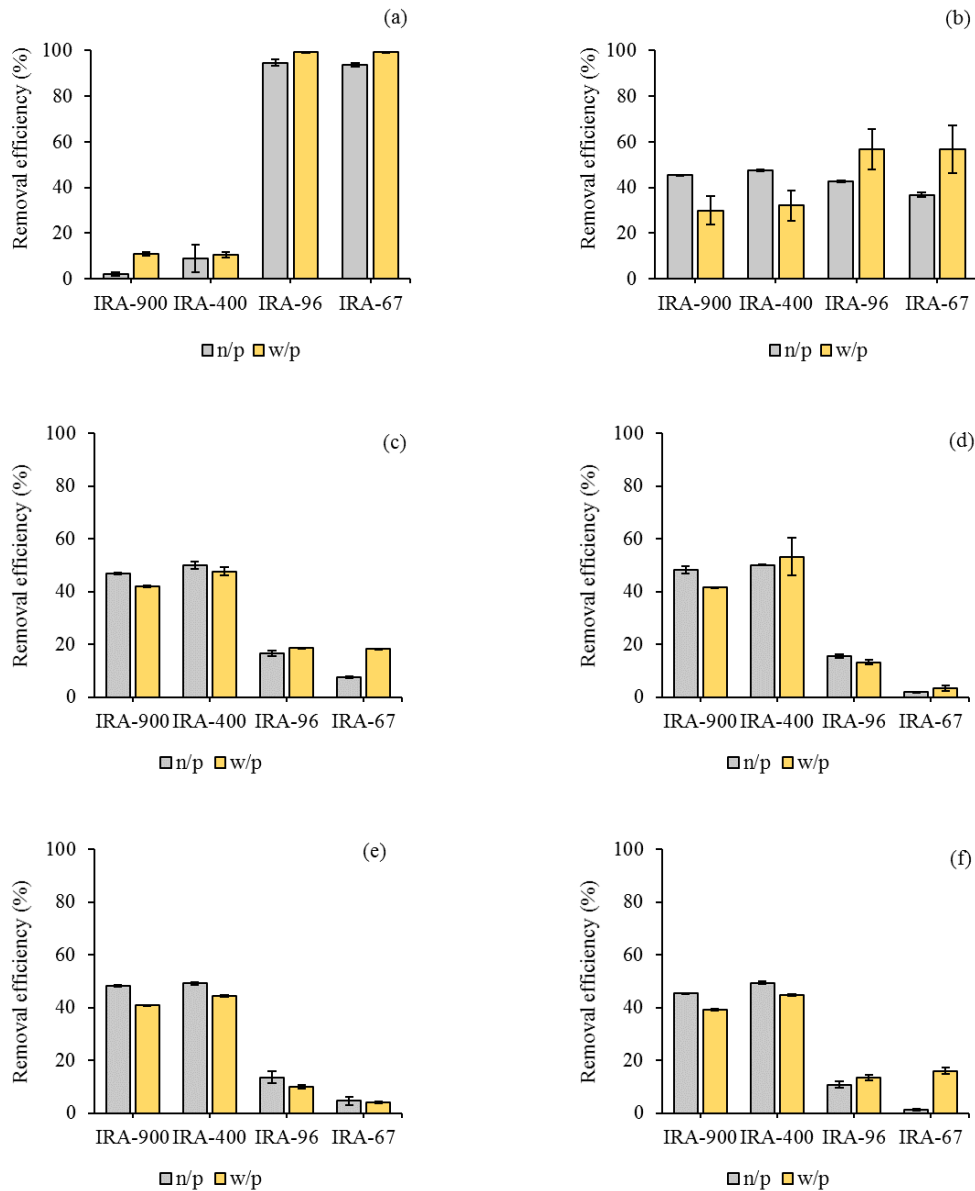
Figure 2. Effect of pH: (a) 2.0, (b) 3.86, (c) 5.0, (d) 5.5, (e) 6.0, and (f) 6.5 on the lactic acid removal efficiency for four anionic resins (IRA-900, IRA-400, IRA-96 and IRA-67). n/p = not pre-treated, w/p = with pre-treatment.

From Figure 3 it is evident that the lactic acid removal efficiency sharply decreased from 67.7% to 27.2% when increasing the initial lactic acid concentration from 1.4 g L^{-1} to 18.0 g L^{-1} for IRA-900 at 30°C. Besides, IRA-400 showed a significant decrease (from 71.1% to 31.6%) in the lactic acid removal efficiency at the same

temperature. Conversely, the weak anionic resins showed minimal changes in the removal efficiencies irrespective of the initial lactic acid concentrations. Specifically, IRA-67 exhibited lactic acid removal efficiencies exceeding 99% for a wide range of initial lactic acid concentrations (Figure 3). The lactic acid recovery efficiency decreased in all experiments carried out at 80°C, except for IRA-67, which maintained a lactic acid removal efficiency > 90% for an initial lactate concentration ranging from 1.4 to 13.5 g L^{-1}.
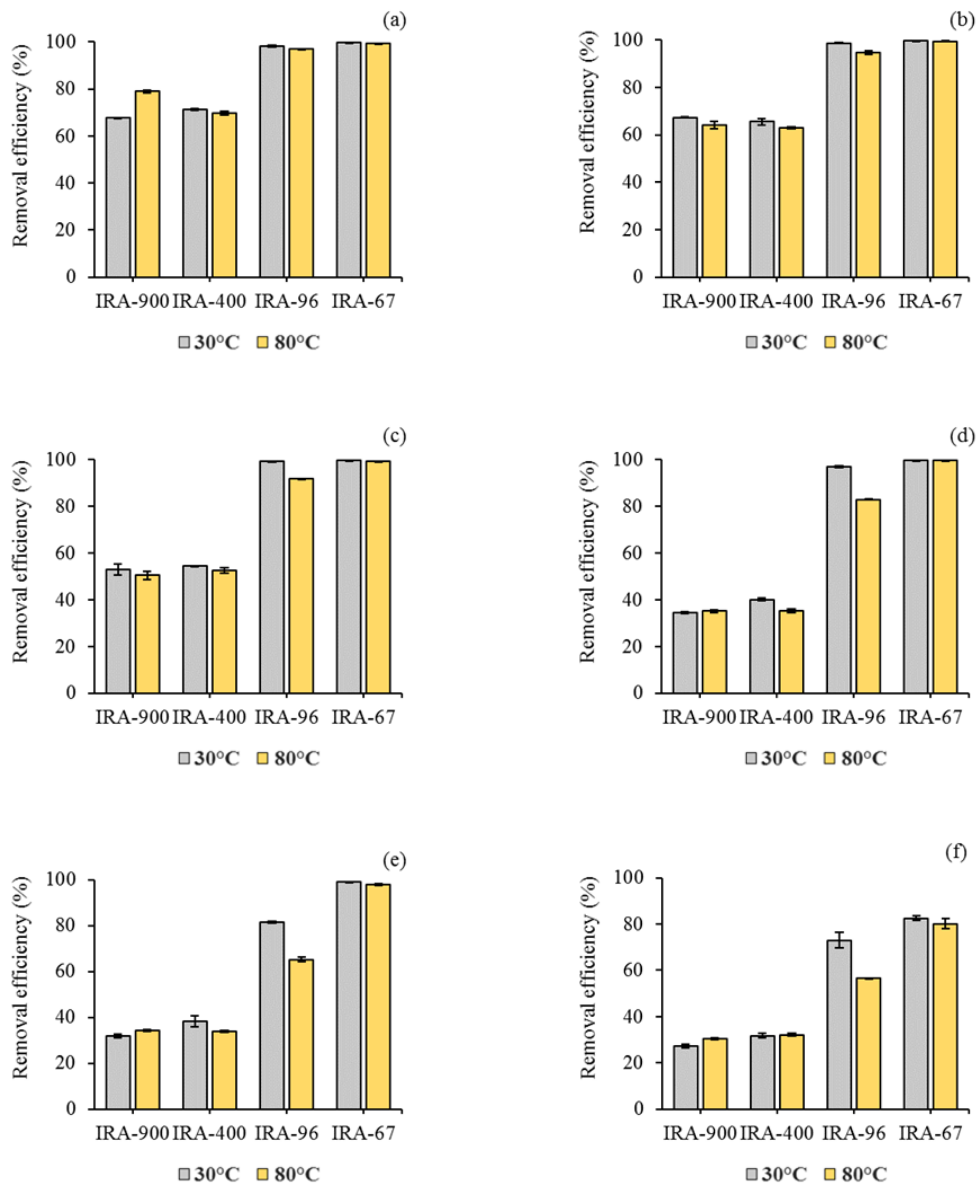
Figure 3. Effect of temperature and different initial lactic acid concentration: (a) 1.4 g L^{-1}, (b) 2.3 g L^{-1}, (c) 4.5 g L^{-1}, (d) 9.0 g L^{-1}, (e) 13.5 g L^{-1}, and (f) 18.0 g L^{-1} on lactic acid removal efficiency for four pre-treated anionic resins (IRA-900 and IRA-400 at pH 5.0 and IRA-96 and IRA-67 at pH 2.0).

To evaluate the effect of contact time on the lactic acid removal efficiency, the most effective pre-treated weak (IRA-67) and strong (IRA-400) anionic resins were further tested at 30°C and at pH 5.0 and 2.0, respectively, in order to ascertain the adsorption behaviour as a function of time with different initial lactic acid concentrations. The results showed that the residual lactic acid concentration significantly decreased after 10 min and reached a constant value after 20 min of operation irrespective of the initial lactic acid concentration (Figure 4).
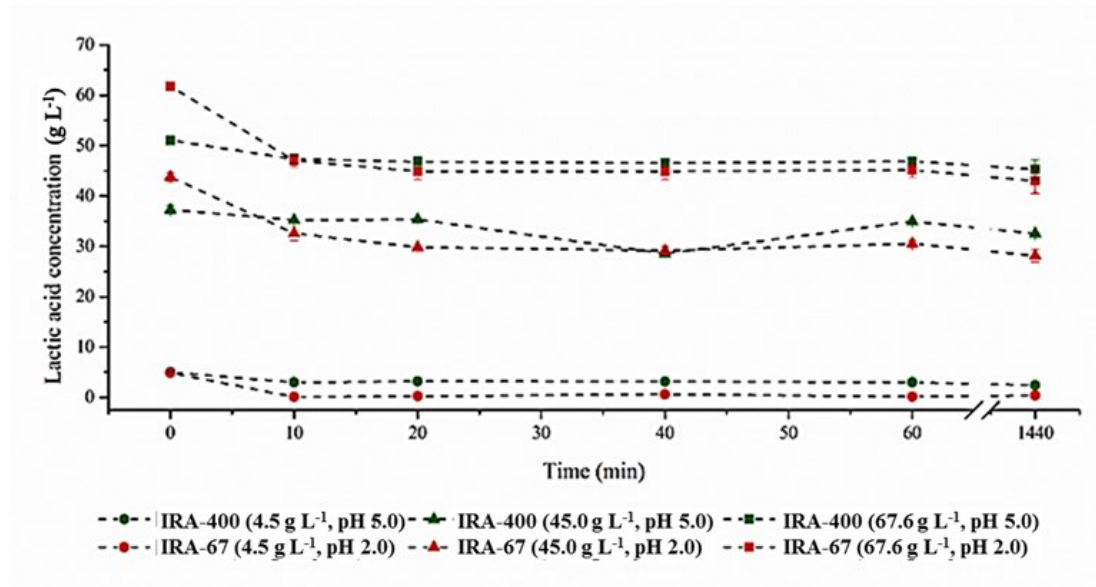
Figure 4. Effect of contact time on residual lactic acid concentration in batch adsorption experiments (0-24 h) using the pre-treated anionic resins IRA-400 (pH 5.0) and IRA-67 (pH 2.0) with three different initial lactic acid concentration (4.5, 45, 67.6 g L^{-1}), at 30 °C.

9.3.2. Adsorption-desorption experiments

The stability of the fresh anionic resins IRA-400 and IRA-67 (40% *w/v*) for lactic acid recovery was assessed over 13 adsorption-desorption cycles using the optimal adsorption contact time achieved in the previous batch experiments. The lactic acid removal efficiency for IRA-67 was > 99% until the ninth cycle and thereafter it steadily decreased to 93% during the last cycle (Figure 5a). In the case of IRA-400 resin, the lactate removal performance slightly decreased steadily during the cycles, with the lactic acid removal efficiency decreasing from 80% to 69% (Figure 5a).
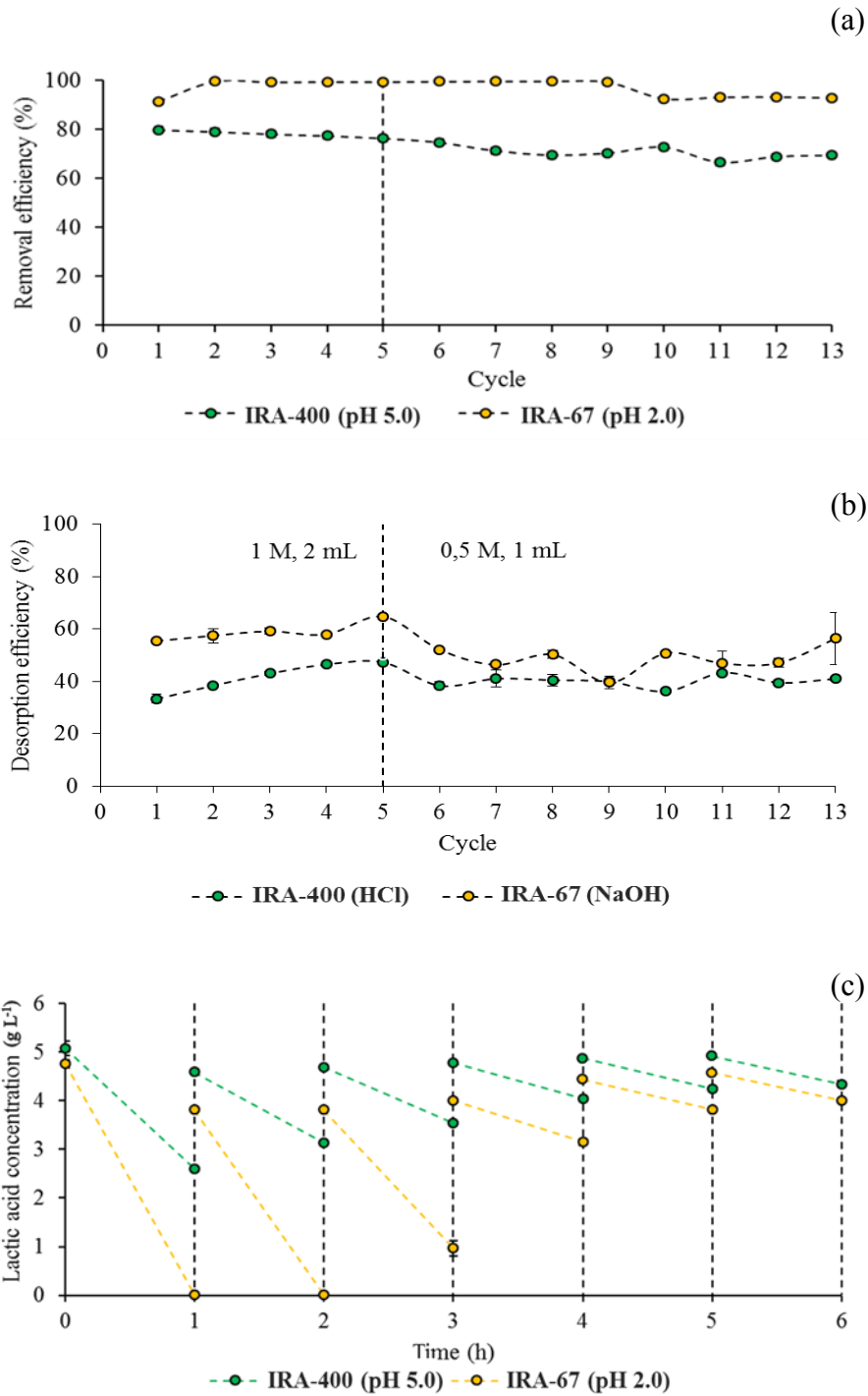
Figure 5. Lactic acid removal (a), and desorption efficiency (b) at varying eluents conditions over thirteen adsorption-desorption cycles for un-treated IRA-400 (pH 5.0) and IRA-67 (pH 2.0) at 30 °C. Time course of lactic acid concentration in fed-batch experiments (0-6 h) for IRA-400 and IRA-67 at 30 °C (c).

Compared to IRA-67, IRA-400 attained a lower desorption efficiency, ranging from 33% to 47% using 2 mL 1 M HCl and from 38% to 41% using 1 mL 0.5 M NaOH as the regenerant. On the other hand, the desorption efficiency of IRA-67 varied between

55 and 65% using 2 mL 1 M NaOH and 52 and 65% using 1 mL 0.5 M NaOH, respectively (Figure 5b). During the desorption step, a lower concentration of the regenerating solutions was used in order to employ a lower amount of chemical without decreasing the lactic acid concentration in the eluate. Despite incomplete regeneration and desorption of lactic acid within the different cycles, IRA-400 and IRA-67 showed stable removal efficiencies. Apparently, resin saturation was not reached during the adsorption phase, allowing additional sorption of lactic acid at the still available active sites.

9.3.3. Fed batch experiments

The results from fed batch experiments highlighted decreasing trends for the lactic acid removal efficiency with time for both resins tested (Figure 5c). IRA-67 showed a lactic acid removal efficiency > 99.8% within the first 2 h of operation. The removal efficiency decreased to 75% at the third hour and successively achieved the final value of 12.5% after 6 h. Differently, the removal efficiency for IRA-400 sharply decreased to 50% after 1 h of operation, gradually reaching a constant value of 12.5% after 6 h (Figure 5c).

9.3.4. Continuous FBR operation

Throughout the first experimental set, the lactic acid removal efficiency was > 85% during the first 2 h of operation of the FBR at a flow rate ranging between 2.5 and 3.5 mL min^{-1} (Figure 6a). Later, it sharply decreased reaching a constant value of 20% at the end of the experiment, at a flow rate of 10 mL min^{-1}. In this phase, the critical lading rate (LA$_{clr}$) was evaluated for the FBR by plotting the lactic acid volumetric loading rate (LA$_{vlr}$) on the x axis and lactic acid volumetric removal rate (LA$_{vrr}$) on the y axis. The FBR was found to have a critical loading rate of 63.1 g L^{-1} h^{-1} after 2 h of operation (Figure 6b). The desorption phase was carried out using 3 BV of 0.5 M NaOH. The lactic acid desorption efficiency was found to be 45.2%, while the lactic acid concentration in the eluent was > 26.5 g L^{-1} for each BV, reaching a value of 36.5 (±1.5) g L^{-1} with the third BV (Figure 6c).
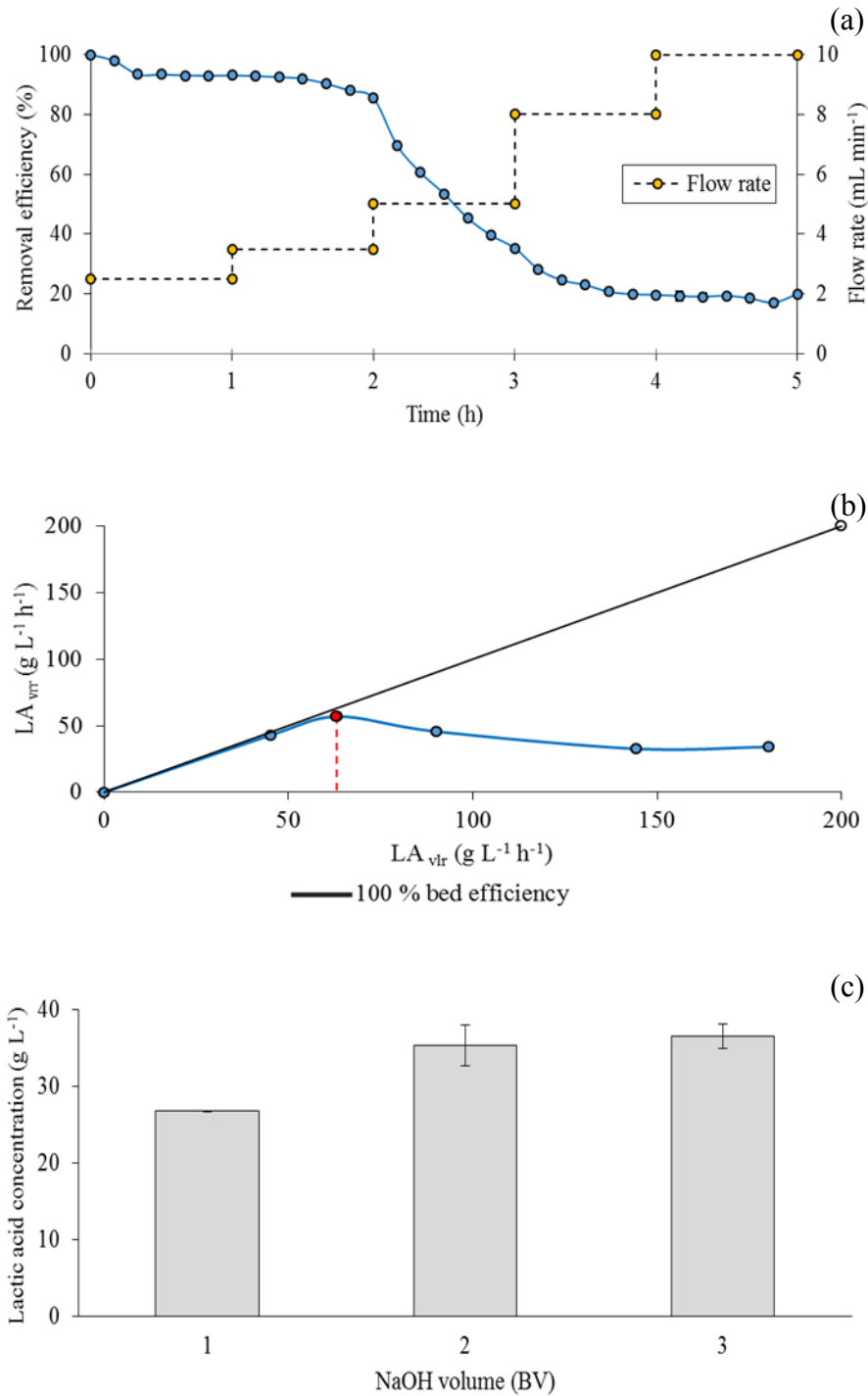
Figure 6. Column experiments with step increase in flow rate once every hour (2.5,
3.5, 5.0, 8.0, 10.0 mL min^{-1}) (a), graphical determination of the critical
lactic acid loading rate (b), and desorbed lactic acid during the regeneration
phase with 3 BV of 0.5 M NaOH, at 25 °C and an initial lactic acid
concentration of 4.5 g L^{-1} (c).

After identifying the critical loading rate (LA$_{clr}$), the results from the second
experimental set showed that IRA-67 maintained the lactic acid removal efficiency >
90% for 2 h at the lowest flow rate tested (1st cycle at 2.5 mL min^{-1}) and lost its

performance as the operation time and flow rate increased. After 5 h, the lactic acid removal efficiencies reached a constant value ranging between 10 and 15% for all flow rates tested, with the exception of the highest one. Breakthrough occurred in less than 30 min, except for the highest flow rate where it occurred between 30 and 60 min (Figure 7a). The bed was completely saturated during the last test after an operation time of 2 h (Figure 8). Afterwards, the experimental breakthrough curves showed decreasing pH of the effluent towards the influent value as the effluent lactic acid concentration steadily increased to values similar to the influent concentration (Figure 8).

(a)

(b)
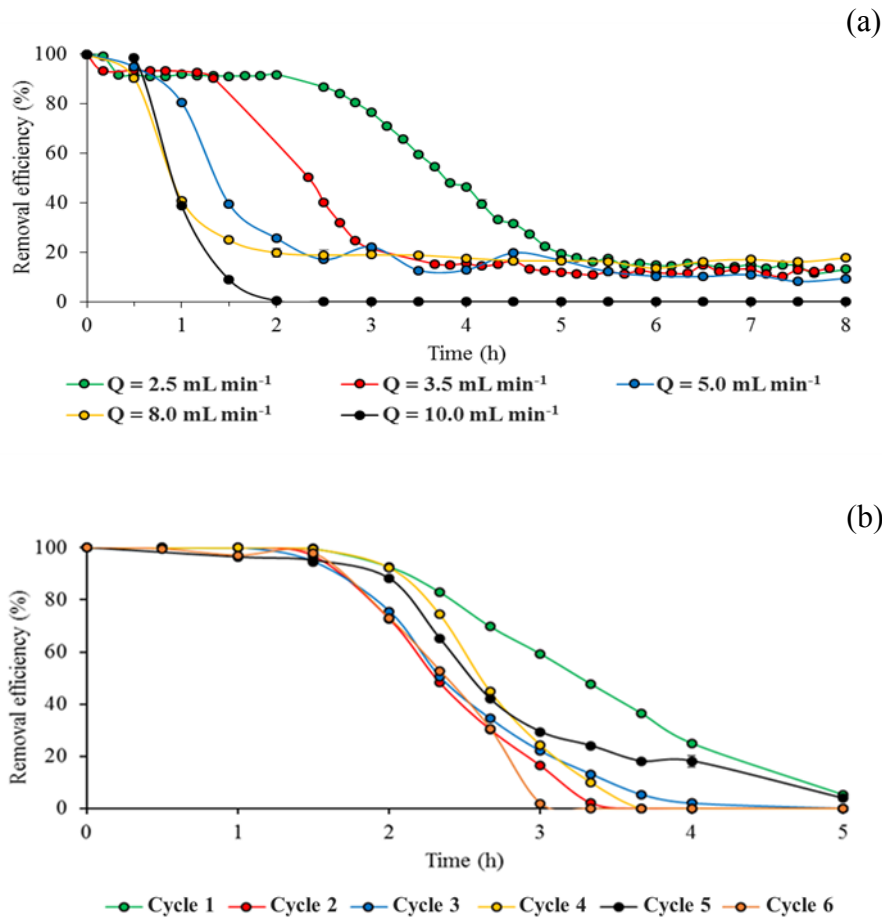
Figure 7. Column experiments (0-8 h) with different flow rates (2.5, 3.5, 5.0, 8.0, 10.0 mL min^{-1}) (a) and column experiments (0-5 h) with adsorption-desorption cycles at a constant flow rate of 3.5 mL min^{-1} (b), at 25 °C and an initial lactic acid concentration of 4.5 g L^{-1}.
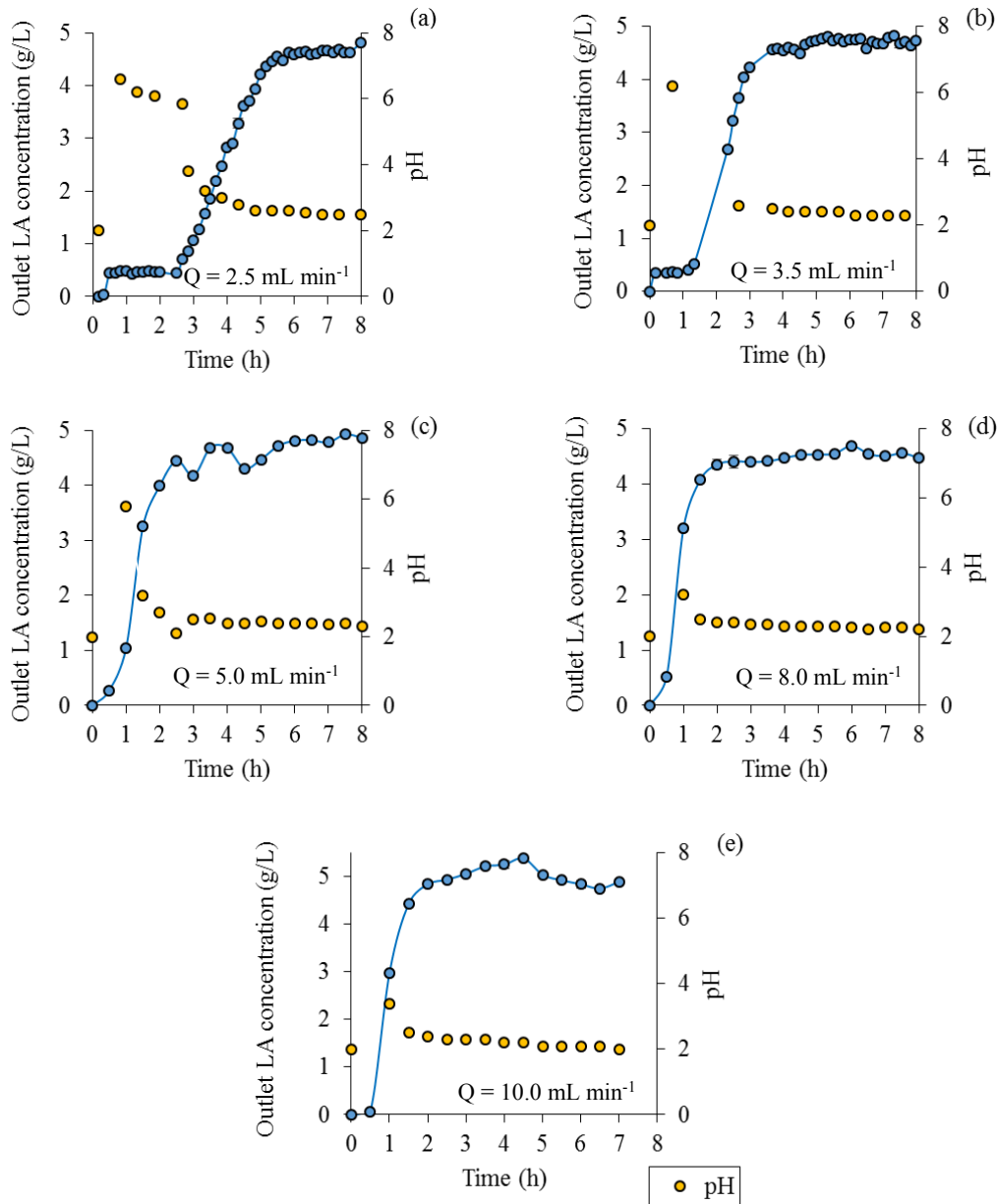
Figure 8. Experimental breakthrough curves and pH trend during five adsorption-desorption cycles in column experiments (a) 2.5 mL min^{-1}, (b) 3.5 mL min^{-1}, (c) 5.0 mL min^{-1}, (d) 8.0 mL min^{-1} and (e) 10 mL min^{-1} (0-8 h), at 25 °C and initial lactic acid concentration of 4.5 g L^{-1}.

The mass balance on lactic acid during the adsorption phase together with other parameters (i.e. removal efficiency and adsorption capacity) are reported in Table 2. The adsorption capacity was similar for the first 3 cycles (2.5, 3.5 and 5 mL min^{-1}), with an unexpected increase after 3 h for the fourth cycle at 8 mL min^{-1}. The uptake of lactic acid reached the minimum value in the last cycle, which was mainly affected by an incomplete desorption during the fourth cycle. The decrease in the amount of lactic acid desorbed until the fourth cycle may be explained by a negative effect of extended desorption and its consequent decrease in the regeneration efficiency of the active

217

sites. As shown in Figures 1e and 1f, the external adsorbate layer was easily removed while the internal adsorbate layer was not cleaned after several adsorption-desorption cycles during column experiments.

Table 2. Lactic acid desorption from IRA-67 during five adsorption-desorption cycles in column experiments using 0.5 M NaOH as eluent (3 BV) at 25 °C.

Cycle	Flow rate (mL min^{-1})	Cumulative lactic acid desorbed (g)	Desorption efficiency (%)	Lactic acid concentration (g L^{-1})
1	2.5	1.80 (± 0.1)	54.4 (± 0.4)	32.3 (± 0.9)
2	3.5	1.65 (± 0.1)	51.2 (± 1.2)	29.6 (± 0.9)
3	5.0	1.67 (± 0.1)	46.3 (± 0.8)	30.0 (± 0.6)
4	8.0	1.19 (± 0.1)	21.7 (± 0.2)	21.3 (± 1.0)
5	10.0	1.46 (± 0.1)	51.1 (± 0.6)	26.2 (± 0.6)

The stability of IRA-67 in recovering lactic acid from a model *T. neapolitana* fermentation broth was finally demonstrated over 6 adsorption-desorption cycles by fixing the inlet flow rate at 3.5 mL min^{-1}. The removal efficiency decreased from 66.3% to 47.2% between the first 2 cycles (Figure 7b), whereas it slightly increased to 56.0% for the fifth cycle and then it reached the lowest value in the last cycle (46.1%). The outlet lactic acid concentration gradually increased up to the feeding value and the pH of the outlet samples decreased until 2.0. Moreover, as the process continued, the breakthrough time decreased from 120 min (first cycle) to 90 min (second and fifth cycle) reaching the minimum of 60 min during the last cycle (Figure 9). The resin IRA-67 was not saturated during the first cycle and showed fluctuations with operating time to reach saturation (more than 210 min) for the remaining cycles. The desorption efficiency sharply increased from 64.7% up to 89.2% during the first 2 cycles and thereafter it decreased to 56.5% during the last cycle. The use of 0.5 M NaOH (3 BV) allowed to achieve a lactic acid concentration in the eluate exceeding 24.5 g L^{-1}, except for the last cycle (19.3 g L^{-1}). The results of the 6 cycles are resumed in Table 3.
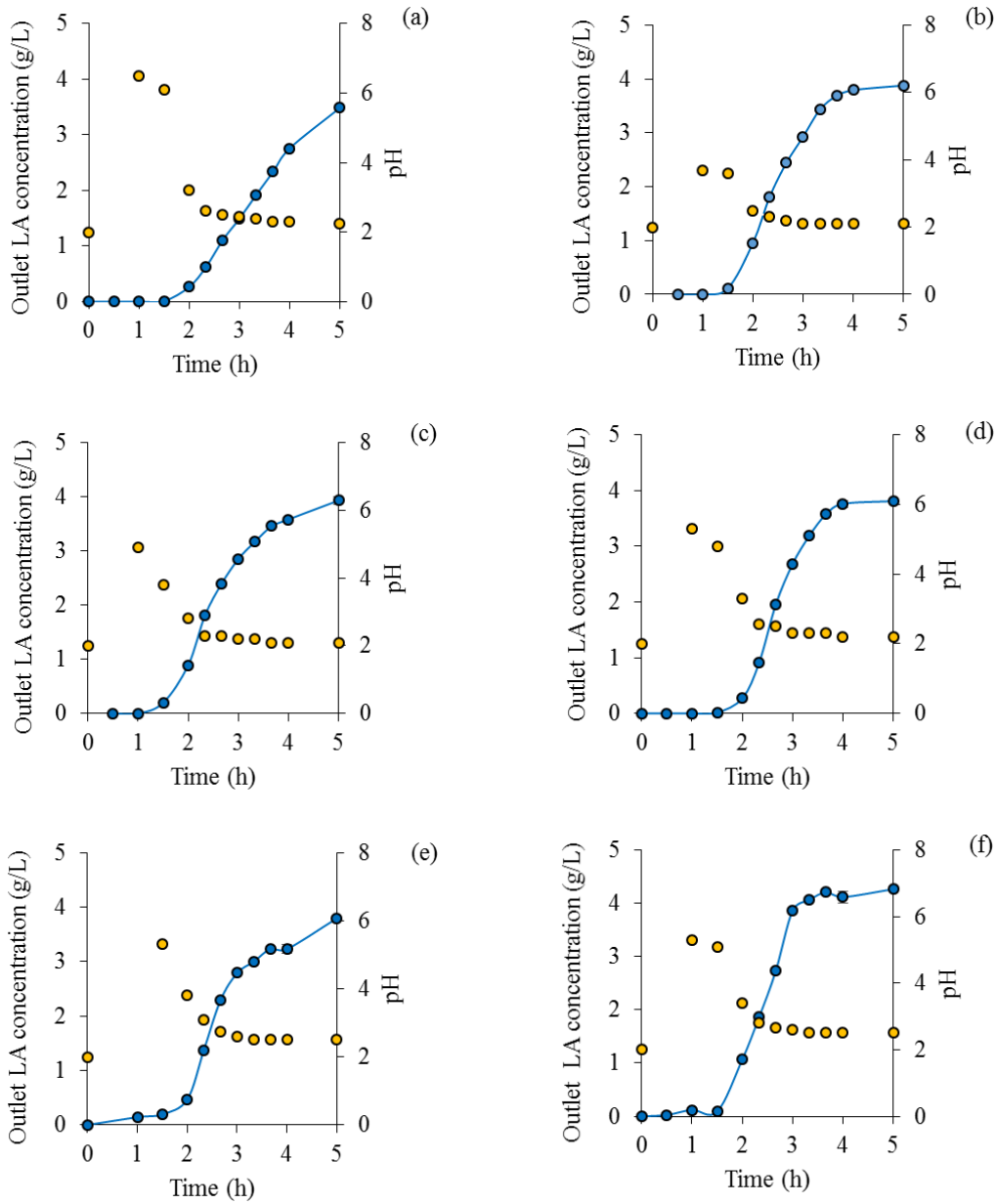
Figure 9. Experimental breakthrough curves and pH trend during six adsorption-
desorption cycles (a-f) in column experiments at a flow rate of 3.5 mL
min^{-1}, at 25 °C and an initial lactic acid concentration of 4.5 g L^{-1}.

Table 3. Lactic acid desorption from IRA-67 during six adsorption-desorption cycles
in column experiments using 0.5 M NaOH as eluent (3 BV) at 25 °C.

Cycle	Cumulative lactic acid desorbed (g)	Desorption efficiency (%)	Lactic acid concentration (g L^{-1})
1	1.7 (± 0.1)	64.7 (± 0.3)	29.7 (± 0.4)
2	1.5 (± 0.1)	89.2 (± 0.4)	27.8 (± 0.4)
3	1.4 (± 0.1)	73.0 (± 1.2)	24.8 (± 0.4)
4	1.4 (± 0.1)	73.6 (± 0.9)	26.0 (± 0.3)
5	1.4 (± 0.1)	59.1 (± 0.7)	24.6 (± 0.3)
6	1.1 (± 0.1)	56.5 (± 2.2)	19.3 (± 0.8)

9.4. Discussion

This study showed that anionic resins can be successfully applied to lactic acid recovery from dark and capnophilic fermentation broths by using the FBR technology. In particular, the weak resin showed better performances during column experiments than in batch and semi-batch configurations in terms of lactic acid recovery. Several purification techniques for lactic acid recovery from fermentation broths for both *in situ* and downstream extraction have been reported in literature [36]. In the case of downstream extraction, the main issue relies on the production of other compounds, such as gypsum, which are produced during the additional washing step prior to obtain pure lactic acid. For *in situ* extraction, it is important to avoid any toxicity effects on fermentative microorganisms that can negatively affect the fermentation process and increase the cost of lactic acid production. The use of ion exchange resins is a cheap and green solution compared to other more complex treatments, i.e. direct distillation, reverse osmosis, conventional electrodialysis or bipolar membrane electrodialysis, and it is well suited to recover lactic acid from low concentration fermentation broths, as in capnophilic fermentation.

9.4.1. Batch experiment to assess in situ and down stream applications

The first set of batch experiments highlighted the higher uptake of lactic acid by the tertiary amine based resins, i.e. IRA-96, than by the strong base resins with quaternary functional groups. Indeed, IRA-96 and IRA-67 showed most of their adsorption capacity up to the lactic acid pKa, revealing a low efficiency up to neutral pH due to the accessibility for the molecular form of lactic acid to the polyamine or tertiary amine functional groups [37, 38]. In comparison, the strong resins IRA-900 and IRA-400 showed a high selectivity at a pH above the lactic acid pKa. This might be due to the presence of quaternary ammonium as functional group in the resin, which mainly interacts with lactate through electrostatic forces (relatively poor attractive interaction) [38]. According to previous studies investigating the adsorption of lactic acid from highly concentrated lactic acid content fermentation broths [39], the weak anionic resins were highly effective for lactic acid recovery at a pH below the pKa of lactic acid, while the strong anionic resins reached their highest removal efficiency at higher pH values.

This study showed that the weak anionic resins IRA-96 and IRA-67 cannot be employed for *in situ* lactic acid recovery as they operate properly at a pH lower than

the optimal pH (5.0-7.0) for lactic acid fermentation [3]. Indeed, there are some applications of weak resins, i.e. IRA-67, for in situ extraction of lactic acid from dark fermentation broths [28], but the uncontrolled pH during the biological process usually leads to high acids accumulation rather than H_2 production [40]. Recently, an interesting result has been obtained by Pradhan et al. [29] comparing the strong anionic resins IRA-400 and granular activated carbon for lactic acid recovery. The better performance of the strong anionic resin than the granular activated carbon was also verified by other studies [41]. The possibility to use IRA-400 for *in situ* lactic acid recovery from high strength lactic acid (> 50 g L^{-1}) fermentation broths was shown by Quintero et al. [42]. Therefore, strong anionic resins, i.e. IRA-400, are effective at pH 5.0 and are often recommended for *in situ* extraction of lactic acid from a fermenter [42].

The adsorption of lactic acid by the four resins tested was differently affected by the temperature (Figure 3). The adsorption by ion exchange resins is an exothermic process with negative heat of adsorption [29, 43] and high operational temperatures can cause irreversible changes in the physio-chemical properties of the resins due to the disrupture of the chemical bonds between the functional groups and the polymeric matrix [44]. Gao et al. [45] indicated that the lactic acid adsorption capacity decreased by ~ 20% for IRA-67 (10% *w/v* adsorbent dose) when the temperature increased from 20 to 50°C with an initial lactic acid concentration of 42.5 g L^{-1}. They underlined that the lactic acid diffusion coefficient is a fundamental parameter to define the adsorption behaviour of anionic resins in the presence of high (> 70 g L^{-1}) or low (< 50g L^{-1}) lactic acid concentrations in the fermentation broth. Moldes et al. [12] reported that the lactic acid adsorption capacities of IRA-900, IRA-400, IRA-96 and IRA-67 (40% *w/v* adsorbent dose) were not influenced by temperature within the range of 25-45°C for an initial lactic acid concentration of 37 g L^{-1}. Similarly, in this study, temperature had a negligible influence on the tested resins, except for IRA-96 which showed a decrease of its maximum adsorption capacity (~ 22%) when operating at 80°C. This difference is probably related to a loss of the weakly bounded tertiary amine groups from the polymeric matrix due to the temperature increase [46]. On the other hand, IRA-400 confirmed its thermal stability as also shown in a previous study [29].

The results obtained by varying the contact time and the lactic acid concentration in the fermentation broth (Figure 4), within the third batch assessment, are comparable

to that presented by Moldes et al. [4] and Rampai et al. [47] in the case of high lactic acid concentration in the influent. A similar behaviour of the resin was observed in this study for low lactic acid concentration (4.5 g L^{-1}). Both the anionic resins (IRA-400 and IRA-67) showed a common kinetic sorption pattern characterized by an initial quick decrease in lactic acid concentration followed by a steady state value. Initially, the active sites are largely available, while the number of occupied sites increases and the repulsive forces between adsorbate molecules as adsorption-ion exchange evolves towards equilibrium.

IRA-67 showed a higher selectivity and stability throughout the 13 adsorption-desorption cycles than IRA-400 (Figure 5b). Eluent selection is a very important parameter for the desorption of carboxylic acids from cationic resins. Commonly, different aliphatic alcohols (e.g. methanol and ethanol), aliphatic ketones (e.g. acetone and methyl ethyl ketone), salts (e.g. NaCl and NH$_4$OH), acids (e.g. HCl and H$_2$SO$_4$) or bases (e.g. NaOH) have been used. The main challenge is the reduction of the costs related to the chemicals employed during the desorbing step. Evangelista and Nikolov [19] employed a mixture of methanol and 5% NH$_4$OH solution for desorbing lactic acid from weakly basic ion exchange resins Dowex MWA-1, Amberlite IRA-35 and Riedel-de-Haen VI-15. Lactic acid was completely desorbed from Riedel-de-Haen VI-15 ion exchange resin using 6.8 BV of methanol. Gao et al. [48] used acetone due to its low volatility and easy recovery from GAC. In particular, the lactic acid recovery rate significantly increased to ~80% with increasing amount of acetone. Quintero et al. [42] observed NaOH (1 M) as the best desorbing agent (92.7% ± 1.9 extraction efficiency) among different eluents (0.1 M HCl, 10% methanol, 1 M H$_2$SO$_4$, 1 M NaCl) using a strong anionic resin Amberlite IRA-400.

Da Silva et al. [43] developed a multistage desorption process for propionic acid (with 1, 3, 4, 5 and 6 tanks) using ethanol and n-propanol as eluent to reduce the amount of solvent and maximize the amount of adsorbate. Cao et al. [49] investigated the elution of lactic acid adsorbed on Amberlite IRA-400, at different pH using several eluents. At pH 5.0, the highest elution recovery of 97.5% was obtained with 2.5 M H$_2$SO$_4$. However, 1.0 M H$_2$SO$_4$ also showed the high elution recovery of 93.6%. On the other hand, the elution of lactic acid was easily performed using simply water as eluent when the adsorption was performed at pH 2.0 (desorption efficiency 73.4%).

In the present study, HCl and NaOH were employed as eluents for desorption of the adsorbed lactic acid onto IRA-400 and IRA-67, respectively. HCl is a common eluent

for regeneration of resins in Cl⁻ form that can be easily separated from lactic acid by selective evaporation [42]. Conversely, NaOH is a non-volatile and low-cost chemical, widely employed for the regeneration of resin in OH⁻ form in other studies [32, 50].

9.4.2. Adsorption capacity in fed batch applications

The scaling-up of the process proceeded with semi-continuous experiments showing a higher selectivity and stability for IRA-67 compared to IRA-400 (Figure 5c). This result was influenced by their different adsorption capacities (134.2 mg g⁻¹ for IRA-67 and 70.1 mg g⁻¹ for IRA-400), evaluated after an operation time of 6 h. In this study, it is important to notice that the adsorption capacities in fed-batch conditions were found higher than those evaluated during the batch experiments. This might be due to the partial removal of the exchanged anions (Cl⁻ and OH⁻) from the liquid solution in semi-continuous conditions.

9.4.3. The role of chemicals for the desorption step in the fixed-bed reactor

The preliminary FBR experiments showed an expected overall decrease of the lactic acid removal efficiency during the adsorption phase when increasing the flow rate due to the higher volumetric loading rate (Figure 6a), the reduction of contact time and irreversible lactic acid adsorption (Figure 1f). During the experimental evaluation of the LA_{clr}, IRA-67 was not saturated during the column operation and the pH of the effluent decreased up to 2.0 (Figure 6b). Moldes et al. [4] tested IRA-67 under similar operational conditions, using variable volumes (from 64 to 106 mL) of 1 N HCl for the regeneration of the resin. Moreover, the lactic acid concentrations in the eluent were lower (10.4-17.2 g L⁻¹) than those obtained in the present work (36.5 g L⁻¹; Figure 6c) with 3 BV of NaOH (0.5 M).

The FBR adsorption capacity of IRA-67 (more than 200 mg g⁻¹) was significantly higher than those observed in batch experiments (35.9 - 45.2 mg g⁻¹) due to the different adsorption conditions (Figure 7), revealing the applicability of the FBR for low concentrations (4.5 g L⁻¹) of lactic acid fermentation broths. As remarked in [12], the OH⁻ ions are continuously eluted during column operation, while they remain in solution in batch operation. Figure 7b shows that the amount of lactic acid removed from the resin during desorption step slightly decreased over the cycles, leading to a gradual decrease of the accumulation performance of lactic acid from the resin. This

was probably due to the not reversible fouling observed for IRA-67 (Figure 1e and 1f).

John et al. 2008 [51] used IRA-67 in Cl^- form for lactic acid recovery from aqueous solutions using several cassava bagasse-based fermentation media in a FBR. Column operation was based on sequential steps and the desorption stage was carried out by employing 100 mL of eluent, reaching comparable lactic acid concentrations in the eluate: 17.6 g L^{-1} for real cassava bagasse broth versus 17.8 g L^{-1} for aqueous lactic acid solution with an average lactic acid recovery of 97% [51]. Similarly, Moldes et al. [4] developed a combined adsorption-desorption system for lactic acid recovery from both aqueous and simultaneous saccharification and fermentation (SSF) media onto IRA-67 in Cl^- form in a FBR. They employed a variable volume of 1 M HCl for lactic acid desorption (70 mL with SSF media, 86 mL with aqueous lactic acid solution) with related lactic acid concentrations in the eluate of 13.3 g L^{-1} with an aqueous lactic acid solution and 15.9 g L^{-1} in SSF media. Moreover, they obtained an average lactic acid recovery of 99.4%.

The lower lactic acid recovery found in the present study (42.9%) can be ascribed to the fact that the adsorption phase was not followed by a washing step to remove the interstitial solution containing lactic acid and to complete the regeneration of the column (Figure 7b). Indeed, the use of a stronger eluent (1 N HCl), powered by a preliminary washing with demineralized water, enables to wash out ions differently from the batch operation where lactate remained in the solution affecting pH and the equilibrium conditions. However, the presence of an additional washing step leads to an increase of the overall time and the complexity of the cycle for scale-up applications. Contextually, the use of a larger quantity of eluent with a high concentration of HCl determines an increase in the costs of desorption as well as a decrease in the lactic acid concentration in the eluate.

For future research, it will be interesting to test different eluents (e.g. NH_4OH, methanol or H_2SO_4) with different concentrations in continuous experiments, making a comparison based on the amount of the eluent required, lactic acid concentration, desorption efficiency and regeneration stability. In addition, the purity of lactic acid is a key parameter that needs to be further investigated.

It is important to take into account the expected decrease in the recovery efficiency that can occur when treating real fermentation media, due to the presence of other competitive anions and the adsorption of external components such as nutrients and

enzymes. Moreover, *in situ* and down stream processes should also be studied with the development of mathematical models for such complex mechanisms [52]. For instance, the mathematical description of the biological processes [53, 54] could be combined with the isotherm adsorption modelling [55], to elucidate the interaction between the fermentation process and the adsorption stage.

9.5. Conclusions

This work assessed the capacity, efficiency and regenerability of strong (IRA-900 and IRA-400) and weak (IRA-96 and IRA-67) anionic resins for lactic acid recovery from solutions that mimic the conditions of *T. neapolitana* fermentation broth at the end of the bacterial culture. The strong anionic resins (IRA-900 and IRA-400) showed a higher lactic acid removal efficiency and capacity at the pH above the pKa of lactic acid (3.86), while for the weak anionic resins (IRA-96 and IRA-67) at a pH below the pKa of lactic acid, irrespective of the resin pre-treatment. Lactic acid recovery can be successfully carried out at 80°C, which is the optimum temperature for *T. neapolitana* fermentation. The ideal contact time of 10 min was suitable for lactic acid adsorption onto both anionic resins IRA-400 and IRA-67, the latter exhibiting the highest lactic acid recovery (> 91%) and stability over 13 batch adsorption-desorption cycles. In column operation, the lactic acid removal efficiency for IRA-67 was highly influenced by the inlet flow rate, especially when the critical loading rate (63.1 g L^{-1} h^{-1}) was exceeded. High concentrations of lactic acid (~30 g L^{-1}) in the eluent were found using 3 BV of NaOH as the regenerant during the desorption step. The practical application of having an integrated adsorption-desorption cycle in the adsorption process has been highlighted for FBR operation in order to recover lactic acid.

References

[1] Yeshanew, M.M., Frunzo, L., Luongo, V., Pirozzi, F., Lens, P.N. and Esposito, G., 2016. Start-up of an anaerobic fluidized bed reactor treating synthetic carbohydrate rich wastewater. Journal of Environmental Management, 184, pp.456-464.

[2] Luongo, V., Ghimire, A., Frunzo, L., Fabbricino, M., d'Antonio, G., Pirozzi, F. and Esposito, G., 2017. Photofermentative production of hydrogen and poly-β-hydroxybutyrate from dark fermentation products. Bioresource Technology, 228, pp.171-175.

[3] Hofvendahl, K. and Hahn-Hägerdal, B., 2000. Factors affecting the fermentative lactic acid production from renewable resources. Enzyme and Microbial Technology, 26(2-4), pp.87-107.

[4] Moldes, A., Alonso, J. and Parajo, J., 2003. Recovery of lactic acid from simultaneous saccharification and fermentation media using anion exchange resins. Bioprocess and Biosystems Engineering, 25(6), pp.357-363.

[5] Martinez, F.A.C., Balciunas, E.M., Salgado, J.M., González, J.M.D., Converti, A., De Souza Oliveira, R.P., 2013. Lactic acid properties, applications and production: a review. Trends in Food Science & Technology, 30(1), pp.70-83.

[6] Ghimire, A., Luongo, V., Frunzo, L., Pirozzi, F., Lens, P.N. and Esposito, G., 2017. Continuous biohydrogen production by thermophilic dark fermentation of cheese whey: Use of buffalo manure as buffering agent. International Journal of Hydrogen Energy, 42(8), pp.4861-4869.

[7] Göksungur, Y., Gündüz, M. and Harsa, Ş., 2005. Optimization of lactic acid production from whey by *L casei* NRRL B-441 immobilized in chitosan stabilized Ca-alginate beads. Journal of Chemical Technology and Biotechnology, 80(11), pp.1282-1290.

[8] Nancib, N. Nancib, A., Boudjelal, A., Benslimane, C., Blanchard, F. and Boudrant, J., 2001. The effect of supplementation by different nitrogen sources on the production of lactic acid from date juice by *Lactobacillus casei subsp. rhamnosus*. Bioresource Technology, 78(2), pp.149-153.

[9]   Huang, L.P., Jin, B., Lant, P. and Zhou, J., 2005. Simultaneous saccharification and fermentation of potato starch wastewater to lactic acid by *Rhizopus oryzae* and *Rhizopus arrhizus*. Biochemical Engineering Journal, 23(3), pp.265-276.

[10]   Fukushima, K., Sogo, K., Miura, S. and Kimura, Y., 2004. Production of D-lactic acid by bacterial fermentation of rice starch. Macromolecular Bioscience, 4(11), pp.1021-1027.

[11]   Jin, B., Yin, P., Ma, Y. and Zhao, L., 2005. Production of lactic acid and fungal biomass by *Rhizopus* fungi from food processing waste streams. Journal of Industrial Microbiology and Biotechnology, 32(11-12), pp.678-686.

[12]   Moldes, A.B., Alonso, J.L. and Parajó, J.C., 2001. Resin selection and single-step production and recovery of lactic acid from pretreated wood. Applied Biochemistry and Biotechnology, 95(2), pp.69-81.

[13]   Garde, A., Jonsson, G., Schmidt, A. and Ahring, B.K., 2002. Lactic acid production from wheat straw hemicellulose hydrolysate by *Lactobacillus pentosus* and *Lactobacillus brevis*. Bioresource Technology, 81(3), pp.217-223.

[14]   Luo, J., Xia, L., Lin, J. and Cen, P., 1997. Kinetics of simultaneous saccharification and lactic acid fermentation processes. Biotechnology Progress, 13(6), pp. 762-767.

[15]   Bishai, M., De, S., Adhikari, B. and Banerjee, R., 2015. A platform technology of recovery of lactic acid from a fermentation broth of novel substrate *Zizyphus oenophlia*. 3 Biotech, 5(4), pp.455-463.

[16]   Wee, Y.-J., Jin-Nam, K. and Hwa-Won R., 2006. Biotechnological production of lactic acid and its recent applications. Food Technology and Biotechnology, 44(2), pp.163-172.

[17]   Datta, R. and Henry, M., 2006. Lactic acid: recent advances in products, processes and technologies-a review. Journal of Chemical Technology and Biotechnology, 81(7), pp.1119-1129.

[18]   Lunt, J., 1998. Large-scale production, properties and commercial applications of polylactic acid polymers. Polymer Degradation and Stability, 59(1), pp.145-152.

[19] Evangelista, R.L. and Nikolov, Z.L., 1996. Recovery and purification of lactic acid from fermentation broth by adsorption. Applied biochemistry and biotechnology, 57(1), pp.471-480.

[20] Joglekar, H.G., Rahman, I., Babu, S., Kulkarni, B.D. and Joshi, A., 2006. Comparative assessment of downstream processing options for lactic acid. Separation and Purification Technology, 52(1), pp.1-17.

[21] Wasewar, K.L., 2005. Separation of lactic acid: recent advances. Chemical and Biochemical Engineering Quarterly, 19(2), pp.159-172.

[22] Raya-Tonetti, G. and Perotti, N., 1998. Expanded bed affinity chromatography using streamline-cibacron red 3ba for simultaneous purification of alcohol dehydrogenase and glucose-6-phosphate dehydrogenase from unclarified yeast homogenate. Latin American Applied Research, 28, pp.89-93.

[23] Dipasquale, L., d'Ippolito, G. and Fontana, A., 2014. Capnophilic lactic fermentation and hydrogen synthesis by *Thermotoga neapolitana*: an unexpected deviation from the dark fermentation model. International Journal of Hydrogen Energy, 39(10), pp.4857-4862.

[24] d'Ippolito, G., Dipasquale, L. and Fontana, A., 2014. Recycling of carbon dioxide and acetate as lactic acid by the hydrogen-producing bacterium *Thermotoga neapolitana*. ChemSusChem, 7(9), pp.2678-2683.

[25] Pradhan, N., Dipasquale, L., d'Ippolito, G., Panico, A., Lens, P.N., Esposito, G. and Fontana, A., 2017. Hydrogen and lactic acid synthesis by the wild-type and a laboratory strain of the hyperthermophilic bacterium *Thermotoga neapolitana* DSMZ 4359 T under capnophilic lactic fermentation conditions. International Journal of Hydrogen Energy, 42, pp.16023-16030.

[26] Zhang, K., Zhang, L. and Yang, S.-T., 2014. Fumaric acid recovery and purification from fermentation broth by activated carbon adsorption followed with desorption by acetone. Industrial & Engineering Chemistry Research, 53(32), pp.12802-12808.

[27] Uslu, H., 2009. Adsorption equilibria of formic acid by weakly basic adsorbent Amberlite IRA-67: Equilibrium, kinetics, thermodynamic. Chemical Engineering Journal, 155, pp.320-325.

[28] Yousuf, A., Bonk, F., Bastidas-Oyanedel, J.-R., Schmidt, J.E., 2016. Recovery of carboxylic acids produced during dark fermentation of food waste by

adsorption on Amberlite IRA-67 and activated carbon. Bioresource Technology, 217, pp.137-140.

[29] Pradhan, N., Rene, E.R., Lens, P.N., Dipasquale, L., d'Ippolito, G., Fontana, A., Panico, A. and Esposito, G., 2017. Adsorption behaviour of lactic acid on granular activated carbon and anionic resins: thermodynamics, isotherms and kinetic studies. Energies, 10(5), pp.665.

[30] Nakano, K., Kataoka, H. and Matsumura, M., 1996. High density culture of *Propionibacterium freudenreichii* coupled with propionic acid removal system with activated charcoal. Journal of Fermentation and Bioengineering, 81(1), pp.37-41.

[31] Aljundi, I.H., Belovich, J.M. and Talu, O., 2005. Adsorption of lactic acid from fermentation broth and aqueous solutions on Zeolite molecular sieves. Chemical Engineering Science, 60(18), pp.5004-5009.

[32] Efe, C., van der Wielen, L.A. and Straathof, A.J., 2010. High silica zeolites as an alternative to weak base adsorbents in succinic acid recovery. Industrial & Engineering Chemistry Research, 49(4), pp.1837-1843.

[33] d'Ippolito, G., Dipasquale, L., Vella, F.M., Romano, I., Gambacorta, A., Cutignano, A. and Fontana, A., 2010. Hydrogen metabolism in the extreme thermophile *Thermotoga neapolitana*. International Journal of Hydrogen Energy, 35(6), pp.2290-2295.

[34] Lützenkirchen, J., Preočanin, T., Kovačević, D., Tomišić, V., Lövgren, L. and Kallay, N., 2012. Potentiometric titrations as a tool for surface charge determination. Croatica Chemica Acta, 85(4), pp.391-417.

[35] Dethe, M.J., Marathe, K. V., Gaikar, V.G., 2006. Adsorption of lactic acid on weak base polymeric resins. Separation Science and Technology, 41(13), pp.2947-2971.

[36] Abdel-Rahman, M.A., Tashiro, Y. and Sonomoto, K., 2013. Recent advances in lactic acid production by microbial fermentation processes. Biotechnology Advances, 31(6), pp.877-902.

[37] Gluszcz, P., Jamroz, T., Sencio, B. and Ledakowicz, S., 2004. Equilibrium and dynamic investigations of organic acids adsorption onto ion-exchange resins. Bioprocess and Biosystems Engineering, 26(3), pp.185-190.

[38] Helfferich, F.G., 1962. Ion exchange. Courier Corporation.

[39] Rincon, J., Fuertes, J., Rodriguez, J.F., Rodriguez, L. and Monteagudo, J.M., 1997. Selection of a cation exchange resin to produce lactic acid solutions from whey fermentation broths. Solvent Extraction and Ion Exchange, 15(2), pp.329-345.

[40] Ghimire, A., Valentino, S., Frunzo, L., Trably, E., Escudié, R., Pirozzi, F., Lens, P.N. and Esposito, G., 2015. Biohydrogen production from food waste by coupling semi-continuous dark-photofermentation and residue post-treatment to anaerobic digestion: a synergy for energy recovery. International Journal of Hydrogen Energy, 40(46), pp.16045-16055.

[41] Bayazit, S.S., Inci, I., and Uslu, H., 2011. Adsorption of lactic acid from model fermentation broth onto activated carbon and Amberlite IRA-67. Journal of Chemical & Engineering Data, 56 (5), pp.1751-1754.

[42] Quintero, J., Acosta, A., Mejía, C., Ríos, R. and Torres, A.M., 2012. Purification of lactic acid obtained from a fermentative process of cassava syrup using ion exchange resins. Revista Facultad de Ingeniería Universidad de Antioquia, 65, pp.139-151.

[43] da Silva, A.H. and Miranda, E.A., 2013. Adsorption/desorption of organic acids onto different adsorbents for their recovery from fermentation broths. Journal of Chemical & Engineering Data, 58(6), pp.1454-1463.

[44] Patel, M., Bassi, A.S., Zhu, J.J.-X and Gomaa, H., 2008. Investigation of a dual-particle liquid-solid circulating fluidized bed bioreactor for extractive fermentation of lactic acid. Biotechnology Progress, 24(4), pp.821-831.

[45] Gao, Q., Liu, F., Zhang, T., Zhang, J., Jia, S., Yu, C., Jiang, K. and Gao, N., 2010. The role of lactic acid adsorption by ion exchange chromatography. Plos One, 5(11), pp.e13948.

[46] Davison, B.H. and Thompson, J.E., 1992. Simultaneous fermentation and separation of lactic acid in a biparticle fluidized-bed bioreactor. Applied Biochemistry and Biotechnology, 34(1), pp.431-439.

[47] Rampai, T., Thitiprasert, S., Boonkong, W., Kodama, K., Tolieng, V. and Thongchul, N., 2016. Improved lactic acid productivity by simultaneous recovery during fermentation using resin exchanger. Asia-Pacific Journal of Science and Technology, 21(2), pp.193-199.

[48] Gao, M.-T., Shimamura, T., Ishida, N. and Takahashi, H., 2011. pH-uncontrolled lactic acid fermentation with activated carbon as an adsorbent. Enzyme and Microbial Technology, 48(6), pp.526-530.

[49] Cao, X., Yun, H.S. and Koo, Y.M., 2002. Recovery of L (+) lactic acid by anion exchange resin Amberlite IRA-400. Biochemical Engineering Journal, 11(2), pp.189-196.

[50] Chen, C.-C. and Ju, L.-K., 1998. Adsorption characteristics of polyvinylpyridine and activated carbon for lactic acid recovery from fermentation of *Lactobacillus delbrueckii*. Separation Science and Technology, 33(10), pp.1423-1437.

[51] John, R.P., Nampoothiri, K.M. and Pandey, A., 2008. L (+) Lactic acid recovery from cassava bagasse based fermented medium using anion exchange resins. Brazilian Archives of Biology and Technology, 51(6), pp.1241-1248.

[52] Sodsai, W. and Sookkumnerd, T., 2014. Modeling of lactic acid adsorption isotherm by anion exchange resin Amberlite IRA-96. King Mongkut's Institute of Technology Ladkrabang Science and Technology Journal, 13(2), pp.82-86.

[53] Pradhan, N., Dipasquale, L., d'Ippolito, G., Fontana, A., Panico, A., Pirozzi, F., Lens, P.N. and Esposito, G., 2016. Model development and experimental validation of capnophilic lactic fermentation and hydrogen synthesis by *Thermotoga neapolitana*. Water research, 99, pp.225-234.

[54] Mattei, M.R., D'Acunto, B., Esposito, G., Frunzo, L. and Pirozzi, F., 2015. Mathematical modeling of competition and coexistence of sulfate-reducing bacteria, acetogens, and methanogens in multispecies biofilms. Desalination and Water Treatment, 55(3), pp.740-748.

[55] D'Acunto, B., Esposito, G., Frunzo, L., Mattei, M.R. and Pirozzi, F., 2015. Mathematical modeling of heavy metal biosorption in multispecies biofilms. Journal of Environmental Engineering, 142(9), pp.1-14.

Chapter 10

Conclusion and future perspectives

Conclusions and future perspectives

Over the last decades, the interest of sustainable alternative technologies for energy and chemicals production highly increased due to the variable price of petroleum-based fuels. The increase in the energy demand, the oil resources depletion and the concern about the greenhouse gases emission due to global climate change motivated the intensification in research efforts in clean and eco-friendly alternatives [1]. Contextually, the production of recalcitrant compounds due to the use of fossil fuels is driving governments to promote more efficient processes to reduce the amount of residues and favour a more sustainable bioeconomy.

In this context, biorefining systems which can use large available biomasses, such as waste biomass, is a promising alternative for biofuel production promoting the use of feedstock which does not contribute to carbon dioxide emissions [2, 3]. One of the issues in the utilization of waste feedstock sources is the selection of the best biorefining system to obtain value added products. The technologies conventionally used for biomass and wastes conversion comprise different physical, biological, and thermo-chemical methods, which need investigations related to their sustainability in application.

10.1 Conclusions

The current study addressed several issues and potential applications of anaerobic processes for waste biomass conversion in a biorefinery concept. The use of well-known biotechnology, i.e. anaerobic digestion (AD), and relatively new bioprocesses, such as dark fermentation (DF) and photo fermentation (PF), led to the valorisation of the organic compounds fed to batch and continuous reactors. These biotechnologies have been combined in original systems to reach higher biogas yields and complete conversion of the organic matter contained in the effluents. The studies presented in Chapters 2 and 3 focussed on AD biofilm reactors. The experimental activity identified different operational factors affecting the start-up process of an AFBR, such as hydrodynamic conditions, substrate characteristics and trace metals bioavailability, which are fundamental to reduce the time of colonization on the biofilm carriers (Yeshanew et al. 2016). To reach the theoretical methane yield of 340 and 345 mL CH_4 g COD^{-1}, methanogenic archaea needed to interact in a synergic way with all the other bacterial species inhabiting the biofilm in the reactor. To clarify the community functions of these complex systems and the mechanisms regulating the methane production in anaerobic biofilm reactors, a mathematical model able to take into account the invasion phenomenon was developed. The numerical results proved that the invasion model is able to effectively describe the invasion of methanogenic

233

archaea into a constituted fermentative biofilm. The model might be used to have a better insight into biofilm dynamics and optimize process designing and practical operation. For what concerns the experimental activity, further developments might involve the microbial characterization of the anaerobic biofilm and the investigation of the reactor performance under diverse feeding and operational conditions. In addition, the results of the microbial analysis might be used to perform model calibration and validation.

Chapters 4 to 9 mainly focused on the application of the DF technology for hydrogen production, with the contextual integration of such process in specific biorefining systems. In particular, in Chapter 4 DF of cheese whey was investigated. The experimental results highlighted that BM, characterized by a higher alkalinity, can be effectively applied as co-substrate for maintaining an operable pH during the DF process around 4.8-5. Therefore, the addition of BM can aid in providing stability to the continuous dark fermentative H_2 production and removing the dependency on chemical buffering agents. Hence, co-fermentation of cheese whey with BM or other locally available feedstock sources might provide economic sustainability to scaled-up applications of DF processes.

In Chapter 5 the feasibility of PF as a post treatment stage of DFE was discussed. DF has the unique capability of utilizing a wide range of complex waste biomass, and the combination of the two processes (DF + PF) can provide the complete conversion of organic substrate in addition to enhanced H_2 yields. In general, DF-PF systems can be integrated in three possible ways; i) utilizing the produced DFE in PF systems, ii) cultivating dark and photofermentative microorganisms in one reactor system or iii) separating the two systems by a physical barrier such as a membrane. In Chapter 6, the first operational strategy was applied to the case of a DFE obtained from the thermophilic DF of the organic fraction of municipal solid wastes (OFMSW). In particular, two different inocula, i.e. *Rhodobacter sphaeroides* AV1b and an enriched mixed culture of PNSB obtained from an anaerobic digestate, were tested under different operating conditions to examine the parameters affecting H_2 and PHB productivities. The results demonstrated the possibility of adapting the mixed PNSB culture for higher hydrogen production compared to the pure cultures. However, higher PHB yields was obtained with pure cultures of *R. sphaeroides* AV1b than the mixed culture. Nonetheless, the use of mixed cultures could be promising in the scale-up application of the PF systems for the treatment of DFE, as it provides a higher COD removal efficiency and saves the asepsis costs increasing process robustness. Conversely, pure *R. sphaeroides* cultures could be specifically applied for PHB production as a value added products from PF process.

In the context of biorefinery, Chapter 7 reviewed the generation of bio-hythane from microalgae via two-stage dark fermentation, with special emphasis on the key issues influencing bio-hythane production. Several crucial factors to be considered prior to technology scale up to boost hydrogen production from DF were discussed. The integrated hydrogen and methane production from microalgae and waste biomass would be a profitable clean energy solution, which would make bio-hythane production sustainable.

Chapter 8 presented a preliminary investigation on an innovative combined system based on a DF and a hydrothermal treatment stages aimed at obtaining an effective and cheaper CAC denaturation. The DF biotechnology has been successfully applied to dissolve the cementitious phase of a composite, simulating a CAC, and to produce H_2. In particular, GFC dissolution was evaluated by using different organic acids synthetic solutions. At this purpose, the results revealed a strong diffusional resistance to VFAs migration through GFC. Specifically, the specific phenomena observed have been explained by imposing the Knudsen diffusion coefficient into the integrated second Fick's law. The DF effluents resulted effective for the dissolution of CAC simulating conglomerates. In fact, in the case of $5.0 \cdot 10^3$ ppm GFC load, the cement matrix was completely dissolved into a real solution deriving from the DF of glucose. Moreover, this process resulted in a H_2 production equal to 284 mmol H_2 L_{sol}^{-1}, which could be used as energy source during the hydrothermal treatment, and in a final pH of the suspension equal to 4.71, which is close to the best conditions for the asbestos fiber denaturation. The adoption of different GFC loads resulted in lower hydrogen productions and/or dissolution efficiencies. According to the other studies, the H_2 yields were low since too acidic pH were reached. On the other hand, the acidity of the solution was necessary for the dissolution of CAC cement matrix.

In Chapter 9, the capacity, efficiency and regenerability of strong (IRA-900 and IRA-400) and weak (IRA-96 and IRA-67) anionic resins for lactic acid recovery from solutions that mimic the conditions of *T. neapolitana* fermentation broth at the end of the bacterial culture were assessed. The strong anionic resins (IRA-900 and IRA-400) showed a higher lactic acid removal efficiency and capacity at the pH above the pKa of lactic acid (3.86), while for the weak anionic resins (IRA-96 and IRA-67) at a pH below the pKa of lactic acid, irrespective of the resin pre-treatment. Lactic acid recovery can be successfully carried out at 80°C, which is the optimum temperature for *T. neapolitana* fermentation. The ideal contact time of 10 min was suitable for lactic acid adsorption onto both anionic resins IRA-400 and IRA-67, the latter exhibiting the highest lactic acid recovery (> 91%) and stability over 13 batch adsorption-desorption cycles. In column operation, the lactic acid removal efficiency for IRA-67 was highly influenced by

the inlet flow rate, especially when the critical loading rate (63.1 g L^{-1} h^{-1}) was exceeded. High concentrations of lactic acid (~30 g L^{-1}) in the eluent were found using 3 BV of NaOH as the regenerant during the desorption step. The practical application of having an integrated adsorption-desorption cycle in the adsorption process was highlighted for FBR operation in order to recover lactic acid.

10.2 Future perspectives

Based on the experimental and modeling results presented in the previous chapters, several open research questions, needing further investigation, can be individuated. For what concerns AD, the scientific literature on the topic demonstrates that such technology has been widely tested on both full and lab scale applications and it identifies the maximisation of biogas yields for a higher net energy production in the form of bio-CH$_4$ as one of the main remaining issues[4, 5, 6]. The use of biofilm technology for the AD of complex organic substrates might represent a valid solution as it is able to enhance the methane productivity and reduce the costs related to the biomass conversion. However, more experimental and modelling efforts are needed to completely understand the dynamic microbial processes occurring during the evolution of such biofilm systems and thus optimize the start-up of these reactors, which usually takes 2 to 9 months [7, 8]. In addition, the biofilm technology has been usually applied in two-stage systems where hydrolysis is performed in a separate reactor prior to the biofilm stage [8]. This implies that the first stage dynamics strongly affect the availability of nutrients and other compounds in the next stage and this might reflect negatively on the biogas production (i.e. lack of bioavailable trace elements, presence of inhibitory compounds).

Relatively to the DF process, the current study has been aimed at valorising the DFEs though the use of recovery technologies or other biochemical processes in complex biorefining systems [3]. The recovery and purification of specific carboxylic acids from real DFE through anionic resins represent a technological challenge due to the presence of other inert salts that can strongly affect the applicability of such separation systems [9]. The presented results demonstrated the applicability of anionic resins in FBR experiments for continuous recovery of lactic acid from a synthetic "fermentation broth". Further investigations might be related to the use of real DFEs and their interactions with the functional groups and porosity characterizing the anionic resins.

For the application of DFE to the dissolution of cement asbestos composites as a pre-treatment substituting the sulphuric acid acidification stage [10], additional experimental activity should be carried out on real waste biomasses to optimize the continuous hydrogen production. In this

way, a complete life cycle assessment could be implemented by taking into account the exchange energy fluxes between the two processes.

Photo fermentation process is probably the most promising light dependent bio-hydrogen production process [11, 12], but only few studies demonstrated its applicability as stand-alone bio conversion system. As demonstrated in this study, the use of mixed adapted consortia can enhance the hydrogen yields compared to pure cultures [13, 14], leading to high versatility of PBRs as they are resilient to the invasion of undesirable micro-organisms detrimental to bioreactor performance. Additional efforts should be devoted to the enhancement of the H_2 yields on both synthetic and real substrates for scaled-up applications.

The use of DFEs in coupled biological systems such as DF-PF or DF-AD is up-to-date the most promising solution to obtain contemporarily the complete biomass conversion and the increase in biogas yields [15, 16]. Future perspectives are mainly related to the use of waste biomass and the production of high value products. A major challenge in this field is related to the selection of the best combination of biological processes, which leads to the most effective biomass valorisation with the lowest costs in terms of operation and waste products disposal.

References

[1] Catalán-Martínez, D., Domine, M.E., Serra, J.M., 2018. Liquid fuels from biomass: An energy self-sustained process integrating H_2 recovery and liquid refining. Fuel, 212, pp.353-363.

[2] Valdez-Vazquez, I., Sanchez, A., 2017. Proposal for biorefineries based on mixed cultures for lignocellulosic biofuel production: a techno-economic analysis. Biofuels, Bioproducts and Biorefining.

[3] Cherubini, F., 2010. The biorefinery concept: using biomass instead of oil for producing energy and chemicals. Energy Conversion and Management, 51(7), pp.1412-1421.

[4] Ariunbaatar, J., Panico, A., Esposito, G., Pirozzi, F., Lens, P.N.L., 2014. Pretreatment methods to enhance anaerobic digestion of organic solid waste. Applied Energy, 123, pp.143-156.

[5] McKeown, R.M., Hughes, D., Collins, G., Mahony, T., O'Flaherty, V., 2012. Low-temperature anaerobic digestion for wastewater treatment. Current Opinion in Biotechnology, 23(3), pp.444-451.

[6] Rajeshwari, K.V., Balakrishnan, M., Kansal, A., Lata, K. and Kishore, V.V.N., 2000. State-of-the-art of anaerobic digestion technology for industrial wastewater treatment. Renewable and Sustainable Energy Reviews, 4(2), pp.135-156.

[7] Wang, W., Hou, H., Hu, S. and Gao, X., 2010. Performance and stability improvements in anaerobic digestion of thermally hydrolyzed municipal biowaste by a biofilm system. Bioresource technology, 101(6), pp.1715-1721.

[8] Picioreanu, C., Batstone, D.J. and Van Loosdrecht, M.C.M., 2005. Multidimensional modelling of anaerobic granules. Water Science and Technology, 52(1-2), pp.501-507.

[9] Yousuf, A., Bonk, F., Bastidas-Oyanedel, J.R., Schmidt, J.E., 2016. Recovery of carboxylic acids produced during dark fermentation of food waste by adsorption on Amberlite IRA-67 and activated carbon. Bioresource Technology, 217, pp.137-140.

[10] Balducci, G., Foresti, E., Lelli, M., Lesci, I.G., Marchetti, M., Pierini, F., Roveri, N., inventors. Process for treating an asbestos containing material. EU patent: EP2428254 B1. 2013 March 27.

[11] Li, R.Y., Fang, H.H., 2009. Heterotrophic photo fermentative hydrogen production. Critical Reviews in Environmental Science and Technology, 39(12), pp.1081-1108.

[12] Das, D., Veziroğlu, T.N., 2001. Hydrogen production by biological processes: a survey of literature. International Journal of Hydrogen Energy, 26(1), pp.13-28.

[13] Ghimire, A., Valentino, S., Frunzo, L., Pirozzi, F., Lens, P.N.L., Esposito, G., 2016. Concomitant biohydrogen and poly-β-hydroxybutyrate production from dark fermentation effluents by adapted *Rhodobacter sphaeroides* and mixed photofermentative cultures. Bioresource Technology, 217, pp.157-164.

[14] Luongo, V., Ghimire, A., Frunzo, L., Fabbricino, M., d'Antonio, G., Pirozzi, F., Esposito, G., 2017. Photofermentative production of hydrogen and poly-β-hydroxybutyrate from dark fermentation products. Bioresource Technology, 228, pp.171-175.

[15] Roy, S. and Das, D., 2016. Biohythane production from organic wastes: present state of art. Environmental Science and Pollution Research, 23(10), pp.9391-9410.

[16] Rai, P.K., Singh, S.P., Asthana, R.K. and Singh, S., 2014. Biohydrogen production from sugarcane bagasse by integrating dark-and photo-fermentation. Bioresource Technology, 152, pp.140-146.